

# **Biophysically characterizing viral particles**

**Dissertation**

with the aim of achieving a doctoral degree at the Faculty of  
Mathematics, Informatics and Natural Sciences

Department of Chemistry

Universität Hamburg

submitted by

Ronja Pogan

born in Heilbronn

Hamburg 2023

## **Reviewers**

### **Prof. Dr. Charlotte Uetrecht**

Leibniz Institute of Virology, Hamburg, Germany; Centre for Structural Systems Biology, Hamburg, Germany; University of Siegen, Siegen, Germany; Deutsches Elektronen-Synchrotron, Hamburg, Germany.

### **Prof. Dr. Hartmut Schlüter**

Institute of Clinical Chemistry and Laboratory Medicine, Section Mass Spectrometry and Proteomics, University Medical Center Hamburg-Eppendorf, Hamburg, Germany.

## **Examination board**

### **Prof. Dr. Kay Grünewald**

Leibniz Institute of Virology, Hamburg, Germany; Centre for Structural Systems Biology, Hamburg, Germany; Institute of Biochemistry and Molecular Biology, University of Hamburg, Hamburg, Germany.

### **Prof. Dr. Hartmut Schlüter**

Institute of Clinical Chemistry and Laboratory Medicine, Section Mass Spectrometry and Proteomics, University Medical Center Hamburg-Eppendorf, Hamburg, Germany.

### **Dr. Pietro Scaturro**

Leibniz Institute of Virology, Hamburg, Germany.

**Date of thesis submission: 13.02.2023**

**Date of disputation and print release: 17.03.2023**

This thesis was prepared from April 2017 to February 2023 under the supervision of Prof. Dr. Charlotte Uetrecht at the Leibniz Institute of Virology in the working group ‘Dynamics of Viral Structures’. Second supervisor was Prof. Dr. Kay Grünewald, Centre for Structural Systems Biology (CSSB) and Leibniz Institute of Virology, associated to the Department of Chemistry of the University of Hamburg



# Table of Contents

---

---

Table of Contents .....	I
List of Publications.....	III
Abbreviations .....	IV
Abstract .....	VI
Zusammenfassung .....	VIII
1. Introduction .....	1
1.1. Structural mass spectrometry.....	1
1.1.1. Characterization of molecular complexes .....	1
1.1.2. Native mass spectrometry .....	2
1.1.3. Charge-detection based instruments.....	8
1.1.4. Gas phase electrophoretic mobility analysis .....	10
1.2. Norovirus Assembly and Stability.....	12
1.2.1. Virus assembly .....	12
1.2.2. Human norovirus .....	12
1.3. Aim of the work.....	21
2. Cumulative Part of the Dissertation .....	23
2.1. Virus-like particle size and molecular weight/mass determination applying gas-phase electrophoresis (native nES GEMMA).....	23
2.2. Norovirus-like VP1 particles exhibit isolate dependent stability profiles. ....	36
2.3. N-terminal VP1 Truncations Favor $T = 1$ Norovirus-Like Particles .....	45
2.4. Synopsis.....	63
3. Discussion .....	67
4. Bibliography.....	73
5. Appendix .....	92

## Table of Contents

5.1.	Hazardous substances according to the Globally Harmonized System (GHS) .....	92
5.2.	Supporting information.....	97
5.2.1.	Virus-like particle size and molecular weight/mass determination applying gas-phase electrophoresis (native nES GEMMA).....	97
5.2.2.	Norovirus-like VP1 particles exhibit isolate-dependent stability profiles .....	100
5.2.3.	N-terminal VP1 truncations favor $T = 1$ norovirus-like particles .....	112
6.	Declaration on Oath/ Eidesstattliche Versicherung.....	128

## List of Publications

---

---

Pogan R, Schneider C, Reimer R, Hansman G, Uetrecht C. Norovirus-like VP1 particles exhibit isolate dependent stability profiles. *J Phys Condens Matter*. 2018;30(6):064006.

\*Weiss VU, \*Pogan R, Zoratto S, Bond KM, Boulanger P, Jarrold MF, Lykтей N, Pahl D, Puffler N, Schelhaas M, Selivanovitch, Uetrecht C and Allmeier G. Virus-like particle size and molecular weight/mass determination applying gas-phase electrophoresis (native nES GEMMA). *Anal Bioanal Chem*. 2019;411(23):5951-62.

\*authors contributed equally

Pogan R, Weiss VU, Bond K, Dülfer J, Krisp C, Lykтей N, Müller-Guhl J, Zoratto S, Allmeier G, Jarrold MF, Muñoz-Fontela C, Schlüter H, Uetrecht C. N-terminal VP1 Truncations Favor  $T = 1$  Norovirus-Like Particles. *Vaccines Basel*. 2021;9(1):8.

Additional:

Review

Pogan R, Dulfer J, Uetrecht C. Norovirus assembly and stability. *Curr Opin Virol*. 2018;31:59-65.

## Abbreviations

---

---

aa	Amino acid
AAV	Adeno associated viruses
AFM	Atomic force microscopy
CC BY	Creative Commons Attribution License
CD	Circular dichroism
CDMS	Charge detection mass spectrometry
CID	Collision-induced dissociation
CRM	Charge residue model
DMA	Differential mobility analyzer
ELIT	Electrostatic linear ion trap
EM	Electron microscopy
EMD	Electrophoretic mobility diameter
FCV	Feline calicivirus
FFT	Fast Fourier transform
FHV	Flockhouse virus
FT ICR	Fourier-transform ion cyclotron resonance
FWHM	Full width half-maximum
GEMMA	Gas phase electrophoretic mobility analysis
HBGA	Human blood group antigens
HDX	Hydrogen deuterium exchange
HIE	Human intestinal enteroid
hNoV	Human norovirus

HPV16	Human papilloma virus type 16
IEM	Ion evaporation model
IM	Ion mobility
MALDI	Matrix-assisted laser desorption
MD	Molecular dynamics
MNV	Murine norovirus
MS	Mass spectrometry
nES, nano ESI	Nano electrospray
NMR	Nuclear magnetic resonance
ORF	Open reading frame
P domain	Protruding domain, norovirus
PTM	Posttranslational modification
QToF	Quadrupole time-of-flight
RF	Radiofrequency
RNA	Ribonucleic acid
S domain	Shell domain, norovirus
SAXS	Small-angle X-ray scattering
STD	Saturation-transfer difference
<i>T</i>	Triangulation number
ToF	Time-of-flight
VLP	Virus-like particle

## Abstract

---

---

Viruses are ubiquitous entities with various structures, that can be summarized into helical, icosahedral or more complex, with or without a viral membrane. Basic component of both enveloped and non-enveloped viruses is a protein shell built from structural subunits called capsomers surrounding the genome. Self-assembly of (nucleo-)capsids is a fundamental cellular process that still lacks full understanding. Helpful systems in unraveling these processes are recombinantly produced virus-like particles (VLPs). In non-enveloped viruses, icosahedral capsids are common. The characterization of capsid self-assembly behavior is of particular interest as icosahedral structures hold innate opportunities for bionanotechnological approaches like bionanocarriers.

The first part of this thesis targets the establishment of biophysical characterization techniques, that help to unravel capsid self-assembly and associated variability of capsomer stoichiometries. I combined different native mass spectrometry approaches and gas phase electrophoretic mobility analysis (GEMMA). This work provides a VLP mass-electrophoretic mobility diameter correlation, which closes the gap between existing correlations and enables mass estimation of spherical, empty assemblies using GEMMA. Furthermore, I applied this correlation to a low-yield example of high medical relevance, Human Papillomavirus 16, where no complementary native MS data could be obtained.

There is growing interest in native MS to aim for measurements of larger and larger species. VLPs and viruses are commonly used in instrumentation development to beat mass records or for characterization of pharmaceutically relevant, well-established systems like adeno-associated virus. The real beauty in the combination of tools as described above however are the niche insights they can give into difficult processes like virus assembly, where dynamic, low-yield assembly intermediates are usually missed with other techniques.

I was able to unravel self-assembly processes of a particularly difficult to work with, yet clinically relevant system. Human norovirus (hNoV), the main cause for viral gastroenteritis outbreaks worldwide, is lacking a robust, easy cell culture system. Norovirus-like particles however, are especially interesting, as the recombinant expression of the major structural protein VP1 is sufficient for self-assembly and norovirus classification into genogroups and genotypes is based on VP1. I established distinctive stability patterns of two different NoV variants using native MS and imaging with electron microscopy with  $T = 3$ , or VP1 180mers

being the prevalent species. Several different intermediate assembly states or disassembly products were identified, with  $T = 1$ , or 60-mers being the most abundant species in both variants. In combination with a recent study, differences on the genotype level were revealed pinpointing to the *N*-terminus has importance for self-assembly.

Indeed, in a second MS study on noroviruses, I identified a *N*-terminal truncation in VLP preparations of several hNoV variants of different genotypes. The most prominent species detected was  $T = 1$  or VP1 60mers, in contrast to the previously described  $T = 3$  particles. This effect was genotype-independent and measurements in varying solution conditions showed stability even in alkaline pH. Although several other intermediate sized assemblies were present in our dataset,  $T = 3$  formations could not be recovered through changing solution conditions.

In summary, this work provides an enormous contribution to the understanding of norovirus assembly as well as a novel tool for characterization of VLPs. The VP1 *N*-terminus was identified as particularly important for assembly. More precisely, a major *N*-terminal truncation in VP1 is leading to the formation of smaller particles. Therefore, this work is paving the way for future studies holding importance especially for norovirus vaccine development and capsid engineering.

## Zusammenfassung

---

---

Viren sind ubiquitäre Infektionserreger mit helikalen, ikosaedrischen oder komplexeren Strukturen, mit oder ohne Virusmembran. Grundbestandteil sowohl umhüllter als auch nicht umhüllter Viren ist eine Proteinhülle, die aus strukturellen Untereinheiten, so genannten Kapsomeren, aufgebaut ist und das Genom umgibt. Das eigenständige Assemblieren von (Nukleo-)Kapsiden ist ein grundlegender zellulärer Prozess, der noch nicht vollständig verstanden ist. Hilfreiche Systeme, um diese Prozesse zu entschlüsseln, sind rekombinant hergestellte virusähnliche Partikel (VLPs). Bei unbehüllten Viren sind ikosaedrische Kapside am häufigsten. Die Charakterisierung des Selbstassemblierungsverhaltens von Kapsiden ist von besonderem Interesse, da ikosaedrische Strukturen Möglichkeiten für bionanotechnologische Ansätze wie Bionanocarrier bieten.

Der erste Teil dieser Arbeit zielt auf die Etablierung biophysikalischer Charakterisierungstechniken ab, die dazu beitragen, die Selbstorganisation von Kapsiden und die damit verbundene Variabilität von Kapsomerstöchiometrien zu entschlüsseln. Es werden verschiedene Ansätze der nativen Massenspektrometrie mit der Analyse der elektrophoretischen Gasphasenmobilität (GEMMA) kombiniert. Das Ergebnis ist eine VLP-Masse-Elektrophorese-Mobilität-Durchmesser-Korrelation, die die Lücke zwischen den bestehenden Korrelationen schließt und die Massenschätzung von sphärischen, leeren Molekularkomplexen mit GEMMA ermöglicht. Darüber hinaus habe ich diese Korrelation auf ein Beispiel mit geringer Aufreinigungsausbeute und hoher medizinischer Relevanz, das humane Papillomavirus 16, angewandt, für das keine ergänzenden nativen MS-Daten gewonnen werden konnten.

Es besteht ein wachsendes Interesse an nativer MS, im speziellen zur Messung größerer Spezies. VLPs und Viren werden häufig bei der Entwicklung von Instrumenten verwendet. Sie dienen dem Brechen von Massenrekorden oder es handelt sich um pharmazeutisch relevante, gut etablierte Systeme wie Adeno-assoziierte Viren. Die beschriebenen Techniken ermöglichen Einblicke in schwierige Prozesse wie die Virusassemblierung, da hier Assemblierungsintermediate mit anderen Techniken oft übersehen werden.

Ich war in der Lage, die Selbstorganisationsprozesse eines besonders schwierig zu bearbeitenden, aber klinisch relevanten Systems zu entschlüsseln. Für das humane Norovirus, die Hauptursache für Ausbrüche viraler Gastroenteritis weltweit, gibt es kein robustes,

einfaches Zellkultursystem. Norovirus-ähnliche Partikel sind jedoch besonders interessant, da die rekombinante Expression des Hauptstrukturproteins VP1 für die Selbstassemblierung ausreicht und die Klassifizierung von Noroviren in Genogruppen und Genotypen auf VP1 basiert.

Wir haben mit Hilfe von nativer MS und elektronenmikroskopischer Bildgebung unterschiedliche Stabilitätsmuster von zwei verschiedenen NoV-Varianten ermittelt, wobei  $T = 3$  oder 180-mere die häufigste Spezies sind. Interessanterweise waren die Muster unter verschiedenen Lösungsbedingungen sowohl auf der Ebene der Genogruppe als auch des Genotyps sehr unterschiedlich. Darüber hinaus konnte ich verschiedene Assemblierungsintermediate identifizieren. Es wurden mehrere verschiedene Assemblierungsintermediate identifiziert, wobei  $T = 1$  bzw. 60-mere in beiden Varianten am häufigsten vorkamen. In Kombination mit einer kürzlich durchgeführten Studie wurden Unterschiede auf der Ebene des Genotyps aufgedeckt, die darauf hindeuten, dass der *N*-Terminus für die Selbstassemblierung von Bedeutung ist.

In einer zweiten MS-Studie über Noroviren identifizierte ich in VLP-Präparaten mehrerer hNoV-Varianten verschiedener Genotypen eine *N*-terminale Trunkierung. Die auffälligste nachgewiesene Spezies war  $T = 1$  oder VP1 60-mere, im Gegensatz zu den zuvor beschriebenen  $T = 3$  Partikeln. Das Vorhandensein dieser Spezies war genotypunabhängig und Messungen unter verschiedenen Lösungsbedingungen zeigten eine hohe Stabilität der Partikel selbst bei alkalischem pH-Wert. Obwohl in unserem Datensatz mehrere andere Assemblierungen von mittlerer Größe vorhanden waren, konnten größere Partikel durch Änderung der Lösungsbedingungen nicht reassembliert werden.

Zusammenfassend lässt sich festhalten, dass diese Arbeit einen enormen Beitrag zum Verständnis der Norovirus-Assemblierung sowie ein neuartiges Werkzeug zur Charakterisierung von VLPs darstellt. Des Weiteren wurden biophysikalische Eigenschaften verschiedener Norovirusvarianten untersucht und es wurden Einblicke in das Deassemblierungsverhalten und Stabilitätsmuster gewonnen. Der VP1 *N*-Terminus wurde als besonders wichtig für die Assemblierung identifiziert. Eine größere *N*-terminale Trunkierung in VP1 führt zur Bildung kleinerer Partikel. Daher ebnet diese Arbeit den Weg für künftige Studien, die insbesondere für die Entwicklung von Norovirus-Impfstoffen und die Entwicklung von Kapsiden von Bedeutung sind.



# 1. Introduction

---

---

## 1.1. Structural mass spectrometry

### 1.1.1. Characterization of molecular complexes

Bionanotechnological applications require extensive knowledge of the targeted biological system. This includes the ability to follow three-dimensional structures of respective molecular assemblies and their non-covalent interactions during protein-protein and protein-ligand interactions. Non-covalent interactions and conformational changes contribute to structural dynamics, which ultimately define a protein's function in its native environment. X-ray crystallography and cryo-electron microscopy (cryo-EM) represent the state of the art in structural biology studies (Adrian et al., 1984; Dubochet et al., 1988). X-ray crystallography provides information up to the atomic level, but proteins need to be crystallized before exposure to diffraction (Eckert, 2012; Perutz et al., 1960). Scattering techniques like small-angle X-ray scattering (SAXS) overcome the need for crystals as samples can be handled in solution or soft matter. Due to high sensitivity, structural difference on the nanoscopic scale can be followed (Khaykelson and Raviv, 2020; Li et al., 2016). For cryo-EM, samples are rapidly frozen and are then either imaged directly, or sequentially tilting the stage (cryo-electron tomography) (Adrian et al., 1984; Dubochet et al., 1988; Koster et al., 1997; Lučić et al., 2005). The individual selection of particles according to similar shape and size tolerates more sample heterogeneity. This includes more complex and flexible structures like (enveloped) viral particles, or particles bound to antibodies or receptor molecules. Therefore, following structural dynamics is generally possible. Nuclear magnetic resonance (NMR) spectroscopy allows measurements in solution or in solid state and provides great sensitivity. Saturation-transfer difference (STD) NMR can give great input on protein-ligand interaction (Mallagaray et al., 2015; Blaum et al., 2018; Creutzmacher et al., 2021). Furthermore, previously generated structural models of megadalton complexes were validated using solid state NMR in combination with *in vitro* and *in silico* data, implicating the general need for structural biology methods to target larger and larger complexes (Gauto et al., 2019; Kaplan et al., 2015; Lecoq et al., 2020). Taken together, the mentioned techniques hold great potential but come with their own limitations. Therefore, structural studies usually include integrative approaches by combining high-resolution data with lower resolution techniques like mass spectrometry (MS) (Liko et al., 2016; Dülfer et al., 2019). Structural MS includes amongst other techniques

## Introduction

hydrogen deuterium exchange (HDX), covalent cross-linking MS or native MS. Native MS, where non-covalent interactions are kept intact, is especially suited to complement structural methods in combination with fragmentation and dissociation, cross-linking or ion mobility (IM) applications. Furthermore, it has been proven beneficial for sample selection prior to cryo-EM imaging (Olinares et al., 2021). The soft electrospray mechanism has further been adopted for sample delivery for imaging techniques (Rauschenbach et al., 2016; Bielecki et al., 2019; Kadek et al., 2021; Esser et al., 2022; Westphall et al., 2022). In the following, I will focus on basic principles of structural mass spectrometry and their applications in characterizing high-mass molecular assemblies in detail.

### 1.1.2. Native mass spectrometry

#### 1.1.2.1. *Sample preparation and requirements*

Ideally, biophysical characterization of molecular assemblies is performed in native-like conditions. A physiological system is usually governed by pH, inorganic ions, and the presence of ligands, lipids and regulatory proteins. For structural biology in cellular context, *e.g.*, the cytoplasm, further factors like metabolites, genomic material, and membrane proteins have to be considered (Theillet, 2022). However, these demands clash tremendously with sample requirements in structural biology where highly purified material is needed. As a further complication, standard MS studies generally use denaturing components like organic solvents and acids for optimized resolution. Regarding structural studies however, protein quaternary structure, intra- and intermolecular interactions need to be kept intact during sample preparation, ionization and detection. Additionally, the analyte is ideally free from solvent and adducts, which interfere with proper mass resolution in native MS. A proper volatile surrogate to imitate a native-like setting is ammonium acetate (Kearle and Verkerk, 2009). Although not a buffer per definition, it can be employed in most common physiologically relevant pH values and the ionic strength can be adjusted over a broad range (Koneremann, 2017). For analyte integrity, low millimolar amounts of salt might be added. Further putative additives are supercharging agents like *m*-nitrobenzyl alcohol, sulfolane and propylene carbonate (Iavarone and Williams, 2003; Lomeli et al., 2009; Teo and Donald, 2014). For desalting, various exchange devices like size-exclusion membranes and dialysis systems can be used. Notably, different systems can yield different protein yields and sample purity (Wu et al., 2018; Zhang et al., 2018).

### 1.1.2.2. *Electrospray ionization of high-mass molecules*

Generally, a mass spectrometer consists of three parts, namely ionization of an analyte, a mass analyzer, where ions are separated according to mass to charge, and finally detection of the analyte. Electrospray ionization (ESI) describes the electrochemically driven transfer of an analyte like proteins or macromolecules into the gas phase to facilitate mass analysis after entering the ultra-high vacuum of a mass spectrometer. Through application of high voltage, either in positive or negative polarity, an aerosol is created as the analyte solution disperses (Van Berkel and Kertesz, 2007). Ionization of proteins is usually performed in positive ion mode where multiple protons are transferred (Van Berkel and Kertesz, 2007; Kebarle and Verkerk, 2009). Conventional ESI approaches use stainless steel capillaries with 100  $\mu\text{m}$  inner capillary diameter resulting in flow rates ranging from 1-10  $\mu\text{L}/\text{min}$  (Wilm and Mann, 1996). For native MS, the solution is transferred to nano ESI capillaries with inner diameters of a few  $\mu\text{m}$ , reducing the flow rate to  $< 20 \text{ nL}/\text{min}$  (Karas et al., 2000). Conductivity is provided through gold-coating or by inserting a platinum wire. Capillaries can be pulled manually or manufactured and used in automated systems. Generally, smaller sized emitters provide smaller initial droplets (Wilm and Mann, 1996). This is favorable as less analyte molecules in a droplet reduce nonspecific clustering, improve desolvation, and provide greater salt tolerance and higher ion yield (Benesch et al., 2007; Konermann et al., 2019; Panczyk et al., 2020). Optimization includes the use of smaller tip sizes even below 1  $\mu\text{m}$ , which however are accompanied by extensive clogging (Gibson et al., 2009; Susa et al., 2017; Kostelic et al., 2022a; Jordan et al., 2022).

Through application of high voltage, a Taylor cone is formed at the emitter tip and charged droplets are emitted (Wilm and Mann, 1994). Starting with approximately 200 nm droplets emanating from the Taylor cone, nanodroplets with increased charge densities are produced through evaporation (Juraschek et al., 1999). On a spherical droplet, the net number of charges  $z_D$  is limited to the so-called Rayleigh limit  $z_R$  defined as

#### Equation 1

$$z_R = \frac{8\pi}{e} \cdot (\varepsilon_0 \gamma r^3)^{1/2}$$

with elementary charge  $e$ , vacuum permittivity  $\varepsilon_0$ , and surface tension  $\gamma$ , and the droplet radius  $r$  (Rayleigh, 1882). With increased charge density on the droplet the Rayleigh limit is

## Introduction

approached ( $z_D/z_R = 1$ ). The droplet becomes electrochemically stressed and unstable until jet fission events are triggered as Coulombic repulsion dominates. Ultimately, analyte ions are released into the gas phase (Gomez and Tang, 1994; Cech and Enke, 2001; Kebarle and Verkerk, 2009; Wu et al., 2012; Konermann et al., 2013).

The release of gaseous proteins from a droplet has been subject to investigation for decades. It has benefitted immensely from molecular dynamics (MD) (McAllister et al., 2015; Metwally et al., 2018; Konermann et al., 2019; Aliyari and Konermann, 2020, 2022). Three models describe this process. For globular proteins, the charge residue model (CRM) is proposed (Dole et al., 1968). Here, the folded protein remains in the droplet interior, while water evaporates gradually as the droplet radius is reduced. Finally, the droplet is dried out completely through repeated evaporation events. Occasionally, low molecular weight ions are ejected from the droplet surface, keeping it at the Rayleigh limit. This process is described in the ion evaporation model (IEM) (Iribarne, 1976; Hogan et al., 2009; Allen et al., 2013). The model can further be applied to peptides and recent MD simulations indicate IEM clustering events during ionization of proteins (Nguyen and Fenn, 2007; Aliyari and Konermann, 2020, 2021). According to the chain ejection model (CEM), unfolded proteins are migrated to the droplet surface through exposed hydrophobic residues, where electrostatic repulsion then drives ejection out of the droplet (Konermann et al., 2013; Metwally et al., 2018). Compared to native ESI, protonation of the extended tail leads to higher charge states. Generally, ESI produces multiply charged ions in contrast to other ionization techniques like Matrix-assisted laser desorption (MALDI). Here, ionization usually yields singly charged, small ions and hence mass and  $m/z$  are identical. Following native ESI, the charge envelope of an analyte results characteristic peak series with adjacent, integer charge states. Assuming that all charges are due to protonation, the charge and subsequently the molecular mass  $M$  can be assigned from this series with  $m/z$  and  $m/z+1$  (Covey et al., 1988; Mann et al., 1989).

### **1.1.2.3. Ion selection, dissociation and fragmentation**

In many setups, a quadrupole is used to direct ions through the mass spectrometer. On a set of four parallel rods, a static voltage is applied to one opposing set of rods and a radiofrequency (RF) voltage is applied to the other pair, respectively. The ions are directed along a helical trajectory by continual oscillation of the RF voltages. Only ions with the proper  $m/z$  range can sustain this trajectory and pass through the quadrupole (Paul, 1990; Chernushevich et al., 2001). Radiofrequency and static voltage magnitudes are varied in transmission mode and ions with

various  $m/z$  can pass successively. To allow mass filtering, the voltages are not varied. This allows selection of the precursor ion, which can be further dissociated or fragmented using different fragmentation techniques.

In collision induced dissociation (CID), the kinetic energy of an ion is partially converted to vibrational energy upon collision with an inert gas (Benesch, 2009). The acceleration voltage and the number of charges of the ion determine the velocity of the ion and hence the energy of the collisions. Small or exposed proteins are dissociated first from the multiprotein complex, whereas large protein complexes disintegrate into sub-complexes. While the overall charge remains the same, small dissociated complexes take a disproportionately high proportion of the protons along (Jurchen and Williams, 2003; Benesch, 2009). Additionally, extra buffer or detergent molecules may be removed during this process (Smith et al., 1990). Furthermore, ion fragmentation can result from fragmentation of the protein backbone. The resultant fragments in peptide bond fragmentation are typically b- and y-ions (Roepstorff and Fohlman, 1984).

#### **1.1.2.4. High-mass QToF modifications**

Quadrupoles are often used in combination with time-of-flight analyzers (ToF, QToF). In a ToF analyzer, ions are accelerated and further pulsed by the pusher. The  $m/z$  of an ion determines the travel time through the analyzer tube and is identified by the detector. In order to study high mass protein complexes, several modifications were introduced to QToF instruments in 2006 (van den Heuvel et al., 2006). A metal cylinder was introduced around the first half of the hexapole ion lens. This allowed increased pressure resulting in collisional cooling (Chernushevich and Thomson, 2004). To transmit ions of higher  $m/z$  than standard quadrupoles, the radio frequency generator was set to lower frequencies (Sobott et al., 2002). In addition, collisional cooling and focusing of ions was further improved by increasing the pressure in the second vacuum chamber. Later, xenon was implemented as collision gas and higher pressure in the collision chamber were introduced (Lorenzen et al., 2007). Further multicomponent ion lenses before the ToF were modified. Despite lowering sensitivity, a decrease of the ToF repetition rate was introduced to allow measurements of high mass  $m/z$  (van den Heuvel et al., 2006)

### 1.1.2.5. *High-masses and high resolution*

Limitations regarding resolution in native mass spectrometry have been subject for discussion in the past. There have been remarkable instrumentation developments in the recent years. It is worthwhile to take a look at basic principles and definitions, especially regarding native high mass measurements. The International Union of Pure and Applied Chemistry (IUPAC) defines mass resolution as  $m/\Delta m$  (McNaught et al., 1997). In line with IUPAC,  $m$  is often the mass to charge ratio of a singly charged ion and  $\Delta m$  can be determined as the peak width at 50% of its height or full width half-maximum (FWHM) (Guilhaus et al., 2000; Makarov et al., 2006). Generally, FWHM is used in mass spectrometry to describe  $\Delta m$  (Murray et al., 2013). The term resolving power describes the capability to distinguish between two peaks and is defined as the peak width,  $\Delta m$  (Murray et al., 2013). In native MS, FWHM can be applied to both terms, in line with IUPAC terminology recommendations for mass spectrometrists, with mass resolving power specifically referring to mass analyzer performance (Murray et al., 2013; Tamara et al., 2022). Other means to describe instrument performance are mass accuracy, detection sensitivity, capability to perform tandem MS and upper mass limits. Mass accuracy is the mass error or fraction of the theoretical mass and given in parts per million (Gross, 1994). Isotopic resolution can be achieved for small molecules at so-called ultrahigh resolution above  $10^6$  at  $m/z = m/z$ . Th *e.g.*, with Fourier-transform ion cyclotron resonance (FT ICR) and Orbitrap MS. Hence, masses resolved to sub-ppm or ppb accuracy give detailed information on exact chemical formulas or posttranslational modifications (PTMs). The ionization process can affect the mass accuracy of the measurement tremendously, especially for high-mass particles. Major limiting factor for ionization is the instrument capability to completely desolvate the analyte (Lössl et al., 2014; Joost Snijder et al., 2013). Next to  $H^+$ , particularly salt cations like  $Na^+$  or  $K^+$  attach and contribute to signal broadening. With increased mass, incomplete desolvation leads to an overlap of various species as simulations of a 150 kDa protein demonstrate. The isotopically resolved spectra overlap and superimpose as shown in **Figure 1**, resulting in a non-gaussian shaped peak (Lössl et al., 2014). Simulated peak widths at different mass resolutions are generally narrower compared to experimental peak widths (Lössl et al., 2014). With increased analyte mass, small mass differences like PTMs are generally hard to follow as the peak width of the isotopic distribution gets narrower. For protein measurements, it is therefore beneficial to rather record average mass of a distribution. Increased microheterogeneity, for example through processing of protein building blocks of subcomplexes, can further prevent charge state resolution. In this case, experimental masses can be estimated using the Rayleigh

limit (**Equation 1**) to define the theoretically maximum charge (Rayleigh, 1882; Loo, 2000; Felitsyn et al., 2002). Following the assumption that the ion is spherical and has the same density as water, the charge limit, or theoretical charge is defined as

### Equation 2

$$z_R = 0.0778 \cdot \sqrt{M}$$

with protein mass  $M$  in Dalton. The validation of this equation has been subject to several studies covering a broad mass range up to 4 MDa, (Heck and van den Heuvel, 2004; Lorenzen et al., 2008; Shoemaker et al., 2010).

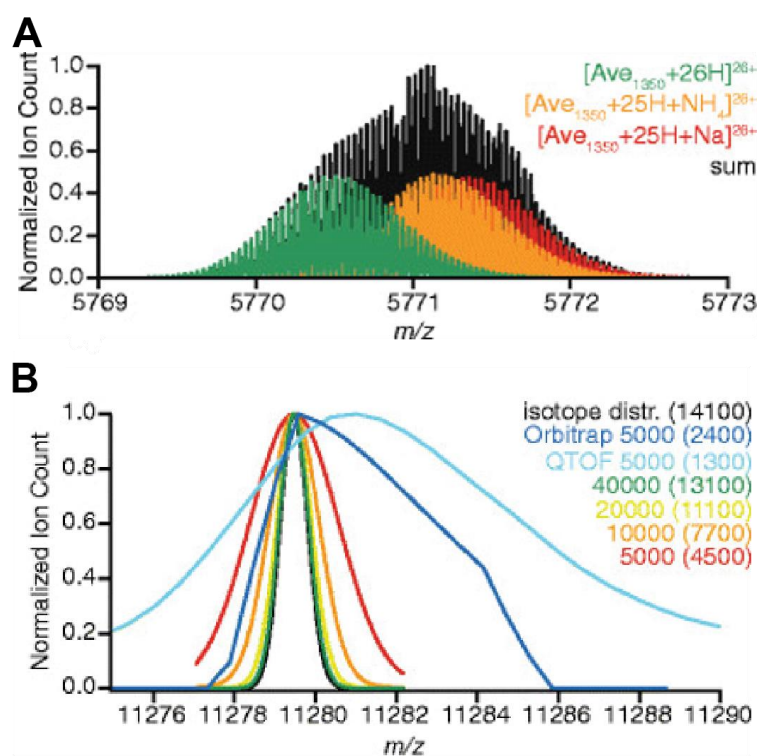


**Figure 1 Limiting factors in high-mass native MS.** **A.** Shown are isotope distributions at assumed baseline resolution ( $R = 500,000$ ) of a bare (green), and ammonium-(orange), sodium- (red) bound 150 kDa protein for the most abundant charge state 26+, respectively. Simulated distributions are shown individually colored and summed up as the final mass spectrum (black). **B.** Experimental peak width exceeds simulated peaks of globular protein complexes. Mass spectra of GroEL 71+ ions are shown measured on an Orbitrap Exactive Plus (blue) and a QToF (cyan) instrument at instrument resolution of 5000. Simulated peaks at mass resolutions 5000 (red), 10000 (orange), 40000 (green) are shown as well as the natural isotope envelope of GroEL (black). Apparent mass resolutions  $R_{nat}$  are given in parentheses, respectively. All simulations were performed with MassLynx ver. 4.1. Reprinted and adapted with permission from (Lössl et al., 2014). Copyright 2014 American Chemical Society

### 1.1.3. Charge-detection based instruments

The beforementioned methods demand deconvolution of  $m/z$  to charge state and subsequently mass from a coherent series of charge states. Generally, mass assignment for proteins and protein complexes becomes more challenging with increased mass in standard native MS as outlined above. While resolution in QToF instruments is comparably low and therefore large assemblies are often assigned mathematically through correlation (see section High-masses and high resolution), a broad overview of size populations can be given as a broad  $m/z$  range is covered. Orbitrap-based instruments have also been optimized for transmission of large assemblies and allowed the measurement of an intact virus (van de Waterbeemd et al., 2016). Resolution however even on high-mass orbitraps is limited by analyte desolvation (**Figure 1**) (Lössl et al., 2014). To overcome the need for deconvolution,  $m/z$  and charge state are measured for the same ion in techniques generally summarized under the term charge-detection MS. For Orbitrap instruments this has been demonstrated recently based on the linear scaling of charge and peak intensity (Kafader et al., 2020; Makarov, 2000; Wörner et al., 2020). However, this requires instrument as well as software modifications, which have been commercialized just recently.

#### 1.1.3.1. *Charge detection mass spectrometry*

Originally developed for mass and velocity assignment of micron-sized metal particles, CDMS was later combined with electrospray, soon allowing measurements of intact viral particles (Fuerstenau and Benner, 1995; Fuerstenau et al., 2001). Following ionization, ions enter the differentially pumped region with a RF hexapole, a RF quadrupole and finally a dual hemispherical deflection energy analyzer. Here, only ions with a narrow band of ion kinetic energies are focused into the following detection cylinder, where an entering ion induces a charge (Benner, 1997). If the energy is known and the cylinder is long enough, the charge can be determined through a charge-sensitive amplifier. Furthermore, the flight-time of the ion through the cylinder gives information on the  $m/z$  ratio (Shockley, 1938; Weinheimer, 1988). Initially, CDMS was restricted to highly charged ions. Starting from a detection limit of a minimum 425  $e$ , constant improvements now allow measurements for even singly charged ions (Todd et al., 2020). Electrical noise is the limiting factor for the accuracy of the charge measurement and therefore mass accuracy. Partial cryogenically cooling of the charge amplifier, using dynamic energy calculations to compensate for collision-induced effects, and signal-averaging can help to diminish electrical noise (Contino et al., 2013; Harper et al., 2018).

Instead of single pass charge detection, ions can be passed through a series of detectors on a linear array, or the detection tube can be implemented into an electrostatic linear ion trap (ELIT). Generally, measurement time increases drastically from single pass, linear array to ion-trap based approaches (Jarrold, 2022). In ion trap CDMS, two end-caps of the ELIT allow transmission or trapping through changing the end-cap potential (Schmidt et al., 2001; Contino and Jarrold, 2013). Through oscillation of the ion back and forth through the tube, charge accuracy is improved proportionally with prolonged trapping time (Benner, 1997; Contino and Jarrold, 2013; Keifer et al., 2015; Pierson et al., 2015). The charge sensitive amplifier detects the periodic signal of trapped ions and the time-domain signals are analyzed in real time using Fourier transforms. While the fast Fourier transform (FFT) magnitude provides information of the charge, the oscillation frequency can be used to determine the  $m/z$  ratio (Contino and Jarrold, 2013). In the prototype CDMS instrument as it was used in this work two trapping modii were possible. In triggered trapping, switching of the end-caps to trapping is induced by an ion entering the detection cylinder at a certain noise threshold. In comparison to continuous trapping, where the trap might be closed without entering of an ion, triggered trapping allows for high sensitivity. However, the limit of detection is rather high with approx. 250  $e$ . Therefore, recent developments focus on optimizing the continuous trapping mode through accumulation of ions before entering the trap and modifications of the charge sensitive amplifier. This allows the detection of single, singly charged ions and highly heterogeneous samples (Todd et al., 2020; Todd and Jarrold, 2020). To further reduce electrical noise, a recent study implemented dynamic calibration using a 129 kHz reference signal superimposed on the ion signal (Todd and Jarrold, 2020). Other improvements include optimizing of the ELIT design by using multielectrode end-caps, which reduces trapping time (Hogan and Jarrold, 2018). Furthermore, the implementation of ion funnel-ion carpet hybrid or FUNPET in the first vacuum stage of the instrument enhances desolvation through thermalization of high mass ions (Draper et al., 2018). Approaches to optimize triggered trapping were done by Williams and coworkers, focusing on trapping multiple ions, which bypasses the omnipresent challenging duration of measurement time (Harper et al., 2019; Harper and Williams, 2019). In a further instrumentation setup by Antoine and coworkers, trapping singular ions in an ELIT is combined with irradiation with a CO<sub>2</sub> laser (Antoine, 2020; Doussineau et al., 2011).

### 1.1.4. Gas phase electrophoretic mobility analysis

Ion mobility spectrometry (IMS) adds the shape of molecular complexes as an additional parameter on which an analyte can be characterized. Ions are separated based on their charge and mobility in an air- or gas-filled electric field. Nowadays, IMS is combined with mass spectrometry, putting the ion mobility tube in front of the detector, so ions are separated according to their shape prior to charge (Utrecht et al., 2010).

Furthermore, this principle can also be used for mass approximation in a basic setup termed gas phase electrophoretic mobility analysis (GEMMA) shown in **Figure 2**, by correlating protein mass and shape or gas phase electrophoretic mobility diameter (EMD). Generally, GEMMA results low mass resolution and can be applied to micrometer-sized analytes. The combination of the differential mobility analyzer (DMA) with electrospray to characterize globular proteins was first described by Kaufmann and colleagues (Knutson and Whitby, 1975; Kaufman et al., 1998). In contrast to standard MS approaches, electrospray ionization is followed by charge reduction, which results mainly neutral ions and a small subpopulation of singly (1%) and multiply charged ions (Fuchs, 1963; Reischl et al., 1996). Furthermore, measurements are performed at atmospheric pressure. Charge reduction can be achieved through controlled contact or thermal collision with ions of positive and negative polarity (Fuchs, 1963; Adachi et al., 1983; Wiedensohler and Fissan, 1988). A radioactive source like  $^{241}\text{Am}$  or  $^{210}\text{Po}$ , a soft X-ray charger or recently also an alternating current corona discharge unit can be used to generate the bipolar atmosphere (Adachi et al., 1983; Shimada et al., 2002; Qi and Kulkarni, 2013; Kallinger and Szymanski, 2015; Weiss et al., 2020b). Using a sheath flow of compressed air and  $\text{CO}_2$ , nanodroplets are dried and carried through different parts of the instrument. In the next unit, the analyte is separated in a tunable electrical field orthogonal to the laminar air flow. Through variation of the electric field, the analytes are deviated from their trajectory and can finally be separated by passing a focused laser beam or ultrafine condensation particle counter. Subsequently, the directly measured electric mobility in air is converted to particle diameter, or electrophoretic mobility diameter using solutions of the Millikan equation (Annis et al., 1972; Tammet, 1995). For consecutive mass estimation, different mass-EMD correlation equations can be used depending on the analyte class. Extensive work using GEMMA has been done on analytes of a wide-spanned size ranging from organic and inorganic compounds, to proteins, liposomes, lipid-based nanoparticles, and intact viruses (Bacher et al., 2001; Bereszczyk et al.,

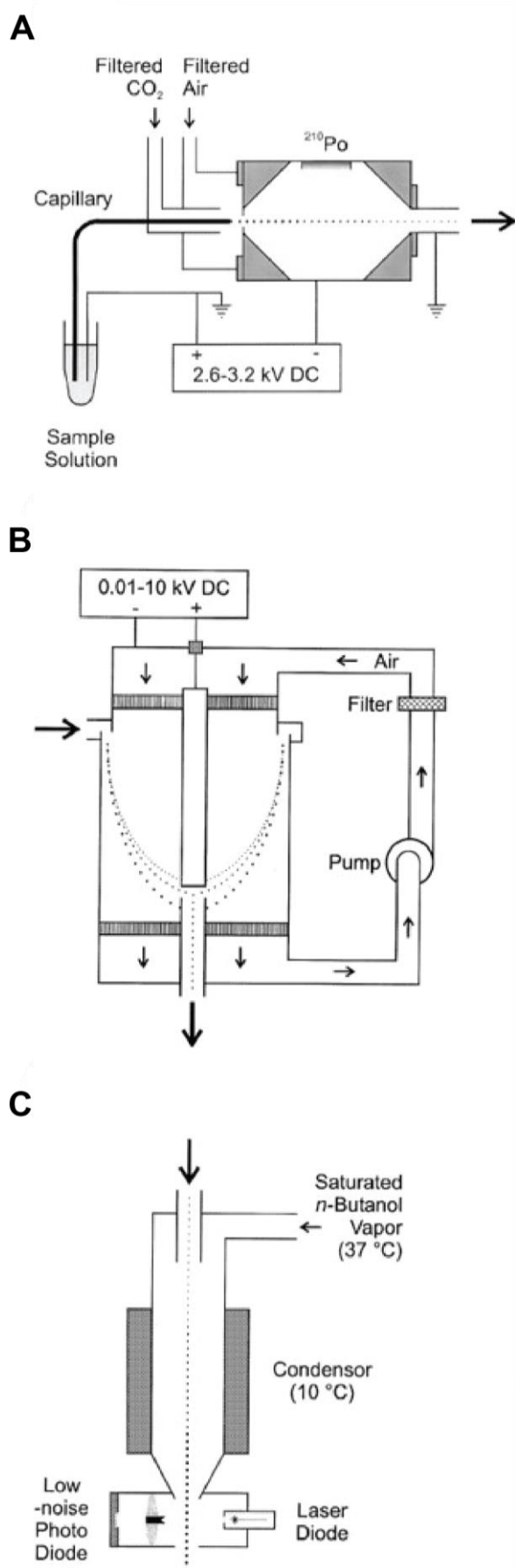


**Figure 2: Instrumentation setup of a GEMMA system.** **A.** Nano ESI spray and charge-reducing chamber, **B.** nano DMA, **C.** condensation particle counter Reprinted from (Bacher et al., 2001), Copyright © 2001 with permission from John Wiley & Sons, Ltd

2014; Bianco et al., 2022; Weiss et al., 2020a, 2015a). Mw/EMD correlations however, have only been established for three analyte classes, namely proteins, polysaccharides and intact viruses (Bacher et al., 2001; Weiss et al., 2015b, 2018, 2020b). Recent instrumentation modifications aim to improve the charge equilibration setup, or the DMA instrumentation for example by tuning resolving power (Fernández-García et al., 2019; Weiss et al., 2020b). Another notable application of the GEMMA setup is size-selection to allow consecutive further analysis. Here, an electrostatic nanoparticle sampler replaces the particle counter. Subsequent applications include the combination with electron-microscopy or atomic force microscopy by landing particles directly on respective substrates. Furthermore, spectroscopic techniques and antibody-based immunological assays were applied (Havlik et al., 2015; Engel et al., 2017). The GEMMA setup was also aligned with size-exclusion chromatography in order to separate analytes prior to ionization (Weiss et al., 2021). Additionally, the differential mobility cell has been applied for analyte-separation prior to

## Introduction

proteomic analysis (Wernisch and Pennathur, 2019).

### 1.2. Norovirus Assembly and Stability

Parts of the Norovirus Assembly and Stability introduction have been published in the following review:

Pogan, R., Dülfer, J., & Uetrecht, C. (2018). Norovirus assembly and stability. *Current opinion in virology*, 31, 59-65. Reprinted (Pogan et al., 2018a) under CC BY 4.0 license. <https://creativecommons.org/licenses/by/4.0/>

To access the publication, see:

DOI: [10.1016/j.coviro.2018.05.003](https://doi.org/10.1016/j.coviro.2018.05.003)

#### 1.2.1. Virus assembly

Virus assembly generally is thought to follow the principle of genetic economy, which ultimately defines how capsids are designed limited through geometric constraints (Crick and Watson 1956, Twarock and Luque 2018). The capsid forms a shell around the genome and can be covered by a lipid membrane originated from the host cells. In non-enveloped viruses, icosahedral capsids are most common. According to Caspar and Klug, multiples of 60 proteins define icosahedral symmetry (Caspar and Klug, 1962). The individual proteins adopt slightly different, or quasi-equivalent, conformations and form morphological units, typically pentamers or hexamers. Exactly 12 pentamers are needed for icosahedral symmetry. Therefore,  $60T$  subunits form a complete capsid, where  $T$  is the triangulation number, or the number of different subunit conformations. Within geometrical reasoning, the allowed  $T$  values are limited to  $T = h^2 + hk + k^2$ , where  $h$  and  $k$  are positive integers (Caspar and Klug, 1962).

#### 1.2.2. Human norovirus

Approximately one-fifth of all acute gastroenteritis outbreaks are caused by human noroviruses (hNoV) (Ahmed et al., 2014). Acute gastroenteritis involves fever, vomiting, cramping and diarrhea (Kapikian et al., 1972). This illness usually persists for several days only but can take longer in children, the elderly and immunocompromised (Lindsay et al., 2015). The prototypical

Norwalk virus was discovered over four decades ago (Kapikian et al., 1972). So far, no vaccines are available and several candidates failed clinical trials (Cates et al., 2020).

Outbreak causing noroviruses emerge frequently and are seasonal especially in temperate regions (Ahmed et al., 2013). The dynamics of this diversity are poorly understood. Contributing factors like population immunity, virus evolution and transmission are mainly followed by epidemiological observations as a robust infection model is still missing. Since the virus is mostly foodborne and has to persist on surfaces and in the environment, particle stability is of interest.

### 1.2.2.1. Genetic diversity

The genus *Norovirus* belongs to the *Caliciviridae* family, which can be divided into ten genera, depicted in **Figure 3** (Chhabra et al., 2019). Noroviruses infecting humans can be found in genogroup I, II, IV, VIII and IX, while murine noroviruses (MNV) are GV and bovine GIII noroviruses (Vinjé, 2015; Chhabra et al., 2019). Genogroups are subdivided into genotypes based on VP1 sequence, differing by at least 43% (Zheng et al., 2006). However, recombination and mutations in both the viral polymerase and the capsid protein VP1 happen frequently. To include both genome regions as nomenclature parameters, P indicates polymerase genotypes (*e.g.*, GII.P4 and GII.4). Thus, recombinant forms can be captured (Hansman et al., 2006; Kroneman et al., 2013; de Graaf et al., 2016, 2017).

Noroviruses of distinct prevalence emerge frequently and surveillance networks like NoroNet help to capture trends of respective genogroups and genotypes (Koopmans et al., 2003). While GI, which also includes the prototype Norwalk virus, is less frequently found nowadays, GII.4 isolates have been known as the most common cause of clinical gastroenteritis cases (Eden et al., 2013; Parra et al., 2023). Surveillance studies also imply that GII.17 variants increase in prevalence (de Graaf et al., 2015). Interestingly, genogroup and transmission route correlate: GII.4 strain transmission was often found to be person-to-person dependent; non GII.4 viruses like several GI isolates, GII.6 and GII.12 were mostly foodborne; and other GI isolates waterborne (de Graaf et al., 2016). These dependencies may be due in part to specific stability patterns of particular isolates.

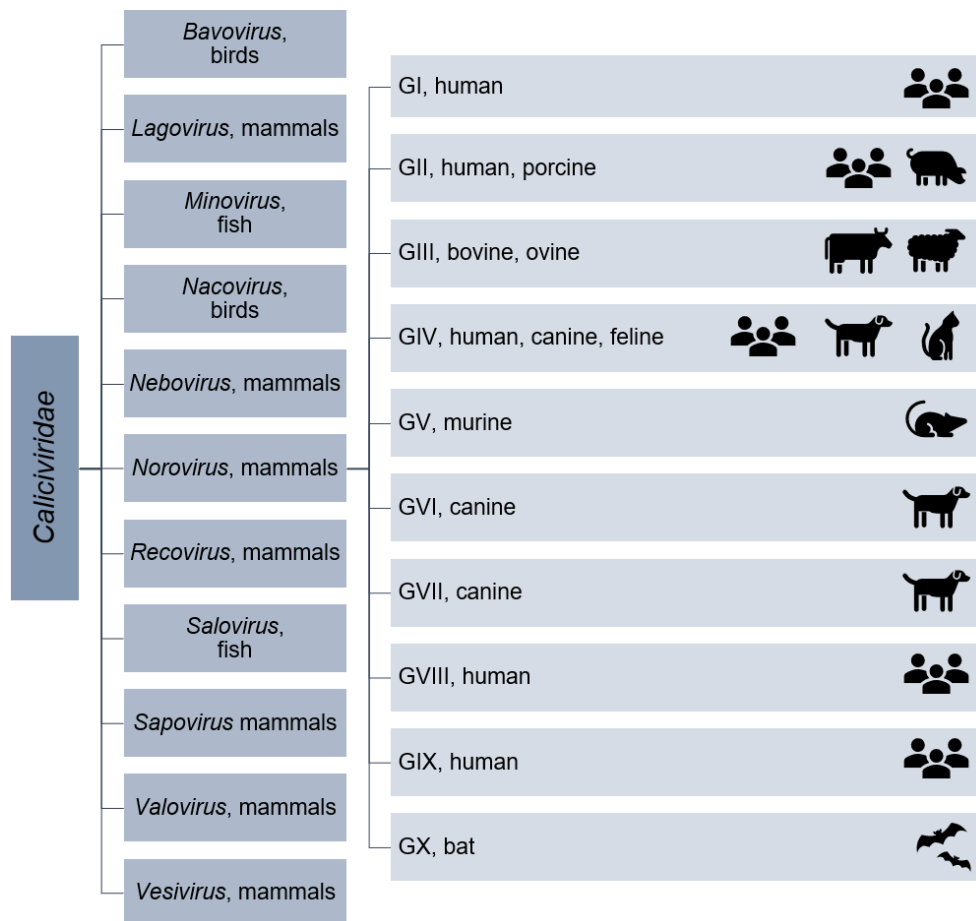


**Figure 3: Schematic diagram of caliciviridae.** The calicivirus family is divided into 11 genera according to (Vinjé et al., 2019). The genus norovirus can be divided into ten genogroups (GI-GX) (Chhabra et al., 2019). Species found within respective groups are also shown.

### 1.2.2.2. *Norovirus virions*

Many NoV mediated gastroenteritis outbreaks originate in the consumption of fecal-contaminated food like mussels, oysters, berries and vegetables (Zainazor et al., 2010). Hence, these enteric pathogenic agents have to persist on various surfaces and in harsh environments. Studies on intact human noroviruses are hampered as no robust cell culture system has been available. hNVoVs are known not to grow in routine cell lines like like Caco-2 or Vero cells (Duizer et al., 2004; Pohl et al., 2022). Replication in B cell lines like BJAB and Raji B cells was shown to be dependent on human blood group antigens (HBGA) (Jones et al., 2014). However, cultivation efforts lack reproducibility (Jones et al., 2015, 2014). Cultivation in monolayer enteroids has been established previously (Ettayebi et al., 2016). The three-dimensional (3D) human intestinal enteroid (HIE) is derived from biopsies and contains several intestinal cell types like enterocytes and others (Ettayebi et al., 2016). Replication of hNoVs is species-specific and dependent on the addition of bile acid, growth factors and other

components (Ettayebi et al., 2016; Costantini et al., 2018; Ettayebi et al., 2021). HIE protocols were further modified and optimized in terms of culture media and virus titer of stool samples (Ettayebi et al., 2021). However, this could not overcome that enteroid systems are costly, time- and labor intensive. Recent efforts therefore aim to adapt these protocols by omitting the differentiation of 3D to 2D monolayers (Mirabelli et al., 2022). Although even more advanced, hNoV were shown to grown in several animal models, amongst others the recently developed zebrafish larvae model (Van Dycke et al., 2021). However, next to their physiological distance to human intestines, they do further not overcome common negative aspects to all approaches, mainly insufficient replication levels, especially to gain decent amounts of viral stock for structural studies. All cell types mentioned derive from the assumption that hNoVs solely replicate in the intestine. Salivary glands have been identified as a further transmission route for enteric viruses. Indeed, hNoVs were shown to replicate in salivary cell lines in comparable numbers to enteroid systems (Ghosh et al., 2022). However, for infectivity assays on virions reliable cultivation systems are inevitable and thus studies focus on norovirus surrogates. Proposed norovirus surrogates are amongst others feline calicivirus (FCV), which belongs to the genus *Vesivirus*, and the *Lagovirus* Rabbit haemorrhagic disease virus (Conley and Bhella, 2019; Katpally et al., 2010).

Due to its transmission by the respiratory route and its general pH instability, FCV is considered less suitable (Cannon et al., 2006; Fallahi and Mattison, 2011). MNV is often used as a surrogate because it shares many genetic and biochemical features with human norovirus and can infect cells in culture as well as replicate in the gastrointestinal tract of its host (Wobus et al., 2004). However, human and murine noroviruses have different cell specificities (Wobus et al., 2006). MNV is more stable than FCV regarding thermal resistance and acid tolerance (Bozkurt et al., 2013; Cannon et al., 2006). Nevertheless, these norovirus surrogates are considered suboptimal due to structural variations within human noroviruses (Donaldson et al., 2010).

### **1.2.2.3. Studying norovirus stability using virus-like particles**

To overcome the limitations of a lacking cultivation system, hNoV studies focus on virus-like particles (VLPs). The Calicivirus capsid is icosahedral and comprises 180 copies of the capsid protein VP1. Expression of VP1 in insect cells leads to self-assembly of VLPs of approximately 36-42 nm in diameter that are morphologically and antigenically comparable to native virions (Jiang et al., 1992). X-ray crystallography of GI.1 Norwalk  $T = 3$  VLPs revealed the division

## Introduction

of the capsid protein into a protruding (P) domain and a shell (S) domain (**Figure 4**) (Prasad et al., 1994, 1999).

The P domain is further divided into P1 and P2 subdomains. Subdomain P2 is highly variable and, as it is exposed to the surface, involved in determination of antigenicity and cell attachment (Prasad et al., 1994, 1999).

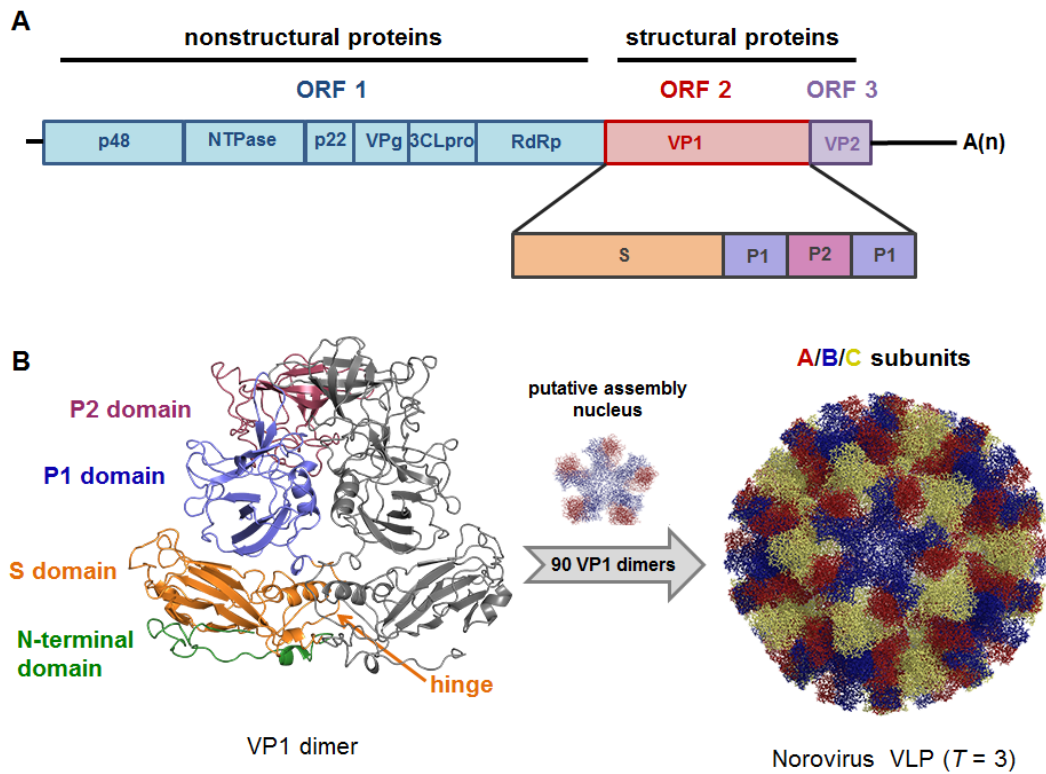


**Figure 4: Genomic organization and structure of human noroviruses.** **A.** Noroviruses are non-enveloped RNA viruses with a positive sense single-stranded genome with three open reading frames (ORFs). A polyprotein, which includes the nonstructural proteins such as the ribonucleic acid (RNA) dependent polymerase, is encoded by ORF1. Two structural proteins, the major and minor capsid protein (VP1 and VP2), are encoded by ORF2 and ORF3, respectively (Jiang et al., 1992, 1990). The VP1 protein is divided into shell (S) and protruding (P) domains. **B.** 90 dimers of the major capsid protein VP1 assemble into icosahedral  $T = 3$  norovirus VLPs. The S domain of the VP1 monomers builds a shell that surrounds the viral RNA in form of a scaffold. The more flexible P-domain is subdivided into P1 and P2 and connected to S via a hinge (Baclayon et al., 2011; Mallagaray et al., 2015; Prasad et al., 1994, 1999). The domains are highlighted in the VP1 dimer structure (left) and the three quasi-equivalent subunits (A/B/C) forming the capsids are shown in the VLP structure (right). PDB accession number 1IHM (Prasad 1999). Reprinted from (Pogan et al., 2018a) under CC BY 4.0 license.

The capsid protein adopts three quasi-equivalent structures, namely A, B and C. The S domain of A/B and C/C dimers is arranged bent and flat, respectively. Switching between A/B and C/C dimers of the S domain is necessary to facilitate curvature whereas P domains build the capsid protrusions. Icosahedral contacts between VP1 dimers are modulated by the S domain, while

intra-dimer contacts are modulated by the P domain (Prasad et al., 1999). The deletion of amino acids in the P domain that are thought to be involved in these contacts leads to heterogeneous particles with increased size (Bertolotti-Ciarlet et al., 2002). Moreover, particles can be formed by assembly of the S domain only showing that the S domain interactions are sufficient for capsid formation (Bertolotti-Ciarlet et al., 2003, 2002). Deletion of the P domain results in smaller, smooth particles ( $T = 3$ , 29 nm) with reduced stiffness compared to wildtype particles indicating that the P domain stabilizes the viral particles (Baclayon et al., 2011). The GI.1  $T = 3$  conformation for VLPs and native virions was confirmed both using X-ray crystallography and cryo-EM on several other variants including GI.7, GII.2, GII.3, GII.10, and GII.17 (Hansman et al., 2012; Jung et al., 2019). Cryo-EM data on GII.4 variants, namely CHDC-1974, NSW-2012 Sydney, GII.4c and Minerva, first revealed assemblies of 240 VP1 with  $T = 4$  icosahedral conformation. Negative stain micrographs of GII.4 virions however could not confirm this organization in stool samples as particles with comparable sizes to  $T = 3$  formation (40 nm) were purified (Devant et al., 2019). For VLPs, observed particle sizes were independent of the expression system and the co-expression of VP2 (Devant and Hansman, 2021; Jung et al., 2019). Notably, both in GII.2 Snow Mountain virus and the vaccine candidate GII.4c several size populations were observed. While the GII.2 variant showed both  $T = 3$  and  $T = 1$  particles, GII.4 NSW-2012 showed  $T = 4$  and  $T = 3$ , and GII.4c  $T = 4$ ,  $T = 3$  and  $T = 1$  particles. In contrast to those findings, a recent study on GII.4 Houston 2002 identified solely  $T = 3$  assemblies, noticeably without imposing icosahedral symmetry (Hu et al., 2022). In  $T = 4$  GII.4 VLPs, the P domain was lifted from the shell domain, a conformation which is generally referred to as ‘rising’ conformation and previously identified in GV MNV. In contrast to that, the P domain was ‘resting’ on the shell domain for some  $T = 3$  particles observed in other studies (Hansman et al., 2012; Devant et al., 2019). Hu and colleagues confirmed both VP1 states in GII.4  $T = 3$  particles (Hu et al., 2022). A conformational change in the hinge induces the switch from resting to rising state of VP1. The capsid diameter increases after removing the bound metal ion by chelation (Hu et al., 2022). Switching between those two states was first identified in GV MNV particles and can be induced by addition of bile acids and pH changes. However, further factors putatively are involved, as another study found VLPs in the resting state independent of presence of bile (Snowden et al., 2020). The resting state allows proper binding to the protein receptor CD300lf in MNV and simultaneously is thought to promote immune evasion through decreased recognition of antibodies. Limited access of antibodies to the resting conformation could also be confirmed for GII.4  $T = 3$  particles (Hu et al., 2022).

Notably, both the HBGA binding site is accessible in both conformations in GII.4  $T = 3$  particles (Hu et al., 2022).

### **1.2.2.4. *Limitations of VP1 VLP studies***

Recombinant norovirus particles are assembled in absence of genome and therefore lack putative RNA-capsid interactions, which could alter capsid stability. These interactions have been shown to play important roles in assembly and stability of other RNA viruses (Dykeman et al., 2013; J. Snijder et al., 2013). Another factor likely contributing to capsid stability and assembly behavior is the presence of the minor capsid protein VP2 (Glass et al., 2000). Although the function of VP2 could not be deciphered completely, comparison of a GII NoV VP1 only and VP1/VP2 particles indicate a slight stabilizing influence under alkaline conditions (Lin et al., 2014). Additionally, VP1/VP2 particles showed decreased protease degradation (Bertolotti-Ciarlet et al., 2003). The amount of incorporated VP2 molecules is still unknown. The protein putatively interacts with the VP1 S-domain and is located in the capsid interior (Vongpunsawad et al., 2013). In FCV, VP2 was shown to be essential for virus entry. Here, VP2 twelve copies form a portal to putatively release genome upon binding of the receptor, the junctional adhesion molecule JAM-A (Conley et al., 2019). Notably, in the P2 domain of VP1 electron densities indicating the presence of metal ions, most likely potassium, were identified and putatively are essential to allow entry (Lu et al., 2018; Conley et al., 2019).

### **1.2.2.5. *Norwalk stability and capsid assembly***

Several studies focus on the effect of pH, temperature and solution additives on capsid stability using various biophysical techniques. GI.1 Norwalk capsids were stable at neutral and acidic pH, whereas disassembly was observed above pH 8 (Ausar et al., 2006; da Silva et al., 2011). Particles remain intact up to 55°C. Above this temperature VLPs start to form aggregates or disintegrate into soluble VP1 oligomers in a pH dependent manner (Ausar et al., 2006). Notably, Norwalk VLP stability was monitored in buffer containing citrate, which can alter capsid morphology as shown for a GII.10 variant (Koromyslova et al., 2015). It would be of interest to disentangle the structural and pH effects of citrate in more detail. Aggregation was prevented by adding various common vaccine-excipients (Kissmann et al., 2008). Nanobodies targeting the P domain have also been shown to influence particle stability and promote disassembly (Koromyslova and Hansman, 2015).

Norwalk capsid disassembly was also followed in detail using native mass spectrometry (MS) (Shoemaker et al., 2010; Utrecht et al., 2011). In line with other studies, complete  $T = 3$  capsids (VP1 180mer) were present at physiological pH (Ausar et al., 2006). At alkaline pH disassembly into different intermediates could be observed with VP1 60mer and VP1 80mer being the most abundant species at high ionic strength (**Figure 5**).

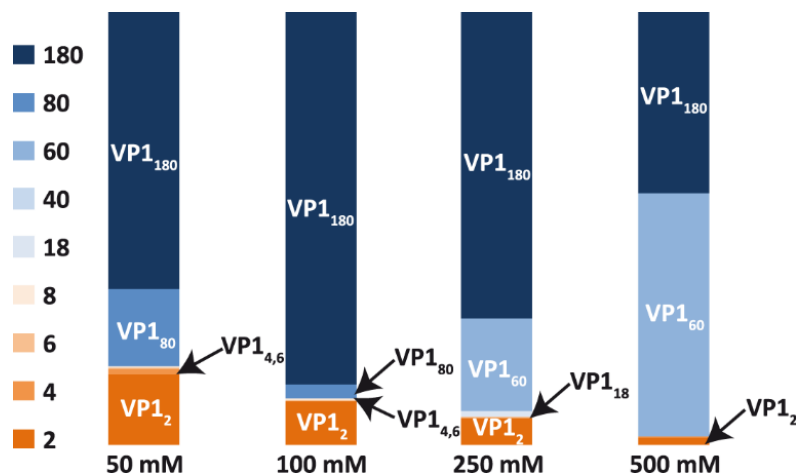


**Figure 5: Effect of ionic strength on assembly of VP1 oligomers at pH 8.** Assembly was monitored by native MS at pH 8 and a range of ammonium acetate concentrations (50–500 mM). This figure was adapted from the originally published in *Molecular & Cellular Proteomics* (Shoemaker et al., 2010) © the American Society for Biochemistry and Molecular Biology or © the Author(s) distributed under the terms of the Creative Commons CC-BY license.

Atomic force microscopy (AFM) images confirmed the presence and spherical morphology of the  $T = 1$  VP1 60mer (Shoemaker et al., 2010). The VP1 60mer was already observed at neutral pH. Smaller particles of  $T = 1$  formation were also found in Norwalk VLP preparations, although in low abundance (White et al., 1997). Further studies on GII variants, also forming these smaller particles, proposed VP1 truncation and variable purification conditions as putative reasons (Huo et al., 2015; Someya et al., 2011). Furthermore, the morphology of the VP1 80mer was probed using native ion mobility MS (IMMS). As the determined collisional cross sections of the VP1 180mer, 80mer and the 60mer increased linearly with mass, a spherical shape was also proposed for the VP1 80mer. The observed oligomers could also be reassembled into the  $T = 3$  native capsids. Further IMMS studies in alkaline, assembly and non-assembly conditions revealed a sheet-like structure of smaller oligomers (Utrecht et al., 2011). The hexamer structure was in line with a partial pentameric vertex. Hence, an assembly pathway starting with a decameric nucleus as predicted previously comprising a fivefold symmetry axis and proceeding via dimer addition was proposed (Prasad et al., 1999; Utrecht et al., 2011). An *in*

## Introduction

*silico* AFM study confirmed this finding, as it could be shown that the interface building a quasi-sixfold symmetry axis (B/C of S domains) is the most instable one (Boyd et al., 2015). Another study on bovine GIII norovirus reported a similar disassembly but distinct assembly mechanism, which indicates that capsid assembly and stability could be genotype specific (Tresset et al., 2013a, 2013b). Stability differences of NoVs from different genogroups were tested with other biophysical techniques. For example, human NoV variants of GI.1 and GII.4, and FCV were compared using circular dichroism (CD) and intrinsic UV fluorescence. Less temperature and pH induced structural changes were observed for GII.4 than for the other particles (Samandoulgou et al., 2015). When solution chemistry properties of GI.1 Norwalk and GII.4 Houston VLPs were compared, Norwalk VLPs aggregated at pH 9 with increasing hydrodynamic radii. The GII.4 variant was stable up to pH 8, however pH 9 was not examined. Furthermore, the two variants showed different attachment efficiencies (da Silva et al., 2011). Sensitivity to alkaline treatment was also observed for a GII.7 isolate via AFM nanoindentation. From pH 8.5 to pH 10, the observed spring constant dropped indicating decreased capsid stability. Notably, capsids of increased size could still be detected at pH 10 (Cuellar et al., 2010). Comparing these findings to AFM on Norwalk VLPs would be of interest.

Norovirus VLPs have been used to study core features of capsid assembly and stability. Biophysical methods like CD spectroscopy are extremely helpful to characterize VLPs. However, they often fail to describe structural changes thoroughly as smaller oligomers are poorly resolved. In AFM nanoindentation, biophysical properties of capsids like size and stiffness can be probed and techniques like IM and native MS are a great tool to monitor stability and decipher smaller capsid assembly states. Insights to capsid disassembly mechanisms could improve the design of capsids for nanotechnological applications and therefore would also be beneficial for norovirus vaccine development. Especially, the latter is extremely hindered by the frequent emergence of outbreak causing variants. Lately, some worldwide outbreaks were caused by an emerging recombinant polymerase genotype showing mutations in the RNA polymerase gene as well as the VP1 (Fu et al., 2017). This indicates that polymerase genotypes can also play a role in emergence, but are usually accompanied by mutations in the capsid protein (Bull et al., 2005).

### 1.3. Aim of the work

Disease prevention and treatment are main drivers for viral structural studies. The ability to follow physical properties and dynamics is a great asset in finding new antivirals or vaccines. Additionally, recent developments more and more target the development of protein nanocages. Based on viral self-assembly mechanisms, protein nanocontainers can be used for various applications like diagnostic tools, delivery vehicles for gene therapy, platforms for antigen presentation, among others (Brune et al., 2016; Holzinger et al., 2014; Wang et al., 2021). Viral proteins, especially derived from viruses with icosahedral symmetry, can be both building blocks or templates to these approaches. Their assemblies differ in various parameters like stability, assembly and disassembly behavior, cargo and presentation capability, and size, to only mention a few. This implies the possibility to actively use these parameters for customization of particles (Glasgow and Tullman-Ercek, 2014). (All-atom) molecular dynamics simulation of whole capsids are driving forces in applying mechanisms of viral self-assembly and disassembly to these nanotechnological approaches (Zhao et al., 2021; Mohajerani et al., 2022). However, they are based on experimental findings. Recent developments in standard structural techniques like cryo-EM putatively allow to capture temporally-limited assembly intermediates (Chmielewski et al., 2022). Additionally, native MS approaches are greatly suited for structural studies (Dülfer et al., 2019; Liko et al., 2016). However, they become more complex with increased size of the studied assemblies.

Self-assembly of empty virus-like particles is vastly different from particle assembly accompanied by genome integration (Bruinsma et al., 2021). However, understanding VLP assembly and disassembly of complex systems like human noroviruses holds innate opportunities in finding antiviral drugs and understanding particle stability for vaccine development, and their utilization as bionanocarriers.

Therefore, this thesis aims to pinpoint important mediators in hNoV assembly and further size-determinants. In order to do so, this work firstly targets to ease characterization of high-mass complexes like VLPs by mass spectrometry and accompanied techniques. Gas phase electrophoretic mobility analysis is a complementary technique to standard and customized native MS. However, in order use this technique for size determination, electrophoretic mobility diameter and mass of respective particles need to be correlated. A correlation which closes the

## Introduction

size-gap of established ones has the potential to allow easy and fast size determination of low-yield particles.

A great advancement of native MS and allied techniques is the ability to simultaneously portray coexisting particle sizes and low-mass multimers. Norovirus assembly has been addressed before but mainly targeted the prototypical Norwalk virus (Shoemaker et al., 2010; Uetrecht et al., 2011). Since its advent, noroviruses classification into genogroups advanced greatly and several genotypes showed increased outbreak-potential. This work therefore addresses strain-dependent differences by applying native MS protocols to other norovirus variants. Main target here is the relationship between capsid size and stability in different pH and ionic strength.

In total, this work addresses the development of novel biophysical characterization techniques as well as their application to noroviruses. Findings on particle stability, particle size, as well as assembly and disassembly behavior are amenable for nanotechnological applications. They further hold potential to decipher other aspects of the norovirus lifecycle, like impact of ligand binding in viral entry.

## 2. Cumulative Part of the Dissertation

---

### 2.1. Virus-like particle size and molecular weight/mass determination applying gas-phase electrophoresis (native nES GEMMA)

Victor U. Weiss, Ronja Pogan, Samuele Zoratto, Kevin M. Bond, Pascale Boulanger, Martin F. Jarrold, Nicholas Lykтей, Dominik Pahl, Nicole Puffler, Mario Schelhaas, Ekaterina Selivanovitch, Charlotte Utrecht and Günter Allmaier

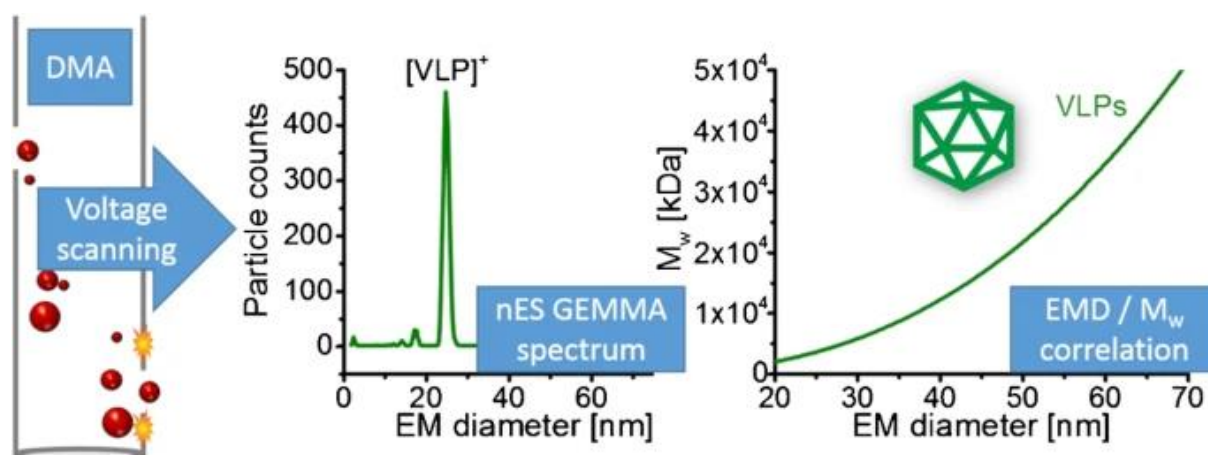
Victor U. Weiss and Ronja Pogan contributed equally to this work.

*Analytical and Bioanalytical Chemistry* volume 411, pages5951–5962 (2019)

This article is distributed under the terms of the Creative Commons Attribution 4.0 International License (<http://creativecommons.org/licenses/by/4.0/>), no changes were made.

To access the publication see

<https://doi.org/10.1007/s00216-019-01998-6>





## Virus-like particle size and molecular weight/mass determination applying gas-phase electrophoresis (native nES GEMMA)

Victor U. Weiss<sup>1</sup> · Ronja Pogan<sup>2,3</sup> · Samuele Zoratto<sup>1</sup> · Kevin M. Bond<sup>4</sup> · Pascale Boulanger<sup>5</sup> · Martin F. Jarrold<sup>4</sup> · Nicholas Lykтей<sup>4</sup> · Dominik Pahl<sup>6</sup> · Nicole Puffler<sup>1</sup> · Mario Schelhaas<sup>6</sup> · Ekaterina Selivanovitch<sup>4</sup> · Charlotte Uetrecht<sup>2,3</sup> · Günter Allmaier<sup>1</sup>

Received: 16 April 2019 / Revised: 29 May 2019 / Accepted: 24 June 2019 / Published online: 6 July 2019  
© The Author(s) 2019

### Abstract

(Bio-)nanoparticle analysis employing a nano-electrospray gas-phase electrophoretic mobility molecular analyzer (native nES GEMMA) also known as nES differential mobility analyzer (nES DMA) is based on surface-dry analyte separation at ambient pressure. Based on electrophoretic principles, single-charged nanoparticles are separated according to their electrophoretic mobility diameter (EMD) corresponding to the particle size for spherical analytes. Subsequently, it is possible to correlate the (bio-)nanoparticle EMDs to their molecular weight ( $M_w$ ) yielding a corresponding fitted curve for an investigated analyte class. Based on such a correlation, (bio-)nanoparticle  $M_w$  determination via its EMD within one analyte class is possible. Turning our attention to icosahedral, non-enveloped virus-like particles (VLPs), proteinaceous shells, we set up an EMD/ $M_w$  correlation. We employed native electrospray ionization mass spectrometry (native ESI MS) to obtain  $M_w$  values of investigated analytes, where possible, after extensive purification. We experienced difficulties in native ESI MS with time-of-flight (ToF) detection to determine  $M_w$  due to sample inherent characteristics, which was not the case for charge detection (CDMS). nES GEMMA exceeds CDMS in speed of analysis and is likewise less dependent on sample purity and homogeneity. Hence, gas-phase electrophoresis yields calculated  $M_w$  values in good approximation even when charge resolution was not obtained in native ESI ToF MS. Therefore, both methods-native nES GEMMA-based  $M_w$  determination via an analyte class inherent EMD/ $M_w$  correlation and native ESI MS-in the end relate (bio-)nanoparticle  $M_w$  values. However, they differ significantly in, e.g., ease of instrument operation, sample and analyte handling, or costs of instrumentation.

**Keywords** Native nES GEMMA · DMA · VLP · Molecular weight/mass · Size · Mass spectrometry

---

Victor U. Weiss and Ronja Pogan contributed equally to this work.

**Electronic supplementary material** The online version of this article (<https://doi.org/10.1007/s00216-019-01998-6>) contains supplementary material, which is available to authorized users.

✉ Victor U. Weiss  
victor.weiss@tuwien.ac.at

<sup>1</sup> Institute of Chemical Technologies and Analytics, TU Wien, Getreidemarkt 9/164, 1060 Vienna, Austria

<sup>2</sup> Heinrich Pette Institute, Leibniz Institute for Experimental Virology, Martinstraße 52, 20251 Hamburg, Germany

<sup>3</sup> European XFEL GmbH, Holzkoppel 4, 22869 Schenefeld, Germany

<sup>4</sup> Department of Chemistry, Indiana University, 800 E Kirkwood Ave, Bloomington, IN 47405, USA

<sup>5</sup> Institute for Integrative Biology of the Cell, CEA, CNRS, Université Paris-Sud, Université Paris-Saclay, 91198 Gif-sur-Yvette, France

<sup>6</sup> Institute of Cellular Virology, WWU Münster, Von-Esmarch-Str. 56, 48149 Münster, Germany

## Introduction

Viruses are nanoparticles of biological origin: A proteinaceous capsid protects the viral genome from the exterior. Additional protection can be conveyed by a lipid membrane, which is additionally modified by (glyco-) proteins to enable attachment to target cells (e.g., [1]). Only upon target cell infection, the genomic material of the virus is intended for release. This concept is of interest for pharmacological applications as virus bionanoparticles can be interpreted as carriers enabling the shielded, targeted transport of cargo material. Alternatively, viral particles without any encapsulated cargo can be employed for vaccination. In both cases, corresponding particles are referred to as virus-like particles (VLPs) (e.g., [2]).

To allow for VLP application in the field of pharmaceuticals, their thorough characterization and preparation batch control, e.g., in terms of particle homogeneity, purity of preparations, particle size, and molecular weight ( $M_w$ ), is of importance. For the latter, native electrospray ionization mass spectrometry (native ESI MS) mostly in combination with time-of-flight (ToF) analyzers evolved as method of choice, yielding  $M_w$  values of bionanoparticles after deconvolution of mass spectra. Such, the  $M_w$  of dimorphic hepatitis B-based VLPs could be obtained already in 2008 [3]. In addition, several other VLPs or subviral particles [4, 5] up to a maximum  $M_w$  of 17.9 MDa with charge state assignment [6] or employing cryodetection with matrix assisted laser desorption/ionization time-of-flight (MALDI TOF) MS [7] could be investigated. ESI with charge detection mass spectrometry (CDMS) [8, 9] even allowed detection of VLPs up to 26.8 MDa, employing bacteriophage P22 as model [10, 11]. Besides enabling the analysis of VLPs, also capsid binding to antibody fragments [12], pH-dependent VLP decomposition [13] or the investigation of VLP capsid assembly [14] was accessible via native ESI MS. However, none of these measurements can be carried out on standard commercial instruments. Employed mass spectrometers are usually customized in terms of, e.g., applied pressures, employed carrier gas or voltage settings, or pose completely new instrumental developments. In 2018, for instance, Dominguez-Medina and coworkers reported the analysis of bacteriophage T5 icosahedral capsids either in their empty VLP form ( $M_w \sim 27$  MDa) or in their DNA-filled native form ( $M_w \sim 108$  MDa) [15]. For these experiments, nanochemical resonators were employed [16, 17].

As alternative,  $M_w$  determination can also be based on gas-phase electrophoresis data employing a nano-electrospray gas-phase electrophoretic mobility molecular analyzer (native nES GEMMA also known as nES differential mobility analyzer, nES DMA) [18]. Bionanoparticles are electrosprayed from a volatile, aqueous electrolyte solution. Subsequently, droplets are dried. At the same time, charge equilibration occurs in a bipolar atmosphere induced by, e.g., an  $\alpha$ -particle emitter like  $^{210}\text{Po}$ , an alternating corona discharger or a soft X-

ray tube [19, 20]. Hence, singly charged particles are obtained (besides a majority of neutral objects), which are then separated according to electrophoretic principles in the gas phase at ambient pressure. A particle charge of one leads to bionanoparticle separation according only to the surface-dry particle size (electrophoretic mobility diameter, EMD) in a high laminar sheath flow of particle-free, dried air, and a tunable electric field. Variation of the field strength enables size separation of sample components. The obtained monodisperse aerosol is subsequently introduced to the detector unit of the instrument (ultrafine condensation particle counter, CPC), where bionanoparticles act as condensation nuclei in a super-saturated atmosphere of either n-butanol or water. Obtained droplets are counted as they pass a focused laser beam. Such an instrumentation has previously been employed for the analysis of liposomes [21, 22], exosomes [23], viruses [24–29], proteins and protein aggregates [30], polysaccharides [31–33], DNA [34], polymers [35–37], and nanoparticles in general [38–42]. Besides yielding information on analyte surface-dry particle size and size distribution, particle number concentration detection is possible in accordance with recommendations of the European Commission for characterization of nanoparticle material (2011/696/EU from October 18<sup>th</sup>, 2011). Furthermore, analytes can be size-selected for further analyses employing orthogonal methods for instance electron microscopy [43], atomic force microscopy [44], spectroscopic techniques [45, 46], or antibody-based nanoparticle recognition [44, 47]. It is of note that LiquiScan ES, MacroIMS, and SMPS are synonyms of the same instrument found in literature.

Furthermore, as first demonstrated in great detail by Bacher and colleagues [48] for proteins, obtained EMD results can be related to particle  $M_w$  values yielding a corresponding correlation. Hence, based on a protein EMD value, its  $M_w$  can be calculated in good approximation. Similar approaches have been demonstrated, e.g., for intact viruses [4] and polysaccharides [32]. It is of note that for the latter two, the obtained EMD/ $M_w$  correlations deviated from the protein case. For instance for polysaccharides, it was reasoned that additional factors might influence the EMD/ $M_w$  correlation, inter alia particle shape, or insufficient characterization of applied, commercially available standards. Likewise, for elongated virus structures (tobacco mosaic virus), effects like bending of analytes due to surface effects of droplets generated during the nES process were observed [49].

In the current manuscript, we focus on nano-objects, namely VLPs, which are approximately spherical (icosahedral) and non-enveloped (empty protein shells). We asked ourselves, if a native nES GEMMA-based EMD/ $M_w$  correlation for VLPs is likewise differing from correlations described for other classes of analytes. In addition, we wanted to investigate if a corresponding EMD/ $M_w$  correlation will allow an approx.  $M_w$  determination of this class of bionanoparticles with a

relatively quick, cheap (~ 80.000 €), less challenging (in terms of sample quality) and easy to handle analytical setup in comparison to native ESI-MS. Mind however, that a high accuracy  $M_w$  determination of VLPs is only possible on the basis of MS-derived data. Hence, both methods have to be regarded as yielding complementary information in terms of analyte size and  $M_w$ , sample quality, and particle number concentration.

## Materials and methods

**Chemicals** Ammonium acetate ( $\text{NH}_4\text{OAc}$ ,  $\geq 99.99\%$ ) and ammonium hydroxide (ACS reagent) were both purchased from Sigma-Aldrich (Steinheim, Germany).

**Electrolyte**  $\text{NH}_4\text{OAc}$ , 40 mM ammonium acetate at pH 7.0 was used as electrolyte solution for desalting of VLPs and for sample dilution for nES GEMMA and ESI MS. Electrolyte solutions for CDMS measurements are detailed with corresponding experiments.  $\text{NH}_4\text{OAc}$  solution was filtered (0.2  $\mu\text{m}$  pore size syringe filters, Sartorius, Göttingen, Germany) prior application. Millipore (Billerica, MA, USA) grade water was employed (18.2  $\text{M}\Omega\text{cm}$  resistivity at 25 °C).

**Biological material** Norovirus West Chester GI.1 VLPs (3 mg/mL in PBS, pH 7.4) were produced in insect cells and kindly provided by Grant Hansman, Heidelberg, Germany, and CPMV VLPs (4 mg/mL in 10 mM sodium phosphate, pH 7.0) were from John Innes Centre (kindly provided by George Lomonosoff, Norwich, UK). Bacteriophage P22 VLPs (2 mg/mL in 50 mM sodium phosphate, pH 7.0 including 100 mM sodium chloride and 200 ppm sodium azide) were obtained from Indiana University Bloomington (Bloomington, IN, USA), bacteriophage T5 VLPs (0.3 mg/mL, i.e.,  $7 \times 10^{12}$  empty capsids/mL in PBS) from the Institute for Integrative Biology of the Cell (I2BC), Gif-sur-Yvette, France). Human papillomavirus type 16 (HPV16, 0.3 mg/mL in PBS additionally including 625 mM sodium chloride, 0.9 mM calcium chloride, 0.5 mM magnesium chloride, and 2.1 mM potassium chloride) VLPs were prepared from mammalian cells as previously described [50].

**Instrumentation** Gas-phase electrophoresis was performed on two setups: a nES GEMMA instrument (TSI Inc., Shoreview, MN, USA) consisting of a nES aerosol generator (model 3480) including a  $^{210}\text{Po}$   $\alpha$ -particle source, an electrostatic classifier (model 3080) with a nano-differential mobility analyzer (nDMA) and an n-butanol-based ultrafine condensation particle counter (model 3025A or 3776C) was applied as instrument A. Instrument B consisted of a model 3482 nES aerosol generator including a soft X-ray source, an electrostatic classifier (model 3082) and a water-based ultrafine condensation particle counter (model 3788). Twenty-five  $\mu\text{m}$  inner

diameter polyimide coated fused silica capillaries (Polymicro, obtained via Optronis, Kehl, Germany) with in-house made tips [51] were employed to transfer analytes from the liquid to the gas phase. Settings for a stable Taylor cone at the nES tip were chosen, typically around 2 kV voltage resulting in approx. – 375 nA current, 0.1 liters per minute (Lpm)  $\text{CO}_2$  (Messer, Gumpoldskirchen, Austria) and 1.0 Lpm filtered, dried ambient air. Four pounds per square inch differential (psid, approx. 27.6 kPa) were applied to additionally move the sample through the capillary. Fifteen Lpm sheath flow filtered ambient air was used to size-separate VLPs in an EMD range from 2 to 65 nm. The corresponding EMD size range was scanned for 120 s. Subsequently, the applied voltage was adjusted to starting values within a 30-s timeframe. Seven datasets (raw data obtained from instrument software, MacroIMS manager v2.0.1.0) were combined via their median to yield a corresponding spectrum. Lastly, Gaussian peaks were fitted to spectra via Origin software (OriginPro v9.1.0) to obtain EMD values.

HPV16 VLPs cannot be produced in high yields. Due to the resulting low VLP concentration, samples were only analyzed between 30 and 65 nm EMD to increase the scanning time in this range. In addition, a 40  $\mu\text{m}$  inner diameter capillary was employed to reduce the surface to volume ratio and hence the probability of analyte loss due to VLP interaction with the fused silica material of the nES capillary. This resulted in significantly higher particle numbers detected per channel and hence a discernible VLP peak.

For CPMV and P22 VLPs, native MS was performed on a Q-ToF 2 instrument (Waters, Manchester, UK, and MS Vision, Almere, the Netherlands) modified for high mass experiments [52, 53] and calibrated with cesium iodide. A nano-ESI source in positive ion mode with a source pressure of 10 mbar was used. Capillaries were produced in-house. Borosilicate glass tubes (inner diameter 0.68 mm, outer diameter 1.2 mm with filament; World Precision Instruments, Sarasota, FL, USA) were pulled using a two-step program in a micropipette puller (model P-1000 from Sutter Instruments, Novato, CA, USA) with a squared box filament (2.5  $\times$  2.5 mm). Subsequently, the capillaries were gold-coated using a sputter coater (Quorum Technologies, East Sussex, UK, 40 mA, 200 s, tooling factor of 2.3 and end bleed vacuum of  $8 \times 10^{-2}$  mbar argon) and opened directly on the sample cone of the mass spectrometer. Voltages of 1.45–1.65 kV and 145–155 V were applied to the capillary and cone, respectively. Xenon (purity 5.0) was used as collision gas at a pressure of  $1.7\text{--}2.0 \times 10^{-2}$  mbar to improve the transmission of large ions [53]. Collision energies were ramped from 10 to 400 V. MS profile and repetition frequency of the pusher pulse were adjusted to high mass range. Mass spectra were analyzed using MassLynx (Waters, Manchester, UK).

Mass spectra of norovirus West Chester VLPs were obtained using a home-built ESI CDMS system, described in detail elsewhere [54]. Briefly, CDMS is a single particle MS technique, which retrieves  $m/z$  and  $z$  for each ion allowing direct mass determination from a charge conducting cylinder functioning also as electrostatic ion trap. Hence, masses of large, heterogeneous biological complexes can be measured. An automated nano-ESI source (Advion, Ithaca, NY, USA) was used to generate ions with a capillary voltage of 1.7 kV. The ions then enter a heated metal capillary and are transmitted using various ion optics to a dual hemispherical deflection energy analyzer which selects ions with energies centered on 100 eV/ $z$ . These ions then enter a modified cone trap. Here, trapped ions oscillate back and forth in a charge detection cylinder for 100 ms. Mass spectra were generated by binning of the single ion masses. Spectra were subsequently analyzed by fitting Gaussian peaks with Origin software (OriginPro 2016).

**Sample preparation** In order to enable native nES-based analysis of VLPs, employed storage buffers (often including additional salt components or stabilizing agents) had to be replaced by a volatile electrolyte solution. Else, these additional sample components were shown to lead to an increased peak heterogeneity of the analytes of interest and, in nES GEMMA, an elevated baseline resulting from clustering of small, non-volatile molecules during the nES process [55]. As in previous studies, we opted for ammonium acetate and carried out removal of small, buffer-associated sample components via spin filtration [42] employing 10 kDa  $M_w$  cutoff filters (Vivaspin-polyethersulfone membrane, Vivacon-regenerated cellulose membrane-both from Sartorius or centrifugal filters-polyethersulfone membrane, VWR, Vienna, Austria). Between 3 and 5 filtration steps were necessary to remove non-volatile additional sample components. Sample concentration for measurements was typically well below 1 mg/mL protein content (based on originally determined values and sample dilution).

## Results and discussion

It was the aim of our investigation to analyze VLP material with gas-phase electrophoresis on a native nES GEMMA instrument and to compare results with data obtained from native ESI MS and from literature. We intended to setup an EMD/ $M_w$  correlation for VLPs to allow for future VLP  $M_w$  determination based on gas-phase electrophoresis directed towards analysis of samples not applicable to native ESI ToF MS.

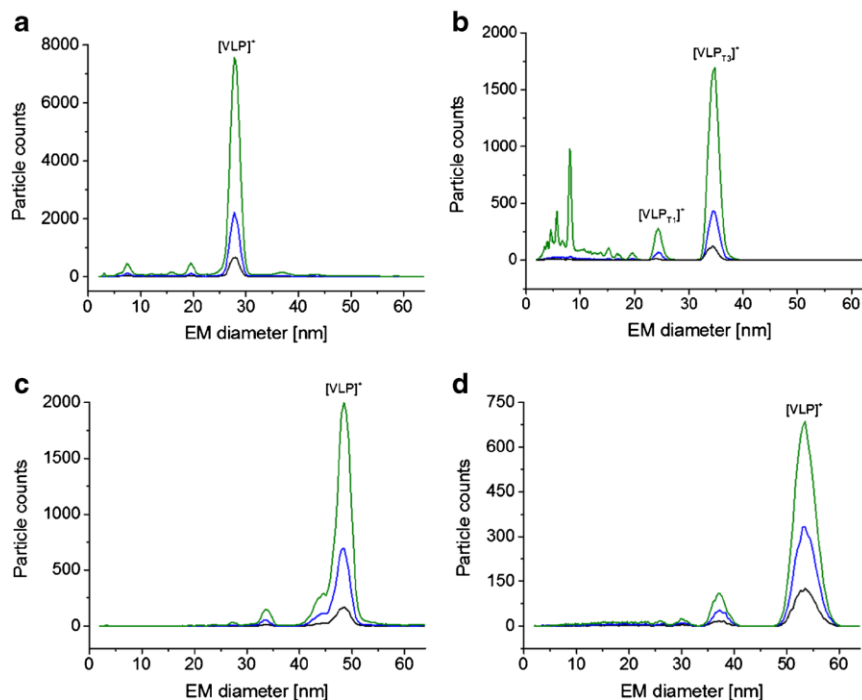
**Native nES GEMMA analysis of VLPs** In previous work, we had already described the analysis of VLP or VLP-like material

based on hepatitis B virus capsids (HBV) with two icosahedral symmetries [12] and subviral particles of a human rhinovirus serotype (HRV-A2) [4]. We now turned to further VLP material and analyzed bionanoparticles derived from cowpea mosaic virus (CPMV), a norovirus strain and particles from bacteriophage P22 and T5 via gas-phase electrophoresis. Figure 1 depicts corresponding native nES GEMMA spectra. An overview of investigated VLPs and resulting EMD values are listed in Table 1. In order to exclude the possibility of unspecific aggregation of sample components, VLPs were electrosprayed from samples diluted to at least three different concentrations. Unspecific aggregation of components was excluded, if peaks remained at identical EMD values for all investigated dilutions.

Besides information on the surface-dry VLP size and an approximation on the bionanoparticle number concentration, two other pieces of information could be gathered from native nES GEMMA spectra. (i) Especially for norovirus West Chester VLPs (Fig. 1b), detection of material below 10 nm EMD hinted the presence of free proteins. Pogan et al. [13] showed that these particles already disassemble at neutral pH and low ionic strengths, which is in line with our results. Moreover, general particle rupture in the nES process is unlikely, as such peaks were only recorded for norovirus West Chester VLPs. (ii) Especially for bacteriophage P22-based VLPs (Fig. 1c) several additional species with significantly lower abundance than the main VLP peak were detected (e.g., at 34 or 45 nm EMD). If these peaks correspond to species simply carrying a higher number of charges from insufficient charge equilibration in the bipolar atmosphere of the nES unit or are analytes of biological relevance (e.g., capsids losing subunits) cannot be determined based on obtained native nES GEMMA results alone. However, ESI ToF MS also showed at least one additional species, which indicates that the observed peaks correspond to different assemblies present in solution (Fig. 2).

**Native ESI MS analysis of VLPs** Next to targeting these VLP analytes via native nES GEMMA, we also applied native ESI MS in VLP characterization. Employing Q-ToF instruments, challenges of VLP  $M_w$  determination in native ESI MS become obvious. For the same samples as with native nES GEMMA, clear peaks were obtained via native ESI ToF MS (Fig. 2). However, the lack of charge state separation hampered exact mass determination. Common sources for lack of resolution are intrinsic VLP heterogeneity mostly on protein level, e.g., the presence of truncated protein or sequence variants, or simply size resulting in overlapping charge states. As was shown in a previous study, the problems in charge state resolution can be instrument, but as well analyte derived [3]. Furthermore, incomplete desolvation can additionally cause peak broadening, which influences native ESI ToF MS to a higher extent than gas-phase electrophoresis. Nevertheless,

**Fig. 1** nES GEMMA data for VLPs: CPMV (a), norovirus West Chester (b), bacteriophage P22 (c), and bacteriophage T5 capsids (d). All VLPs are shown in three different dilutions of obtained material after solution exchange to 40 mM NH<sub>4</sub>OAc, pH 7.0 employing 10 kDa M<sub>w</sub> cutoff membrane filters. (Typically, overall dilutions were in the range of 1:10 to 1:250 [v:v] of the original VLP stock solutions resulting from solution exchange and sample dilution steps)



using an experimentally derived equation [57], also in such cases, the M<sub>w</sub> can be estimated from the obtained *m/z* values. Taking for instance *m/z* of 22,600 for CPMV into consideration, a M<sub>w</sub> of 3107 kDa is obtained, for bacteriophage P22, an *m/z* of 55,600 yields a M<sub>w</sub> of 18,807 kDa. Both M<sub>w</sub> values are in the same range as data found in literature (see Table 1). In general, the spectra show that the number of different observed sizes is in line with the nES GEMMA results. Moreover, the norovirus VLPs were also analyzed on an ESI CDMS instrument to provide M<sub>w</sub> values without the need for charge state resolution and obtain more values for the correlation (Electronic Supplementary Material (ESM) Fig. S1). Additionally, application of an Orbitrap instrument with

higher resolution might help to resolve charge states in a future study.

**Combining native nES GEMMA and native ESI MS data yields an EMD/M<sub>w</sub> correlation for VLPs** Based on our analyses of VLP material via native nES GEMMA and accurate mass values from native ESI MS including literature values (given in Table 1), we set up a corresponding EMD/M<sub>w</sub> correlation:  $y [M_w \text{ in kDa}] = 0.7601 [EMD \text{ in nm}]^{2.6319}$  (Fig. 3). Notably, this deviates from a correlation for proteins as was the case for filled virions [32]. Hence, a basic knowledge concerning the analyte class prior EMD-based M<sub>w</sub> calculation (but not for gas-phase electrophoresis itself) is necessary.

**Table 1** Overview on investigated VLP material as well as data taken from literature as indicated

VLP	EM diameter (nm)	Based on	M <sub>w</sub> (kDa)	Based on	
1	Norovirus West Chester T1 VLP	24.22 ± 0.21	–	3320 ± 30	CDMS
2	Hepatitis B virus (HBV) T3 VLP	24.22 ± 0.40	[12]	3004 ± 3	MS [12]
3	Hepatitis B virus (HBV) T4 VLP	26.84 ± 0.44	[12]	4006 ± 3	MS [12]
4	Cowpea mosaic virus (CPMV) VLP	27.88 ± 0.04	–	3940 ± n.a.	[56]
5	Subviral B particle of human rhinovirus 2	28.68 ± 0.07	[4]	5210 ± 2	MS [4]
6	Norovirus West Chester T3 VLP	34.47 ± 0.15	–	10,260 ± 40	CDMS
7	Bacteriophage P22 VLP	48.44 ± 0.12	–	19,840 ± n.a.	MS [11]
8	Bacteriophage T5 VLP	53.45 ± 0.09	–	27,200 ± 2300	MS [15]

New data is presented in italics. An exemplary CDMS spectrum of investigated VLPs is shown in the ESM (Fig. S1). At least *N* = 3 technical replicates were used per EMD value. Errors provided are standard deviations

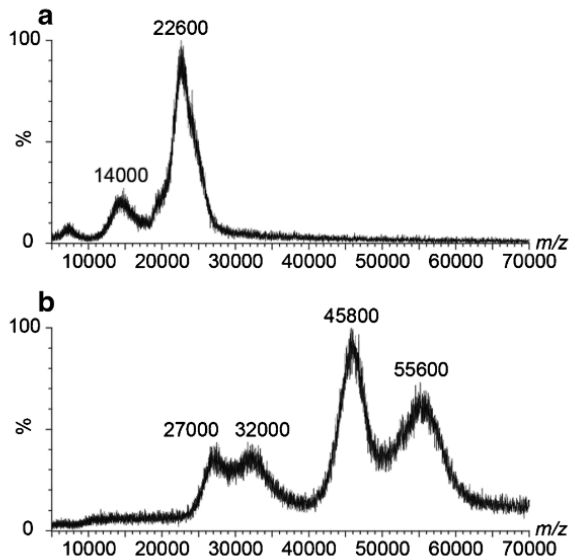


**Fig. 2** QTOF native ESI MS data for VLPs: CPMV at 50 V collision energy (a) and bacteriophage P22 at 100 V collision energy (b) are shown. Although in both cases signals are detected, analyte heterogeneity precluded charge state resolution.  $m/z$  values at peak apices are given. VLPs were exchanged to 40 mM  $\text{NH}_4\text{OAc}$ , pH 7.0, using 10 kDa  $M_w$  cutoff filters. Peaks at 14,000, 27,000, and 32,000  $m/z$  may represent metastable ions

A collapse of VLP particles during gas-phase electrophoresis upon stripping of solvent molecules from their interior seems highly unlikely as AFM and dot-blot analyses of a vaccine VLP demonstrated particle integrity after gas-phase electrophoresis [44]. Instead, due to protein analyte inherent  $M_w$  limitations, especially a direct comparison of a protein correlation with an EMD/ $M_w$  correlation for VLPs is to date not feasible. Simply because VLPs are analyzed in an EMD/ $M_w$  range, in which pure protein complexes (in a non-aggregated or structured form) rarely exist, the extrapolation

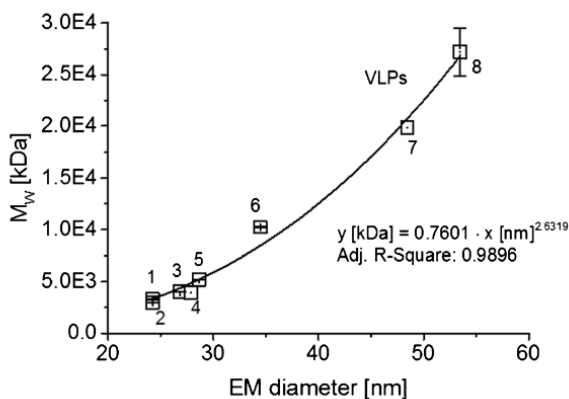


**Fig. 3** nES GEMMA and MS data can be related to yield an EMD/ $M_w$  correlation valid for VLPs. The numbering of data points correlates to Table 1

of the protein EMD/ $M_w$  correlation to larger EMD and  $M_w$  values has to be taken with extreme caution. It is of note that the largest protein analyzed in [32] was the octamer of  $\beta$ -galactosidase with an EMD of 16.83 nm and a  $M_w$  of 931.28 kDa.

In contrast, the VLP-based EMD/ $M_w$  correlation is based on data points for larger EMD/ $M_w$  values. VLPs with low EMD/ $M_w$  value are not reasonable as the proteinaceous sphere has to be of a certain lower size limit (around 20 nm) in order to allow for genome encapsulation within the capsid. Therefore, there is poor overlap between pure protein complex and VLP curves. Extrapolation of either the protein correlation to large or the VLP correlation to lower EMD/ $M_w$  values is problematic. Hence, we advise against taking one single EMD/ $M_w$  correlation for all investigated analyte classes in order to calculate  $M_w$  values based on a particle EMD.

**EMD/ $M_w$  correlations on different native nES GEMMA instruments** As it was our intention to setup an EMD/ $M_w$  correlation for VLPs applicable to as many as possible corresponding native nES GEMMA instrumentations, we asked ourselves, if obtained results can be ported between setups. Laschober and colleagues already reported in 2007 differences of up to 15% in obtained EMD values for globular proteins up to 660 kDa [58]. Especially slight variations in nDMA geometries, length values of connecting tubes between instrument parts or differences in sheath flow values may lead to deviations observed between instruments. Therefore, we analyzed a set of analytes on another gas-phase electrophoretic setup besides our standard native nES GEMMA (instrument A). This instrument corresponded to a next-generation setup with differences in the geometry of the nES source and a soft X-ray source for charge equilibration (instrument B). Detection on the latter instrumentation was carried out on a water-based CPC. We

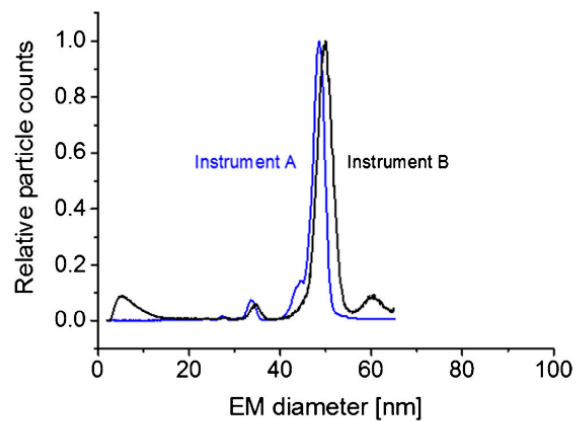


**Fig. 4** Comparing gas-phase electrophoresis data obtained on two instrument generations. As shown for bacteriophage P22, a significant shift in obtained EMD values on both instruments is found. Corresponding EMD data is found in Table 2

**Table 2** Comparison of averaged EMD values obtained on several gas-phase electrophoretic instrumentations

Analyte	MW (kDa)	Instrument A			Instrument B	
		EMD (nm)	STDEV	(%) value instrument B	EMD (nm)	STDEV
IgG	M 147.27	9.03	0.10	95.19	9.49	0.04
IgG	D 294.54	11.26	0.10	95.58	11.78	0.04
$\beta$ -Gal	M 116.41	8.33	0.11	95.76	8.70	0.03
$\beta$ -Gal	D 232.82	10.57	0.11	95.52	11.07	0.02
Dextran 150	M 147.6	8.17	0.15	98.67	8.28	0.01
Dextran 670	M 667.8	10.05	0.41	92.88	10.82	0.12
Oat $\beta$ glucan 80	M 81	7.12	0.04	93.81	7.59	0.03
Oat $\beta$ glucan 1500	M 1508	7.71	0.15	94.83	8.13	0.04
CPMV VLP	M 3940	27.88	0.04	99.32	28.07	0.07
P22 VLP	M 19,840	48.44	0.12	97.21	49.83	0.07

At least  $N=3$  measurements were considered per EMD value.  $M_W$  values and data for instrument A either taken from [32] or Table 1. *M* monomer, *D* dimer; errors provided are standard deviations

opted for immunoglobulin G (IgG),  $\beta$ -galactosidase ( $\beta$ -Gal), several polysaccharides (dextrans and oat  $\beta$  glucans), CPMV VLP, and bacteriophage P22 VLP as analytes.

Resulting spectra from gas-phase electrophoresis carried out on the two instrumentations are depicted in Fig. 4 as exemplified by P22 VLPs. Corresponding data for all analytes is given in Table 2. As can be seen, indeed slight differences between instrumentations were detected. For instance, the EMD of investigated proteins deviated on average by 4.5% at the peak apex between our standard instrumentation (instrument A) and the next-generation setup (instrument B). Less variation was found for VLPs, more for polysaccharides. Based on this data, we strongly suggest calibration of each instrument for corresponding EMD-based  $M_W$  calculation: Instrument specific parameters have to be regarded in order to obtain reliable EMD-based  $M_W$

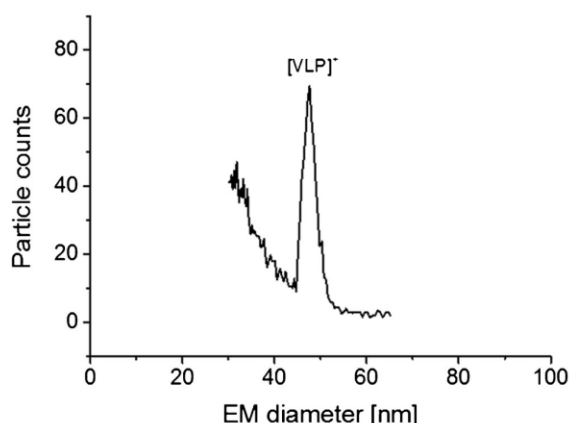


**Fig. 5** nES GEMMA yields a peak for HPV16-based VLPs allowing its subsequent  $M_W$  determination based on the correlation presented in Fig. 3. The calculated  $M_W$  (19,975 kDa) is in good accordance with the theoretically expected  $M_W$  value (20,260 kDa, based on VLP stoichiometry and database  $M_W$  values for individual viral proteins)

values via gas-phase electrophoresis. A simple porting of EMD/ $M_W$  correlations between instrumentations without considering a corresponding deviation would lead to significant systematic errors in EMD-based particle  $M_W$  calculation.

**Application of the developed EMD/ $M_W$  correlation in VLP research, an example** Following the setup of our EMD/ $M_W$  correlation for VLPs, we turned to another VLP based on HPV16, for which no native MS data was obtained so far. We carried out our analyses on our standard instrumentation (instrument A). Employing native nES GEMMA, we could obtain a peak at  $47.78 \pm 0.29$  nm EM diameter ( $N=4$  measurements, Fig. 5). Subsequently, we employed our EMD/ $M_W$  correlation for the calculation of the VLP  $M_W$ . A result of 19,975 kDa is in good accordance with the expected value of 20,260 kDa (based on 72 pentamers of coat protein L1, Uniprot data, P03101, retrieved on January 17<sup>th</sup>, 2019); the deviation is in fact below 1.5%. Reasons for this deviation could be inter alia (i) a still relatively low number of data points available for the VLP EMD/ $M_W$  correlation, (ii) the shape, surface texture, or tightness of the proteinaceous shell itself, (iii) additional material encapsulated within VLPs, or (iv) differences between VLP material measured via native nES GEMMA and material described in the database. Nevertheless, employing HPV16 as an exemplary VLP bionanoparticle, we were able to demonstrate the applicability of native nES GEMMA-based  $M_W$  determination of VLP analytes.

## Concluding remarks

For pharmaceutical applications as pointed out above, the thorough characterization of VLPs in terms of particle size,

$M_w$ , sample, and analyte heterogeneity and particle number-based concentration is a necessary prerequisite. In general, it can be seen that ESI MS, whether from ToF or CDMS instruments, is in good agreement with nES GEMMA in terms of species detected. Hence, ESI MS results can be used to interpret nES GEMMA data of unknown samples. However, although native ESI ToF MS is unrivaled in VLP  $M_w$  determination, it often experiences problems due to sample specific problems, like heterogeneity or low particle numbers. Even though ESI CDMS is not suffering from sample heterogeneity, it is slow, requiring several hours per mass spectrum, and the home-built instrumentation is not widely accessible. nES GEMMA on the other hand is less prone to the mentioned sample inherent characteristics and is relatively cheap facilitating wide application. Analytes are separated according to electrophoretic principles in the gas-phase at ambient pressure based on their size yielding particle number-based concentrations. As has already been shown for other analyte classes, a subsequent correlation between the nES GEMMA-derived EMD and the particle  $M_w$  allows (bio-)nanoparticle  $M_w$  calculation in good approximation. We now focused on spherical VLPs and analyzed a variety of these bionanoparticles to setup an EMD/ $M_w$  correlation, which we found significantly different from correlations known for, e.g., proteins or intact virus particles. As such, it is crucial to know the nature of samples prior to  $M_w$  determination. As demonstrated, application of this correlation allowed us to calculate the  $M_w$  of a VLP, for which native ESI MS data is not available to date. Especially through the combination of both methods, nES GEMMA and native ESI MS, as exemplified here, a thorough VLP characterization will be feasible in the future.

**Acknowledgments** Open access funding provided by TU Wien (TUW). VUW acknowledges funding of the Austrian Theodor Körner Fonds. VUW and RP both acknowledge funding of COST Action BM1403 - Native Mass Spectrometry and Related Methods for Structural Biology. The Heinrich-Pette-Institute, Leibniz Institute for Experimental Virology is supported by the Freie und Hansestadt Hamburg and the Bundesministerium für Gesundheit (BMG). CU acknowledges funding from the Leibniz Association through SAW-2014-HPI-4 grant. RP acknowledges funding from EU Horizon 2020 project VIRUSCAN 731868 and thanks MINGS. CU, RP, DP and MS further thank the DFG FOR2327 Virocarb for support. We thank Grant Hansman and George Lomonosoff for providing VLPs. ES was supported by the Graduate Training Program in Quantitative and Chemical Biology under Award T32 GM109825 and Indiana University.

**Author contributions** Initial idea: VUW, GA; nES GEMMA measurements: VUW, RP, SZ; MS measurements: RP, KB, NL; sample preparation: PB, DP, MS, ES; data interpretation: VUW, RP, CU, GA; instrumentation: GA, CU, MFJ; funding: GA, CU, VUW; scientific guidance: GA, CU, VUW; organization: VUW; all authors contributed to the manuscript.

## Compliance with ethical standards

**Conflict of interest** The authors declare that they have no conflict of interest.

**Open Access** This article is distributed under the terms of the Creative Commons Attribution 4.0 International License (<http://creativecommons.org/licenses/by/4.0/>), which permits unrestricted use, distribution, and reproduction in any medium, provided you give appropriate credit to the original author(s) and the source, provide a link to the Creative Commons license, and indicate if changes were made.

## References

1. Sieben C, Kappel C, Zhu R, Wozniak A, Rankl C, Hinterdorfer P, et al. Influenza virus binds its host cell using multiple dynamic interactions. *P Natl Acad Sci USA*. 2012;109(34):13626–31.
2. Zeltins A. Construction and characterization of virus-like particles: a review. *Mol Biotechnol*. 2013;53(1):92–107.
3. Uetrecht C, Versluis C, Watts NR, Roos WH, Wuite GJ, Wingfield PT, et al. High-resolution mass spectrometry of viral assemblies: molecular composition and stability of dimorphic hepatitis B virus capsids. *Proc Natl Acad Sci U S A*. 2008;105(27):9216–20.
4. Weiss VU, Bereszczak JZ, Havlik M, Kallinger P, Gosler I, Kumar M, et al. Analysis of a common cold virus and its subviral particles by gas-phase electrophoretic mobility molecular analysis and native mass spectrometry. *Anal Chem*. 2015;87(17):8709–17.
5. Snijder J, van de Waterbeemd M, Damoc E, Denisov E, Grinfeld D, Bennett A, et al. Defining the stoichiometry and cargo load of viral and bacterial nanoparticles by Orbitrap mass spectrometry. *J Am Chem Soc*. 2014;136(20):7295–9.
6. Snijder J, Rose RJ, Veessler D, Johnson JE, Heck AJR. Studying 18 MDa virus assemblies with native mass spectrometry. *Angew Chem Int Edit*. 2013;52(14):4020–3.
7. Sipe DM, Ozdemir A, Firek B, Hendrix RW, Bier ME. Analysis of viral CapsidHK97 via cryodetection MALDI TOF in the megadalton mass range. In: 56th ASMS Conference on Mass Spectrometry and Allied Topics. June 1st–5th, 2008; Denver, CO, USA(# 571).
8. Keifer DZ, Pierson EE, Jarrold MF. Charge detection mass spectrometry: weighing heavier things. *Analyst*. 2017;142(10):1654–71.
9. Keifer DZ, Motwani T, Teschke CM, Jarrold MF. Measurement of the accurate mass of a 50 MDa infectious virus. *Rapid Commun Mass Spectrom*. 2016;30(17):1957–62.
10. Keifer DZ, Motwani T, Teschke CM, Jarrold MF. Acquiring structural information on virus particles with charge detection mass spectrometry. *J Am Soc Mass Spectrom*. 2016;27(6):1028–36.
11. Keifer DZ, Pierson EE, Hogan JA, Bedwell GJ, Prevelige PE, Jarrold MF. Charge detection mass spectrometry of bacteriophage P22 procapsid distributions above 20 MDa. *Rapid Commun Mass Spectrom*. 2014;28(5):483–8.
12. Bereszczak JZ, Havlik M, Weiss VU, Marchetti-Deschmann M, van Duijn E, Watts NR, et al. Sizing up large protein complexes by electrospray ionisation-based electrophoretic mobility and native mass spectrometry: morphology selective binding of Fabs to hepatitis B virus capsids. *Anal Bioanal Chem*. 2014;406(5):1437–46.

13. Pogan R, Schneider C, Reimer R, Hansman G, Utrecht C. Norovirus-like VP1 particles exhibit isolate dependent stability profiles. *J Phys Condens Matter*. 2018;30(6):064006.
14. Shoemaker GK, van Duijn E, Crawford SE, Utrecht C, Baclayon M, Roos WH, et al. Norwalk virus assembly and stability monitored by mass spectrometry. *Mol Cell Proteomics*. 2010;9(8):1742–51.
15. Dominguez-Medina S, Fostner S, Defoort M, Sansa M, Stark AK, Halim MA, et al. Neutral mass spectrometry of virus capsids above 100 megadaltons with nanomechanical resonators. *Science*. 2018;362(6417):918–22.
16. Naik AK, Hanay MS, Hiebert WK, Feng XL, Roukes ML. Towards single-molecule nanomechanical mass spectrometry. *Nat Nanotechnol*. 2009;4(7):445–50.
17. Malvar O, Ruz JJ, Kosaka PM, Dominguez CM, Gil-Santos E, Calleja M, et al. Mass and stiffness spectrometry of nanoparticles and whole intact bacteria by multimode nanomechanical resonators. *Nat Commun*. 2016;7:13452.
18. Kaufman SL, Skogen JW, Dorman FD, Zarrin F, Lewis KC. Macromolecule analysis based on electrophoretic mobility in air: globular proteins. *Anal Chem*. 1996;68(11):1895–904.
19. Kallinger P, Szymanski WW. Experimental determination of the steady-state charging probabilities and particle size conservation in non-radioactive and radioactive bipolar aerosol chargers in the size range of 5–40 nm. *J Nanopart Res*. 2015;17(4):171.
20. Allmaier G, Weiss VU, Engel NY, Marchetti-Deschmann M, Szymanski WW. Soft X-ray radiation applied in the analysis of intact viruses and antibodies by means of nano electrospray differential mobility analysis. In: Banoub JH, Caprioli RM, editors. *Molecular technologies for detection of chemical and biological agents*. Dordrecht: Springer Netherlands; 2017. p. 149–57.
21. Epstein H, Afergan E, Moise T, Richter Y, Rudich Y, Golomb G. Number-concentration of nanoparticles in liposomal and polymeric multiparticulate preparations: empirical and calculation methods. *Biomaterials*. 2006;27(4):651–9.
22. Weiss VU, Urey C, Gondikas A, Golesne M, Friedbacher G, von der Kammer F, et al. Nano electrospray gas-phase electrophoretic mobility molecular analysis (nES GEMMA) of liposomes: applicability of the technique for nano vesicle batch control. *Analyst*. 2016;141(21):6042–50.
23. Chernyshev VS, Rachamadugu R, Tseng YH, Belnap DM, Jia YL, Branch KJ, et al. Size and shape characterization of hydrated and desiccated exosomes. *Anal Bioanal Chem*. 2015;407(12):3285–301.
24. Hogan CJ Jr, Kettleleson EM, Ramaswami B, Chen DR, Biswas P. Charge reduced electrospray size spectrometry of mega- and gigadalton complexes: whole viruses and virus fragments. *Anal Chem*. 2006;78(3):844–52.
25. TJ J, Bothner B, Traina J, Benner WH, Siuzdak G. Electrospray ion mobility spectrometry of intact viruses. *Spectroscopy*. 2004;18:31–6.
26. Pease LF 3rd. Physical analysis of virus particles using electrospray differential mobility analysis. *Trends Biotechnol*. 2012;30(4):216–24.
27. Pease LF 3rd, Lipin DI, Tsai DH, Zachariah MR, Lua LH, Tarlov MJ, et al. Quantitative characterization of virus-like particles by asymmetrical flow field flow fractionation, electrospray differential mobility analysis, and transmission electron microscopy. *Biotechnol Bioeng*. 2009;102(3):845–55.
28. Pease LF 3rd, Tsai DH, Brorson KA, Guha S, Zachariah MR, Tarlov MJ. Physical characterization of icosahedral virus ultra structure, stability, and integrity using electrospray differential mobility analysis. *Anal Chem*. 2011;83(5):1753–9.
29. Laschober C, Wruss J, Blaas D, Szymanski WW, Allmaier G. Gas-phase electrophoretic molecular mobility analysis of size and stoichiometry of complexes of a common cold virus with antibody and soluble receptor molecules. *Anal Chem*. 2008;80(6):2261–4.
30. Kaddis CS, Lomeli SH, Yin S, Berhane B, Apostol MI, Kickhoefer VA, et al. Sizing large proteins and protein complexes by electrospray ionization mass spectrometry and ion mobility. *J Am Soc Mass Spectrom*. 2007;18(7):1206–16.
31. Malm L, Hellman U, Larsson G. Size determination of hyaluronan using a gas-phase electrophoretic mobility molecular analysis. *Glycobiology*. 2012;22(1):7–11.
32. Weiss VU, Golesne M, Friedbacher G, Alban S, Szymanski WW, Marchetti-Deschmann M, et al. Size and molecular weight determination of polysaccharides by means of nano electrospray gas-phase electrophoretic mobility molecular analysis (nES GEMMA). *Electrophoresis*. 2018;39(9–10):1142–50.
33. Szymanski WW, Bacher G, Allmaier G. Applicability of nanoaerosol techniques for measurements of high-mass biopolymers and complexes. In: Szymanski WW, Wagner P, Itoh M, Ohachi T, editors. *Nanostructured materials and their applications*. Vienna: Facultas; 2004. p. 157–66.
34. Mouradian S, Skogen JW, Dorman FD, Zarrin F, Kaufman SL, Smith LM. DNA analysis using an electrospray scanning mobility particle sizer. *Anal Chem*. 1997;69(5):919–25.
35. Saucy DA, Ude S, Lenggoro IW, Fernandez de la Mora J. Mass analysis of water-soluble polymers by mobility measurement of charge-reduced ions generated by electrosprays. *Anal Chem*. 2004;76(4):1045–53.
36. Ude S, Fernandez de la Mora J, Thomson BA. Charge-induced unfolding of multiply charged polyethylene glycol ions. *J Am Chem Soc*. 2004;126(38):12184–90.
37. Muller R, Laschober C, Szymanski WW, Allmaier G. Determination of molecular weight, particle size, and density of high number generation PAMAM dendrimers using MALDI-TOF-MS and nES-GEMMA. *Macromolecules*. 2007;40(15):5599–605.
38. Dudkiewicz A, Wagner S, Lehner A, Chaudhry Q, Pietravalle S, Tiede K, et al. A uniform measurement expression for cross method comparison of nanoparticle aggregate size distributions. *Analyst*. 2015;140(15):5257–67.
39. Grombe R, Charoud-Got J, Emteborg H, Linsinger TP, Seghers J, Wagner S, et al. Production of reference materials for the detection and size determination of silica nanoparticles in tomato soup. *Anal Bioanal Chem*. 2014;406(16):3895–907.
40. Hinterwirth H, Wiedmer SK, Moilanen M, Lehner A, Allmaier G, Waitz T, et al. Comparative method evaluation for size and size-distribution analysis of gold nanoparticles. *J Sep Sci*. 2013;36(17):2952–61.
41. Kallinger P, Weiss VU, Lehner A, Allmaier G, Szymanski WW. Analysis and handling of bio-nanoparticles and environmental nanoparticles using electrostatic aerosol mobility. *Particuology*. 2013;11(1):14–9.
42. Weiss VU, Lehner A, Kerul L, Grombe R, Kratzmeier M, Marchetti-Deschmann M, et al. Characterization of cross-linked gelatin nanoparticles by electrophoretic techniques in the liquid and the gas phase. *Electrophoresis*. 2013;34(24):3267–76.
43. Tsai DH, DelRio FW, Pettibone JM, Lin PA, Tan J, Zachariah MR, et al. Temperature-programmed electrospray-differential mobility analysis for characterization of ligated nanoparticles in complex media. *Langmuir*. 2013;29(36):11267–74.
44. Havlik M, Marchetti-Deschmann M, Friedbacher G, Winkler W, Messner P, Perez-Burgos L, et al. Comprehensive size-determination of whole virus vaccine particles using gas-phase

- electrophoretic mobility macromolecular analyzer, atomic force microscopy, and transmission electron microscopy. *Anal Chem.* 2015;87(17):8657–64.
45. Wieland K, Ramer G, Weiss VU, Allmaier G, Lendl B, Centrone A. Nanoscale chemical imaging of individual chemotherapeutic cytarabine-loaded liposomal nanocarriers. *Nano Res.* 2019;12(1):197–203.
  46. Weiss VU, Wieland K, Schwaighofer A, Lendl B, Allmaier G. Native nano-electrospray differential mobility analyzer (nES GEMMA) enables size selection of liposomal nanocarriers combined with subsequent direct spectroscopic analysis. *Anal Chem.* 2019;91(6):3860–8.
  47. Engel NY, Weiss VU, Marchetti-Deschmann M, Allmaier G. nES GEMMA analysis of lectins and their interactions with glycoproteins - separation, detection, and sampling of noncovalent biospecific complexes. *J Am Soc Mass Spectrom.* 2017;28(1):77–86.
  48. Bacher G, Szymanski WW, Kaufman SL, Zollner P, Blaas D, Allmaier G. Charge-reduced nano electrospray ionization combined with differential mobility analysis of peptides, proteins, glycoproteins, noncovalent protein complexes and viruses. *J Mass Spectrom.* 2001;36(9):1038–52.
  49. Allmaier G, Laschober C, Szymanski WW. Nano ES GEMMA and PDMA, new tools for the analysis of nanobiotopes-protein complexes, lipoparticles, and viruses. *J Am Soc Mass Spectrom.* 2008;19(8):1062–8.
  50. Buck CB, Thompson CD. Production of papillomavirus-based gene transfer vectors. *Curr Protoc Cell Biol.* 2007. <https://doi.org/10.1002/0471143030.cb2601s37>.
  51. Tycova A, Prikryl J, Foret F. Reproducible preparation of nanospray tips for capillary electrophoresis coupled to mass spectrometry using 3D printed grinding device. *Electrophoresis.* 2016;37(7–8):924–30.
  52. van den Heuvel RH, van Duijn E, Mazon H, Synowsky SA, Lorenzen K, Versluis C, et al. Improving the performance of a quadrupole time-of-flight instrument for macromolecular mass spectrometry. *Anal Chem.* 2006;78:7473–83.
  53. Lorenzen K, Versluis C, van Duijn E, van den Heuvel RHH, Heck AJR. Optimizing macromolecular tandem mass spectrometry of large non-covalent complexes using heavy collision gases. *Int J Mass Spectrom.* 2007;268(2–3):198–206.
  54. Contino NC, Pierson EE, Keifer DZ, Jarrold MF. Charge detection mass spectrometry with resolved charge states. *J Am Soc Mass Spectrom.* 2013;24(1):101–8.
  55. Weiss VU, Kerul L, Kallinger P, Szymanski WW, Marchetti-Deschmann M, Allmaier G. Liquid phase separation of proteins based on electrophoretic effects in an electrospray setup during sample introduction into a gas-phase electrophoretic mobility molecular analyzer (CE-GEMMA/CE-ES-DMA). *Anal Chim Acta.* 2014;841:91–8.
  56. Wang Q, Kaltgrad E, Lin T, Johnson JE, Finn MG. Natural supra-molecular building blocks. Wild-type cowpea mosaic virus. *Chem Biol.* 2002;9(7):805–11.
  57. Catalina MI, van den Heuvel RH, van Duijn E, Heck AJ. Decharging of globular proteins and protein complexes in electrospray. *Chemistry.* 2005;11(3):960–8.
  58. Laschober C, Kaddis CS, Reischl GP, Loo JA, Allmaier G, Szymanski WW. Comparison of various nano-differential mobility analysers (nDMAs) applying globular proteins. *J Exp Nanosci.* 2007;2(4):291–301.

**Publisher's note** Springer Nature remains neutral with regard to jurisdictional claims in published maps and institutional affiliations.



**Victor U. Weiss** is an Assistant Professor in the research group “Mass Spectrometric Bio- and Polymer Analytics” at TU Wien, Institute of Chemical Technologies and Analytics, Vienna, Austria. In his research, he focuses on the characterization and detection of nanoparticle material (organic, inorganic, and biological, e.g., liposomes, viruses, and virus-like particles) by application of electrophoretic techniques (liquid-phase electrophoresis in the capillary and the chip

format as well as gas-phase electrophoresis). Furthermore, he works on the on- and offline hyphenation of gas-phase electrophoresis to orthogonal analysis methods.



**Ronja Pogan** is a PhD student at Charlotte Uetrecht's lab at the Heinrich Pette Institute, Leibniz Institute for Experimental Virology in Hamburg, Germany. She studied biology in Hamburg. Her work within the Horizon 2020 project VIRUSCAN aims to characterize viral particles with mass spectrometry focusing on capsid assembly and stability.



**Samuele Zoratto** is a PhD student in the research group “Mass Spectrometric Bio- and Polymer Analytics” at TU Wien, Institute of Chemical Technologies and Analytics, Vienna, Austria. His current project focuses on methods development for the characterization of nano(bio)particles (i.e., virus-like particles) by means of gas-phase electrophoresis (nES GEMMA), atomic force microscopy (AFM), and native mass spectrometry (nMS).



**Kevin M. Bond** is a PhD candidate in Professor Martin F. Jarrold's research lab at Indiana University in Bloomington, Indiana. His research in the Jarrold group has primarily involved investigation of the assembly pathways and products of virus-like particles and the analysis of viral vaccines using charge detection mass spectrometry.



**Nicholas Lykтей** is a PhD candidate in Professor Martin F. Jarrold's research lab at Indiana University in Bloomington, Indiana. His research in the Jarrold group has primarily involved investigation of the gene therapy vector AAV as well as studies of micellular formation using charge detection mass spectrometry.



**Pascale Boulanger** is Head of the Team Bacteriophage T5 of the Institute for Integrative Biology of the Cell (I2BC) in Gif-sur-Yvette, France. She has been studying for many years the mechanisms of infection of bacteria by their natural predators, the bacteriophages, using both in vivo and in vitro approaches. She has been a major contributor in deciphering the structure of phage T5 particle as well as the molecular basis of phage/host recognition and delivery of viral



**Dominik Pahl** is a PhD student in the Institute of Cellular Virology in Münster, Germany. His work is focused on structural features of the human papillomavirus capsid during cell entry.

DNA into the host cell.



**Martin F. Jarrold** is Full Professor and Robert and Marjorie Mann Chair in the Chemistry Department at Indiana University in Bloomington, Indiana. His current research focusses on the development and applications of charge detection mass spectrometry.



**Nicole Puffler** graduated with her Master's from TU Wien where she studied "Technical Chemistry." She focused on analytical chemistry and wrote her bachelor and master thesis within the Institute of Chemical Technologies and Analytics (TU Wien, Vienna, Austria).



**Mario Schelhaas** is Director of the Institute of Cellular Virology at the University of Münster, Germany. His work is focussed on structural and cell biological aspects of virus entry (particularly of small non-enveloped DNA viruses) into host cells with a strong emphasis on imaging techniques.



**Charlotte Utrecht** is Junior Group Leader at the Heinrich Pette Institute, Leibniz Institute for Experimental Virology, Hamburg, Germany, and guest scientist at the European XFEL GmbH, Schenefeld, Germany. Her research focuses on dynamics of viral structures using structural mass spectrometry. She studied biochemistry in Potsdam, Germany, obtained her PhD from Utrecht University in the lab of Albert Heck and did a postdoc in Uppsala, Sweden, and at

European XFEL.



**Ekaterina Selivanovitch** is a 4th year chemistry PhD student in the Douglas Lab at Indiana University. Her current research is based on the development of biomimetic materials using virus-like particles. She received a B.S. in chemistry from St. Francis College in Brooklyn, NY, and a M.S. in chemistry from St. John's University in Queens, NY.



**Günter Allmaier** is Full Professor of Analytical Chemistry in the research group "Mass Spectrometric Bio- and Polymer Analytics" at TU Wien, Institute of Chemical Technologies and Analytics, Vienna, Austria. Since the beginning of the 1980s, he has been working in the field of mass spectrometry and analysis of bioactive compounds with emphasis on therapeutic proteins and proteomics/lipidomics. During the last 15 years, he has also been engaged in the field of electrophoretic separation in the liquid and gas phase of various classes of biomolecules and nano(bio)particles.

retic separation in the liquid and gas phase of various classes of biomolecules and nano(bio)particles.

## **2.2. Norovirus-like VP1 particles exhibit isolate dependent stability profiles.**

Ronja Pogan, Carola Schneider, Rudolph Reimer, Grant Hansman, and Charlotte Uetrecht

*J. Phys.: Condens. Matter* 30 064006 (2018)

This article is distributed under the terms of the [Creative Commons Attribution 3.0 licence](https://creativecommons.org/licenses/by/3.0/).

<https://creativecommons.org/licenses/by/3.0/>, listed in this work under the reference (Pogan et al., 2018b).

To access the publication see

<https://doi.org/10.1088/1361-648X/aaa43b>

# Norovirus-like VP1 particles exhibit isolate dependent stability profiles

Ronja Pogan<sup>1</sup>, Carola Schneider<sup>1</sup>, Rudolph Reimer<sup>1</sup>, Grant Hansman<sup>2,3</sup>  
and Charlotte Uetrecht<sup>1,4</sup> 

<sup>1</sup> Heinrich Pette Institute, Leibniz Institute for Experimental Virology, Hamburg, Germany

<sup>2</sup> Department of Infectious Diseases, Virology, Heidelberg University, Heidelberg, Germany

<sup>3</sup> Schaller Research Group at the University of Heidelberg and the DKFZ, Heidelberg, Germany

<sup>4</sup> European XFEL, Schenefeld, Germany

E-mail: [charlotte.uetrecht@xfel.eu](mailto:charlotte.uetrecht@xfel.eu)

Received 1 November 2017, revised 19 December 2017

Accepted for publication 28 December 2017

Published 18 January 2018



## Abstract

Noroviruses are the main cause of viral gastroenteritis with new variants emerging frequently. There are three norovirus genogroups infecting humans. These genogroups are divided based on the sequence of their major capsid protein, which is able to form virus-like particles (VLPs) when expressed recombinantly. VLPs of the prototypical GI.1 Norwalk virus are known to disassemble into specific capsid protein oligomers upon alkaline treatment. Here, native mass spectrometry and electron microscopy on variants of GI.1 and of GII.17 were performed, revealing differences in terms of stability between these groups. Beyond that, these experiments indicate differences even between variants within a genotype. The capsid stability was monitored in different ammonium acetate solutions varying both in ionic strength and pH. The investigated GI.1 West Chester isolate showed comparable disassembly profiles to the previously studied GI.1 Norwalk virus isolate. However, differences were observed with the West Chester being more sensitive to alkaline pH. In stark contrast to that, capsids of the variant belonging to the currently prevalent genogroup GII were stable in all tested conditions. Both variants formed smaller capsid particles already at neutral pH. Certain amino acid substitutions in the S domain of West Chester relative to the Norwalk virus potentially result in the formation of these  $T = 1$  capsids.

Keywords: virus assembly, native mass spectrometry, structural virology, capsid stability, VLP size

 Supplementary material for this article is available [online](#)

(Some figures may appear in colour only in the online journal)

## 1. Introduction

Human noroviruses cause the majority of nonbacterial gastroenteritis outbreaks worldwide (Ahmed *et al* 2014). Symptoms include fever, vomiting, and diarrhea that usually last for several days (Kaplan *et al* 1982). In addition to the surface of fecal contaminated food, noroviruses can be found in

environmental samples such as sewage and spread through person-to-person contact (Kaplan *et al* 1982, Hedberg and Osterholm 1993, Ozawa *et al* 2007). A small number of particles of this pathogen is sufficient for infection. Severe disease is mostly observed in the elderly, children and immunocompromised people (Teunis *et al* 2008).

Noroviruses belong to the *Caliciviridae* family and are non-enveloped, single-stranded, positive-sense ribonucleic acid (RNA) viruses. Human norovirus genomes are 7.4–7.7 kb in length and have three open reading frames (ORFs). The non-structural proteins, such as the RNA dependent polymerase

 Original content from this work may be used under the terms of the [Creative Commons Attribution 3.0 licence](#). Any further distribution of this work must maintain attribution to the author(s) and the title of the work, journal citation and DOI.

(RdRp), are encoded by ORF1, while the structural proteins are encoded by ORF2 (VP1) and ORF3 (VP2) (Xi *et al* 1990, Jiang *et al* 1993). The major capsid protein VP1 forms dimers, which assemble into the viral capsid with  $T = 3$  icosahedral symmetry of approximately 36–42 nm diameter. VP2 is considered as minor capsid protein and carries multiple functions, which are still not completely deciphered (Vongpunsawad *et al* 2013). VP1 can be divided into a shell (S) domain and a protruding (P) domain, which is further subdivided into P1 and P2. The S domain forms a scaffold surrounding the viral RNA with a diameter of 30 nm, whereas the genetically more variable P domain builds the viral spikes and facilitates cell attachment (Prasad *et al* 1994, 1999). Research on human noroviruses has been limited by the lack of a robust cell culture system. Nevertheless, production of virus-like VP1 particles (VLPs) show comparable characteristics to the native virion (Jiang *et al* 1992). Electron microscopy (EM) and x-ray crystallography studies have deepened the understanding of capsid assembly and interactions with potential receptors like human histo-blood group antigens (Harrington *et al* 2002, Tan and Jiang 2005).

Native mass spectrometry (MS) has further elucidated these processes (Shoemaker *et al* 2010, Utrecht and Heck 2011, Mallagaray *et al* 2015). Here, intact non-covalent protein complexes are transferred into the gas phase from an aqueous solution of a volatile buffer surrogate, such as ammonium acetate, via nano-electrospray ionization (ESI). All coexisting oligomers can be detected with high sensitivity, allowing to monitor assembly processes. Recently, charge detection MS has been introduced, enabling simultaneous charge and mass-to-charge ( $m/z$ ) ratio determination and therefore mass assignment of single ions (Keifer *et al* 2017). VLPs can also be analyzed by mobility-based approaches (Weiss *et al* 2015). However, ESI with time-of-flight (ToF) detectors are mostly employed, which rely on charge state resolution for exact mass assignment of  $m/z$  signals.

Remarkably, Shoemaker *et al* demonstrated the alkaline and ionic strength sensitivity of norovirus VLPs, and showed that capsid disassembly was reversible (Shoemaker *et al* 2010). VLPs completely disassembled at low ionic strength and alkaline pH, whereas smaller particles formed at high ionic strength in alkaline conditions. Most importantly, they showed that small VLPs, which were previously observed in EM under alkaline conditions, corresponded to  $T = 1$  capsids. The dynamic behavior of VP1 upon changing pH may have implications for the infection process as the virus passes through very different environments in the intestinal tract. Using ion mobility, pH dependent intermediates were shown to be consistent with partial capsid structures and an assembly pathway was proposed (Utrecht *et al* 2011). These findings confirmed previous studies, which combined EM with spectroscopic techniques like circular dichroism and high resolution second-derivative UV absorption spectroscopy (Ausar *et al* 2006).

Importantly, MS studies focused on the prototypical Norwalk virus first isolated in 1972 in Ohio (Kapikian *et al* 1972), disregarding the emergence of new variants, which could exhibit altered assembly behavior. Noroviruses can be

divided into at least seven genogroups (GI–GVII), with GI, GII, and GIV causing infections in human. Each genogroup can be further subdivided into numerous genotypes based on the capsid amino acid sequences (Kageyama *et al* 2004, Hansman *et al* 2006). The prototypical Norwalk virus (GI.1 Norwalk) is rarely found to cause outbreaks nowadays. It is replaced by strains of the genogroup II, where GII.4 noroviruses have been prevalent (Eden *et al* 2013). A reemerging genotype of this genogroup, GII.17, seems to become a major threat nowadays in East Asia. First isolated in 1978, they were the cause of several outbreaks in Asia in 2014 to 2015 (Chan *et al* 2015, Lee *et al* 2015, Zhang *et al* 2015, Singh *et al* 2016).

Here, GI.1 West Chester noroviruses closely related to and isolated three decades after the Norwalk strain and a newly emerging GII.17 variant isolated 2015 in Kawasaki, Japan, are compared. The VLP stability in different pH and ionic strength conditions of these genotypes was examined using native MS and negative stain EM. Surprisingly, the outbreak-causing isolate showed a much stronger resistance to pH. Furthermore, both variants form smaller  $T = 1$  capsids at neutral pH, which points to amino acid substitutions potentially influencing the particle size. Differences between variants in terms of mass and stability hint towards new approaches for virus identification.

## 2. Experimental details

### 2.1. VLP production and preparation

In order to produce norovirus VLPs, recombinant VP1 protein was expressed in insect cells as described previously (Hansman *et al* 2005, 2007). Genebank accession numbers are AY602016.1 and Kawasaki308 for the GI.1 and GII.17 variant, respectively. Briefly, recombinant VP1 bacmid was transfected into *Spodoptera frugiperda* (Sf9) cells using Effectene. After incubation for five days at 27 °C, the cell culture medium was clarified by low-speed centrifugation. The supernatant containing the baculovirus was used to infect high five (H5) insect cells for 6 d at 27 °C. To separate secreted VLPs from the cell medium and cells, the solution was centrifuged at low speed and then concentrated by ultracentrifugation at 35 000 rpm for 2 h at 4 °C. VLPs were purified using a caesium chloride (CsCl) equilibrium gradient ultracentrifugation at 35 000 rpm for 18 h at 4 °C and then stored in phosphate buffered saline at 4 °C at a concentration of 3–5 mg ml<sup>-1</sup>.

Prior to MS and EM analysis, the VLPs were exchanged into 50 and 250 mM ammonium acetate solutions at different pH using Vivaspin 500 centrifugal concentrators (10 000 MWCO, Sartorius, Göttingen, Germany). Zeba micro spin™ desalting columns 0.5 ml (7000 MWCO, Thermo Fisher Scientific, Massachusetts, USA) were used if protein yields were too low for analysis using Vivaspin.

### 2.2. Mass spectrometry

Native MS measurements on VLPs were performed on a Q-ToF 2 instrument (Waters, Manchester, UK and MS Vision, Almere, the Netherlands) with modifications enabling high

mass experiments (van den Heuvel *et al* 2006). All spectra were recorded in positive ion mode. Generally, samples were measured at a VP1 concentration of 10  $\mu\text{M}$ . Ions were introduced via a nano-ESI source into the vacuum at a source pressure of 10 mbar using both premade (Waters, Manchester, UK) and handmade capillaries. For the in-house production, borosilicate glass tubes (inner diameter 0.68 mm, outer diameter 1.2 mm with filament; World Precision Instruments, Sarasota, USA) were pulled using a two-step program in a micropipette puller (Sutter Instruments, Novato, USA) with a squared box filament ( $2.5 \times 2.5$  mm). The capillaries were gold-coated using a sputter coater (Quorum Technologies Ltd., East Sussex, UK, 40 mA, 200 s, tooling factor of 2.3 and end bleed vacuum of  $8 \times 10^{-2}$  mbar argon) and opened directly on the sample cone of the mass spectrometer. Voltages of 1.55–1.65 kV and 145–155 V were applied to the capillary and cone, respectively. Xenon was used as a collision gas at a pressure of  $2.0 \times 10^{-2}$  mbar to improve the transmission of large ions (Lorenzen *et al* 2007). Starting from 10 V, collision energies were increased up to 200 V in steps of 25 V. The presented spectra were generally recorded at 50 V collision energy. MS profile and pusher settings were kept constant for all measurements. A caesium iodide spectrum was recorded the same day in order to test the performance of the instrument and to calibrate spectra where necessary. Analysis was performed using MassLynx™ (Waters, Manchester, UK). In order to generate intensity fraction plots, signals were accumulated over 100 s and in a respective  $m/z$  range all signals belonging to the broad ion distributions of a given oligomer were summed. The range was kept constant for both variants to simplify comparison, although ion distribution widths varied. Tables S2 and S3 ([stacks.iop.org/JPhysCM/30/064006/mmedia](https://stacks.iop.org/JPhysCM/30/064006/mmedia)) list respective  $m/z$  ranges that correspond to different VP1 oligomers and their intensity fractions.

### 2.3. Electron microscopy

After buffer exchange to ammonium acetate solutions, the norovirus VLPs were stored at 4 °C. The samples were adsorbed onto glow discharge-activated carbon coated grids (Science Services, Munich, Germany) after storage in ammonium acetate solution. The sample coated grids were washed three times with distilled water, following a negative staining with 1% uranyl acetate. Images were acquired using the FEI Tecnai™ G2 transmission electron microscope and the wide angle Veleta CCD camera (FEI, Thermo Fisher Scientific, USA and Olympus, Tokyo, Japan) at 80 kV.

## 3. Results and discussion

### 3.1. Altered capsid stability and size distribution in Gl.1 isolates

In order to compare the stability of VLPs within a genotype, native MS measurements in varying solution conditions were performed according to Shoemaker *et al* (2010). They observed the intact  $T = 3$  capsid, at neutral and near neutral pH, which disassembled upon alkaline treatment into VP1 oligomers.

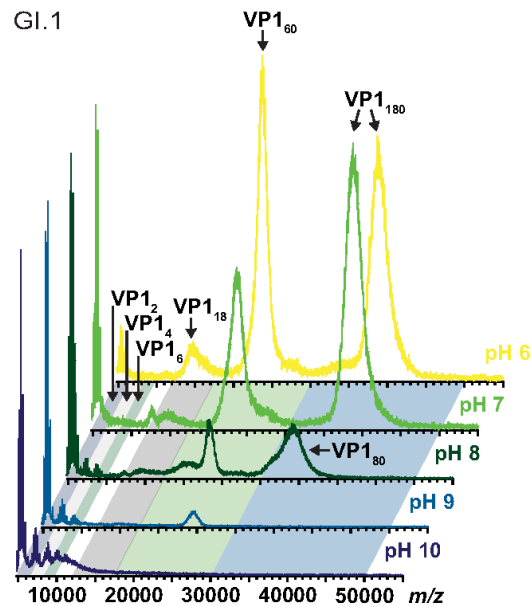


**Figure 1.** Norovirus GI.1 West Chester VLP stability monitored by native MS. Representative mass spectra of norovirus VLPs (10  $\mu\text{M}$  VP1) at pH values indicated (from top to bottom pH 6–10) in 250 mM ammonium acetate. Data are normalized to the highest peak.

Whereas the prototypical GI.1 Norwalk virus was investigated previously, the GI.1 West Chester variant is studied here. Our assignment of ion distributions is analogous to the Norwalk results (Shoemaker *et al* 2010), since VP1 heterogeneity again precluded charge state resolution (figure S1). The broad ion distribution around  $m/z$  40 000 indicates the presence of intact VLPs consisting of 180 copies of the VP1 protein (figure 1). The observed  $m/z$  is in line with the linear relation of charge state to the square root of the mass (Heck and van den Heuvel 2004) and is therefore assigned to  $T = 3$  particles. Following this scheme, further VP1 oligomers, namely VP1 80 mers and 60 mers ( $T = 1$ ), can be assigned in high ionic strength solutions (250 mM ammonium acetate) at pH ranging from 6–10 (figure 1). Intact  $T = 3$  is observed at pH 6 and pH 7. A shift of the corresponding ion distribution at pH 8 indicates that  $T = 3$  disassembles and instead VP1 80 mers form. A second dominant ion distribution is located around  $m/z$  20 000. Ions in this  $m/z$  region can be assigned to the  $T = 1$  capsid. These ions are detected at pH 6 up to pH 9 and high ionic strength, although with strongly decreasing signals at alkaline pH. Several smaller oligomers are detected up to pH 8 between  $m/z$  10 000–20 000 in line with disassembly of  $T = 3$  and reformation of 80 mer particles. The dominant signal around  $m/z$  15 000 corresponds to VP1 18 mers already detected at pH 6. VP1 6 mers and 4 mers are observed in solutions at pH 7 and higher. VP1 dimers are present in all tested solutions with strongly increasing signals upon alkaline treatment. To further illustrate and confirm the different VP1 oligomers, the ammonium acetate VLP preparations were imaged in negative

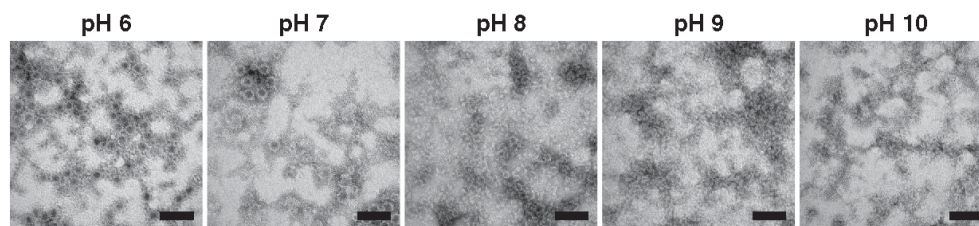


**Figure 2.** EM images of norovirus GI.1 West Chester VLPs. VLPs are in 250mM ammonium acetate solutions with increasing pH from left to right. The bar represents 100nm. All images are taken at the same magnification.

stain EM (figure 2). At pH 6 and pH 7, round structures with a diameter of about 40 nm corresponding to intact  $T = 3$  capsids can be found. Smaller particles with a diameter of about 20 nm are also seen in pH 6–8, likely the detected  $T = 1$  particles. Size estimation is affected by aggregation. However, a clear trend in line with the MS measurements is observed as bigger spherical structures are no longer visible at pH 9 and 10.

Notably, West Chester VP1 60 mers are present in ammonium acetate solutions from pH 6 up to pH 9, whereas 60 mers were only observed at pH 8 and pH 9 for the Norwalk virus despite comparable measurement conditions and very similar purification protocols. In both protocols a baculovirus expression system was used and VLPs were purified via CsCl gradient centrifugation. The  $T = 1$  particles with a diameter of approximately 21 nm are a known byproduct in VLP production and also found in stool samples (Taniguchi *et al* 1981, White *et al* 1997). Truncated VP1 proteins were described as a possible reason for formation of smaller particles (Huo *et al* 2015). The versions of West Chester VP1 observed in the low  $m/z$  region after particle disassembly show differences in methionine processing ( $\Delta m \sim 270$ Da per monomer) as was previously described for Norwalk VP1 (Shoemaker *et al* 2010). Therefore, the  $T = 1$  formation likely represents an intrinsic property of the VP1 protein. This is also in agreement with the observation of  $T = 3$  particles at neutral pH of the Norwalk virus S domain (Baclayon *et al* 2011). Nevertheless, it cannot be ruled out that small particles in stool samples are  $T = 3$  particles lacking the P domain or other aberrant assemblies. Furthermore, West Chester VLPs are more sensitive to alkaline treatment as they disassemble at even lower pH than the previously described Norwalk virus (Shoemaker *et al* 2010). Smaller oligomers, such as the VP1 18 mer, are also detected at lower pH values for the West Chester. Importantly like Norwalk, the West Chester virus retained the ability to reversibly assemble when diluted from a high pH solution into a low pH solution including reformation of  $T = 1$  particles (figure S2).

### 3.2. GII.17 Kawasaki norovirus shows vast stability at alkaline pH

Although the Norwalk virus is known as the prototype strain, GI noroviruses have been replaced by emerging GII noroviruses (Blanton *et al* 2006). It is therefore of interest, whether these still exhibit a similar stability profile as GI noroviruses, in other words whether particle stability is a conserved

feature in noroviruses. Therefore, GII.17 Kawasaki VLPs are also analyzed with native MS (figure 3). Broad ion distributions corresponding to the  $T = 3$  and  $T = 1$  intact capsids are detected throughout the whole pH range (pH 6–10) both at low (50 mM ammonium acetate, figure 3) and high ionic strength (250 mM ammonium acetate, figure S3(A)). The ratios of the capsid sizes remain unchanged up to pH 9. At pH 10, mild disassembly is observed, as is evident from the arising dimer signal. Based on the intensity fractions, no preference for disassembly of either capsid form is observed. Disulfide bonds as cause of this extraordinary stabilization can be excluded, as no additional bands corresponding to oligomers are observed under non-reducing conditions in SDS-PAGE (figure S4).

Ions in the  $m/z$  range of 30000–50000  $m/z$  assigned to  $T = 3$  signal cannot be detected above pH 7 for the GI.1 West Chester in 50 mM ammonium acetate (figure 3(B)). At pH 7 however, the signal already shifts to lower  $m/z$  as it does in 250 mM ammonium acetate, pH 8; therefore it likely corresponds to VP1 80 mers and not complete  $T = 3$  particles. At pH 9, also  $T = 1$  particles have disappeared. Thus, West Chester VLPs maintain a lower stability at lower ionic strength as was shown for Norwalk VLPs (Shoemaker *et al* 2010). Conversely, the Kawasaki VLPs show a more intense VP1 dimer signal at pH 10 at higher ionic strength indicative of decreased stability (figures 3(C) and S3(C)). VLP solutions were further imaged in negative stain EM (figure 4). Spherical structures with a diameter of about 40 nm can be found in all conditions for GII.17 Kawasaki VLPs. For GI.1 West Chester VLPs, the  $T = 3$  is most obvious at pH 6. Consistent with the findings at high ionic strength, several smaller West Chester VP1 oligomers arise with alkaline treatment albeit with less defined size (figures 1 and 3).

The mass spectra and intensity fractions are normalized and therefore do not include information on the absolute amount of assemblies or altered electrospray ionization due to pH induced changes. To further illustrate differences between the strains, absolute intensities for  $m/z$  ranges corresponding to  $T = 3$ ,  $T = 1$  and a combined lower  $m/z$  range (corresponding to VP1 oligomers between 4800 to 9600  $m/z$  at 50 mM and 4800–17500  $m/z$  at 250 mM) are plotted (figure S5). The GII.17 ion signals for both capsid forms are increasing up to pH 9 until they drop again at pH 10 in 250 mM ammonium acetate. The ion counts for both forms are overall lower at 50 mM ammonium acetate but less affected by pH. Furthermore, the spray is more stable at low ionic strength as is evident from smaller error bars. In contrast,

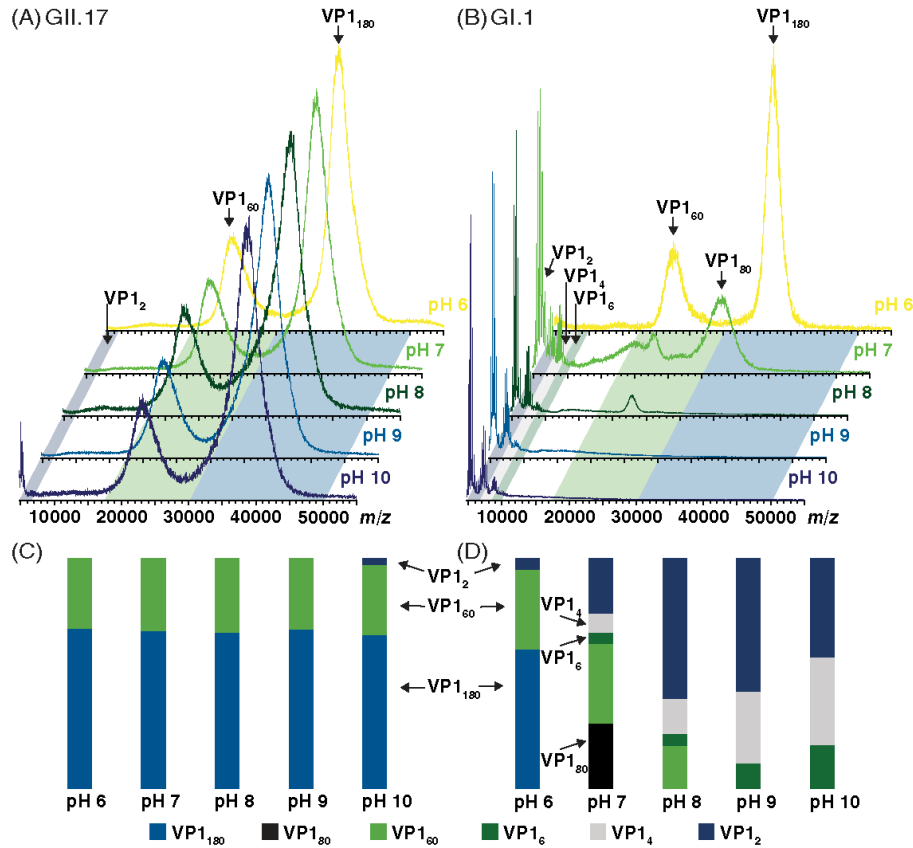


**Figure 3.** Comparison of norovirus VLP stability monitored by native MS at low ionic strength. Representative mass spectra of norovirus VLPs ( $10 \mu\text{M}$  VP1) in 50mM ammonium acetate at pH values indicated (from top to bottom pH 6–10) (A) mass spectra obtained for the GII.17 Kawasaki virus and (B) for the GI.1 West Chester virus. Data are normalized to the highest peak. Colored inlets indicate the respective  $m/z$  range, where intensities were summed for the respective VP1 oligomers. Due to overlapping distributions, the VP1 80 mer falls into the same  $m/z$  range as VP1 180 mers, the descriptor therefore changes at pH 7 in (D). The intensity fractions of oligomers are shown for GII.17 Kawasaki (C) and for GI.1 West Chester (D) viruses. Spectra for measurements in 250mM ammonium acetate can be found in figure S3 of both variants.

ion counts for GI.1 West Chester capsids are always lower but reproducible. High intensity counts can only be obtained for the signal corresponding to low mass VP1 oligomers upon VLP dissociation.

#### 4. Discussion

The two human norovirus strains GI.1 West Chester and GII.17 Kawasaki show a completely different pattern when monitored in ammonium acetate solutions of increasing pH. The GI.1 West Chester virus behaves similar to Norwalk virus (Shoemaker *et al* 2010) and disassembles upon alkaline treatment into capsid protein oligomers. The alkaline sensitivity is furthermore dependent on ionic strength, as higher ionic strength favors higher-mass oligomers. In stark contrast, GII.17 Kawasaki VLPs exhibit immense stability throughout the tested pH range up to pH 10. Capsid destabilization is indicated only at pH 10 as VP1 dimer peaks arise in low

abundance. For GII.17 Kawasaki VLPs, the influence of ionic strength is low but inverted compared to GI.1 West Chester and Norwalk viruses.

Previous studies using various techniques on norovirus VLP stability were able to show alkaline sensitivity for the Norwalk virus (Ausar *et al* 2006, Shoemaker *et al* 2010, da Silva *et al* 2011). Stability studies on noroviruses are of special interest, as these are foodborne and need to persist in various environmental settings. The influence of temperature, ionic strength and pH on the adhesion of VLPs to surfaces also revealed higher stability and more adhesion for GII.4 viruses than GI.1 (da Silva *et al* 2011, Samandoulgou *et al* 2015). However, the investigated pH range was limited. In 2010, Donath and coworkers investigated the norovirus genotype GII.7 with atomic force microscopy (AFM) in a pH range of 2–10 (Cuellar *et al* 2010). Despite belonging to GII genotype, VLPs were found to be sensitive to alkaline treatment. GII.7 noroviruses were reported as slowly evolving genotypes

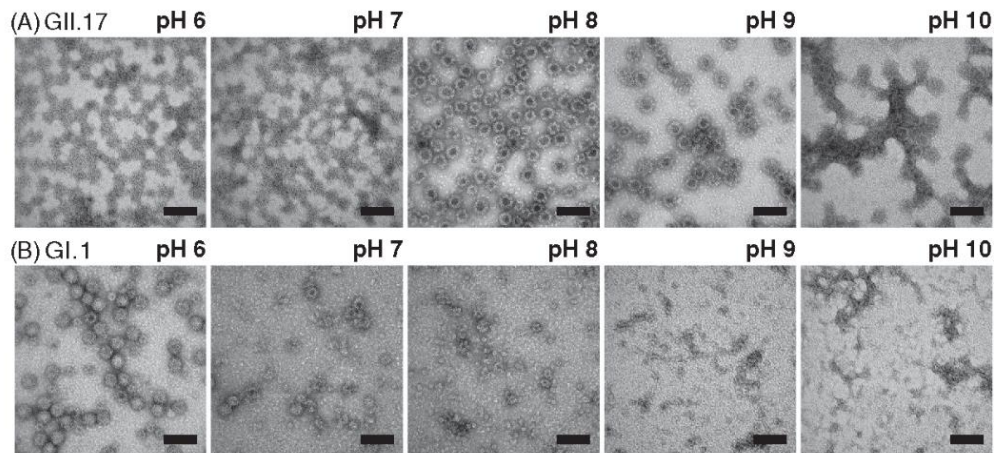


**Figure 4.** EM images of norovirus VLPs in 50mM ammonium acetate. Images of VLPs of GII.17 Kawasaki virus (A) and of GI.1 West Chester virus (B) in increasing pH solutions from left to right (pH 6–10, respectively). The bar represents 100 nm. Images were taken at the same magnification.

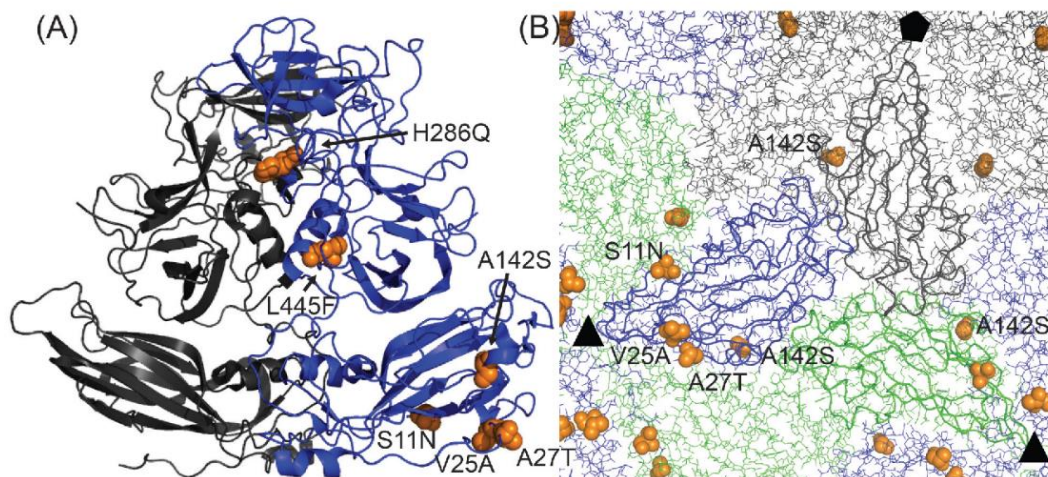


**Figure 5.** Norovirus GI.1 Norwalk and GI.1 West Chester capsid protein VP1 show six dissimilar substitutions. (A) Cartoon structure of a Norwalk VP1 dimer (PDB: 1IHM, residues 10–520) with quasi-equivalent monomers A (grey) and B (blue). Amino acids substituted for similar residues are not shown. Only the B subunit has a sufficiently resolved N-terminal arm to observe all four dissimilar amino acids in the S domain (bottom). The upper P domain only contains two major substitutions at the intra-dimer interface. All dissimilar residues are depicted as orange spheres and the substitution from Norwalk to West Chester is annotated. (B) S domains in the capsid context viewed from the interior with one subunit each (A—grey, B—blue, C—green) highlighted as ribbon. All substituted residues locate to the inter-dimer interface. Threefold and fivefold symmetry axes are labelled with black symbols.

with decreasing prevalence (Hoffmann *et al* 2012). Based on these and our own findings on GI.1 and emerging GII.17 viruses, it is tempting to speculate whether increased VLP stability could be related to prevalence. However, other causes cannot be excluded and genome containing viruses likely have altered stability profiles.

A sequence alignment of VP1 of GI.1 Norwalk and West Chester virus reveals 13 substitutions (figure S6), with seven amino acids exchanged for similar residues. Four out of the six dissimilar residues are located in the S domain (N-terminal 225 amino acids); all of them are located at the dimer surface

and potentially involved in inter-dimer contacts (figure 5). Substitutions for similar amino acids are exclusively found in the P domain together with two dissimilar residues close to the intra-dimer interface and therefore unlikely to cause the differences in assembly behavior. The P domain also contains the only substitution involving charged residues (H286Q), therefore altered electrostatic interactions are an unlikely cause of the observed changes. In light of the Norwalk S domain, which assembles into  $T = 3$  particles like the full length protein VP1 albeit with lower stability (Baclayon *et al* 2011), the amino acid exchanges in the S domain most likely cause

the occurrence of the smaller West Chester  $T = 1$  at neutral pH. Which amino acids contribute to stability or alteration of capsid size requires further investigations by mutagenesis. Nevertheless, the quasi-equivalent *B* subunit shows a serine to asparagine substitution at residue 11 in the N-terminal arm, which directly interfaces with the  $\beta$ -sheet of subunit *C*. *A/B* and *C/C* dimers show a different arrangement of the *S* domain, bent and flat, respectively (Prasad *et al* 1999). The substitution at residue 11 may alter the capability of the VP1 protein to switch to the alternate *C* conformation and therefore also small particles can form at neutral pH. The GI.1 Norwalk and GII.17 Kawasaki sequences are 46% identical (figure S6). The substitutions are located across the entire sequence but with higher frequency in the *P* domain. However, in all three variants the pI remains similar (Norwalk virus pI 5.64, West Chester isolate pI 5.57 and Kawasaki isolate pI 5.24). Given the number of substitutions, it is impossible to link the increased stability to any specific residues. Interestingly, residue 11 is not substituted in Kawasaki virus but flanked by two substitutions, S10P and V12N, which could again be an explanation for the increased  $T = 1$  amount compared to Norwalk virus. Again, further studies are required to pinpoint the residues responsible for the observed stability and size differences.

This study demonstrates that native MS is the method of choice to investigate genotype and even isolate specific stability differences as it can resolve the different assembly states. The combination with negative stain EM confirmed the observed differences between norovirus-like particles of different genogroups. Notably, also isolates from the same genotype show distinct profiles and can pinpoint residues altering the assembly. The results are therefore informative for designing capsids with specific properties for nanotechnological applications (Worsdorfer *et al* 2011). It is of interest to test whether ligand binding to e.g. glycans alters the stability profiles, which would be indicative of structural changes. Furthermore, if stability differences persist at the virion level, mass determination in conjunction with determination of mechanical properties from AFM or similar methods could have potential as a diagnostic tool with the capability to distinguish specific isolates. Especially for rapidly evolving RNA viruses like noroviruses, this is a promising approach to identify new variants without the need for prior knowledge.

## Acknowledgments

The Heinrich-Pette-Institute, Leibniz Institute for Experimental Virology is supported by the Freie und Hansestadt Hamburg and the Bundesministerium für Gesundheit (BMG). CU acknowledges funding from the Leibniz Association through SAW-2014-HPI-4 grant. RP acknowledges funding from EU Horizon 2020 project VIRUSCAN 731868. CU, RP and GH further thank the DFG FOR2327 Viocarbo for support. We thank the HPI microscopy technology platform for help acquiring the electron microscopy images.

## ORCID iDs

Charlotte Uetrecht  <https://orcid.org/0000-0002-1991-7922>

## References

- Ahmed S M, Hall A J, Robinson A E, Verhoef L, Premkumar P, Parashar U D, Koopmans M and Lopman B A 2014 Global prevalence of norovirus in cases of gastroenteritis: a systematic review and meta-analysis *Lancet Infect. Dis.* **14** 725–30
- Ausar S F, Foubert T R, Hudson M H, Vedvick T S and Middaugh C R 2006 Conformational stability and disassembly of Norwalk virus-like particles. Effect of pH and temperature *J. Biol. Chem.* **281** 19478–88
- Baclayon M, Shoemaker G K, Uetrecht C, Crawford S E, Estes M K, Prasad B V, Heck A J, Wuite G J and Roos W H 2011 Prestress strengthens the shell of Norwalk virus nanoparticles *Nano Lett.* **11** 4865–9
- Blanton L H, Adams S M, Beard R S, Wei G, Bulens S N, Widdowson M-A, Glass R I and Monroe S S 2006 Molecular and epidemiologic trends of caliciviruses associated with outbreaks of acute gastroenteritis in the United States, 2000–2004 *J. Infect. Dis.* **193** 413–21
- Chan M C, Lee N, Hung T N, Kwok K, Cheung K, Tin E K, Lai R W, Nelson E A, Leung T F and Chan P K 2015 Rapid emergence and predominance of a broadly recognizing and fast-evolving norovirus GII.17 variant in late 2014 *Nat. Commun.* **6** 10061
- Cuellar J L, Meinhoevel F, Hoehne M and Donath E 2010 Size and mechanical stability of norovirus capsids depend on pH: a nanoindentation study *J. Gen. Virol.* **91** 2449–56
- da Silva A K, Kavanagh O V, Estes M K and Elimelech M 2011 Adsorption and aggregation properties of norovirus GI and GII virus-like particles demonstrate differing responses to solution chemistry *Environ. Sci. Technol.* **45** 520–6
- Eden J S, Tanaka M M, Boni M F, Rawlinson W D and White P A 2013 Recombination within the pandemic norovirus GII.4 lineage *J. Virol.* **87** 6270–82
- Hansman G S *et al* 2006 Genetic and antigenic diversity among noroviruses *J. Gen. Virol.* **87** 909–19
- Hansman G S, Natori K, Oka T, Ogawa S, Tanaka K, Nagata N, Ushijima H, Takeda N and Katayama K 2005 Cross-reactivity among sapovirus recombinant capsid proteins *Arch. Virol.* **150** 21–36
- Hansman G S, Saito H, Shibata C, Ishizuka S, Oseto M, Oka T and Takeda N 2007 Outbreak of gastroenteritis due to sapovirus *J. Clin. Microbiol.* **45** 1347–9
- Harrington P R, Lindesmith L, Yount B, Moe C L and Baric R S 2002 Binding of norwalk virus-like particles to ABH histo-blood group antigens is blocked by antisera from infected human volunteers or experimentally vaccinated mice *J. Virol.* **76** 12335–43
- Heck A J R and van den Heuvel R H H 2004 Investigation of intact protein complexes by mass spectrometry *Mass Spectrom. Rev.* **23** 368–89
- Hedberg C W and Osterholm M T 1993 Outbreaks of food-borne and waterborne viral gastroenteritis *Clin. Microbiol. Rev.* **6** 199–210
- Hoffmann D, Hutzenthaler M, Seebach J, Panning M, Umgelter A, Menzel H, Protzer U and Metzler D 2012 Norovirus GII.4 and GII.7 capsid sequences undergo positive selection in chronically infected patients *Infect. Genet. Evol.* **12** 461–6
- Huo Y, Wan X, Wang Z, Meng S and Shen S 2015 Production of norovirus VLPs to size homogeneity *Virus Res.* **204** 1–5

- Jiang X, Wang M, Graham D Y and Estes M K 1992 Expression, self-assembly, and antigenicity of the Norwalk virus capsid protein *J. Virol.* **66** 6527–32
- Jiang X, Wang M, Wang K and Estes M K 1993 Sequence and genomic organization of Norwalk virus *Virology* **195** 51–61
- Kageyama T, Shinohara M, Uchida K, Fukushi S, Hoshino F B, Kojima S, Takai R, Oka T, Takeda N and Katayama K 2004 Coexistence of multiple genotypes, including newly identified genotypes, in outbreaks of gastroenteritis due to Norovirus in Japan *J. Clin. Microbiol.* **42** 2988–95
- Kapikian A Z, Wyatt R G, Dolin R, Thornhill T S, Kalica A R and Chanock R M 1972 Visualization by immune electron microscopy of a 27 nm particle associated with acute infectious nonbacterial gastroenteritis *J. Virol.* **10** 1075–81
- Kaplan J E, Feldman R, Campbell D S, Lookabaugh C and Gary G W 1982 The frequency of a Norwalk-like pattern of illness in outbreaks of acute gastroenteritis *Am. J. Public Health* **72** 1329–32
- Keifer D Z, Pierson E E and Jarrold M F 2017 Charge detection mass spectrometry: weighing heavier things *Analyst* **142** 1654–71
- Lee C-C, Feng Y, Chen S-Y, Tsai C-N, Lai M-W and Chiu C-H 2015 Emerging Norovirus GII.17 in Taiwan *Clin. Infect. Dis.* **61** 1762–4
- Lorenzen K, Versluis C, Van Duijn E, Van Den Heuvel R H H and Heck A J R 2007 Optimizing macromolecular tandem mass spectrometry of large non-covalent complexes using heavy collision gases *Int. J. Mass Spectrom.* **268** 198–206
- Mallagaray A, Lockhauserbaumer J, Hansman G, Uetrecht C and Peters T 2015 Attachment of norovirus to histo blood group antigens: a cooperative multistep process *Angew. Chem., Int. Ed. Engl.* **54** 12014–9
- Ozawa K, Oka T, Takeda N and Hansman G S 2007 Norovirus infections in symptomatic and asymptomatic food handlers in Japan *J. Clin. Microbiol.* **45** 3996–4005
- Prasad B V, Hardy M E, Dokland T, Bella J, Rossmann M G and Estes M K 1999 X-ray crystallographic structure of the Norwalk virus capsid *Science* **286** 287–90
- Prasad B V, Rothnagel R, Jiang X and Estes M K 1994 Three-dimensional structure of baculovirus-expressed Norwalk virus capsids *J. Virol.* **68** 5117–25
- Samandougou I, Hammami R, Morales Rayas R, Fliess I and Jean J 2015 Stability of secondary and tertiary structures of virus-like particles representing noroviruses: effects of pH, ionic strength, and temperature and implications for adhesion to surfaces *Appl. Environ. Microbiol.* **81** 7680–6
- Shoemaker G K, Van Duijn E, Crawford S E, Uetrecht C, Baclayon M, Roos W H, Wuite G J, Estes M K, Prasad B V and Heck A J 2010 Norwalk virus assembly and stability monitored by mass spectrometry *Mol. Cell. Proteomics* **9** 1742–51
- Singh B K, Koromyslova A, Hefele L, Gurth C and Hansman G S 2016 Structural evolution of the emerging 2014–2015 GII.17 noroviruses *J. Virol.* **90** 2710–5
- Tan M and Jiang X 2005 The p domain of norovirus capsid protein forms a subviral particle that binds to histo-blood group antigen receptors *J. Virol.* **79** 14017–30
- Taniguchi K, Urasawa S and Urasawa T 1981 Further studies of 35–40 nm virus-like particles associated with outbreaks of acute gastroenteritis *J. Med. Microbiol.* **14** 107–18
- Teunis P F M, Moe C L, Liu P, Miller S E, Lindesmith L, Baric R S, Le Pendu J and Calderon R L 2008 Norwalk virus: how infectious is it? *J. Med. Virol.* **80** 1468–76
- Uetrecht C, Barbu I M, Shoemaker G K, Van Duijn E and Heck A J 2011 Interrogating viral capsid assembly with ion mobility-mass spectrometry *Nat. Chem.* **3** 126–32
- Uetrecht C and Heck A J 2011 Modern biomolecular mass spectrometry and its role in studying virus structure, dynamics, and assembly *Angew. Chem., Int. Ed. Engl.* **50** 8248–62
- Van Den Heuvel R H *et al* 2006 Improving the performance of a quadrupole time-of-flight instrument for macromolecular mass spectrometry *Anal. Chem.* **78** 7473–83
- Vongpunsawad S, Venkataram Prasad B V and Estes M K 2013 Norwalk virus minor capsid protein VP2 associates within the VP1 shell domain *J. Virol.* **87** 4818–25
- Weiss V U *et al* 2015 Analysis of a common cold virus and its subviral particles by gas-phase electrophoretic mobility molecular analysis and native mass spectrometry *Anal. Chem.* **87** 8709–17
- White L J, Hardy M E and Estes M K 1997 Biochemical characterization of a smaller form of recombinant Norwalk virus capsids assembled in insect cells *J. Virol.* **71** 8066–72
- Worsdorfer B, Woycechowsky K J and Hilvert D 2011 Directed evolution of a protein container *Science* **331** 589–92
- Xi J, Graham D, Wang K and Estes M 1990 Norwalk virus genome cloning and characterization *Science* **250** 1580–3
- Zhang X F *et al* 2015 An outbreak caused by GII.17 norovirus with a wide spectrum of HBGA-associated susceptibility *Sci. Rep.* **5** 17687

## 2.3. N-terminal VP1 Truncations Favor $T = 1$ Norovirus-Like Particles

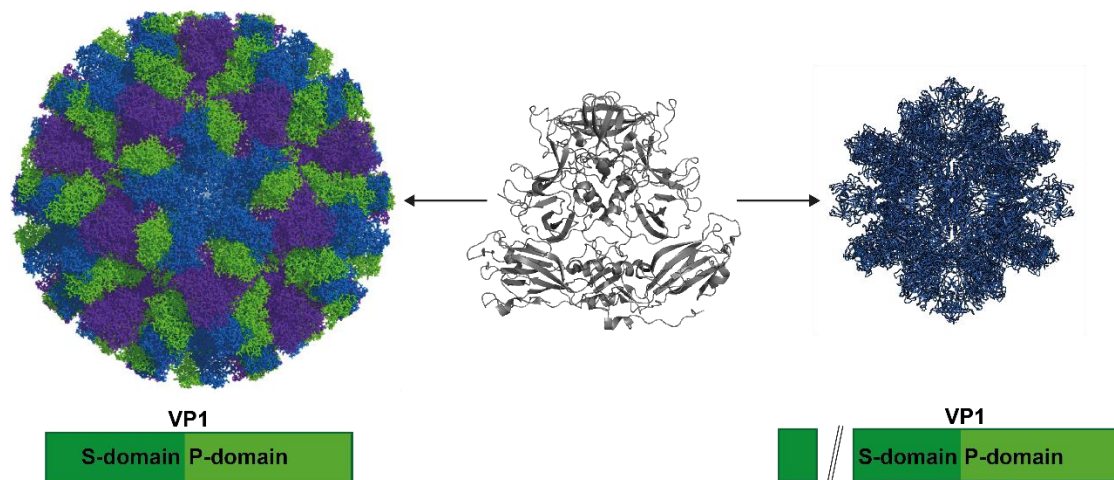
Ronja Pogan, Victor U. Weiss, Kevin Bond, Jasmin Dülfer, Christoph Krisp, Nicholas Lykтей, Jürgen Müller-Guhl, Samuele Zoratto, Günter Allmaier, Martin F. Jarrold, Cesar Muñoz-Fontela, Hartmut Schlüter and Charlotte Uetrecht,

*Vaccines*, 9(1), 8 (2021)

This article is distributed under the terms of the Creative Commons Attribution 4.0 International License (<http://creativecommons.org/licenses/by/4.0/>), Copyright © 2020 by the authors. Licensee MDPI, Basel, Switzerland. No changes were made.

To access the publication see

<https://doi.org/10.3390/vaccines9010008>



## Article

# N-Terminal VP1 Truncations Favor $T = 1$ Norovirus-Like Particles

Ronja Pogan<sup>1,2</sup>, Victor U. Weiss<sup>3</sup> , Kevin Bond<sup>4</sup>, Jasmin Dülfer<sup>1</sup> , Christoph Krisp<sup>5</sup>, Nicholas Lykтей<sup>4</sup>, Jürgen Müller-Guhl<sup>1,6</sup>, Samuele Zoratto<sup>3</sup> , Günter Allmaier<sup>3</sup>, Martin F. Jarrold<sup>4</sup>, Cesar Muñoz-Fontela<sup>6</sup> , Hartmut Schlüter<sup>5</sup>  and Charlotte Uetrecht<sup>1,2,\*</sup> 

- <sup>1</sup> Heinrich Pette Institute, Leibniz Institute for Experimental Virology, 20251 Hamburg, Germany; ronja.pogan@leibniz-hpi.de (R.P.); jasmin.duelfer@leibniz-hpi.de (J.D.); juergen.mueller@leibniz-hpi.de (J.M.-G.)
- <sup>2</sup> European XFEL GmbH, 22869 Schenefeld, Germany
- <sup>3</sup> Institute of Chemical Technologies and Analytics, TU Wien, 1060 Vienna, Austria; victor.weiss@tuwien.ac.at (V.U.W.); samuele.zoratto@tuwien.ac.at (S.Z.); guenter.allmaier@tuwien.ac.at (G.A.)
- <sup>4</sup> Department of Chemistry, Indiana University, Bloomington, IN 47405, USA; kmbond@iu.edu (K.B.); nalykтей@iu.edu (N.L.); mfj@indiana.edu (M.F.J.)
- <sup>5</sup> Mass Spectrometric Proteomics Group, Institute of Clinical Chemistry and Laboratory Medicine, University Medical Center Hamburg-Eppendorf, 20246 Hamburg, Germany; c.krisp@uke.de (C.K.); hschluet@uke.de (H.S.)
- <sup>6</sup> Partner Site Hamburg-Lübeck-Borstel-Riems, Bernhard Nocht Institute for Tropical Medicine and German Center for Infection Research (DZIF), 20359 Hamburg, Germany; munoz-fontela@bnitm.de
- \* Correspondence: charlotte.uetrecht@xfel.eu

**Abstract:** Noroviruses cause immense sporadic gastroenteritis outbreaks worldwide. Emerging genotypes, which are divided based on the sequence of the major capsid protein VP1, further enhance this public threat. Self-assembling properties of the human norovirus major capsid protein VP1 are crucial for using virus-like particles (VLPs) for vaccine development. However, there is no vaccine available yet. Here, VLPs from different variants produced in insect cells were characterized in detail using a set of biophysical and structural tools. We used native mass spectrometry, gas-phase electrophoretic mobility molecular analysis, and proteomics to get clear insights into particle size, structure, and composition, as well as stability. Generally, noroviruses have been known to form mainly  $T = 3$  particles. Importantly, we identified a major truncation in the capsid proteins as a likely cause for the formation of  $T = 1$  particles. For vaccine development, particle production needs to be a reproducible, reliable process. Understanding the underlying processes in capsid size variation will help to produce particles of a defined capsid size presenting antigens consistent with intact virions. Next to vaccine production itself, this would be immensely beneficial for bio-/nano-technological approaches using viral particles as carriers or triggers for immunological reactions.

**Keywords:** norovirus; capsid assembly; native mass spectrometry; nES GEMMA; differential mobility analysis; CDMS



**Citation:** Pogan, R.; Weiss, V.U.; Bond, K.; Dülfer, J.; Krisp, C.; Lykтей, N.; Müller-Guhl, J.; Zoratto, S.; Allmaier, G.; Jarrold, M.F.; et al. N-Terminal VP1 Truncations Favor  $T = 1$  Norovirus-Like Particles.

*Vaccines* **2021**, *9*, 8. <https://dx.doi.org/10.3390/vaccines9010008>

Received: 25 November 2020

Accepted: 21 December 2020

Published: 24 December 2020

**Publisher's Note:** MDPI stays neutral with regard to jurisdictional claims in published maps and institutional affiliations.



**Copyright:** © 2020 by the authors. Licensee MDPI, Basel, Switzerland. This article is an open access article distributed under the terms and conditions of the Creative Commons Attribution (CC BY) license (<https://creativecommons.org/licenses/by/4.0/>).

## 1. Introduction

A vast number of nonbacterial gastroenteritis cases worldwide is caused by human noroviruses (hNoVs) [1]. Norovirus infection especially poses an acute threat to children, immunocompromised individuals and elderly people. Already a small number of particles is sufficient for infection [2]. Gastroenteritis outbreaks happen worldwide with new hNoV-variants occurring sporadically.

Human noroviruses are non-enveloped and a member of the *Caliciviridae* family. They have a positive sense, single strand, approx. 7.7 kb RNA genome organized into three open reading frames (ORFs) and a poly(A) tail. ORF1 encodes non-structural proteins, ORF2 the major capsid protein VP1, and ORF 3 the minor structural protein VP2 [3,4].

Based on VP1, noroviruses can be classified into up to ten genogroups (GI–GX) and further into genotypes [5]. Genogroups I, II, IV, VIII, and IX infect humans. The prototypical GI.1 Norwalk was isolated from stool samples in Norwalk, Ohio in 1968 [6]. Today, mostly GII.4 and GII.17 strains have been identified as a cause of viral gastroenteritis outbreaks [7,8].

There is no norovirus vaccine available yet. The lack of a robust cell culture system and small animal models as well as the immense genetic diversity of hNoVs have hindered its development to date. Although breakthroughs in developing a cell-culture system have been made in 2016 by Ettayebi et al. [9], hNoV research has mostly been based on virus-like particles (VLPs). Current vaccine candidates are also using VLPs, mostly GI.1 and GII.4 VLPs. hNoVLPs can be produced by expressing VP1 in various systems, including insect cells, yeast, mammalian cells, and plants [10–13].

Generally, VP1 can be divided into two functionally and structurally distinct domains. The shell (S)-domain, forming a scaffold around the genome, and a protruding (P)-domain. In GI.1 Norwalk, the N-terminal 225 amino acids (aa) belong to the S-domain. The P-domain is further divided into subdomains P1 and an insertion P2, with P2 being most variable and involved in host-attachment and immunogenicity [14,15]. Self-assembling properties of VP1 allow for next to fully formed  $T = 3$  particles, particles of several other forms [16]. The isolated P-domain expressed in *Escherichia coli* with or without a tag can form P-dimers as well as 12-mer and 24-mer P-particles [17]. Expression of the S-domain in the baculovirus-expression system results in thin-layered, small, and smooth  $T = 3$  particles [18]. In full-length VP1 particles, S- and P-domains are connected via a flexible hinge region [14]. When expressed in eukaryotic systems, caliciviruses generally are known to assemble into VP1 180-mers with  $T = 3$  icosahedral symmetry. However, VP1 60-mers of  $T = 1$  symmetry have been described as byproducts of hNoVLP production coexisting with other particle sizes and independent of the expression system [19]. Recently, VP1 240-mers of  $T = 4$  symmetry have also been described so far only for GII.4 variants expressed in insect cells as well as in plants [20,21]. In studies on virions of different norovirus variants  $T = 3$  as well as  $T = 1$ , formations were detected [22].

Thus, hNoVLP particle sizes are polymorphic and dynamic. Native mass spectrometry (MS) is a perfect biophysical tool to characterize these structural dynamics [23]. Previously, VLPs of three different norovirus variants have been investigated with native MS [24,25]. In our previous work, we established the pH stability pattern of two norovirus variants, GI.1 West Chester and GII.17 Kawasaki [25]. Stability was assessed in different ionic strengths as well as pH levels and compared to results on Norwalk VLPs [24]. In all three variants,  $T = 3$  particles were identified as the major population. Furthermore, GII.17 Kawasaki was resistant to changing conditions, while both GI variants disassembled upon alkaline treatment.

In order to characterize hNoVLPs in detail and gain more insights into size determination, we extended our previous native MS studies with a set of biophysical methods. Next to charge detection mass spectrometry (CDMS) for mass determination of heterogeneous particle populations and proteomics, we used nano electrospray gas-phase electrophoretic mobility molecular analysis (nES GEMMA) [26], especially suited to measure high-mass particles at low concentrations [27,28]. Notably, this fast technique allows for measurements at low ionic strength and with less concentrated sample.

We described particle preparations from insect cells with sample batches, where only  $T = 1$  particles were detected. A major VP1 truncation was identified in all particle preparations forming these  $T = 1$  particles. We found that this size-limitation was genogroup- and genotype-independent and could not be rescued in different buffer conditions. This provides great implications for vaccine design and other applications of bio-nanoparticles, where size-homogeneity is highly favored.

## 2. Materials and Methods

### 2.1. VLP Production and Preparation

Full-length VP1 genes for GI.1 West Chester, GII.4 Saga 2006, GII.10 Vietnam, GII.17 Kawasaki308, and GII.17 Saitama T87 (GenBank accession numbers: AY502016.1, AB447457.1, AF504671.2, LC037415.1, AII73747.1) were cloned and expressed in a baculovirus system [29,30]. After transfection of a bacmid containing the recombinant VP1 gene in Sf9 insect cells and incubation for 5–7 days, the culture medium was collected and centrifuged for 10 min at 3000 rpm at 4 °C. Subsequently, Hi5 insect cells were infected with recovered baculovirus and incubated for 5 days. After centrifuging the culture medium for 10 min at 3000 rpm at 4 °C and then 1 h at 6500 rpm at 4 °C, VLPs in the supernatant were concentrated by ultracentrifugation at 35,000 rpm (Beckman Ti45 rotor, Krefeld, Germany) for 2 h at 4 °C. Furthermore, VLPs were further purified using CsCl equilibrium gradient ultracentrifugation at 35,000 rpm (Beckman SW56 rotor, Krefeld, Germany) for 18 h at 4 °C. VLPs were pelleted for 2 h at 40,000 rpm (Beckman TLA55 rotor, Krefeld, Germany) at 4 °C and solved in PBS (pH 7.4).

### 2.2. VP1 Mapping

Trypsin digestion. For tryptic digestion followed by proteomic analysis, VLP samples in PBS at 15 µM VP1 were separated via sodium dodecyl sulfate polyacrylamide gel electrophoresis (SDS-PAGE) following the reported method [31]. After staining with a solution containing 0.5% Coomassie brilliant blue R250, 50% ethanol, and 7% acetic acid, respective gel bands were cut into small pieces and further processed according to Shevchenko et al. [32]. After digestion, the samples were dried and thereafter dissolved in 0.1% formic acid and transferred into the autosampler. Tryptic peptides were either separated on a nano-UPLC system (Dionex Ultimate 3000 UPLC system, Thermo Fisher Scientific, Bremen, Germany) with a 50 cm C18 analytical column (Acclaim PepMap 100, 75, 3 µm, Thermo Fisher Scientific, Darmstadt, Germany) or a nano-UPLC system (nanoAcquity, Waters, Manchester, Great Britain) with a 25 cm C18 analytical column (BEH C18 Column, 75, 1.7 µm, 100 Å, Waters) using a 60 min gradient with increasing acetonitrile concentration from 2% to 30%. Eluting peptides were desorbed and ionized with an electrospray ionization (ESI) source into a Tribrid mass spectrometer consisting of a quadrupole, linear ion-trap, and an Orbitrap (Fusion; Thermo Fisher Scientific, Bremen, Germany) with the Dionex setup or a quadrupole Orbitrap mass spectrometer (QExactive; Thermo Fisher Scientific, Bremen, Germany) with nanoAcquity setup operated in data-dependent acquisition (DDA) mode. MS/MS spectra were searched with the Sequest algorithm integrated in the Proteome Discoverer software version 2.0, against AY502016.1, AB447457.1, AF504671.2, LC037415.1, AII73747, and a common contaminant protein database. Precursor ion mass tolerance was set to 10 ppm, and fragment ion mass tolerances was set to 0.02 (QExactive) or 0.6 Da (Fusion). Carbamidomethylation was set as a fixed modification on cysteine residues. Acetylation of the protein N-terminus, N-terminal methionine loss, the oxidation of methionine, deamidation of asparagine and glutamine, and glutamine to pyroglutamate on the peptide N-terminus were set as variable modifications. Only peptides with a high confidence (FDR of <1%) using a decoy database approach were accepted as identified.

Pepsin digestion. VLP samples were mixed 1:1 with denaturing buffer (300 mM phosphate buffer, pH 2.3, 6 M urea). Pepsin digestion of 100 pmol VP1 was performed online (Agilent Infinity 1260, Agilent Technologies, Waldbronn, Germany) on a home-packed pepsin column (IDEX guard column with an internal volume of 60 µL, Porozyme immobilized pepsin beads, Thermo Scientific, Darmstadt, Germany) at a flow rate of 75 µL/min (0.4% formic acid in water). Peptides were trapped in a trap column (OPTI-TRAP for peptides, Optimize Technologies, Oregon City, OR, USA.) and separated on a reversed-phase analytical column (PLRP-S for Biomolecules, Agilent Technologies) using a 27 min gradient of 8–40% organic solvent (0.4% formic acid in acetonitrile) at 150 µL/min. MS was performed using an Orbitrap Fusion Tribrid in positive ESI data-dependent MS/MS acquisition mode (Orbitrap resolution 120,000, 1 microscan, HCD 30 with dynamic

exclusion). Precursor and fragment ions were searched and matched against a local protein database containing the proteins of interest in MaxQuant (version 1.5.7.0, Max-Planck-Institute, Munich, Germany) using the Andromeda search engine. The digestion mode was set to “unspecific” and N-terminal acetylation, deamidation, oxidation, and disulfide bond formation were included as variable modifications with a maximum number of 5 modifications per peptide. Peptides between 5 and 30 amino acids length were accepted. The MaxQuant default mass tolerances for precursor (4.5 ppm) and fragment (20 ppm) ions defined for the Orbitrap instrument (Thermo Fisher Scientific, Bremen, Germany) were used for data search. The minimum score for successful identifications was set to 20 for unmodified and 40 for modified peptides.

The mass spectrometry proteomics data have been deposited to the ProteomeXchange Consortium via the PRIDE [33] partner repository with the dataset identifier PXD023182.

### 2.3. Sample Preparation

For mass spectrometry as well as nES GEMMA analysis, hNoVLP sample solutions were exchanged to 40 and 250 mM ammonium acetate solutions. Solution pH was adjusted between 5 and 9 using acetic acid and ammonia. For the solution exchange, Vivaspin 500 centrifugal concentrators (10,000 MWCO, Sartorius, Göttingen, Germany) or Zeba micro spin<sup>TM</sup> desalting columns 0.5 mL (7000 MWCO, Thermo Fisher Scientific, Rockford, IL, USA) were used. Generally, 5 filtration steps using spin filters and 3 steps using size-exclusion columns were employed. Samples were diluted to 10  $\mu$ M VP1 protein or further diluted, if necessary, to obtain spectra.

### 2.4. Mass Spectrometry

Conventional native MS measurements of VLPs were performed using a quadrupole time-of-flight (QToF) instrument Q-ToF 2 (Waters, Manchester, UK and MS Vision, Almere, the Netherlands) modified for high mass experiments [34]. For ESI, capillaries were handmade by pulling borosilicate glass tubes (inner diameter 0.68 mm, outer diameter 1.2 mm with filament, World Precision Instruments, Sarasota, FL, USA) using a two-step program in a micropipette puller (Sutter Instruments, Novato, CA, USA) with a squared box filament (2.5  $\times$  2.5 mm). Gold-coating of capillaries was performed using a sputter coater (Quorum Technologies., East Sussex, UK, 40 mA, 200 s, tooling factor of 2.3 and end bleed vacuum of 8  $\times$  10<sup>-2</sup> mbar argon or Safematic (Zizers, Switzerland), process pressure 5  $\times$  10<sup>-2</sup> mbar, process current 30.0 mA, coating time 100 s, 3 runs to vacuum limit 3  $\times$  10<sup>-2</sup> mbar Argon). Capillaries were opened on the sample cone of the mass spectrometer. Using a nanoESI source, ions were introduced into the vacuum at a source pressure of 10 mbar. The positive ion mode was used to record spectra. Generally, voltages of 1.45 kV and 165 V to the capillary and cone, respectively, were used and adjusted during spray-optimization. Xenon was used as a collision gas at a pressure of 1.7  $\times$  10<sup>-2</sup> mbar in order to enable better transmission of high-mass ions [35]. MS profile and repetition frequency of the pusher pulse were adjusted to high mass range. For instrument calibration, a cesium iodide spectrum was recorded the same day. Analysis was performed using MassLynx V4.1 SCN 566 (Waters, Manchester, UK) and Massign [36].

Charge detection mass spectrometry (CDMS) was performed on a home-built CDMS instrument described in detail elsewhere [37] in order to enable measurements of heterogeneous complexes in the MDa range or larger. Briefly, charge and  $m/z$  of single ions are measured simultaneously using a charge conduction cylinder and electrostatic ion trap. In contrast to conventional QToF MS, CDMS sidesteps the need for charge states to be assigned. Ions were generated using an automated nano-ESI source (Nanomate, Advion, Ithaca, NY, USA) with a capillary voltage of approximately 1.7 kV. After entering a heated metal capillary, ions are transmitted using various ion optics to a dual hemispherical deflection energy analyzer, which selects ions with energies centered on 100 eV/z. Subsequently, ions enter a modified cone trap where they oscillate back and forth in a charge detection

cylinder for 100 ms. Single ion masses were binned to generate mass spectra. Mass spectra were analyzed by fitting Gaussian peaks with Origin software (OriginPro 2016).

Gas-phase electrophoresis was performed on a nES GEMMA instrument (TSI Inc, Shoreview, MN, USA) consisting of a nES aerosol generator (model 3480) including a  $^{210}\text{Po}$   $\alpha$ -particle source, an electrostatic classifier (model 3080) with a nano differential mobility analyzer (nDMA), and an n-butanol based ultrafine condensation particle counter (model 3025A). Briefly, particle-size determination is a function of the particles' trajectory in the nDMA chamber. The trajectory of a size-specific particle is based on the sheath flow of particle-free ambient air and an orthogonal electric field applied. Therefore, with a constant high laminar sheath flow of air and a variable electrical field, only specific particle sizes can successfully be transported to the particle counter device for detection. For electrospraying, polyimide-coated fused silica capillaries (25  $\mu\text{m}$  inner diameter, Polymicro, obtained via Optronis, Kehl, Germany) with in-house-made tips [38] were used. Settings for a stable Taylor cone at the nES tip were chosen, typically around 2 kV, resulting in approx.  $-375$  nA current, 0.1 L/min  $\text{CO}_2$  (Messer, Gumpoldskirchen, Austria), and 1.0 L/min filtered, dried ambient air. Four pounds per square inch differential (psid, approx. 27.6 kPa) were applied to additionally move the sample through the capillary, and 15 L/min sheath flow filtered ambient air was used to size-separate VLPs in an electrophoretic mobility diameter (EMD) range from 2 to 65 nm. The corresponding EMD size range was scanned for 120 s. Subsequently, the applied voltage was adjusted to starting values within a 30 s timeframe. Seven datasets (raw data obtained from instrument software, MacroIMS manager v2.0.1.0) were combined via their median to yield a corresponding spectrum. Lastly, Gauss peaks were fit to spectra via Origin software (OriginPro 2016) to obtain EMD values. EMD values were correlated to particle mass using MW-correlation either based on proteins [39] or VLPs [28].

### 2.5. Electron Microscopy

For imaging using transmission electron microscopy (EM), hNoVLPs stored in PBS were adsorbed onto glow discharge-activated carbon-coated grids (Science Services, Munich, Germany). After three consecutive washing steps with distilled water, the sample coated grids were stained with 1% uranyl acetate. Image acquisition was performed using a FEI Tecnai<sup>TM</sup> G2 transmission electron microscope and wide-angle Veleta CCD camera (FEI, Thermo Fisher Scientific, USA and Olympus, Tokyo, Japan) at 80 kV.

## 3. Results

### 3.1. Truncated GII.4 Saga VP1 Forms Homogeneous $T = 1$ Particles

Here, we extended our previous investigations on GI.1 West Chester and GII.17 Kawasaki to other hNoVLP constructs. VLPs of an outbreak strain GII.4 Saga are produced in the same baculovirus-expression system. Native mass spectra reveal the lack of  $T = 3$  particles at neutral pH and moderate ionic strength (Figure 1). Notably, the identified peak distribution is almost baseline resolved, indicating a highly homogeneous population annotated to VP1 60-mers or  $T = 1$  particles. An additional, unresolved peak distribution around 15,000  $m/z$  relates to metastable ions. Metastable ions are commonly accompanying high-mass ions as these disintegrate partially in the ToF-analyzer, as such they cannot be targeted by selection in the quadrupole, allowing differentiation from ions originating from the sample solution. Figure 1 also illustrates collision-induced dissociation (CID) products for GII.4 Saga. The  $T = 1$  ions ( $\sim 150+$  charges) dissociate via consecutive losses of VP1 monomers, with at least two subspecies in mass, as well as corresponding high mass ions, VP1 59-mer, 58-mer, and 57-mer. Mass-assignment of the dissociated monomer suggests an N-terminal truncation of 45 amino acids (aa) of the main species and a subpopulation lacking 45 aa. Proteomics data following trypsin-digestion as well as pepsin-digestion (Table 1) results in VP1 sequence coverage of 95 and 90% with the N-terminal coverage starting from residues 25 and 27, indicating additional subpopulations, which are low abundant. Notably, the C-terminus is complete up to several arginine residues (C-terminal

three to six residues), which exclude coverage for both proteins due to small peptides. This suggests exclusive N-terminal truncation. An assembly into a 60-mer of the full-length VP1 would result in a theoretical  $T = 1$  mass of 3.54 MDa, and VP1 lacking 45 aa would form 3.28 MDa  $T = 1$  particles. The assigned mass of 3.27 MDa using QToF MS and 3.35 MDa using native CDMS (Supplementary Table S1; note, masses in CDMS are always higher, indicating incomplete desolvation) suggests that detected 60-mer particles are indeed formed mainly from VP1 lacking at least 45 aa. To conclude, in this case, heterologous expression of GII.4 Saga VP1 results in a truncated VP1 species with the mere ability to form  $T = 1$  but not  $T = 3$  particles.

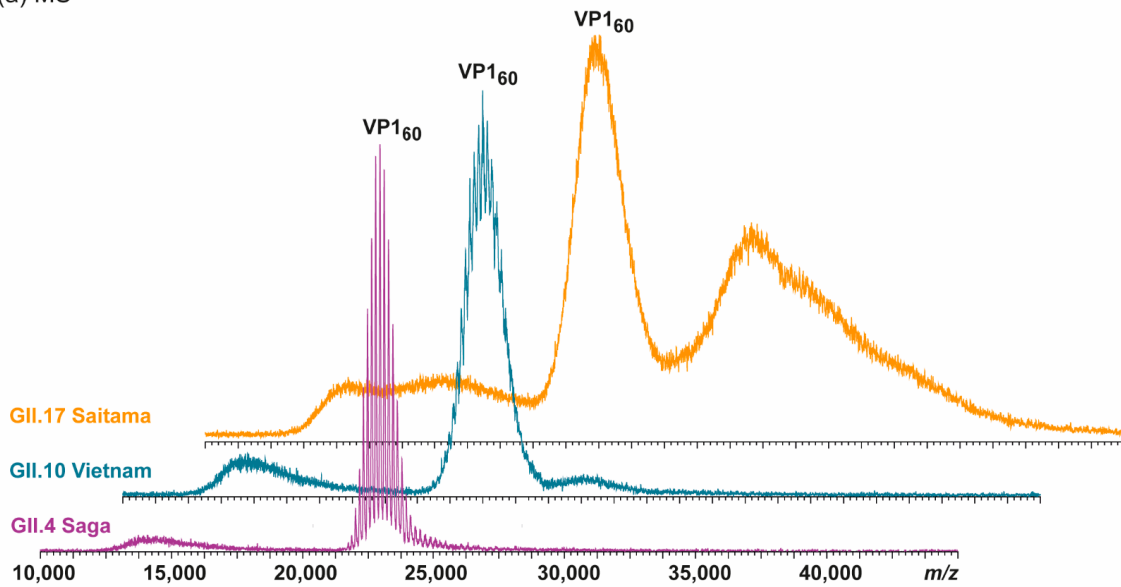
### 3.2. $T = 1$ Capsid Formation Is Genotype-Independent

Additional hNoVLPs were investigated to pinpoint whether the truncation seen in GII.4 Saga causes  $T = 1$  formation. Norovirus-like particle polymorphism has been described as putatively genotype-dependent [20,21,40]. Therefore, we extended our sampling to GII.10 Vietnam and GII.17 Saitama (Figure 1). In line with GII.4 Saga measurements, most abundant peak distributions were assigned to VP1 60-mers for both variants. Notably, more acceleration energy compared to GII.4 Saga was needed to gain charge-resolution for VP1 60-mer peaks, which indicated increased VP1 heterogeneity in these samples (Supplementary Figure S1). Furthermore,  $T = 1$  ions in GII.10 Vietnam showed tailing with a non-resolved shoulder peak, indicating either aggregation or a further low-intensity assembly of slightly higher mass. In GII.17 Saitama mass spectra, heterogeneity was even more prominent as multiple higher-mass assemblies gave rise to complex ion distributions between 30,000 and 40,000  $m/z$ . GII.17 Saitama ion distributions were overlapping with the respective  $T = 3$   $m/z$  range observed in previous mass spectra, but clear mass assignment was hindered due to high heterogeneity in the sample. Dissociated VP1 monomer species for all listed variants except GII.17 Saitama, where signal intensities were too low for selective dissociation experiments and monomer mass was inferred from CDMS (Table S1), are listed in Table 1. If a similar incomplete desolvation for GII.17 Saitama as for GII.4 Saga was assumed in CDMS, the VP1 monomer mass further reduced by ~1500 Da corresponding to an additional 14 aa missing, resulting in a total of 31 aa, closer to the values observed for the other hNoVLPs. Mutual in most VP1 monomer measurements was a major truncation of at least 45 aa (45 aa in GII.4, 45 aa in GII.10, and 17 aa/31 aa in GII.17). Although VP1 truncation was similar in all three variants, the putative cleavage site did not reside in a conserved region, and a putative protease could not be assigned (Table 1).

### 3.3. Heterologous Expression of GI.1 West Chester Results in Either $T = 1$ or $T = 3$ Preparations

To provide further evidence of truncation influence, we compared two GI.1 West Chester batches. Batch 1 is identical to the sample used in our previous work [25]. In the second batch, no  $T = 3$  particles were detected at neutral pH using native MS (Figure 2). The main peak distribution was assigned to  $T = 1$  particles, which was accompanied by a low-intense shoulder peak comparable to GII.10 Vietnam. At increased acceleration voltage, the  $T = 1$  ions released VP1 monomers. A close-up of these monomers showed that at least two subspecies were present. This directly contributed to heterogeneity and therefore low peak resolution of higher-mass species. The dominating VP1 species was assigned to  $52,760 \pm 10$  Da, or the theoretical VP1 mass lacking 40 N-terminal aa. Proteomics data, which hinted to subspecies with minor truncations, was consistent with other variants tested in this study (Table 1). In our previous study, we could identify GI.1 West Chester VP1 monomers with the major species lacking only three amino acids, forming mainly  $T = 3$  particles [25]. Taken together, we can assume that with the VP1 N-terminus of GI.1 West Chester lacking three amino acids the formation of  $T = 3$  particles is possible, while with an expanded truncation of 40 amino acids this is no longer the case.

(a) MS



(b) MS/MS GII.4 Saga

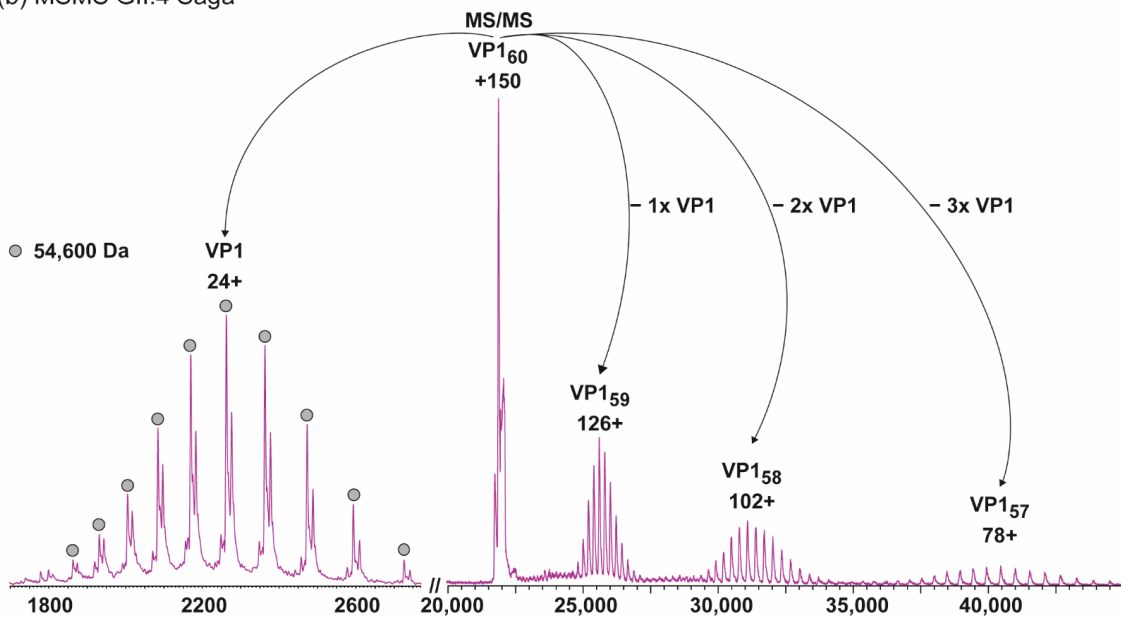


**Figure 1.** Native MS of different human norovirus-like particles (hNoVLPs) suggests that a major truncation of VP1 leads to  $T = 1$  particles. (a) From bottom to top spectra of GII.4 Saga (purple), GII.10 Vietnam (blue), and GII.17 Saitama (orange) in 250 mM ammonium acetate pH 7 at 10  $\mu$ M VP1 are shown. All variants have main ion distributions between 20,000 and 25,000  $m/z$ , which are assigned to VP1<sub>60</sub> complexes. GII.10 Vietnam and especially GII.17 Saitama also form larger assemblies as indicated by additional signal above 25,000  $m/z$ . (b) Collision-induced dissociation MS/MS is shown exemplarily for GII.4 Saga. The dissociation of the 150+ charged VP1 60-mer into VP1-monomer (top left) and residual VP1 59-, 58-, and 57-mer (top right) is shown. Charge states and average monomer mass are annotated. The MS/MS confirms stoichiometry assignment and reveals monomer truncation.

**Table 1.** Overview of investigated samples forming mainly  $T = 1$  particles. Theoretical (th.) VP1 mass and amino acid (aa) number given for constructs West Chester, Saga, Vietnam, and Saitama constructs. Experimental (exp) mass and truncation given for main observed monomeric species after dissociation in conventional MS for all variants except GII.17 Saitama. For Saitama, mass was approximated using charge detection mass spectrometry (CDMS) (Table S1, for nMS see Table S2). MW: Molecular weight.

Variant	VP1 th.	VP1 exp.	Putative Cleavage Site	Trypsin Digestion	Pepsin Digestion
	MW, Total MW Truncation	Main Species MW Truncation	According to exp. VP1 MW	Sequence Coverage %, Minimal N-terminal Truncation	
GI.1 West Chester	56,609 Da, 530 aa	52,760 Da, −40 aa	LAMDVPAGSS/TAVATAGQVN	80%, −6 aa	98%, −2 aa
GI.4 Saga	59,005 Da 540 aa	54,600 Da, −45 aa	AIAAPVAGQQ/NVIDPWIRNN	95%, −25 aa	90%, −27 aa
GI.10 Vietnam	59,901 Da 548 aa	55,560 Da, −aa	SLAAPVTGQT/NIIDPWIRMN	95%, −27 aa	94%, −27 aa
GI.17 Saitama	58,957 Da 540 aa	57,300 Da, −17 aa	SNDGATGLVP/EINNETLPLE	91%, −32 aa	99%, −3 aa

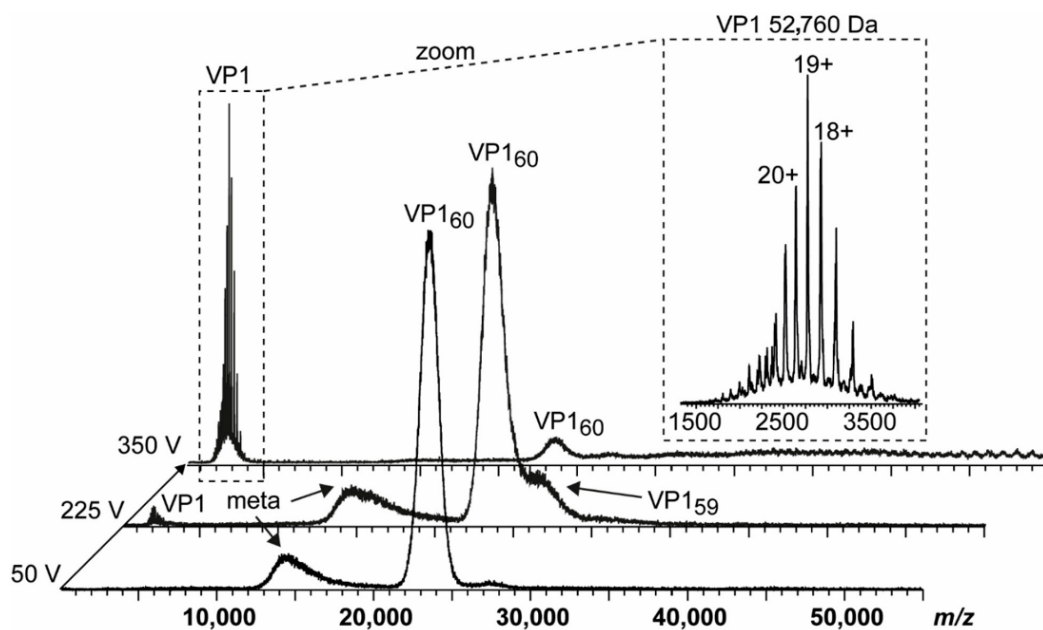


**Figure 2.** Native MS of a GI.1 West Chester batch forming merely VP1<sub>60</sub> complexes. Dissociation pathway without selection in the quadrupole is shown for GI.1 West Chester in 250 mM ammonium acetate pH 7 at 10  $\mu$ M VP1. From bottom to top, illustrative mass spectra are shown for 50, 225, and 350 V acceleration into the collision cell. While at 225 V, VP1 monomers dissociate with the main population of VP1 60-mer still intact, the signal ratio of VP1 monomer:60-mer is reversed at 350 V. An insert shows a zoom of dissociated VP1 monomer with annotated charge states and average mass. As lower mass ions at approximately 15,000  $m/z$  are annotated as metastable ions (meta), monomer lacking at least 40 aa most likely dissociate from  $T = 1$  species.

Furthermore, we characterized particle size and stoichiometry in further detail using nES GEMMA. Measurements of both GI.1 West Chester preparations are superimposed in Figure 3. In order to exclude artefacts, all samples were measured at different dilutions (Supplementary Figure S2). Putative artefacts included unspecific, nES-based aggregates at high sample concentrations, as well as multiply charged particles obtained at low

percentage values during charge equilibration in the bipolar atmosphere of the spray chamber. Comparison of both batches at neutral pH reveals a clear shift in particle size and their counts. In the first GI.1 West Chester batch, most prominent particle counts were at  $34.37 \pm 0.13$  nm, which was assigned to  $T = 3$  particles. Further particle counts at  $8.10 \pm 0.05$  and  $24.09 \pm 0.27$  nm were assigned to VP1 dimer and VP1 60-mer. nES GEMMA spectra of the second batch showed a predominant species at  $24.50 \pm 0.12$  nm equalling  $T = 1$ , as well as a species with low counts at  $30.71 \pm 0.17$  nm. The population at  $30.71$  nm was assigned to  $6.24$  MDa using VLP correlation fitting approximately 120 VP1 (Table S3) [28]. At pH 9, high-mass particles in batch 1 were fragile, complementing our previous findings with native MS [25], while the  $T = 1$  VLPs in batch 2 were resistant to pH 9. Other particles in the second batch bigger than  $24.18 \pm 0.06$  nm disappeared. Interestingly, comparing EMDs of this 60-mer species at neutral pH and pH 9 did not indicate swelling or shrinking of the particles. Notably, the VP1 dimers released in alkaline conditions were slightly smaller in the second batch in line with the observed truncation. Moreover, size difference was not observed for  $T = 1$  particles in the two batches in line with an N-terminal truncation located at the inner face of the capsids. We can conclude that no  $T = 3$  particles were detected with nES GEMMA in the second West Chester batch, which indicated that at least a certain amount of full-length or less truncated VP1 subpopulation was needed to form  $T = 3$  particles. Intermediate-sized populations could stem from either truncated, full-length VP1, or a mixture.

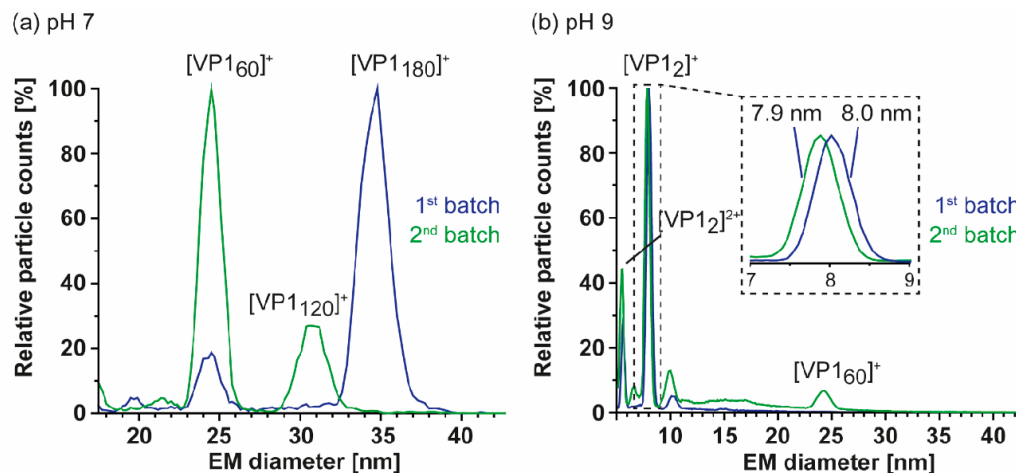


**Figure 3.** Comparison of two GI.1 West Chester VLP preparations using nano electrospray gas-phase electrophoretic mobility molecular analysis (nES GEMMA). Illustrative spectra are shown for both samples in 40 mM ammonium acetate at pH 7 (a) and pH 9 (b) at approximately 2–10  $\mu$ M VP1. Depicted are exemplary spectra for two batches in blue (1) and green (2). (a) Batch 1 shows a clear pattern with a main population of  $34.37 \pm 0.13$  nm and less particle counts at  $24.09 \pm 0.27$  nm, assigned to VP1 180-mer and VP1 60-mer. In batch 2, VP1 60-mer detected at  $24.50 \pm 0.12$  nm is the most abundant species. Furthermore, a species at  $30.71 \pm 0.17$  nm assigned to VP1 120-mer is present and VP1 180-mer is missing. (b) At pH 9, no VP1 complexes other than VP1 dimer were detected for batch 1. The second batch shows a small particle distribution at  $24.18 \pm 0.06$ , indicating higher stability of VP1 60-mers. A zoom at the electrophoretic mobility diameter (EMD) range depicts a minor difference in VP1 dimer size of  $8.03 \pm 0.01$  nm for batch 1 and  $7.89 \pm 0.01$  nm for batch 2. For both conditions, the shown EMD range was adjusted and the complete range including multiply charged species in the low EMD range are shown in Supplementary Figure S2.

#### 3.4. Detailed nES GEMMA and CDMS Profiling

As nES GEMMA is fast and sensitive, all samples were further profiled to see if  $T = 3$  assemblies could be rescued and/or  $T = 1$  particles from truncated VP1 were in general

more stable at alkaline pH. At neutral pH and low ionic strength, particle size patterns of all variants were in line with conventional native MS. Next to the GI.1 West Chester second batch, GII.4 Saga and GII.10 Vietnam formed  $T = 1$  particles but not  $T = 3$  particles. GII.17 Saitama showed some signals, which may have originated from  $T = 3$  particles. Similar to the low-count species in GI.1 West Chester batch 2 of  $30.71 \pm 0.17$  nm (120-mer), in GII.4 Saga and even more prominent in GII.10 Vietnam, further particles were detected at around 33 nm, equaling 7.7 MDa (VP1 140-mer). In line with native MS data, enormous heterogeneity was observed in GII.17 Saitama, and multiple species other than VP1 60-mer could be distinguished with nES GEMMA (Figure 4). Measurements at pH 5 up to pH 9 revealed that  $T = 1$  formations of all samples were mostly resistant to changing solution conditions (Figure 5). Starting from pH 8, free VP1 dimer was detected in all variants in low counts. At pH 9, GII.10 Vietnam and GII.17 Saitama showed reversed particle count ratios of VP1 60-mer and VP1 dimer and larger assemblies did not disintegrate. In GII.4 Saga, no complexes were detected at pH 9 and the employed low VP1 concentrations. However, GII.4 Saga 60-mers remained intact at alkaline pH and low ionic strength in conventional native MS measurements at  $10 \mu\text{M}$  VP1 (50 mM ammonium acetate, Supplementary Figure S3). For all samples, particle-size patterns were also consistent at pH 5, although with lower particle counts and with increased background noise. Taken together, this indicated that  $T = 1$  particles were highly stable, resisting alkaline pH, and  $T = 3$  particle formation could not be rescued by changing solution conditions.

So far, several different size-populations have been detected outside the scope of the Caspar–Klug capsid assembly theory [41], where multiples of 60 (with 120 being formally not allowed) form particles of icosahedral symmetry. CDMS measurements in conditions comparable to our conventional QToF measurements at 250 mM ammonium acetate were used to unambiguously assign such assemblies (Figure 6). For GII.4 Saga, no species but  $T = 1$  particles were observed in sufficient counts to fit peaks. Albeit peaks at approximately 33 nm appeared in low-salt nES GEMMA measurements, no respective peak could be assigned to VP1 140-mer with CDMS. At notably lower ion counts, GII.10 Vietnam showed  $T = 1$  particles, as well as two further species with approximately 4.5 and 6.9 MDa assigned to VP1 79-mer and VP1 121-mer, respectively. Note that those species were approximations due to very low counts, and stoichiometry was based on assuming that 60 VP1 formed the 3.41 MDa population. For both variants, the VP1 mass inferred from the 60-mer was higher than determined in conventional native MS (CDMS/nMS: GII.4 Saga 55.8/54.6 and GII.10 Vietnam 56.8/55.6 kDa). This indicated mixed subpopulations of different VP1-size forming particles or less efficient desolvation in CDMS compared to QToF measurements. Notably, the species at 4.5 MDa was repetitive in GII.10 Vietnam, as well as GI.1 West Chester batch 1 (Supplementary Figure S4). In GII.17 Saitama, CDMS helped to elucidate mass heterogeneity observed in the other methods. Next to a distinct population of 3.44 MDa assigned to VP1 60-mer, five additional high mass species could be deconvoluted. CDMS clearly showed the absence of fully-formed  $T = 3$  particles. Proteomics data for Saitama indicated a subpopulation of VP1 with a minor truncation of 3 aa. This subpopulation would putatively be able to form  $T = 3$  particles in low amounts, which would likely be prone to disassemble at varying concentrations, ionic strengths, and pH levels. Given a mass of approximately 57.3 kDa, CDMS Saitama high-mass species fit VP1 71-, 91-, 100-, 108-, and 120-mers. In contrast, the stability at alkaline pH and low concentrations of these species suggested distinct assemblies. Particle size-heterogeneity was also observed using EM (Figure S5), where various larger assemblies were detected in GII.17 Saitama micrographs. Moreover, although formally not allowed according to triangulation theory, observed VP1 intermediates were repeatedly found in all tested variants and with different techniques.

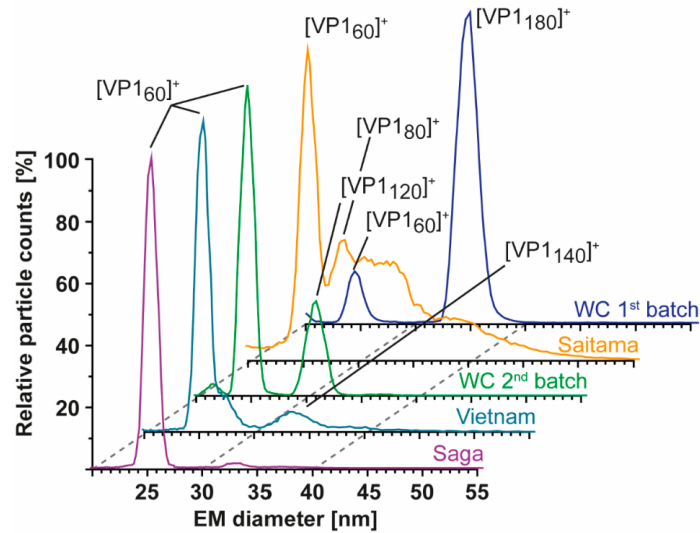


**Figure 4.** Size-distribution overview of different hNoVLPs with nES GEMMA. All variants are measured at 40 mM ammonium acetate pH 7 and approximately 2–10  $\mu$ M VP1. From bottom to top GII.4 Saga (purple), GII.10 Vietnam (light blue), GI.1 West Chester batch 2 (WC, green), GII.17 Saitama (orange), and GI.1 West Chester batch 1 (WC, dark blue). West Chester batch 1 is shown as an indication of the expected EMD range for  $T = 3$  particles. Assigned species are annotated. VP1 60-mers were detected in all variants, with less counts in WC batch 1. Next to 60-mers, GII.4 Saga and GII.10 Vietnam show distributions at approx. 33 nm assigned to VP1 140-mer, and WC second batch shows a distinct peak at 30 nm assigned to VP1-120mer. In GII.17 Saitama, at least two peaks can be fitted in the particle distribution accompanying VP1 60-mer annotated as VP1 80-mer and putatively VP1 180-mer.

(a) GII.4 Saga

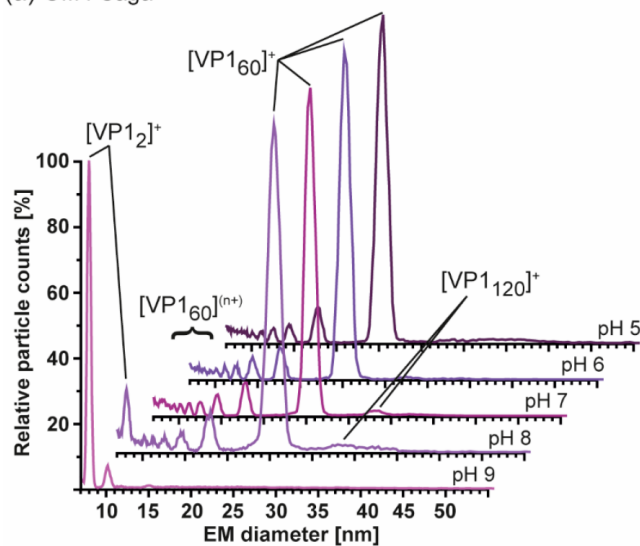


**Figure 5.** *Cont.*

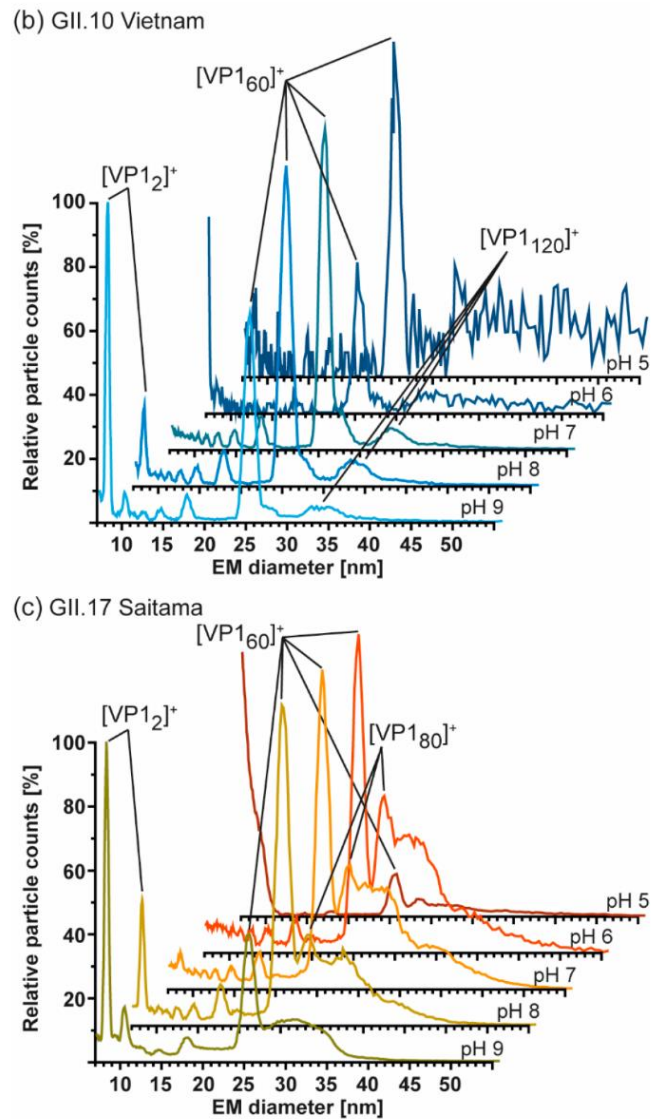


**Figure 5.** Measurements at different pH of hNoVLPs with GEMMA indicates high pH-resistance of  $T = 1$  particles formed from truncated VP1. All measurements were performed at 40 mM ammonium acetate at pH 5–9 from top to bottom at approximately 2–10  $\mu$ M. (a) GII.4 Saga (purple) shows mainly VP1 60-mer accompanied by multiply charged VP1-60-mer. Particle patterns differ only at pH 8, where VP1 dimers are present in low counts as well as pH 9, where merely VP1 dimer is detected. (b) GII.10 Vietnam (blue) shows intact  $T = 1$  particles at all tested pH values. Increased particle counts at pH 7–9 are accompanied with multiply charged VP1 60-mer. Disassembly into VP1 dimer is seen at pH 8 but is only resulting in less VP1-mer counts at pH 9. This pattern is comparable to measurements of GII.17 Saitama (c). Here, main VP1-mers are accompanied by heterogeneous subspecies, which are reduced under alkaline conditions.

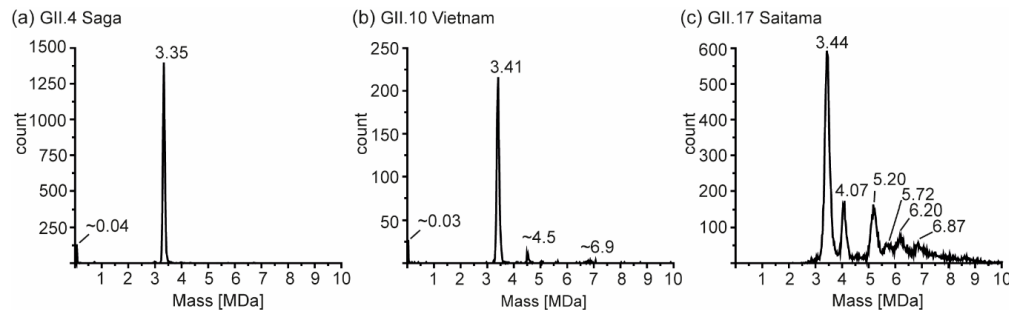


**Figure 6.** Charge detection mass spectrometry of hNoVLPs at 250 mM ammonium acetate pH 7 and 10  $\mu$ M VP1. Illustrative spectra shown for (a) GII.4 Saga (b) GII.10 Vietnam, and (c) GII.17 Saitama. Distinct peaks are annotated; for GII.4 Saga and GII.10 Vietnam low-count species, masses are approximations.

#### 4. Discussion

In this study, different hNoVLP variants were investigated with a set of biophysical tools in order to obtain insights into particle size, stoichiometry, and shape. hNoVLP preparations forming  $T = 1$  particles were identified.  $T = 1$  particles were repeatedly described in hNoVLP preparations [19,21,24,25]. In our previous study,  $T = 1$  and  $T = 3$  particles were coexisting in GI.1 West Chester and GII.17 Kawasaki preparations at neutral pH. In line with a former study on GI.1 Norwalk [24], GI.1 West Chester formed  $T = 3$  particles, which were prone to disassemble in alkaline pH [25]. Here, we identified a major VP1 N-terminal truncation of more than 40 aa in several hNoV variants, leading to  $T = 1$  particles only. The origin of this truncation was unclear. As no clear conserved cleavage motif could be identified, various or unspecific proteases were proposed, likely originating from the insect cell expression system [42,43]. Moreover, this pointed at a structurally defined proteolytic site, which was in line with the flexibility observed in the N-terminal arm. Notably, in all investigated preparations, less populated subspecies with limited truncations building the observed particle formations could not be excluded as proteomics data suggest. This was further supported by a  $T = 1$  structure from cryo-EM [21], which showed no electron density for the N-terminal stretch, indicating that it was either flexible or absent in the preparation.

The ability of truncated VP1 to form mainly  $T = 1$  particles was genogroup- and genotype-independent, as several hNoV variants were targeted here. This indicated a major truncation was sufficient for VP1 to form  $T = 1$  only, and therefore, homogenous, small-sized hNoVLP production was reproducible. Interestingly, several intermediate species were observed repeatedly. In GI.1 West Chester batch 2, GII.4 Saga, and GII.10 Vietnam intermediates were detected in very low proportions. In GII.17 Saitama, spectra suggested a heterogeneous size distribution of several high-mass species with increased counts. A repetitive species that overlapped between preparations was VP1 120-mer. VP1 dimer has been described as a building block for capsid assembly, which suggests that intermediate species must be even integers [14,15,40,44]. Therefore, GII.17 Saitama CDMS measurements resulting in odd numbered complexes were rounded here. Using a combination of characterizing tools like nES GEMMA, conventional MS, and CDMS, VP1 120-mer appeared biologically relevant, although not allowed according to triangulation theory [41]. Moreover, the agreement in GEMMA mass assignment based on a VLP calibration and CDMS revealed that these assemblies resemble hollow spheres like regular capsids. Putative, non-allowed  $T = 2$  particles were described for bluetongue virus and brome mosaic virus among others [45–47]. Another intermediate observed in different hNoVLP preparations was VP1 80-mer. Interestingly, it was detected in preparations, in which  $T = 3$  particles were also observed like GI.1 Norwalk [24], GI.1 West Chester [25] (Supplementary Figure S4). This indicated different behavior of full-length and truncated

VP1 and mixtures thereof. General observed particle plasticity suggested that these species could be trapped formations or overgrown particles, as observed for hepatitis B virus and woodchuck hepatitis virus [48,49]. However, it has to be noted that assemblies have specific sizes as evident from CDMS, rather than covering a broad distribution. The inability to form full  $T = 3$  particles indicated that the N-terminus was required to form flat C/C dimers, leading to lattice expansion. We already proposed an influence of the N-terminus in capsid size determination in our previous study [25]. In turn, the truncated VP1 would likely form mainly bent A/B-like dimers, forming the pentameric vertices present in both VLP formations. This would then likely preclude  $T = 2$  capsids. An alternative assembly route would follow octahedral symmetry, which has been described for SV40 polyomavirus [50]. This requires strongly bent dimer interactions and a 24-mer octahedron formed from pentamers exactly matching the VP1 120-mers detected here. This interpretation was further appealing as it offered an explanation for the aberrant GII.17 Saitama assemblies of 70/72, 90/92, 100, and 108/110 VP1 subunits being octahedrons lacking multiple pentamers. Polymorphism in hNoVLP production, independent of the expression system, have been described both for VP1 forming  $T = 1$  and  $T = 3$  particles at neutral pH levels and intermediates upon changing conditions. In an assembly study on GI.1 Norwalk, three N-terminal deletion mutants were compared [18]. Full-length as well as deletion of N-terminal 20 aa still resulted in  $T = 3$  particles. Deletion of 34 and 98 aa N-terminally did not result in any particles detectable with electron microscopy. However, N-terminal 34 aa mutant expression was described as low, hampering the assessment of how this deletion is involved in capsid assembly. Furthermore, N-terminal deletions of 26 and 38 aa were introduced in GI.4 Sydney VLPs. Both constructs were found to form mainly small particles when examined with electron microscopy [51]. Next to deletion itself, culture conditions were also described as a putative reason for size heterogeneity. Another attempt to gain size-homogeneity in hNoVLP preparations was performed by Someya et al. using GI.4 Chiba VLPs [52]. Truncation of 45 aa N-terminally, similar as observed in this study, was identified and the subsequent introduction of a mutation Leu43Val in this region resulted in the formation of merely  $T = 3$  particles. However, in a follow-up study, GI.4 Chiba mutants were shown to form 23 nm or  $T = 1$  particles, putatively due to freezing and thawing of preparations or pH-dependent processes [53]. Previously,  $T = 4$  particles were identified in hNoVLP preparations [20,21]. Interestingly, one study included GII.2 Snow Mountain virus forming  $T = 1$  particles [21]. Here, residues 1 to 46 were not covered in electron density maps. Hence, truncation as the origin of small particles similar to our observations could not be excluded.

Next to particle size distribution, the influence of solution pH was investigated.  $T = 1$  particles, as well as higher-mass assemblies in GII.17 Saitama, were found to be pH-independent. Moreover, in preparations forming mainly  $T = 1$  particles, like GI.1 West Chester batch 2,  $T = 1$  particles showed increased stability in alkaline conditions. Therefore, truncated VP1 was able to build particles with increased stability. This implies great advances for bio-nanotechnology, as especially in approaches using VLPs as carrier particles, they need to be stable independently of environmental conditions. The contribution of the N-terminus to pH stability suggests a way to obtain S-particles of increased stability by truncation.

## 5. Conclusions

There is no hNoV vaccine available yet and hNoVLP size polymorphism could contribute to this circumstance. Therefore, N-terminally truncated particles have great potential to be beneficial as they imply size homogeneity. An N-terminal truncation of VP1 also leaves P-domains and therefore protrusions on assembled particles intact, as evident from EM data on all tested variants. Studies on P-particles imply the necessity of protrusions for antigen recognition and immunogenicity [54]. Furthermore, P-particles were shown to putatively enable other immunological approaches like antigen presentation [55]. There are clear structural differences between  $T = 1$  particles of truncated VP1 and P-particles as the

S-domain is missing in the latter. Furthermore, the S-domain is generally more conserved among hNoVs, putatively allowing induction of cross-reactive antibodies. Orientation of dimeric protrusions, and therefore their interaction is likely to be different in P-particles missing the S-domain, truncated VP1  $T = 1$  or full-length  $T = 3$  particles. Whether this affects antibody raising and therefore immunogenic reaction needs to be investigated. Additionally, increased stability would likely allow for simplified and prolonged storage. Our results indicate that such small particles from truncated VP1 can be produced independent of genotype by introducing N-terminal deletion mutants.

**Supplementary Materials:** The following are available online at <https://www.mdpi.com/2076-393X/9/1/8/s1>, Figure S1: Native MS of a GII.10 Vietnam VLPs, Figure S2: GEMMA spectra of different hNoVLPs in 40 mM ammonium acetate at pH 7, 3 different tested dilutions exemplarily shown for (a) West Chester batch 1, (b) West Chester batch 2, (c) GII.4 Saga, (d) GII.10 Vietnam, and (e) GII.17 Saitama, Figure S3: Native mass spectrum of GII.4 Saga VLPs at 50 mM ammonium pH 9 at 10  $\mu$ M VP1, Figure S4: Charge detection mass spectra of GI.1 West Chester batch 1 VLPs in 250 mM ammonium acetate at (a) pH 7 and (b) pH 8, Figure S5: Electron micrographs of different hNoVLPs in PBS, Figure S6: VP1 mapping overview of hNoVLP GI.1 West Chester batch 1 after pepsin digestion, Figure S7: VP1 mapping overview of hNoVLP GI.1 West Chester batch 2 after pepsin digestion, Figure S8: VP1 mapping overview of hNoVLP GII.4 Saga after pepsin digestion, Figure S9: VP1 mapping overview of hNoVLP GII.10 Vietnam after pepsin digestion, Figure S10: VP1 mapping overview of hNoVLP GII.17 Saitama after pepsin digestion, Figure S11: VP1 mapping overview of hNoVLP GI.1 West Chester batch 1 after trypsin digestion (coverage 72%), Figure S12: VP1 mapping overview of hNoVLP GI.1 West Chester batch 2 after trypsin digestion (coverage 80%), Figure S13: VP1 mapping overview of hNoVLP GII.4 Saga after trypsin digestion (coverage 95%), Figure S14: VP1 mapping overview of hNoVLP GII.10 Vietnam after trypsin digestion (coverage 95%), Figure S15: VP1 mapping overview of hNoVLP GII.17 Saitama after trypsin digestion (coverage 91%), Table S1: Data mass table for charge detection mass spectrometry measurements, Table S2: Data mass table for conventional QToF measurements, Table S3: GEMMA data mass table for gas-phase electrophoretic molecular mobility analysis.

**Author Contributions:** Conceptualization, C.U.; methodology, C.U., M.F.J., G.A.; validation, R.P.; formal analysis, R.P., V.U.W.; investigation, R.P., V.U.W., S.Z., K.B., N.L., J.D., C.K., J.M.-G.; resources, C.U., M.F.J., G.A., H.S., C.M.-F.; data curation, R.P.; writing—original draft preparation, R.P., C.U.; writing—review and editing, R.P., V.U.W., K.B., J.D., C.K., N.L., J.M.-G., S.Z., G.A., M.F.J., C.M.-F., H.S., C.U. visualization, R.P.; supervision, C.U.; project administration, C.U.; funding acquisition, C.U., C.M.-F. All authors have read and agreed to the published version of the manuscript.

**Funding:** The Heinrich-Pette-Institute, Leibniz Institute for Experimental Virology is supported by the Free and Hanseatic City Hamburg and the Federal Ministry of Health (Bundesministerium für Gesundheit, BMG). C.U. acknowledges funding from the Leibniz Association through SAW-2014-HPI-4 grant. R.P., J.M.-G., C.U., and C.M.-F. acknowledge funding from EU Horizon 2020 project VIRUSCAN 731868. R.P. further acknowledges funding from MIN Graduate School Universität Hamburg. J.D. was funded by DFG FOR2327 Virocarb. V.U.W. acknowledges funding of the Austrian Theodor Körner Fonds. V.U.W. and R.P. both acknowledge funding of COST Action BM1403 Native Mass Spectrometry and Related Methods for Structural Biology.

**Data Availability Statement:** The mass spectrometry proteomics data have been deposited to the ProteomeXchange Consortium via the PRIDE [33] partner repository with the dataset identifier PXD023182. All other data are available on request from the corresponding author.

**Acknowledgments:** We thank Grant Hansman for providing VLPs. We thank the HPI microscopy technology platform, especially Carola Schneider, for assistance in electron microscopy.

**Conflicts of Interest:** The authors declare no conflict of interest.

## References

- Ahmed, S.M.; Hall, A.J.; Robinson, A.E.; Verhoef, L.; Premkumar, P.; Parashar, U.D.; Koopmans, M.; Lopman, B.A. Global prevalence of norovirus in cases of gastroenteritis: A systematic review and meta-analysis. *Lancet Infect. Dis.* **2014**, *14*, 725–730. [[CrossRef](#)]
- Teunis, P.F.; Moe, C.L.; Liu, P.; Miller, S.E.; Lindesmith, L.; Baric, R.S.; Le Pendu, J.; Calderon, R.L. Norwalk virus: How infectious is it? *J. Med. Virol.* **2008**, *80*, 1468–1476. [[CrossRef](#)]
- Xi, J.N.; Graham, D.Y.; Wang, K.N.; Estes, M.K. Norwalk virus genome cloning and characterization. *Science* **1990**, *250*, 1580–1583. [[CrossRef](#)]
- Jiang, X.; Wang, M.; Wang, K.; Estes, M.K. Sequence and genomic organization of Norwalk virus. *Virology* **1993**, *195*, 51–61. [[CrossRef](#)]
- Chhabra, P.; de Graaf, M.; Parra, G.I.; Chan, M.C.; Green, K.; Martella, V.; Wang, Q.; White, P.A.; Katayama, K.; Vennema, H.; et al. Updated classification of norovirus genogroups and genotypes. *J. Gen. Virol.* **2019**, *100*, 1393–1406. [[CrossRef](#)]
- Kapikian, A.Z.; Wyatt, R.G.; Dolin, R.; Thornhill, T.S.; Kalica, A.R.; Chanock, R.M. Visualization by immune electron microscopy of a 27-nm particle associated with acute infectious nonbacterial gastroenteritis. *J. Virol.* **1972**, *10*, 1075–1081. [[CrossRef](#)]
- Eden, J.S.; Tanaka, M.M.; Boni, M.F.; Rawlinson, W.D.; White, P.A. Recombination within the Pandemic Norovirus GII.4 Lineage. *J. Virol.* **2013**, *87*, 6270–6282. [[CrossRef](#)]
- De Graaf, M.; van Beek, J.; Vennema, H.; Podkolzin, A.T.; Hewitt, J.; Bucardo, F.; Templeton, K.; Mans, J.; Nordgren, J.; Reuter, G.; et al. Emergence of a novel GII.17 norovirus—End of the GII.4 era? *Eurosurveillance* **2015**, *20*, 8–15. [[CrossRef](#)]
- Ettayebi, K.; Crawford, S.E.; Murakami, K.; Broughman, J.R.; Karandikar, U.; Tenge, V.R.; Neill, F.H.; Blutt, S.E.; Zeng, X.L.; Qu, L.; et al. Replication of human noroviruses in stem cell-derived human enteroids. *Science* **2016**. [[CrossRef](#)]
- Tome-Amat, J.; Fleischer, L.; Parker, S.A.; Bardlving, C.L.; Batt, C.A. Secreted production of assembled Norovirus virus-like particles from *Pichia pastoris*. *Microb. Cell Fact.* **2014**, *13*, 134. [[CrossRef](#)]
- Taube, S.; Kurth, A.; Schreier, E. Generation of recombinant norovirus-like particles (VLP) in the human endothelial kidney cell line 293T. *Arch. Virol.* **2005**, *150*, 1425–1431. [[CrossRef](#)] [[PubMed](#)]
- Diamos, A.G.; Mason, H.S. High-level expression and enrichment of norovirus virus-like particles in plants using modified geminiviral vectors. *Protein Expr. Purif.* **2018**, *151*, 86–92. [[CrossRef](#)] [[PubMed](#)]
- Mason, H.S.; Ball, J.M.; Shi, J.J.; Jiang, X.; Estes, M.K.; Arntzen, C.J. Expression of Norwalk virus capsid protein in transgenic tobacco and potato and its oral immunogenicity in mice. *Proc. Natl. Acad. Sci. USA* **1996**, *93*, 5335–5340. [[CrossRef](#)] [[PubMed](#)]
- Prasad, B.V.; Rothnagel, R.; Jiang, X.; Estes, M.K. Three-dimensional structure of baculovirus-expressed Norwalk virus capsids. *J. Virol.* **1994**, *68*, 5117–5125. [[CrossRef](#)] [[PubMed](#)]
- Prasad, B.V.; Hardy, M.E.; Dokland, T.; Bella, J.; Rossmann, M.G.; Estes, M.K. X-ray crystallographic structure of the Norwalk virus capsid. *Science* **1999**, *286*, 287–290. [[CrossRef](#)]
- Jiang, X.; Wang, M.; Graham, D.Y.; Estes, M.K. Expression, self-assembly, and antigenicity of the Norwalk virus capsid protein. *J. Virol.* **1992**, *66*, 6527–6532. [[CrossRef](#)] [[PubMed](#)]
- Tan, M.; Jiang, X. The p domain of norovirus capsid protein forms a subviral particle that binds to histo-blood group antigen receptors. *J. Virol.* **2005**, *79*, 14017–14030. [[CrossRef](#)]
- Bertolotti-Ciarlet, A.; White, L.J.; Chen, R.; Prasad, B.V.; Estes, M.K. Structural requirements for the assembly of Norwalk virus-like particles. *J. Virol.* **2002**, *76*, 4044–4055. [[CrossRef](#)]
- White, L.J.; Hardy, M.E.; Estes, M.K. Biochemical characterization of a smaller form of recombinant Norwalk virus capsids assembled in insect cells. *J. Virol.* **1997**, *71*, 8066–8072. [[CrossRef](#)]
- Devant, J.M.; Hofhaus, G.; Bhella, D.; Hansman, G.S. Heterologous expression of human norovirus GII.4 VP1 leads to assembly of T = 4 virus-like particles. *Antivir. Res.* **2019**, *168*, 175–182. [[CrossRef](#)]
- Jung, J.; Grant, T.; Thomas, D.R.; Diehnelt, C.W.; Grigorieff, N.; Joshua-Tor, L. High-resolution cryo-EM structures of outbreak strain human norovirus shells reveal size variations. *Proc. Natl. Acad. Sci. USA* **2019**, *116*, 12828–12832. [[CrossRef](#)] [[PubMed](#)]
- Taniguchi, K.; Urasawa, S.; Urasawa, T. Further studies of 35–40 nm virus-like particles associated with outbreaks of acute gastroenteritis. *J. Med. Microbiol.* **1981**, *14*, 107–118. [[CrossRef](#)] [[PubMed](#)]
- Dulfer, J.; Kadek, A.; Kopicki, J.D.; Krichel, B.; Uetrecht, C. Structural mass spectrometry goes viral. *Adv. Virus Res.* **2019**, *105*, 189–238. [[CrossRef](#)] [[PubMed](#)]
- Shoemaker, G.K.; van Duijn, E.; Crawford, S.E.; Uetrecht, C.; Baclayon, M.; Roos, W.H.; Wuite, G.J.; Estes, M.K.; Prasad, B.V.; Heck, A.J. Norwalk virus assembly and stability monitored by mass spectrometry. *Mol. Cell Proteom.* **2010**, *9*, 1742–1751. [[CrossRef](#)] [[PubMed](#)]
- Pogan, R.; Schneider, C.; Reimer, R.; Hansman, G.; Uetrecht, C. Norovirus-like VP1 particles exhibit isolate dependent stability profiles. *J. Phys. Condens. Matter* **2018**, *30*, 064006. [[CrossRef](#)]
- Kaufman, S.L.; Skogen, J.W.; Dorman, F.D.; Zarrin, F.; Lewis, K.C. Macromolecule analysis based on electrophoretic mobility in air: Globular proteins. *Anal. Chem.* **1996**, *68*, 1895–1904. [[CrossRef](#)]
- Weiss, V.U.; Berezczak, J.Z.; Havlik, M.; Kallinger, P.; Gosler, I.; Kumar, M.; Blaas, D.; Marchetti-Deschmann, M.; Heck, A.J.; Szymanski, W.W.; et al. Analysis of a common cold virus and its subviral particles by gas-phase electrophoretic mobility molecular analysis and native mass spectrometry. *Anal. Chem.* **2015**, *87*, 8709–8717. [[CrossRef](#)]
- Weiss, V.U.; Pogan, R.; Zoratto, S.; Bond, K.M.; Boulanger, P.; Jarrold, M.F.; Lyktey, N.; Pahl, D.; Puffler, N.; Schelhaas, M.; et al. Virus-like particle size and molecular weight/mass determination applying gas-phase electrophoresis (native nES GEMMA). *Anal. Bioanal. Chem.* **2019**, *411*, 5951–5962. [[CrossRef](#)]

29. Hansman, G.S.; Natori, K.; Oka, T.; Ogawa, S.; Tanaka, K.; Nagata, N.; Ushijima, H.; Takeda, N.; Katayama, K. Cross-reactivity among sapovirus recombinant capsid proteins. *Arch. Virol.* **2005**, *150*, 21–36. [[CrossRef](#)]
30. Hansman, G.S.; Saito, H.; Shibata, C.; Ishizuka, S.; Oseto, M.; Oka, T.; Takeda, N. Outbreak of gastroenteritis due to sapovirus. *J. Clin. Microbiol.* **2007**, *45*, 1347–1349. [[CrossRef](#)]
31. Laemmli, U.K. Cleavage of structural proteins during the assembly of the head of bacteriophage T4. *Nature* **1970**, *227*, 680–685. [[CrossRef](#)]
32. Shevchenko, A.; Tomas, H.; Havlis, J.; Olsen, J.V.; Mann, M. In-gel digestion for mass spectrometric characterization of proteins and proteomes. *Nat. Protoc.* **2006**, *1*, 2856–2860. [[CrossRef](#)]
33. Perez-Riverol, Y.; Csordas, A.; Bai, J.; Bernal-Llinares, M.; Hewapathirana, S.; Kundu, D.J.; Inuganti, A.; Griss, J.; Mayer, G.; Eisenacher, M.; et al. The PRIDE database and related tools and resources in 2019: Improving support for quantification data. *Nucleic Acids Res.* **2019**, *47*, D442–D450. [[CrossRef](#)] [[PubMed](#)]
34. Van den Heuvel, R.H.; van Duijn, E.; Mazon, H.; Synowsky, S.A.; Lorenzen, K.; Versluis, C.; Brouns, S.J.; Langridge, D.; van der Oost, J.; Hoyes, J.; et al. Improving the performance of a quadrupole time-of-flight instrument for macromolecular mass spectrometry. *Anal. Chem.* **2006**, *78*, 7473–7483. [[CrossRef](#)] [[PubMed](#)]
35. Lorenzen, K.; Versluis, C.; van Duijn, E.; van den Heuvel, R.H.H.; Heck, A.J.R. Optimizing macromolecular tandem mass spectrometry of large non-covalent complexes using heavy collision gases. *Int. J. Mass Spectrom.* **2007**, *268*, 198–206. [[CrossRef](#)]
36. Morgner, N.; Robinson, C.V. Massign: An assignment strategy for maximizing information from the mass spectra of heterogeneous protein assemblies. *Anal. Chem.* **2012**, *84*, 2939–2948. [[CrossRef](#)]
37. Contino, N.C.; Pierson, E.E.; Keifer, D.Z.; Jarrold, M.F. Charge detection mass spectrometry with resolved charge states. *J. Am. Soc. Mass Spectrom.* **2013**, *24*, 101–108. [[CrossRef](#)]
38. Tycova, A.; Prikryl, J.; Foret, F. Reproducible preparation of nanospray tips for capillary electrophoresis coupled to mass spectrometry using 3D printed grinding device. *Electrophoresis* **2016**, *37*, 924–930. [[CrossRef](#)]
39. Bacher, G.; Szymanski, W.W.; Kaufman, S.L.; Zollner, P.; Blaas, D.; Allmaier, G. Charge-reduced nano electrospray ionization combined with differential mobility analysis of peptides, proteins, glycoproteins, noncovalent protein complexes and viruses. *J. Mass Spectrom.* **2001**, *36*, 1038–1052. [[CrossRef](#)]
40. Caspar, D.L.; Klug, A. Physical principles in the construction of regular viruses. *Cold Spring Harb. Symp. Quant. Biol.* **1962**, *27*, 1–24. [[CrossRef](#)]
41. Gotoh, T.; Miyazaki, Y.; Kikuchi, K.; Bentley, W.E. Investigation of sequential behavior of carboxyl protease and cysteine protease activities in virus-infected Sf-9 insect cell culture by inhibition assay. *Appl. Microbiol. Biotechnol.* **2001**, *56*, 742–749. [[CrossRef](#)]
42. Gotoh, T.; Ono, H.; Kikuchi, K.; Nirasawa, S.; Takahashi, S. Purification and characterization of aspartic protease derived from Sf9 insect cells. *Biosci. Biotechnol. Biochem.* **2010**, *74*, 2154–2157. [[CrossRef](#)] [[PubMed](#)]
43. Uetrecht, C.; Barbu, I.M.; Shoemaker, G.K.; van Duijn, E.; Heck, A.J. Interrogating viral capsid assembly with ion mobility-mass spectrometry. *Nat. Chem.* **2011**, *3*, 126–132. [[CrossRef](#)] [[PubMed](#)]
44. Pogan, R.; Dulfer, J.; Uetrecht, C. Norovirus assembly and stability. *Curr. Opin. Virol.* **2018**, *31*, 59–65. [[CrossRef](#)] [[PubMed](#)]
45. Grimes, J.M.; Burroughs, J.N.; Gouet, P.; Diprose, J.M.; Malby, R.; Zientara, S.; Mertens, P.P.; Stuart, D.I. The atomic structure of the bluetongue virus core. *Nature* **1998**, *395*, 470–478. [[CrossRef](#)] [[PubMed](#)]
46. Baker, T.S.; Olson, N.H.; Fuller, S.D. Adding the third dimension to virus life cycles: Three-dimensional reconstruction of icosahedral viruses from cryo-electron micrographs. *Microbiol. Mol. Biol. Rev.* **1999**, *63*, 862–922. [[CrossRef](#)] [[PubMed](#)]
47. Krol, M.A.; Olson, N.H.; Tate, J.; Johnson, J.E.; Baker, T.S.; Ahlquist, P. RNA-controlled polymorphism in the in vivo assembly of 180-subunit and 120-subunit virions from a single capsid protein. *Proc. Natl. Acad. Sci. USA* **1999**, *96*, 13650–13655. [[CrossRef](#)]
48. Lutomski, C.A.; Lykтей, N.A.; Zhao, Z.; Pierson, E.E.; Zlotnick, A.; Jarrold, M.F. Hepatitis B Virus Capsid Completion Occurs through Error Correction. *J. Am. Chem. Soc.* **2017**, *139*, 16932–16938. [[CrossRef](#)]
49. Pierson, E.E.; Keifer, D.Z.; Kukreja, A.A.; Wang, J.C.; Zlotnick, A.; Jarrold, M.F. Charge Detection Mass Spectrometry Identifies Preferred Non-Icosahedral Polymorphs in the Self-Assembly of Woodchuck Hepatitis Virus Capsids. *J. Mol. Biol.* **2016**, *428*, 292–300. [[CrossRef](#)]
50. Salunke, D.M.; Caspar, D.L.; Garcea, R.L. Polymorphism in the assembly of polyomavirus capsid protein VP1. *Biophys. J.* **1989**, *56*, 887–900. [[CrossRef](#)]
51. Huo, Y.Q.; Wan, X.; Wang, Z.J.; Meng, S.L.; Shen, S. Production of Norovirus VLPs to size homogeneity. *Virus Res.* **2015**, *204*, 1–5. [[CrossRef](#)] [[PubMed](#)]
52. Someya, Y.; Shirato, H.; Hasegawa, K.; Kumasaka, T.; Takeda, N. Assembly of homogeneous norovirus-like particles accomplished by amino acid substitution. *J. Gen. Virol.* **2011**, *92*, 2320–2323. [[CrossRef](#)] [[PubMed](#)]
53. Hasegawa, K.; Someya, Y.; Shigematsu, H.; Kimura-Someya, T.; Nuemket, N.; Kumasaka, T. Crystallization and X-ray analysis of 23 nm virus-like particles from Norovirus Chiba strain. *Acta Crystallogr. F Struct. Biol. Commun.* **2017**, *73*, 568–573. [[CrossRef](#)] [[PubMed](#)]
54. Tan, M.; Fang, P.; Chachiyo, T.; Xia, M.; Huang, P.; Fang, Z.; Jiang, W.; Jiang, X. Noroviral P particle: Structure, function and applications in virus-host interaction. *Virology* **2008**, *382*, 115–123. [[CrossRef](#)]
55. Tan, M.; Jiang, X. Norovirus P particle: A subviral nanoparticle for vaccine development against norovirus, rotavirus and influenza virus. *Nanomedicine* **2012**, *7*, 889–897. [[CrossRef](#)] [[PubMed](#)]

## 2.4. Synopsis

This thesis aims to characterize biophysical properties of viruses focusing on norovirus-like particles with especially targeting capsid assembly and disassembly.

In 2.1, we address the process of characterization and how current routine techniques can be applied and combined in order to facilitate mass measurements of viral capsids or capsid-like structures. In a collaborative study together with colleagues from the Technical University of Vienna and several other institutions, we established a mass and electrophoretic mobility diameter (EMD) correlation of virus-like particles (VLPs) covering a mass range from 3 to 27 MDa using gas phase electrophoretic mobility molecular analysis (GEMMA) and native mass spectrometry (nMS). This work focused on high-mass, spherical and empty capsid particles compared to previous work by our collaborators on proteins and virions. Measurements were performed on VLPs of cowpea mosaic virus (CPMV), human norovirus (hNoV) and bacteriophages T5 and P22. Additionally, previous work by our collaborator was incorporated in our study. Here, hepatitis B virus-like particles (HBV) and subviral particles of human rhinovirus serotype A2 were studied. Generally, particles were produced by expressing either the major or both the major and minor capsid protein in a suitable expression system followed by extensive purification of self-assembled particles. In all methods used, VLPs were ionized using nanoelectrospray (nano ESI). Technical details of ionization instrumentation varied between methods differing in capillary inner diameter, capillary material and static, manually operated and automated spray mechanism. In GEMMA, analytes are transferred to the gas phase using nanoelectrospray following charge reduction to singly charged, surface-dry ions. At ambient pressure, singly charged particles are separated according to their size or EMD. Subsequently, the aerosol is introduced to an ultrafine condensation counter for quantification of respective signals. For mass measurements, samples were measured on a quadrupole time-of-flight (QToF) as well as a charge detection mass spectrometry (CDMS) instrument when charge state resolution was not given or literature values were not available. Notably, hNoV and HBV, showed two different particle formations with icosahedral symmetry. More precisely, these formations are assemblies of 60 and 180 ( $T = 1$  and  $T = 3$  capsids) and 180 and 240 ( $T = 3$  and  $T = 4$  capsids) structural proteins for hNoV and HBV-like particles, respectively

In order to check transferability of the established correlation, a set of measurements on two instrumentation setups was performed including measurements on proteins, polysaccharides

and VLPs. This study implicates that a calibration of instrument is needed per sample type. Furthermore, the established correlation was tested on human papilloma virus type 16 (HPV16) VLPs. HPV particle production generally generates small protein yields and were not sufficient for ESI MS in this study. However, GEMMA data combined with our correlation provided a mass measurement deviating approximately 1.5% to the theoretical mass based on theoretical structural protein mass.

Finally, this work provides a contrasting juxtaposition of GEMMA, QToF and CDMS for measurement of high-mass particles. Consequently, all three techniques can be considered complementary with regards to differences in instrument sensitivity, commercial availability and cost, as well as duration of measurement.

Next, I focus on the investigation of human norovirus-like particles with the three techniques described. The following will target NoV assembly and disassembly. Furthermore, I set out to examine relations between norovirus strain and particle stability.

In 2.2, we study two norovirus variants, namely GI.1 West Chester and GII.17 Kawasaki, with native QToF MS and negative stain electron microscopy (EM). Generally, noroviruses can be classified into genogroups and genotypes based on the major structural protein VP1. VLPs were investigated with EM and native MS in a set of solution conditions varying in ionic strength and pH. Compared to the previously studied prototype GI.1 Norwalk, the West Chester variant was generally more susceptible to alkaline treatment maintaining  $T = 3$  particles only up to pH 7, but not at pH 8. Disassembly was further indicated by detection of VP1 low mass multimers, namely tetramers, hexamers, putative 18mers and 80mers. VP1 dimers were detected in all tested solution conditions with increased intensities at high pH and low ionic strength. Furthermore, West Chester showed smaller  $T = 1$  particles already at pH 6 whereas Norwalk formed  $T = 1$  assemblies at pH 8 at the respective ionic strength. Both  $T = 1$  and  $T = 3$  assemblies could be reassembled following complete disassembly to VP1 dimers. Interestingly, VP1 sequences differed in 13 amino acids (aa) with 6 dissimilar residues out of which four were located in the N-terminal scaffolding domain.

GI.17 Kawasaki on the other hand did not show disassembly induced by solution condition changes. Native  $T = 3$  particles were formed at all conditions tested. Surprisingly, a further species assigned to  $T = 1$  particles was also observed for this variant at all tested conditions. At pH 10 in 50 mM and 250 mM ammonium acetate, VP1 dimers indicated starting disassembly of particles. Compared to GI.1 West Chester, Genogroup II variants are generally known as

newly emerging, prevalent strains with GII.17 Kawasaki being an outbreak-causing strain isolated in Asia starting 2014. Next to variation of solution pH, samples were measured in different ionic strength, namely 50 mM and 250 mM ammonium acetate. For GII.17 Kawasaki, spectra showed similar species patterns in both molarities, while high ionic strength showed increased impact on GI.1 West Chester. Here,  $T = 3$  particles disassembled at lower pH at 250 mM than at 50 mM ammonium acetate.

In this work, we studied NoV disassembly and reassembly behavior. Several VP1 multimers were identified as putative intermediates. We identified norovirus-like particle stability patterns in different solution conditions with differences on the genogroup and genotype level, which are attributable to VP1 sequence.

Subsequently, further genotypes were included in our next approach studying NVLPs with mass spectrometry as shown in chapter 2.3. Namely, I worked with GI.1 West Chester (2 batch preparations), GII.4 Saga, GII.10 Vietnam and GII.17 Saitama. Samples were characterized using GEMMA, QToF MS, CDMS and trypsin- and pepsin-based proteomics. Measurements on further variants showed VP1 60mers particles but were lacking signal for  $T = 3$  formations at neutral pH in several tested VLP preparations. MSMS studies on VP1 60mer ion distributions showed that dissociating VP1 monomers were truncated. More precisely, detected VP1 was lacking 40 aa in GI.1 West Chester and 45 aa GII:4 Saga and GII.10 Vietnam. In GII.17 Saitama, MSMS could not be performed on VP1 60mer ions successfully. However, CDMS data suggested a truncation of at least 17 aa or 31 aa corrected for adducts. Proteomics following pepsin digestion suggested the presence of at least subspecies with near-intact N-terminus lacking three residues due to methionine processing. Subspecies with minor truncations (2-27 aa) were also indicated for all variants based on both trypsin and pepsin-based proteomics. Generally, C-terminal coverage was considered complete as the sequence was covered up to several arginine residues resulting in small proteins that are considered undetectable. Notably,  $T = 1$  peak distributions of GI.1 West Chester and GII.10 Vietnam showed tailing indicating further species. In GII.17 Saitama, further high-mass ion distributions partially overlapping with the respective  $T = 3$   $m/z$  range were detected.

Having set up the mass-EMD correlation for VLPs in chapter 2.1, I now employed it for rigorous characterization of all variants. As particle formation has been shown to be solution condition dependent before, this should be excluded as a reason for preparations lacking  $T = 3$  formations. Measurements were performed at 40 mM ranging from pH 5 to pH 9. Reassembly

of  $T = 3$  particles was not observed. Next to VP1 60mers observed throughout the data set, except for GII.4 Saga at pH 9, several other species were detected in very low counts hampering mass assignment. Additionally, CDMS helped to elucidate sample heterogeneity. Notable species were putative VP1 80mers detected with CDMS in GI.1 West Chester batch 1 and GII.10 Vietnam, and putative VP1 120mers detected in GII.10 Vietnam and GII.17 Saitama. Furthermore, CDMS measurements of GII.17 Saitama showed VP1 71-, 91-, 100- and 108-mers, or assemblies of 70/72, 90/92, 100 and 108/110 subunits corrected for integers, respectively.

In conclusion, we identified a major N-terminal truncation leading to  $T = 1$  assemblies independent of genogroup and genotype. Generating mutants lacking the respective aa likely results in homogenous VP1 60mer assemblies. Therefore, our findings provide important benefit to vaccine development and other biological application of bionanoparticles as homogeneous particle preparations are generally favored in both approaches.

### 3. Discussion

---

Generally, viruses and their recombinant assemblies are excellent systems for mass spectrometry due to their size and the remarkable feature to self-assemble even from a single protein. In terms of mass measurable with standard native MS approaches, they close the gap between proteins up to approx. 2 MDa, and an extended mass range of GDa complexes like bacteria. Therefore, some viral systems like P22, Flockhouse virus (FHV) and Adeno associated viruses (AAV) are often used as mass standards. So far, they demonstrated great advancements in instrumentation like Orbitraps or CDMS by breaking mass records on said systems (Keifer et al., 2014; Snijder et al., 2014; van de Waterbeemd et al., 2017; Wörner et al., 2020). On the other hand, it is of great importance to understand virus assembly and stability. Assembly states, in particular sizes of fully-assembled particles and their intermediates, need to be followed. Especially the latter are approachable by MS, but less with non-dynamic imaging techniques like cryo EM. A notable example how native MS was aiding to understand these processes is AAV. Using native MS, the proposed assembly pattern of 1:1:10 of the capsid proteins VP1, VP2, and VP3 was confirmed for recombinant particles although electron densities of low-amount VP1 and VP2 were not resolved with imaging techniques. Furthermore, stoichiometric differences were identified in other particle expression systems, and recent instrumentation advancements even elucidated incorporation quantities of genomic material (Snijder et al., 2014; Wörner et al., 2022, 2021; Barnes et al., 2021, 2022). Taken together, these findings and instrumentation developments have potential not only to optimize AAV gene therapy but furthermore hold capabilities for novel MS-based quality control (Kostelic et al., 2022b). This demonstrates how mass spectrometry can aid to optimize nanobiotechnological approaches and also how beneficial the proper characterization of particles for such applications can be. Fundamental characterization parameters are biophysical properties like particle size and morphology of intact and misshaped particles or artefacts, as well as sample preparation purity, and particle stability. VLP-based approaches demand the ability to monitor particle stability for example over the time-span of storage in the cold-chain as vaccines have been shown to disintegrate over time (Kumru et al., 2014). Therefore, the characterization technique must be fast and inexpensive. The instrumentation techniques discussed so far however are expensive, require further instrument modifications, software extensions, or are home-built instruments. Hence, they are not applicable to a broad audience. A technique that can overcome this burden

## Discussion

is GEMMA. This work provides a novel opportunity to characterize low-concentrated, high-mass globular particles. The MW-EMD correlation established in this work targets the mass-range generally covered by VLPs, extending the previously covered mass range focusing on protein complexes (Bacher et al., 2001). In contrast to a further correlation targeting globular, filled particles or intact virions (Weiss et al., 2015b). Recently, our correlation was applied to characterize AAV particle stability using GEMMA (Zoratto et al., 2021).

To follow and understand viral assembly ultimately enables the use of VLPs as protein carriers or vehicle, capsules, platforms for antigen display, and other bionanotechnological applications. A notable viral system that was investigated in great detail using structural studies is HBV. Studies using MS, CDMS, AFM, and SAXS, amongst others, identified intermediates next to the generally known  $T = 3$  and  $T = 4$  particles (Asor et al., 2020; Buzón et al., 2021; Chevreuil et al., 2020; Lutomski et al., 2018, 2017; Pierson et al., 2014; Utrecht et al., 2011). Next to immense insights to self-assembly, this facilitated particle assembly with distinct stopping points with great potential for capsid engineering (Zhao et al., 2021).

Another viral system with great potential for technological applications is human norovirus, the main target of my work. In a study using native MS and EM, I established stability patterns of hNoV VP1-only particles of two variants in different ammonium acetate solutions differing in ionic strength and pH. The tested variants GI.1 West Chester and GII.17 Kawasaki were further compared to previously investigated prototypical GI.1 Norwalk particles (Shoemaker et al., 2010). The different VP1 oligomer-patterns were clearly distinguishable on the genogroup level (GI and GII). Furthermore, several VP1-oligomerisation states also differed on the genotype-level (GI.1 Norwalk and GI.1 West Chester). In all three tested variants, the predominant and largest particle population was of  $T = 3$  symmetry, in line with the common understanding of hNoV virion size (Prasad et al., 1994). Several smaller intermediate sizes were identified. Oligomers smaller than the proposed nucleation complex, a pentamer of a dimer, namely VP1 dimers, tetramers, hexamers were observed for Norwalk and West Chester. In the tested conditions and with the exceeded resolution, VP1 8mers were not observed in our study on West Chester, although observed for Norwalk. Larger oligomeric states were VP1 18- and 40mers for Norwalk only, as well as 60- and 80mers for (full-length) Norwalk and West Chester. Despite these minor differences regarding smaller-sized assemblies, the main discrepancy was the presence of  $T = 1$  particles in neutral conditions for the West Chester, but not the Norwalk variant. First, this was contributed to 13 aa substitutions, out of which 6 were dissimilar, of the West Chester VP1 sequence compared to Norwalk. A substitution at residue

11 putatively enabled a switch from A/B to C/C dimers. Notably,  $T = 1$  particles were also observed in all conditions tested of the Kawasaki variant and substitutions flanking the respective residue 11 were also noted in this variant. The assembly states discussed so far were composed of full length VP1. In contrast to my following study on several other hNoV variants. Here, an N-terminal truncation of approx. 40-45 aa was observed as the putative cause for the assembly of merely  $T = 1$  particles. Additionally, several other VP1 oligomers were observed, namely assemblies of 71 (70/72), 91 (90/92), 80, 100, 109 (108/110) and 120 VP1. As proteomics data suggested, some VP1 assemblies putatively originate from subspecies of full-length or less truncated VP1. Furthermore, I reviewed the strain-stability correlation as a clear dependency was indicated (Pogan et al., 2018a). Studies on virions, surrogates and VLPs were reviewed regarding particle size, stoichiometry and stability. In this review, the lack of following variant or even strain-specifics throughout the literature became apparent. In contrast to that, later structural hNoVLP studies included information on the variant and larger assemblies,  $T = 4$  particles or 240mers were identified by different labs (Devant and Hansman, 2021, 2021; Jung et al., 2019). The array of particle sizes and intermediates is evident. However, the question arises which assembly states hold intrinsic function in the norovirus virion, are kinetically trapped states, or assembly artefacts due to missing components in VLPs compared to virions. I have demonstrated so far, that most complexes are repetitive in various norovirus variants and experimental conditions. Dimeric, tetrameric and hexameric assemblies of full-length VP1 are rather expected sizes in line with nucleation theory assuming the putative assembly nucleus of a pentamer of a dimer (Utrecht et al., 2011). The occurrence of 80mers can be correlated to full length VP1 as they coexist  $T = 3$  particles. Other multimers however, including 120mers hint to an alternative assembly route starting from pentamers following octahedral symmetry (Salunke et al., 1989). Therefore, the next step must be to determine the symmetry of this complex. As evident from our data however, this needs to involve advanced techniques that are able to detect low intense assemblies like a combination of mass spectrometry and X-ray free electron lasers (Kadek et al., 2021).

In other viruses like brome mosaic virus (BMV) and Bluetongue virus, pseudo  $T = 2$  particles have been described (Krol et al., 1999). In BMV, pseudo  $T = 2$  and  $T = 3$  formation is reversible following RNA-protein interaction.  $T = 1$  particles are formed after N-terminal cleavage of 63 or 35 aa of the capsid protein after endogenous enzyme or trypsin digestion, respectively (Bol et al., 1974; Cuillel et al., 1981; Lucas et al., 2001). Furthermore, encapsulation of RNA of

## Discussion

different length was identified as a switch from  $T = 1$  to pseudo  $T = 2$  capsids (Choi 2002). In the dsRNA virus phage phi6, major and minor capsid proteins form an inner capsid of pseudo  $T = 2$  formation (Nemecek et al., 2013). Twarock and Luque have introduced alternative models to CP theory, based on kite, rhomb and triangle tiling, which consider geometries of different sized proteins and several protein domains (Twarock and Luque, 2019). According to this theory, phage phi6 pseudo  $T = 2$  particles follow a gyrated layout with trihexagonal lattice architecture (Twarock and Luque, 2019).

These studies pinpoint to general particle polymorphism in small viruses and their recombinant VLP systems. Furthermore, N-terminal modifications are an underlying principle allowing the formation of different assemblies as it was also observed in this work. Cowpea chlorotic mottle virus (CCMV) capsid proteins were N-terminally linked to an elastin-like polypeptide (ELP). Due to the hydrophobicity of the ELP, capsid assembly from  $T = 3$  to  $T = 1$  is reversible following pH change from pH 5 to pH 7.5. Notably, the conversion from  $T = 3$  to  $T = 1$  is 10 times faster than reverse (Timmermans et al., 2022). In several hNoV studies with  $T = 1$  formations where no truncation or mutation of the N-terminal region was reported, electron densities of this region were missing. This was the case for example for  $T = 1$  particles of a ssRNA virus satellite tobacco necrosis virus, but also in the above mentioned hNoV studies (Bunka et al., 2011; Jung et al., 2019).

Furthermore, post translational modification of VP1 or subunits thereof putatively impact viral dynamics and thereby likely the accessibility of proteases to capsids. For example, deamidation of P-dimers were found to modulate glycan binding in certain hNoV variants (Dülfer et al., 2021; Mallagaray et al., 2019). Although noroviruses in line with other small, non-enveloped viruses are generally known not to carry glycosylation, several VP1 modifications were found in GII.4 Sydney VLPs recently (Hanisch, 2022). Glycosylation is generally hard to follow due to their low abundance and further studies on hNoVLPs might require enrichment of glycosylated peptides. Next to their putative impact on capsid dynamics and size polymorphism, post-translational modifications might play a role in the lacking efficiency of current norovirus vaccine candidates (Hanisch, 2022).

Generally, bigger particles can accommodate more cargo and have greater resources for antigen presentation on their surface. On the other hand, smaller assemblies can be associated with increased stability as the integrity of truncated VP1 forming  $T = 1$  particles in alkaline conditions observed in this work suggests. Furthermore, the studies discussed so far indicate a trend to natural formation of smaller particles than bigger ones. Recently identified bigger

assemblies in noroviruses on the other hand appear to be species-dependent and the role of sample solution conditions needs to be investigated in detail (Devant et al., 2019; Devant and Hansman, 2021; Jung et al., 2019).

Next to particle size polymorphism, structural dynamics of the capsid protrusions were detected for several noroviruses (Hu et al., 2022; Sherman et al., 2021). The flexibility of the P-domain, which is either resting or floating on top of the shell domain, has vast impact on receptor and antibody binding in murine norovirus (MNV). In the extended, open state, the P domain is accessible to antibody binding, but receptor binding in MNV was shown to be reduced. The closed conformation on the other hand enables CD300lf binding to MNV (Nelson et al., 2018). In enveloped viruses, conformational dynamics of the fusionglycoprotein are critical for vaccine development. Here, the fusionprotein undergoes conformational changes from a metastable closed to an open postfusion form upon cell entry. However, only the closed unstable form allows recognition by antibodies and therefore a stabilized, closed conformation is required for vaccine development (Munro et al., 2014; Rey and Lok, 2018). This overall suggests, that the observed VP1 dynamics in noroviruses are important mediators in norovirus entry. Studies on the entry mechanism and identification of a putative hNoV receptor therefore likely lack particles in the right conformation and would benefit from a stabilized closed form. A process, which is well suited to be followed by structural MS techniques.

Understanding the dynamics of the protruding domain in hNoV has great potential for norovirus vaccine development and the outcome of cell culture propagation approaches. Ultimately, norovirus vaccine development would further benefit immensely from a system based on the presentation of multivalent antigens. In this work, the potential to build size controlled hNoV  $T = 1$  particles was identified. Next, chimeric particles presenting antigens need to follow. Chimeric particles can be prepared using the spytag-spycatcher system as used for example for MS2 chimeras presenting SARS-CoV-2 antigens for diagnostics (Brune et al., 2016; Wang et al., 2021).

The traditional approach in vaccine development is based on fundamental principles of immunology. Usually, tedious steps are necessary regardless if the vaccine is produced in animals, eggs, or in cell-based systems. This work however contributes to emerging, integrative approaches that are based on structural studies like particle engineering, where insights to self-assembly mechanisms are crucial (Olshefsky et al., 2022).

## Discussion

This work presents an ideal base to transform such approaches to norovirus disease prevention. The truncations identified in this work and their effect on capsid assembly and capsid size need to be unraveled in detail and are fundamental for subsequent mutational studies. Once, the interplay between N-terminal length and capsid size are defined, putative  $T = 1$  particles can be used for approaches like antigen presentation. Furthermore, the impact of different capsid protein length can be tested for stability with the applications and workflows established in this work or additionally with other techniques like AFM.

## 4. Bibliography

---

---

- Adachi, M., Okuyama, K., Kousaka, Y., 1983. Electrical neutralization of charged aerosol particles by bipolar ions. *J. Chem. Eng. Jpn.* 16, 229–235. <https://doi.org/10.1252/jcej.16.229>
- Adrian, M., Dubochet, J., Lepault, J., McDowell, A.W., 1984. Cryo-electron microscopy of viruses. *Nature* 308, 32–36. <https://doi.org/10.1038/308032a0>
- Ahmed, S.M., Hall, A.J., Robinson, A.E., Verhoef, L., Premkumar, P., Parashar, U.D., Koopmans, M., Lopman, B.A., 2014. Global prevalence of norovirus in cases of gastroenteritis: a systematic review and meta-analysis. *Lancet Infect. Dis.* 14, 725–730. [https://doi.org/10.1016/S1473-3099\(14\)70767-4](https://doi.org/10.1016/S1473-3099(14)70767-4)
- Ahmed, S.M., Lopman, B.A., Levy, K., 2013. A Systematic Review and Meta-Analysis of the Global Seasonality of Norovirus. *PLoS ONE* 8, e75922. <https://doi.org/10.1371/journal.pone.0075922>
- Aliyari, E., Konermann, L., 2022. Formation of Gaseous Peptide Ions from Electrospray Droplets: Competition between the Ion Evaporation Mechanism and Charged Residue Mechanism. *Anal. Chem.* 94, 7713–7721. <https://doi.org/10.1021/acs.analchem.2c01355>
- Aliyari, E., Konermann, L., 2021. Atomistic Insights into the Formation of Nonspecific Protein Complexes during Electrospray Ionization. *Anal. Chem.* 93, 12748–12757. <https://doi.org/10.1021/acs.analchem.1c02836>
- Aliyari, E., Konermann, L., 2020. Formation of Gaseous Proteins via the Ion Evaporation Model (IEM) in Electrospray Mass Spectrometry. *Anal. Chem.* 92, 10807–10814. <https://doi.org/10.1021/acs.analchem.0c02290>
- Allen, S.J., Schwartz, A.M., Bush, M.F., 2013. Effects of Polarity on the Structures and Charge States of Native-Like Proteins and Protein Complexes in the Gas Phase. *Anal. Chem.* 85, 12055–12061. <https://doi.org/10.1021/ac403139d>
- Annis, B.K., Malinauskas, A.P., Mason, E.A., 1972. Theory of drag on neutral or charged spherical aerosol particles. *J. Aerosol Sci.* 3, 55–64. [https://doi.org/10.1016/0021-8502\(72\)90141-3](https://doi.org/10.1016/0021-8502(72)90141-3)
- Antoine, R., 2020. Weighing synthetic polymers of ultra-high molar mass and polymeric nanomaterials: What can we learn from charge detection mass spectrometry? *Rapid Commun. Mass Spectrom.* 34. <https://doi.org/10.1002/rcm.8539>
- Asor, R., Schlicksup, C.J., Zhao, Z., Zlotnick, A., Raviv, U., 2020. Rapidly Forming Early Intermediate Structures Dictate the Pathway of Capsid Assembly. *J. Am. Chem. Soc.* 142, 7868–7882. <https://doi.org/10.1021/jacs.0c01092>
- Ausar, S.F., Foubert, T.R., Hudson, M.H., Vedvick, T.S., Middaugh, C.R., 2006. Conformational Stability and Disassembly of Norwalk Virus-like Particles. *J. Biol. Chem.* 281, 19478–19488. <https://doi.org/10.1074/jbc.M603313200>
- Bacher, G., Szymanski, W.W., Kaufman, S.L., Zöllner, P., Blaas, D., Allmaier, G., 2001. Charge-reduced nano electrospray ionization combined with differential mobility analysis of peptides, proteins, glycoproteins, noncovalent protein complexes and

## Bibliography

- viruses: ESI GEMMA of proteins and noncovalent complexes. *J. Mass Spectrom.* 36, 1038–1052. <https://doi.org/10.1002/jms.208>
- Baclayon, M., Shoemaker, G.K., Uetrecht, C., Crawford, S.E., Estes, M.K., Prasad, B.V.V., Heck, A.J.R., Wuite, G.J.L., Roos, W.H., 2011. Prestress Strengthens the Shell of Norwalk Virus Nanoparticles. *Nano Lett.* 11, 4865–4869. <https://doi.org/10.1021/nl202699r>
- Barnes, L.F., Draper, B.E., Chen, Y.-T., Powers, T.W., Jarrold, M.F., 2021. Quantitative analysis of genome packaging in recombinant AAV vectors by charge detection mass spectrometry. *Mol. Ther. - Methods Clin. Dev.* 23, 87–97. <https://doi.org/10.1016/j.omtm.2021.08.002>
- Barnes, L.F., Draper, B.E., Jarrold, M.F., 2022. Analysis of thermally driven structural changes, genome release, disassembly, and aggregation of recombinant AAV by CDMS. *Mol. Ther. - Methods Clin. Dev.* 27, 327–336. <https://doi.org/10.1016/j.omtm.2022.10.008>
- Benesch, J.L.P., 2009. Collisional activation of protein complexes: Picking up the pieces. *J. Am. Soc. Mass Spectrom.* 20, 341–348. <https://doi.org/10.1016/j.jasms.2008.11.014>
- Benesch, J.L.P., Ruotolo, B.T., Simmons, D.A., Robinson, C.V., 2007. Protein Complexes in the Gas Phase: Technology for Structural Genomics and Proteomics. *Chem. Rev.* 107, 3544–3567. <https://doi.org/10.1021/cr068289b>
- Benner, W.H., 1997. A Gated Electrostatic Ion Trap To Repetitiously Measure the Charge and  $m/z$  of Large Electrospray Ions. *Anal. Chem.* 69, 4162–4168. <https://doi.org/10.1021/ac970163e>
- Bereszczak, J.Z., Havlik, M., Weiss, V.U., Marchetti-Deschmann, M., van Duijn, E., Watts, N.R., Wingfield, P.T., Allmaier, G., Steven, A.C., Heck, A.J.R., 2014. Sizing up large protein complexes by electrospray ionisation-based electrophoretic mobility and native mass spectrometry: morphology selective binding of Fabs to hepatitis B virus capsids. *Anal. Bioanal. Chem.* 406, 1437–1446. <https://doi.org/10.1007/s00216-013-7548-z>
- Bertolotti-Ciarlet, A., Crawford, S.E., Hutson, A.M., Estes, M.K., 2003. The 3' End of Norwalk Virus mRNA Contains Determinants That Regulate the Expression and Stability of the Viral Capsid Protein VP1: a Novel Function for the VP2 Protein. *J. Virol.* 77, 11603–11615. <https://doi.org/10.1128/JVI.77.21.11603-11615.2003>
- Bertolotti-Ciarlet, A., White, L.J., Chen, R., Prasad, B.V.V., Estes, M.K., 2002. Structural Requirements for the Assembly of Norwalk Virus-Like Particles. *J. Virol.* 76, 4044–4055. <https://doi.org/10.1128/JVI.76.8.4044-4055.2002>
- Bianco, A., Neefjes, I., Alfaouri, D., Vehkamäki, H., Kurtén, T., Ahonen, L., Passananti, M., Kangasluoma, J., 2022. Separation of isomers using a differential mobility analyser (DMA): Comparison of experimental vs modelled ion mobility. *Talanta* 243, 123339. <https://doi.org/10.1016/j.talanta.2022.123339>
- Bielecki, J., Hantke, M.F., Daurer, B.J., Reddy, H.K.N., Hasse, D., Larsson, D.S.D., Gunn, L.H., Svenda, M., Munke, A., Sellberg, J.A., Flueckiger, L., Pietrini, A., Nettelblad, C., Lundholm, I., Carlsson, G., Okamoto, K., Timneanu, N., Westphal, D., Kulyk, O., Higashiura, A., van der Schot, G., Loh, N.-T.D., Wysong, T.E., Bostedt, C., Gorkhover, T., Iwan, B., Seibert, M.M., Osipov, T., Walter, P., Hart, P., Bucher, M., Ulmer, A., Ray, D., Carini, G., Ferguson, K.R., Andersson, I., Andreasson, J., Hajdu, J., Maia, F.R.N.C., 2019. Electrospray sample injection for single-particle imaging with x-ray lasers. *Sci. Adv.* 5, eaav8801. <https://doi.org/10.1126/sciadv.aav8801>

- Blaum, B.S., Neu, U., Peters, T., Stehle, T., 2018. Spin ballet for sweet encounters: saturation-transfer difference NMR and X-ray crystallography complement each other in the elucidation of protein–glycan interactions. *Acta Crystallogr. Sect. F Struct. Biol. Commun.* 74, 451–462. <https://doi.org/10.1107/S2053230X18006581>
- Bol, J.F., Kraal, B., Brederode, F.T., 1974. Limited proteolysis of alfalfa mosaic virus: Influence on the structural and biological function of the coat protein. *Virology* 58, 101–110. [https://doi.org/10.1016/0042-6822\(74\)90144-5](https://doi.org/10.1016/0042-6822(74)90144-5)
- Boyd, K.J., Bansal, P., Feng, J., May, E.R., 2015. Stability of Norwalk Virus Capsid Protein Interfaces Evaluated by in Silico Nanoindentation. *Front. Bioeng. Biotechnol.* 3. <https://doi.org/10.3389/fbioe.2015.00103>
- Bozkurt, H., D'souza, D.H., Davidson, P.M., 2013. Determination of the Thermal Inactivation Kinetics of the Human Norovirus Surrogates, Murine Norovirus and Feline Calicivirus. *J. Food Prot.* 76, 79–84. <https://doi.org/10.4315/0362-028X.JFP-12-327>
- Bruinsma, R.F., Wuite, G.J.L., Roos, W.H., 2021. Physics of viral dynamics. *Nat. Rev. Phys.* 3, 76–91. <https://doi.org/10.1038/s42254-020-00267-1>
- Brune, K.D., Leneghan, D.B., Brian, I.J., Ishizuka, A.S., Bachmann, M.F., Draper, S.J., Biswas, S., Howarth, M., 2016. Plug-and-Display: decoration of Virus-Like Particles via isopeptide bonds for modular immunization. *Sci. Rep.* 6, 19234. <https://doi.org/10.1038/srep19234>
- Bull, R.A., Hansman, G.S., Clancy, L.E., Tanaka, M.M., Rawlinson, W.D., White, P.A., 2005. Norovirus Recombination in ORF1/ORF2 Overlap. *Emerg. Infect. Dis.* 11, 1079–1085. <https://doi.org/10.3201/eid1107.041273>
- Bunka, D.H.J., Lane, S.W., Lane, C.L., Dykeman, E.C., Ford, R.J., Barker, A.M., Twarock, R., Phillips, S.E.V., Stockley, P.G., 2011. Degenerate RNA Packaging Signals in the Genome of Satellite Tobacco Necrosis Virus: Implications for the Assembly of a T= 1 Capsid. *J. Mol. Biol.* 413, 51–65. <https://doi.org/10.1016/j.jmb.2011.07.063>
- Buzón, P., Maity, S., Christodoulis, P., Wiertsema, M.J., Dunkelbarger, S., Kim, C., Wuite, G.J.L., Zlotnick, A., Roos, W.H., 2021. Virus self-assembly proceeds through contact-rich energy minima. *Sci. Adv.* 7, eabg0811. <https://doi.org/10.1126/sciadv.abg0811>
- Cannon, J.L., Papafragkou, E., Park, G.W., Osborne, J., Jaykus, L.-A., Vinjé, J., 2006. Surrogates for the Study of Norovirus Stability and Inactivation in the Environment: A Comparison of Murine Norovirus and Feline Calicivirus. *J. Food Prot.* 69, 2761–2765. <https://doi.org/10.4315/0362-028X-69.11.2761>
- Caspar, D.L.D., Klug, A., 1962. Physical Principles in the Construction of Regular Viruses. *Cold Spring Harb. Symp. Quant. Biol.* 27, 1–24. <https://doi.org/10.1101/SQB.1962.027.001.005>
- Cates, J.E., Vinjé, J., Parashar, U., Hall, A.J., 2020. Recent advances in human norovirus research and implications for candidate vaccines. *Expert Rev. Vaccines* 19, 539–548. <https://doi.org/10.1080/14760584.2020.1777860>
- Cech, N.B., Enke, C.G., 2001. Practical implications of some recent studies in electrospray ionization fundamentals. *Mass Spectrom. Rev.* 20, 362–387. <https://doi.org/10.1002/mas.10008>

## Bibliography

- Chernushevich, I.V., Loboda, A.V., Thomson, B.A., 2001. An introduction to quadrupole-time-of-flight mass spectrometry. *J. Mass Spectrom.* 36, 849–865. <https://doi.org/10.1002/jms.207>
- Chernushevich, I.V., Thomson, B.A., 2004. Collisional Cooling of Large Ions in Electrospray Mass Spectrometry. *Anal. Chem.* 76, 1754–1760. <https://doi.org/10.1021/ac035406j>
- Chevreuril, M., Lecoq, L., Wang, S., Gargowitsch, L., Nhiri, N., Jacquet, E., Zinn, T., Fieulaine, S., Bressanelli, S., Tresset, G., 2020. Nonsymmetrical Dynamics of the HBV Capsid Assembly and Disassembly Evidenced by Their Transient Species. *J. Phys. Chem. B* 124, 9987–9995. <https://doi.org/10.1021/acs.jpcc.0c05024>
- Chhabra, P., de Graaf, M., Parra, G.I., Chan, M.C.-W., Green, K., Martella, V., Wang, Q., White, P.A., Katayama, K., Vennema, H., Koopmans, M.P.G., Vinjé, J., 2019. Updated classification of norovirus genogroups and genotypes. *J. Gen. Virol.* 100, 1393–1406. <https://doi.org/10.1099/jgv.0.001318>
- Chmielewski, D., Schmid, M.F., Simmons, G., Jin, J., Chiu, W., 2022. Chikungunya virus assembly and budding visualized in situ using cryogenic electron tomography. *Nat. Microbiol.* 7, 1270–1279. <https://doi.org/10.1038/s41564-022-01164-2>
- Conley, M.J., Bhella, D., 2019. Asymmetric analysis reveals novel virus capsid features. *Biophys. Rev.* 11, 603–609. <https://doi.org/10.1007/s12551-019-00572-9>
- Conley, M.J., McElwee, M., Azmi, L., Gabrielsen, M., Byron, O., Goodfellow, I.G., Bhella, D., 2019. Calicivirus VP2 forms a portal-like assembly following receptor engagement. *Nature* 565, 377–381. <https://doi.org/10.1038/s41586-018-0852-1>
- Contino, N.C., Jarrold, M.F., 2013. Charge detection mass spectrometry for single ions with a limit of detection of 30 charges. *Int. J. Mass Spectrom.* 345–347, 153–159. <https://doi.org/10.1016/j.ijms.2012.07.010>
- Contino, N.C., Pierson, E.E., Keifer, D.Z., Jarrold, M.F., 2013. Charge Detection Mass Spectrometry with Resolved Charge States. *J. Am. Soc. Mass Spectrom.* 24, 101–108. <https://doi.org/10.1007/s13361-012-0525-5>
- Costantini, V., Morantz, E.K., Browne, H., Ettayebi, K., Zeng, X.-L., Atmar, R.L., Estes, M.K., Vinjé, J., 2018. Human Norovirus Replication in Human Intestinal Enteroids as Model to Evaluate Virus Inactivation. *Emerg. Infect. Dis.* 24, 1453–1464. <https://doi.org/10.3201/eid2408.180126>
- Covey, T.R., Bonner, R.F., Shushan, B.I., Henion, J., Boyd, R.K., 1988. The determination of protein, oligonucleotide and peptide molecular weights by ion-spray mass spectrometry. *Rapid Commun. Mass Spectrom.* 2, 249–256. <https://doi.org/10.1002/rcm.1290021111>
- Creutzmacher, R., Maass, T., Ogrissek, P., Wallmann, G., Feldmann, C., Peters, H., Lingemann, M., Taube, S., Peters, T., Mallagaray, A., 2021. NMR Experiments Shed New Light on Glycan Recognition by Human and Murine Norovirus Capsid Proteins. *Viruses* 13, 416. <https://doi.org/10.3390/v13030416>
- Cuellar, J.L., Meinhoevel, F., Hoehne, M., Donath, E., 2010. Size and mechanical stability of norovirus capsids depend on pH: a nanoindentation study. *J. Gen. Virol.* 91, 2449–2456. <https://doi.org/10.1099/vir.0.021212-0>
- Cuillet, M., Jacrot, B., Zulauf, M., 1981. A T = 1 capsid formed by protein of brome mosaic virus in the presence of trypsin. *Virology* 110, 63–72. [https://doi.org/10.1016/0042-6822\(81\)90008-8](https://doi.org/10.1016/0042-6822(81)90008-8)

- da Silva, A.K., Kavanagh, O.V., Estes, M.K., Elimelech, M., 2011. Adsorption and Aggregation Properties of Norovirus GI and GII Virus-like Particles Demonstrate Differing Responses to Solution Chemistry. *Environ. Sci. Technol.* 45, 520–526. <https://doi.org/10.1021/es102368d>
- de Graaf, M., van Beek, J., Koopmans, M.P.G., 2016. Human norovirus transmission and evolution in a changing world. *Nat. Rev. Microbiol.* 14, 421–433. <https://doi.org/10.1038/nrmicro.2016.48>
- de Graaf, M., van Beek, J., Vennema, H., Podkolzin, A.T., Hewitt, J., Bucardo, F., Templeton, K., Mans, J., Nordgren, J., Reuter, G., Lynch, M., Rasmussen, L.D., Iritani, N., Chan, M.C., Martella, V., Ambert-Balay, K., Vinjé, J., White, P.A., Koopmans, M.P., 2015. Emergence of a novel GII.17 norovirus – End of the GII.4 era? *Eurosurveillance* 20. <https://doi.org/10.2807/1560-7917.ES2015.20.26.21178>
- de Graaf, M., Villabruna, N., Koopmans, M.P., 2017. Capturing norovirus transmission. *Curr. Opin. Virol.* 22, 64–70. <https://doi.org/10.1016/j.coviro.2016.11.008>
- Devant, J.M., Hansman, G.S., 2021. Structural heterogeneity of a human norovirus vaccine candidate. *Virology* 553, 23–34. <https://doi.org/10.1016/j.virol.2020.10.005>
- Devant, J.M., Hofhaus, G., Bhella, D., Hansman, G.S., 2019. Heterologous expression of human norovirus GII.4 VP1 leads to assembly of T=4 virus-like particles. *Antiviral Res.* 168, 175–182. <https://doi.org/10.1016/j.antiviral.2019.05.010>
- Dole, M., Mack, L.L., Hines, R.L., Mobley, R.C., Ferguson, L.D., Alice, M.B., 1968. Molecular Beams of Macroions. *J. Chem. Phys.* 49, 2240–2249. <https://doi.org/10.1063/1.1670391>
- Donaldson, E.F., Lindesmith, L.C., LoBue, A.D., Baric, R.S., 2010. Viral shape-shifting: norovirus evasion of the human immune system. *Nat. Rev. Microbiol.* 8, 231–241. <https://doi.org/10.1038/nrmicro2296>
- Doussineau, T., Yu Bao, C., Clavier, C., Dagany, X., Kerleroux, M., Antoine, R., Dugourd, P., 2011. Infrared multiphoton dissociation tandem charge detection-mass spectrometry of single megadalton electrosprayed ions. *Rev. Sci. Instrum.* 82, 084104. <https://doi.org/10.1063/1.3628667>
- Draper, B.E., Anthony, S.N., Jarrold, M.F., 2018. The FUNPET—a New Hybrid Ion Funnel-Ion Carpet Atmospheric Pressure Interface for the Simultaneous Transmission of a Broad Mass Range. *J. Am. Soc. Mass Spectrom.* 29, 2160–2172. <https://doi.org/10.1007/s13361-018-2038-3>
- Dubochet, J., Adrian, M., Chang, J.-J., Homo, J.-C., Lepault, J., McDowell, A.W., Schultz, P., 1988. Cryo-electron microscopy of vitrified specimens. *Q. Rev. Biophys.* 21, 129–228. <https://doi.org/10.1017/S0033583500004297>
- Duizer, E., Schwab, K.J., Neill, F.H., Atmar, R.L., Koopmans, M.P.G., Estes, M.K., 2004. Laboratory efforts to cultivate noroviruses. *J. Gen. Virol.* 85, 79–87. <https://doi.org/10.1099/vir.0.19478-0>
- Dülfer, J., Kadek, A., Kopicki, J.-D., Krichel, B., Uetrecht, C., 2019. Structural mass spectrometry goes viral, in: *Advances in Virus Research*. Elsevier, pp. 189–238. <https://doi.org/10.1016/bs.aivir.2019.07.003>
- Dülfer, J., Yan, H., Brodmerkel, M.N., Creutzmacher, R., Mallagaray, A., Peters, T., Caleman, C., Marklund, E.G., Uetrecht, C., 2021. Glycan-Induced Protein Dynamics in Human

## Bibliography

- Norovirus P Dimers Depend on Virus Strain and Deamidation Status. *Molecules* 26, 2125. <https://doi.org/10.3390/molecules26082125>
- Dykeman, E.C., Stockley, P.G., Twarock, R., 2013. Packaging Signals in Two Single-Stranded RNA Viruses Imply a Conserved Assembly Mechanism and Geometry of the Packaged Genome. *J. Mol. Biol.* 425, 3235–3249. <https://doi.org/10.1016/j.jmb.2013.06.005>
- Eckert, M., 2012. Max von Laue and the discovery of X-ray diffraction in 1912. *Ann. Phys.* 524, A83–A85. <https://doi.org/10.1002/andp.201200724>
- Eden, J.-S., Tanaka, M.M., Boni, M.F., Rawlinson, W.D., White, P.A., 2013. Recombination within the Pandemic Norovirus GII.4 Lineage. *J. Virol.* 87, 6270–6282. <https://doi.org/10.1128/JVI.03464-12>
- Engel, N.Y., Weiss, V.U., Marchetti-Deschmann, M., Allmaier, G., 2017. nES GEMMA Analysis of Lectins and Their Interactions with Glycoproteins – Separation, Detection, and Sampling of Noncovalent Biospecific Complexes. *J. Am. Soc. Mass Spectrom.* 28, 77–86. <https://doi.org/10.1007/s13361-016-1483-0>
- Esser, T.K., Böhning, J., Fremdling, P., Agasid, M.T., Costin, A., Fort, K., Konijnenberg, A., Gilbert, J.D., Bahm, A., Makarov, A., Robinson, C.V., Benesch, J.L.P., Baker, L., Bharat, T.A.M., Gault, J., Rauschenbach, S., 2022. Mass-selective and ice-free electron cryomicroscopy protein sample preparation via native electrospray ion-beam deposition. *PNAS Nexus* 1, pgac153. <https://doi.org/10.1093/pnasnexus/pgac153>
- Ettayebi, K., Crawford, S.E., Murakami, K., Broughman, J.R., Karandikar, U., Tenge, V.R., Neill, F.H., Blutt, S.E., Zeng, X.-L., Qu, L., Kou, B., Opekun, A.R., Burrin, D., Graham, D.Y., Ramani, S., Atmar, R.L., Estes, M.K., 2016. Replication of human noroviruses in stem cell-derived human enteroids. *Science* 353, 1387–1393. <https://doi.org/10.1126/science.aaf5211>
- Ettayebi, K., Tenge, V.R., Cortes-Penfield, N.W., Crawford, S.E., Neill, F.H., Zeng, X.-L., Yu, X., Ayyar, B.V., Burrin, D., Ramani, S., Atmar, R.L., Estes, M.K., 2021. New Insights and Enhanced Human Norovirus Cultivation in Human Intestinal Enteroids. *mSphere* 6, e01136-20. <https://doi.org/10.1128/mSphere.01136-20>
- Fallahi, S., Mattison, K., 2011. Evaluation of Murine Norovirus Persistence in Environments Relevant to Food Production and Processing. *J. Food Prot.* 74, 1847–1851. <https://doi.org/10.4315/0362-028X.JFP-11-081>
- Felitsyn, N., Peschke, M., Kebarle, P., 2002. Origin and number of charges observed on multiply-protonated native proteins produced by ESI. *Int. J. Mass Spectrom.* 219, 39–62. [https://doi.org/10.1016/S1387-3806\(02\)00588-2](https://doi.org/10.1016/S1387-3806(02)00588-2)
- Fernández-García, J., Compton, S., Wick, D., Fernandez de la Mora, J., 2019. Virus Size Analysis by Gas-Phase Mobility Measurements: Resolution Limits. *Anal. Chem.* 91, 12962–12970. <https://doi.org/10.1021/acs.analchem.9b03023>
- Fu, J.-G., Shi, C., Xu, C., Lin, Q., Zhang, J., Yi, Q.-H., Zhang, J., Bao, C.-J., Huo, X., Zhu, Y.-F., Ai, J., Xing, Z., 2017. Outbreaks of acute gastroenteritis associated with a re-emerging GII.P16-GII.2 norovirus in the spring of 2017 in Jiangsu, China. *PLOS ONE* 12, e0186090. <https://doi.org/10.1371/journal.pone.0186090>
- Fuchs, N.A., 1963. On the stationary charge distribution on aerosol particles in a bipolar ionic atmosphere. *Geofis. Pura E Appl.* 56, 185–193. <https://doi.org/10.1007/BF01993343>

- Fuerstenau, S.D., Benner, W.H., 1995. Molecular weight determination of megadalton DNA electrospray ions using charge detection time-of-flight mass spectrometry. *Rapid Commun. Mass Spectrom.* 9, 1528–1538. <https://doi.org/10.1002/rcm.1290091513>
- Fuerstenau, S.D., Benner, W.H., Thomas, J.J., Brugidou, C., Bothner, B., Siuzdak, G., 2001. Mass Spectrometry of an Intact Virus. *Angew. Chem. Int. Ed.* 40, 541–544. [https://doi.org/10.1002/1521-3773\(20010202\)40:3<541::AID-ANIE541>3.0.CO;2-K](https://doi.org/10.1002/1521-3773(20010202)40:3<541::AID-ANIE541>3.0.CO;2-K)
- Gauto, D.F., Estrozi, L.F., Schwieters, C.D., Effantin, G., Macek, P., Sounier, R., Sivertsen, A.C., Schmidt, E., Kerfah, R., Mas, G., Colletier, J.-P., Güntert, P., Favier, A., Schoehn, G., Schanda, P., Boisbouvier, J., 2019. Integrated NMR and cryo-EM atomic-resolution structure determination of a half-megadalton enzyme complex. *Nat. Commun.* 10. <https://doi.org/10.1038/s41467-019-10490-9>
- Ghosh, S., Kumar, M., Santiana, M., Mishra, A., Zhang, M., Labayo, H., Chibly, A.M., Nakamura, H., Tanaka, T., Henderson, W., Lewis, E., Voss, O., Su, Y., Belkaid, Y., Chiorini, J.A., Hoffman, M.P., Altan-Bonnet, N., 2022. Enteric viruses replicate in salivary glands and infect through saliva. *Nature* 607, 345–350. <https://doi.org/10.1038/s41586-022-04895-8>
- Gibson, G.T.T., Mugo, S.M., Oleschuk, R.D., 2009. Nanoelectrospray emitters: Trends and perspective. *Mass Spectrom. Rev.* 28, 918–936. <https://doi.org/10.1002/mas.20248>
- Glasgow, J., Tullman-Ercek, D., 2014. Production and applications of engineered viral capsids. *Appl. Microbiol. Biotechnol.* 98, 5847–5858. <https://doi.org/10.1007/s00253-014-5787-3>
- Glass, P.J., White, L.J., Ball, J.M., Leparac-Goffart, I., Hardy, M.E., Estes, M.K., 2000. Norwalk Virus Open Reading Frame 3 Encodes a Minor Structural Protein. *J. Virol.* 74, 6581–6591. <https://doi.org/10.1128/JVI.74.14.6581-6591.2000>
- Gomez, A., Tang, K., 1994. Charge and fission of droplets in electrostatic sprays. *Phys. Fluids* 6, 404–414. <https://doi.org/10.1063/1.868037>
- Gross, M.L., 1994. Accurate masses for structure confirmation. *J. Am. Soc. Mass Spectrom.* 5, 57–57. [https://doi.org/10.1016/1044-0305\(94\)85036-4](https://doi.org/10.1016/1044-0305(94)85036-4)
- Guilhaus, M., Selby, D., Mlynski, V., 2000. Orthogonal acceleration time-of-flight mass spectrometry. *Mass Spectrom. Rev.* 19, 65–107. [https://doi.org/10.1002/\(SICI\)1098-2787\(2000\)19:2<65::AID-MAS1>3.0.CO;2-E](https://doi.org/10.1002/(SICI)1098-2787(2000)19:2<65::AID-MAS1>3.0.CO;2-E)
- Hanisch, F.-G., 2022. Recombinant norovirus capsid protein VP1 (GII.4) expressed in H5 insect cells exhibits post-translational modifications with potential impact on lectin activity and vaccine design. *Glycobiology* 32, 496–505. <https://doi.org/10.1093/glycob/cwac017>
- Hansman, G.S., Guntapong, R., Pongsuwanna, Y., Natori, K., Katayama, K., Takeda, N., 2006. Development of an antigen ELISA to detect sapovirus in clinical stool specimens. *Arch. Virol.* 151, 551–561. <https://doi.org/10.1007/s00705-005-0630-x>
- Hansman, G.S., Taylor, D.W., McLellan, J.S., Smith, T.J., Georgiev, I., Tame, J.R.H., Park, S.-Y., Yamazaki, M., Gondaira, F., Miki, M., Katayama, K., Murata, K., Kwong, P.D., 2012. Structural Basis for Broad Detection of Genogroup II Noroviruses by a Monoclonal Antibody That Binds to a Site Occluded in the Viral Particle. *J. Virol.* 86, 3635–3646. <https://doi.org/10.1128/JVI.06868-11>

## Bibliography

- Harper, C.C., Elliott, A.G., Lin, H.-W., Williams, E.R., 2018. Determining Energies and Cross Sections of Individual Ions Using Higher-Order Harmonics in Fourier Transform Charge Detection Mass Spectrometry (FT-CDMS). *J. Am. Soc. Mass Spectrom.* 29, 1861–1869. <https://doi.org/10.1007/s13361-018-1987-x>
- Harper, C.C., Elliott, A.G., Oltrogge, L.M., Savage, D.F., Williams, E.R., 2019. Multiplexed Charge Detection Mass Spectrometry for High-Throughput Single Ion Analysis of Large Molecules. *Anal. Chem.* 91, 7458–7465. <https://doi.org/10.1021/acs.analchem.9b01669>
- Harper, C.C., Williams, E.R., 2019. Enhanced Multiplexing in Fourier Transform Charge Detection Mass Spectrometry by Decoupling Ion Frequency from Mass to Charge Ratio. *J. Am. Soc. Mass Spectrom.* 30, 2637–2645. <https://doi.org/10.1007/s13361-019-02330-3>
- Havlik, M., Marchetti-Deschmann, M., Friedbacher, G., Winkler, W., Messner, P., Perez-Burgos, L., Tauer, C., Allmaier, G., 2015. Comprehensive Size-Determination of Whole Virus Vaccine Particles Using Gas-Phase Electrophoretic Mobility Macromolecular Analyzer, Atomic Force Microscopy, and Transmission Electron Microscopy. *Anal. Chem.* 87, 8657–8664. <https://doi.org/10.1021/acs.analchem.5b01198>
- Heck, A.J.R., van den Heuvel, R.H.H., 2004. Investigation of intact protein complexes by mass spectrometry. *Mass Spectrom. Rev.* 23, 368–389. <https://doi.org/10.1002/mas.10081>
- Hogan, C.J., Carroll, J.A., Rohrs, H.W., Biswas, P., Gross, M.L., 2009. Combined Charged Residue-Field Emission Model of Macromolecular Electrospray Ionization. *Anal. Chem.* 81, 369–377. <https://doi.org/10.1021/ac8016532>
- Hogan, J.A., Jarrold, M.F., 2018. Optimized Electrostatic Linear Ion Trap for Charge Detection Mass Spectrometry. *J. Am. Soc. Mass Spectrom.* 29, 2086–2095. <https://doi.org/10.1007/s13361-018-2007-x>
- Holzinger, M., Le Goff, A., Cosnier, S., 2014. Nanomaterials for biosensing applications: a review. *Front. Chem.* 2. <https://doi.org/10.3389/fchem.2014.00063>
- Hu, L., Salmen, W., Chen, R., Zhou, Y., Neill, F., Crowe, J.E., Atmar, R.L., Estes, M.K., Prasad, B.V.V., 2022. Atomic structure of the predominant GII.4 human norovirus capsid reveals novel stability and plasticity. *Nat. Commun.* 13, 1241. <https://doi.org/10.1038/s41467-022-28757-z>
- Huo, Y., Wan, X., Wang, Z., Meng, S., Shen, S., 2015. Production of Norovirus VLPs to size homogeneity. *Virus Res.* 204, 1–5. <https://doi.org/10.1016/j.virusres.2015.04.009>
- Iavarone, A.T., Williams, E.R., 2003. Mechanism of Charging and Supercharging Molecules in Electrospray Ionization. *J. Am. Chem. Soc.* 125, 2319–2327. <https://doi.org/10.1021/ja021202t>
- Iribarne, J.V., 1976. On the evaporation of small ions from charged droplets. *J. Chem. Phys.* 64, 2287. <https://doi.org/10.1063/1.432536>
- Jarrold, M.F., 2022. Applications of Charge Detection Mass Spectrometry in Molecular Biology and Biotechnology. *Chem. Rev.* 122, 7415–7441. <https://doi.org/10.1021/acs.chemrev.1c00377>
- Jiang, X., Graham, D.Y., Wang, K., Estes, M.K., 1990. Norwalk Virus Genome Cloning and Characterization. *Science* 250, 1580–1583. <https://doi.org/10.1126/science.2177224>

- Jiang, X., Wang, M., Graham, D.Y., Estes, M.K., 1992. Expression, self-assembly, and antigenicity of the Norwalk virus capsid protein. *J. Virol.* 66, 6527–6532. <https://doi.org/10.1128/jvi.66.11.6527-6532.1992>
- Jones, M.K., Grau, K.R., Costantini, V., Kolawole, A.O., de Graaf, M., Freiden, P., Graves, C.L., Koopmans, M., Wallet, S.M., Tibbetts, S.A., Schultz-Cherry, S., Wobus, C.E., Vinjé, J., Karst, S.M., 2015. Human norovirus culture in B cells. *Nat. Protoc.* 10, 1939–1947. <https://doi.org/10.1038/nprot.2015.121>
- Jones, M.K., Watanabe, M., Zhu, S., Graves, C.L., Keyes, L.R., Grau, K.R., Gonzalez-Hernandez, M.B., Iovine, N.M., Wobus, C.E., Vinjé, J., Tibbetts, S.A., Wallet, S.M., Karst, S.M., 2014. Enteric bacteria promote human and mouse norovirus infection of B cells. *Science* 346, 755–759. <https://doi.org/10.1126/science.1257147>
- Jordan, J.S., Xia, Z., Williams, E.R., 2022. Tips on Making Tiny Tips: Secrets to Submicron Nanoelectrospray Emitters. *J. Am. Soc. Mass Spectrom.* 33, 607–611. <https://doi.org/10.1021/jasms.1c00372>
- Jung, J., Grant, T., Thomas, D.R., Diehnelt, C.W., Grigorieff, N., Joshua-Tor, L., 2019. High-resolution cryo-EM structures of outbreak strain human norovirus shells reveal size variations. *Proc. Natl. Acad. Sci.* 116, 12828–12832. <https://doi.org/10.1073/pnas.1903562116>
- Juraschek, R., Dülcks, T., Karas, M., 1999. Nanoelectrospray—More than just a minimized-flow electrospray ionization source. *J. Am. Soc. Mass Spectrom.* 10, 300–308. [https://doi.org/10.1016/S1044-0305\(98\)00157-3](https://doi.org/10.1016/S1044-0305(98)00157-3)
- Jurchen, J.C., Williams, E.R., 2003. Origin of Asymmetric Charge Partitioning in the Dissociation of Gas-Phase Protein Homodimers. *J. Am. Chem. Soc.* 125, 2817–2826. <https://doi.org/10.1021/ja0211508>
- Kadek, A., Lorenzen, K., Uetrecht, C., 2021. In a flash of light: X-ray free electron lasers meet native mass spectrometry. *Drug Discov. Today Technol.* 39, 89–99. <https://doi.org/10.1016/j.ddtec.2021.07.001>
- Kafader, J.O., Melani, R.D., Durbin, K.R., Ikwuagwu, B., Early, B.P., Fellers, R.T., Beu, S.C., Zabrouskov, V., Makarov, A.A., Maze, J.T., Shinholt, D.L., Yip, P.F., Tullman-Ercek, D., Senko, M.W., Compton, P.D., Kelleher, N.L., 2020. Multiplexed mass spectrometry of individual ions improves measurement of proteoforms and their complexes. *Nat. Methods* 17, 391–394. <https://doi.org/10.1038/s41592-020-0764-5>
- Kallinger, P., Szymanski, W.W., 2015. Experimental determination of the steady-state charging probabilities and particle size conservation in non-radioactive and radioactive bipolar aerosol chargers in the size range of 5–40 nm. *J. Nanoparticle Res.* 17. <https://doi.org/10.1007/s11051-015-2981-x>
- Kapikian, A.Z., Wyatt, R.G., Dolin, R., Thornhill, T.S., Kalica, A.R., Chanock, R.M., 1972. Visualization by Immune Electron Microscopy of a 27-nm Particle Associated with Acute Infectious Nonbacterial Gastroenteritis. *J. Virol.* 10, 1075–1081. <https://doi.org/10.1128/jvi.10.5.1075-1081.1972>
- Kaplan, M., Cukkemane, A., van Zundert, G.C.P., Narasimhan, S., Daniëls, M., Mance, D., Waksman, G., Bonvin, A.M.J.J., Fronzes, R., Folkers, G.E., Baldus, M., 2015. Probing a cell-embedded megadalton protein complex by DNP-supported solid-state NMR. *Nat. Methods* 12, 649–652. <https://doi.org/10.1038/nmeth.3406>

## Bibliography

- Karas, M., Bahr, U., Dülcks, T., 2000. Nano-electrospray ionization mass spectrometry: addressing analytical problems beyond routine. *Fresenius J. Anal. Chem.* 366, 669–676. <https://doi.org/10.1007/s002160051561>
- Katpally, U., Voss, N.R., Cavazza, T., Taube, S., Rubin, J.R., Young, V.L., Stuckey, J., Ward, V.K., Virgin, H.W., Wobus, C.E., Smith, T.J., 2010. High-Resolution Cryo-Electron Microscopy Structures of Murine Norovirus 1 and Rabbit Hemorrhagic Disease Virus Reveal Marked Flexibility in the Receptor Binding Domains. *J. Virol.* 84, 5836–5841. <https://doi.org/10.1128/JVI.00314-10>
- Kaufman, S.L., Kuchumov, A.R., Kazakevich, M., Vinogradov, S.N., 1998. Analysis of a 3.6-MDa Hexagonal Bilayer Hemoglobin from *Lumbricus terrestris* Using a Gas-Phase Electrophoretic Mobility Molecular Analyzer. *Anal. Biochem.* 259, 195–202. <https://doi.org/10.1006/abio.1998.2644>
- Kebarle, P., Verkerk, U.H., 2009. Electrospray: From ions in solution to ions in the gas phase, what we know now. *Mass Spectrom. Rev.* 28, 898–917. <https://doi.org/10.1002/mas.20247>
- Keifer, D.Z., Pierson, E.E., Hogan, J.A., Bedwell, G.J., Prevelige, P.E., Jarrold, M.F., 2014. Charge detection mass spectrometry of bacteriophage P22 procapsid distributions above 20 MDa: CDMS of bacteriophage P22 procapsid distributions above 20 MDa. *Rapid Commun. Mass Spectrom.* 28, 483–488. <https://doi.org/10.1002/rcm.6809>
- Keifer, D.Z., Shinholt, D.L., Jarrold, M.F., 2015. Charge Detection Mass Spectrometry with Almost Perfect Charge Accuracy. *Anal. Chem.* 87, 10330–10337. <https://doi.org/10.1021/acs.analchem.5b02324>
- Khaykelson, D., Raviv, U., 2020. Studying viruses using solution X-ray scattering. *Biophys. Rev.* 12, 41–48. <https://doi.org/10.1007/s12551-020-00617-4>
- Kissmann, J., Ausar, S.F., Foubert, T.R., Brock, J., Switzer, M.H., Detzi, E.J., Vedvick, T.S., Middaugh, C.R., 2008. Physical Stabilization of Norwalk Virus-Like Particles\*\*The views, opinions and/or findings contained in this report are those of the author(s) and should not be construed as an official Department of the Army position, policy or decision unless so designated by other documentation. *J. Pharm. Sci.* 97, 4208–4218. <https://doi.org/10.1002/jps.21315>
- Knutson, E.O., Whitby, K.T., 1975. Aerosol classification by electric mobility: apparatus, theory, and applications. *J. Aerosol Sci.* 6, 443–451. [https://doi.org/10.1016/0021-8502\(75\)90060-9](https://doi.org/10.1016/0021-8502(75)90060-9)
- Konermann, L., 2017. Addressing a Common Misconception: Ammonium Acetate as Neutral pH “Buffer” for Native Electrospray Mass Spectrometry. *J. Am. Soc. Mass Spectrom.* 28, 1827–1835. <https://doi.org/10.1007/s13361-017-1739-3>
- Konermann, L., Ahadi, E., Rodriguez, A.D., Vahidi, S., 2013. Unraveling the Mechanism of Electrospray Ionization. *Anal. Chem.* 85, 2–9. <https://doi.org/10.1021/ac302789c>
- Konermann, L., Metwally, H., Duez, Q., Peters, I., 2019. Charging and supercharging of proteins for mass spectrometry: recent insights into the mechanisms of electrospray ionization. *The Analyst* 144, 6157–6171. <https://doi.org/10.1039/C9AN01201J>
- Koopmans, M., Vennema, H., Heersma, H., van Strien, E., van Duynhoven, Y., Brown, D., Reacher, M., Lopman, B., for the European Consortium on Foodborne Viruses, 2003. Early Identification of Common-Source Foodborne Virus Outbreaks in Europe. *Emerg. Infect. Dis.* 9, 1136–1142. <https://doi.org/10.3201/eid0909.020766>

- Koromyslova, A.D., Hansman, G.S., 2015. Nanobody Binding to a Conserved Epitope Promotes Norovirus Particle Disassembly. *J. Virol.* 89, 2718–2730. <https://doi.org/10.1128/JVI.03176-14>
- Koromyslova, A.D., White, P.A., Hansman, G.S., 2015. Treatment of norovirus particles with citrate. *Virology* 485, 199–204. <https://doi.org/10.1016/j.virol.2015.07.009>
- Kostelic, M.M., Hsieh, C.-C., Sanders, H.M., Zak, C.K., Ryan, J.P., Baker, E.S., Aspinwall, C.A., Marty, M.T., 2022a. Surface Modified Nano-Electrospray Needles Improve Sensitivity for Native Mass Spectrometry. *J. Am. Soc. Mass Spectrom.* 33, 1031–1037. <https://doi.org/10.1021/jasms.2c00087>
- Kostelic, M.M., Ryan, J.P., Brown, L.S., Jackson, T.W., Hsieh, C.-C., Zak, C.K., Sanders, H.M., Liu, Y., Chen, V.S., Byrne, M., Aspinwall, C.A., Baker, E.S., Marty, M.T., 2022b. Stability and Dissociation of Adeno-Associated Viral Capsids by Variable Temperature-Charge Detection-Mass Spectrometry. *Anal. Chem.* 94, 11723–11727. <https://doi.org/10.1021/acs.analchem.2c02378>
- Koster, A.J., Grimm, R., Typke, D., Hegerl, R., Stoschek, A., Walz, J., Baumeister, W., 1997. Perspectives of Molecular and Cellular Electron Tomography. *J. Struct. Biol.* 120, 276–308. <https://doi.org/10.1006/jsbi.1997.3933>
- Krol, M.A., Olson, N.H., Tate, J., Johnson, J.E., Baker, T.S., Ahlquist, P., 1999. RNA-controlled polymorphism in the *in vivo* assembly of 180-subunit and 120-subunit virions from a single capsid protein. *Proc. Natl. Acad. Sci.* 96, 13650–13655. <https://doi.org/10.1073/pnas.96.24.13650>
- Kroneman, A., Vega, E., Vennema, H., Vinjé, J., White, P.A., Hansman, G., Green, K., Martella, V., Katayama, K., Koopmans, M., 2013. Proposal for a unified norovirus nomenclature and genotyping. *Arch. Virol.* 158, 2059–2068. <https://doi.org/10.1007/s00705-013-1708-5>
- Kumru, O.S., Joshi, S.B., Smith, D.E., Middaugh, C.R., Prusik, T., Volkin, D.B., 2014. Vaccine instability in the cold chain: Mechanisms, analysis and formulation strategies. *Biologicals* 42, 237–259. <https://doi.org/10.1016/j.biologicals.2014.05.007>
- Lecoq, L., Fogeron, M.-L., Meier, B.H., Nassal, M., Böckmann, A., 2020. Solid-State NMR for Studying the Structure and Dynamics of Viral Assemblies. *Viruses* 12, 1069. <https://doi.org/10.3390/v12101069>
- Li, T., Senesi, A.J., Lee, B., 2016. Small Angle X-ray Scattering for Nanoparticle Research. *Chem. Rev.* 116, 11128–11180. <https://doi.org/10.1021/acs.chemrev.5b00690>
- Liko, I., Allison, T.M., Hopper, J.T., Robinson, C.V., 2016. Mass spectrometry guided structural biology. *Curr. Opin. Struct. Biol.* 40, 136–144. <https://doi.org/10.1016/j.sbi.2016.09.008>
- Lin, Y., Fengling, L., Lianzhu, W., Yuxiu, Z., Yanhua, J., 2014. Function of VP2 protein in the stability of the secondary structure of virus-like particles of genogroup II norovirus at different pH levels: Function of VP2 protein in the stability of NoV VLPs. *J. Microbiol.* 52, 970–975. <https://doi.org/10.1007/s12275-014-4323-6>
- Lindsay, L., Wolter, J., De Coster, I., Van Damme, P., Verstraeten, T., 2015. A decade of norovirus disease risk among older adults in upper-middle and high income countries: a systematic review. *BMC Infect. Dis.* 15, 425. <https://doi.org/10.1186/s12879-015-1168-5>

## Bibliography

- Lomeli, S.H., Yin, S., Ogorzalek Loo, R.R., Loo, J.A., 2009. Increasing charge while preserving noncovalent protein complexes for ESI-MS. *J. Am. Soc. Mass Spectrom.* 20, 593–596. <https://doi.org/10.1016/j.jasms.2008.11.013>
- Loo, J.A., 2000. Electrospray ionization mass spectrometry: a technology for studying noncovalent macromolecular complexes. *Int. J. Mass Spectrom.* 200, 175–186. [https://doi.org/10.1016/S1387-3806\(00\)00298-0](https://doi.org/10.1016/S1387-3806(00)00298-0)
- Lorenzen, K., Olia, A.S., Uetrecht, C., Cingolani, G., Heck, A.J.R., 2008. Determination of Stoichiometry and Conformational Changes in the First Step of the P22 Tail Assembly. *J. Mol. Biol.* 379, 385–396. <https://doi.org/10.1016/j.jmb.2008.02.017>
- Lorenzen, K., Versluis, C., van Duijn, E., van den Heuvel, R.H.H., Heck, A.J.R., 2007. Optimizing macromolecular tandem mass spectrometry of large non-covalent complexes using heavy collision gases. *Int. J. Mass Spectrom.* 268, 198–206. <https://doi.org/10.1016/j.ijms.2007.06.012>
- Lössl, P., Snijder, J., Heck, A.J.R., 2014. Boundaries of Mass Resolution in Native Mass Spectrometry. *J. Am. Soc. Mass Spectrom.* 25, 906–917. <https://doi.org/10.1007/s13361-014-0874-3>
- Lu, Z., Ledgerwood, E.D., Hinchman, M.M., Dick, R., Parker, J.S.L., 2018. Conserved Surface Residues on the Feline Calicivirus Capsid Are Essential for Interaction with Its Receptor Feline Junctional Adhesion Molecule A (fJAM-A). *J. Virol.* 92, e00035-18. <https://doi.org/10.1128/JVI.00035-18>
- Lucas, R.W., Kuznetsov, Y.G., Larson, S.B., McPherson, A., 2001. Crystallization of Brome Mosaic Virus and T = 1 Brome Mosaic Virus Particles Following a Structural Transition. *Virology* 286, 290–303. <https://doi.org/10.1006/viro.2000.0897>
- Lučić, V., Förster, F., Baumeister, W., 2005. STRUCTURAL STUDIES BY ELECTRON TOMOGRAPHY: From Cells to Molecules. *Annu. Rev. Biochem.* 74, 833–865. <https://doi.org/10.1146/annurev.biochem.73.011303.074112>
- Lutomski, C.A., Lykтей, N.A., Pierson, E.E., Zhao, Z., Zlotnick, A., Jarrold, M.F., 2018. Multiple Pathways in Capsid Assembly. *J. Am. Chem. Soc.* 140, 5784–5790. <https://doi.org/10.1021/jacs.8b01804>
- Lutomski, C.A., Lykтей, N.A., Zhao, Z., Pierson, E.E., Zlotnick, A., Jarrold, M.F., 2017. Hepatitis B Virus Capsid Completion Occurs through Error Correction. *J. Am. Chem. Soc.* 139, 16932–16938. <https://doi.org/10.1021/jacs.7b09932>
- Makarov, A., 2000. Electrostatic Axially Harmonic Orbital Trapping: A High-Performance Technique of Mass Analysis. *Anal. Chem.* 72, 1156–1162. <https://doi.org/10.1021/ac991131p>
- Makarov, A., Denisov, E., Kholomeev, A., Balschun, W., Lange, O., Strupat, K., Horning, S., 2006. Performance Evaluation of a Hybrid Linear Ion Trap/Orbitrap Mass Spectrometer. *Anal. Chem.* 78, 2113–2120. <https://doi.org/10.1021/ac0518811>
- Mallagaray, A., Creutzmacher, R., Dülfer, J., Mayer, P.H.O., Grimm, L.L., Orduña, J.M., Trabjerg, E., Stehle, T., Rand, K.D., Blaum, B.S., Uetrecht, C., Peters, T., 2019. A post-translational modification of human Norovirus capsid protein attenuates glycan binding. *Nat. Commun.* 10. <https://doi.org/10.1038/s41467-019-09251-5>
- Mallagaray, A., Lockhauserbäumer, J., Hansman, G., Uetrecht, C., Peters, T., 2015. Attachment of Norovirus to Histo Blood Group Antigens: A Cooperative Multistep Process. *Angew. Chem. Int. Ed.* 54, 12014–12019. <https://doi.org/10.1002/anie.201505672>

- Mann, M., Meng, C.K., Fenn, J.B., 1989. Interpreting mass spectra of multiply charged ions. *Anal. Chem.* 61, 1702–1708. <https://doi.org/10.1021/ac00190a023>
- McAllister, R.G., Metwally, H., Sun, Y., Konermann, L., 2015. Release of Native-like Gaseous Proteins from Electrospray Droplets via the Charged Residue Mechanism: Insights from Molecular Dynamics Simulations. *J. Am. Chem. Soc.* 137, 12667–12676. <https://doi.org/10.1021/jacs.5b07913>
- McNaught, A.D., Wilkinson, A., International Union of Pure and Applied Chemistry (Eds.), 1997. *Compendium of chemical terminology: IUPAC recommendations*, 2nd ed. ed. Blackwell Science, Oxford [England] ; Malden, MA, USA.
- Metwally, H., Duez, Q., Konermann, L., 2018. Chain Ejection Model for Electrospray Ionization of Unfolded Proteins: Evidence from Atomistic Simulations and Ion Mobility Spectrometry. *Anal. Chem.* 90, 10069–10077. <https://doi.org/10.1021/acs.analchem.8b02926>
- Mirabelli, C., Santos-Ferreira, N., Gilliland, M.G., Cieza, R.J., Colacino, J.A., Sexton, J.Z., Neyts, J., Taube, S., Rocha-Pereira, J., Wobus, C.E., 2022. Human Norovirus Efficiently Replicates in Differentiated 3D-Human Intestinal Enteroids. *J. Virol.* e00855-22. <https://doi.org/10.1128/jvi.00855-22>
- Mohajerani, F., Tyukodi, B., Schlicksup, C.J., Hadden-Perilla, J.A., Zlotnick, A., Hagan, M.F., 2022. Multiscale Modeling of Hepatitis B Virus Capsid Assembly and Its Dimorphism. *ACS Nano* 16, 13845–13859. <https://doi.org/10.1021/acsnano.2c02119>
- Munro, J.B., Gorman, J., Ma, X., Zhou, Z., Arthos, J., Burton, D.R., Koff, W.C., Courter, J.R., Smith, A.B., Kwong, P.D., Blanchard, S.C., Mothes, W., 2014. Conformational dynamics of single HIV-1 envelope trimers on the surface of native virions. *Science* 346, 759–763. <https://doi.org/10.1126/science.1254426>
- Murray, K.K., Boyd, R.K., Eberlin, M.N., Langley, G.J., Li, L., Naito, Y., 2013. Definitions of terms relating to mass spectrometry (IUPAC Recommendations 2013). *Pure Appl. Chem.* 85, 1515–1609. <https://doi.org/10.1351/PAC-REC-06-04-06>
- Nelson, C.A., Wilen, C.B., Dai, Y.-N., Orchard, R.C., Kim, A.S., Stegeman, R.A., Hsieh, L.L., Smith, T.J., Virgin, H.W., Fremont, D.H., 2018. Structural basis for murine norovirus engagement of bile acids and the CD300lf receptor. *Proc. Natl. Acad. Sci.* 115. <https://doi.org/10.1073/pnas.1805797115>
- Nemecek, D., Boura, E., Wu, W., Cheng, N., Plevka, P., Qiao, J., Mindich, L., Heymann, J.B., Hurley, J.H., Steven, A.C., 2013. Subunit Folds and Maturation Pathway of a dsRNA Virus Capsid. *Structure* 21, 1374–1383. <https://doi.org/10.1016/j.str.2013.06.007>
- Nguyen, S., Fenn, J.B., 2007. Gas-phase ions of solute species from charged droplets of solutions. *Proc. Natl. Acad. Sci.* 104, 1111–1117. <https://doi.org/10.1073/pnas.0609969104>
- Olinares, P.D.B., Kang, J.Y., Llewellyn, E., Chiu, C., Chen, J., Malone, B., Saecker, R.M., Campbell, E.A., Darst, S.A., Chait, B.T., 2021. Native Mass Spectrometry-Based Screening for Optimal Sample Preparation in Single-Particle Cryo-EM. *Structure* 29, 186-195.e6. <https://doi.org/10.1016/j.str.2020.11.001>
- Olshefsky, A., Richardson, C., Pun, S.H., King, N.P., 2022. Engineering Self-Assembling Protein Nanoparticles for Therapeutic Delivery. *Bioconjug. Chem.* 33, 2018–2034. <https://doi.org/10.1021/acs.bioconjchem.2c00030>

## Bibliography

- Panczyk, E.M., Gilbert, J.D., Jagdale, G.S., Stiving, A.Q., Baker, L.A., Wysocki, V.H., 2020. Ion Mobility and Surface Collisions: Submicrometer Capillaries Can Produce Native-like Protein Complexes. *Anal. Chem.* 92, 2460–2467. <https://doi.org/10.1021/acs.analchem.9b03666>
- Parra, G.I., Tohma, K., Ford-Siltz, L.A., Eguino, P., Kendra, J.A., Pilewski, K.A., Gao, Y., 2023. Minimal Antigenic Evolution after a Decade of Norovirus GII.4 Sydney\_2012 Circulation in Humans. *J. Virol.* <https://doi.org/10.1128/jvi.01716-22>
- Paul, W., 1990. Electromagnetic Traps for Charged and Neutral Particles(Nobel Lecture). *Angew. Chem. Int. Ed. Engl.* 29, 739–748. <https://doi.org/10.1002/anie.199007391>
- Perutz, M.F., Rossmann, M.G., Cullis, A.F., Muirhead, H., Will, G., North, A.C.T., 1960. Structure of Hæmoglobin: A Three-Dimensional Fourier Synthesis at 5.5-Å. Resolution, Obtained by X-Ray Analysis. *Nature* 185, 416–422. <https://doi.org/10.1038/185416a0>
- Pierson, E.E., Contino, N.C., Keifer, D.Z., Jarrold, M.F., 2015. Charge Detection Mass Spectrometry for Single Ions with an Uncertainty in the Charge Measurement of 0.65 e. *J. Am. Soc. Mass Spectrom.* 26, 1213–1220. <https://doi.org/10.1007/s13361-015-1126-x>
- Pierson, E.E., Keifer, D.Z., Selzer, L., Lee, L.S., Contino, N.C., Wang, J.C.-Y., Zlotnick, A., Jarrold, M.F., 2014. Detection of Late Intermediates in Virus Capsid Assembly by Charge Detection Mass Spectrometry. *J. Am. Chem. Soc.* 136, 3536–3541. <https://doi.org/10.1021/ja411460w>
- Pogan, R., Dülfer, J., Uetrecht, C., 2018a. Norovirus assembly and stability. *Curr. Opin. Virol.* 31, 59–65. <https://doi.org/10.1016/j.coviro.2018.05.003>
- Pogan, R., Schneider, C., Reimer, R., Hansman, G., Uetrecht, C., 2018b. Norovirus-like VP1 particles exhibit isolate dependent stability profiles. *J. Phys. Condens. Matter* 30, 064006. <https://doi.org/10.1088/1361-648X/aaa43b>
- Pohl, C., Szczepankiewicz, G., Liebert, U.G., 2022. Analysis and optimization of a Caco-2 cell culture model for infection with human norovirus. *Arch. Virol.* 167, 1421–1431. <https://doi.org/10.1007/s00705-022-05437-3>
- Prasad, B.V., Rothnagel, R., Jiang, X., Estes, M.K., 1994. Three-dimensional structure of baculovirus-expressed Norwalk virus capsids. *J. Virol.* 68, 5117–5125. <https://doi.org/10.1128/jvi.68.8.5117-5125.1994>
- Prasad, B.V.V., Hardy, M.E., Dokland, T., Bella, J., Rossmann, M.G., Estes, M.K., 1999. X-ray Crystallographic Structure of the Norwalk Virus Capsid. *Science* 286, 287–290. <https://doi.org/10.1126/science.286.5438.287>
- Qi, C., Kulkarni, P., 2013. Miniature Dual-Corona Ionizer for Bipolar Charging of Aerosol. *Aerosol Sci. Technol.* 47, 81–92. <https://doi.org/10.1080/02786826.2012.728301>
- Rauschenbach, S., Ternes, M., Harnau, L., Kern, K., 2016. Mass Spectrometry as a Preparative Tool for the Surface Science of Large Molecules. *Annu. Rev. Anal. Chem.* 9, 473–498. <https://doi.org/10.1146/annurev-anchem-071015-041633>
- Rayleigh, Lord, 1882. XX. *On the equilibrium of liquid conducting masses charged with electricity.* *Lond. Edinb. Dublin Philos. Mag. J. Sci.* 14, 184–186. <https://doi.org/10.1080/14786448208628425>

- Reischl, G.P., Mäkelä, J.M., Karch, R., Nucid, J., 1996. Bipolar charging of ultrafine particles in the size range below 10 nm. *J. Aerosol Sci.* 27, 931–949. [https://doi.org/10.1016/0021-8502\(96\)00026-2](https://doi.org/10.1016/0021-8502(96)00026-2)
- Rey, F.A., Lok, S.-M., 2018. Common Features of Enveloped Viruses and Implications for Immunogen Design for Next-Generation Vaccines. *Cell* 172, 1319–1334. <https://doi.org/10.1016/j.cell.2018.02.054>
- Roepstorff, P., Fohlman, J., 1984. Letter to the editors. *Biol. Mass Spectrom.* 11, 601–601. <https://doi.org/10.1002/bms.1200111109>
- Salunke, D.M., Caspar, D.L., Garcea, R.L., 1989. Polymorphism in the assembly of polyomavirus capsid protein VP1. *Biophys. J.* 56, 887–900. [https://doi.org/10.1016/S0006-3495\(89\)82735-3](https://doi.org/10.1016/S0006-3495(89)82735-3)
- Samandoulgou, I., Hammami, R., Morales Rayas, R., Fliss, I., Jean, J., 2015. Stability of Secondary and Tertiary Structures of Virus-Like Particles Representing Noroviruses: Effects of pH, Ionic Strength, and Temperature and Implications for Adhesion to Surfaces. *Appl. Environ. Microbiol.* 81, 7680–7686. <https://doi.org/10.1128/AEM.01278-15>
- Schmidt, H.T., Cederquist, H., Jensen, J., Fardi, A., 2001. Conetrap: A compact electrostatic ion trap. *Nucl. Instrum. Methods Phys. Res. Sect. B Beam Interact. Mater. At.* 173, 523–527. [https://doi.org/10.1016/S0168-583X\(00\)00415-8](https://doi.org/10.1016/S0168-583X(00)00415-8)
- Sherman, M.B., Williams, A.N., Smith, H.Q., Pettitt, B.M., Wobus, C.E., Smith, T.J., 2021. Structural Studies on the Shapeshifting Murine Norovirus. *Viruses* 13, 2162. <https://doi.org/10.3390/v13112162>
- Shimada, M., Han, B., Okuyama, K., Otani, Y., 2002. Bipolar Charging of Aerosol Nanoparticles by a Soft X-ray Photoionizer. *J. Chem. Eng. Jpn.* 35, 786–793. <https://doi.org/10.1252/jcej.35.786>
- Shockley, W., 1938. Currents to Conductors Induced by a Moving Point Charge. *J. Appl. Phys.* 9, 635–636. <https://doi.org/10.1063/1.1710367>
- Shoemaker, G.K., van Duijn, E., Crawford, S.E., Uetrecht, C., Baclayon, M., Roos, W.H., Wuite, G.J.L., Estes, M.K., Prasad, B.V.V., Heck, A.J.R., 2010. Norwalk Virus Assembly and Stability Monitored by Mass Spectrometry. *Mol. Cell. Proteomics* 9, 1742–1751. <https://doi.org/10.1074/mcp.M900620-MCP200>
- Smith, R.D., Loa, J.A., Barinaga, C.J., Edmonds, C.G., Udseth, H.R., 1990. Collisional activation and collision-activated dissociation of large multiply charged polypeptides and proteins produced by electrospray ionization. *J. Am. Soc. Mass Spectrom.* 1, 53–65. [https://doi.org/10.1016/1044-0305\(90\)80006-9](https://doi.org/10.1016/1044-0305(90)80006-9)
- Snijder, Joost, Rose, R.J., Veessler, D., Johnson, J.E., Heck, A.J.R., 2013. Studying 18 MDa Virus Assemblies with Native Mass Spectrometry. *Angew. Chem. Int. Ed.* 52, 4020–4023. <https://doi.org/10.1002/anie.201210197>
- Snijder, J., Uetrecht, C., Rose, R.J., Sanchez-Eugenía, R., Marti, G.A., Agirre, J., Guérin, D.M.A., Wuite, G.J.L., Heck, A.J.R., Roos, W.H., 2013. Probing the biophysical interplay between a viral genome and its capsid. *Nat. Chem.* 5, 502–509. <https://doi.org/10.1038/nchem.1627>

## Bibliography

- Snijder, J., van de Waterbeemd, M., Damoc, E., Denisov, E., Grinfeld, D., Bennett, A., Agbandje-McKenna, M., Makarov, A., Heck, A.J.R., 2014. Defining the Stoichiometry and Cargo Load of Viral and Bacterial Nanoparticles by Orbitrap Mass Spectrometry. *J. Am. Chem. Soc.* 136, 7295–7299. <https://doi.org/10.1021/ja502616y>
- Snowden, J.S., Hurdiss, D.L., Adeyemi, O.O., Ranson, N.A., Herod, M.R., Stonehouse, N.J., 2020. Dynamics in the murine norovirus capsid revealed by high-resolution cryo-EM. *PLOS Biol.* 18, e3000649. <https://doi.org/10.1371/journal.pbio.3000649>
- Sobott, F., Hernández, H., McCammon, M.G., Tito, M.A., Robinson, C.V., 2002. A Tandem Mass Spectrometer for Improved Transmission and Analysis of Large Macromolecular Assemblies. *Anal. Chem.* 74, 1402–1407. <https://doi.org/10.1021/ac0110552>
- Someya, Y., Shirato, H., Hasegawa, K., Kumasaka, T., Takeda, N., 2011. Assembly of homogeneous norovirus-like particles accomplished by amino acid substitution. *J. Gen. Virol.* 92, 2320–2323. <https://doi.org/10.1099/vir.0.033985-0>
- Susa, A.C., Xia, Z., Williams, E.R., 2017. Small Emitter Tips for Native Mass Spectrometry of Proteins and Protein Complexes from Nonvolatile Buffers That Mimic the Intracellular Environment. *Anal. Chem.* 89, 3116–3122. <https://doi.org/10.1021/acs.analchem.6b04897>
- Tamara, S., den Boer, M.A., Heck, A.J.R., 2022. High-Resolution Native Mass Spectrometry. *Chem. Rev.* 122, 7269–7326. <https://doi.org/10.1021/acs.chemrev.1c00212>
- Tammet, H., 1995. Size and mobility of nanometer particles, clusters and ions. *J. Aerosol Sci.* 26, 459–475. [https://doi.org/10.1016/0021-8502\(94\)00121-E](https://doi.org/10.1016/0021-8502(94)00121-E)
- Teo, C.A., Donald, W.A., 2014. Solution Additives for Supercharging Proteins beyond the Theoretical Maximum Proton-Transfer Limit in Electrospray Ionization Mass Spectrometry. *Anal. Chem.* 86, 4455–4462. <https://doi.org/10.1021/ac500304r>
- Theillet, F.-X., 2022. In-Cell Structural Biology by NMR: The Benefits of the Atomic Scale. *Chem. Rev.* 122, 9497–9570. <https://doi.org/10.1021/acs.chemrev.1c00937>
- Timmermans, S.B.P.E., Ramezani, A., Montalvo, T., Nguyen, M., van der Schoot, P., van Hest, J.C.M., Zandi, R., 2022. The Dynamics of Viruslike Capsid Assembly and Disassembly. *J. Am. Chem. Soc.* 144, 12608–12612. <https://doi.org/10.1021/jacs.2c04074>
- Todd, A.R., Alexander, A.W., Jarrold, M.F., 2020. Implementation of a Charge-Sensitive Amplifier without a Feedback Resistor for Charge Detection Mass Spectrometry Reduces Noise and Enables Detection of Individual Ions Carrying a Single Charge. *J. Am. Soc. Mass Spectrom.* 31, 146–154. <https://doi.org/10.1021/jasms.9b00010>
- Todd, A.R., Jarrold, M.F., 2020. Dynamic Calibration Enables High-Accuracy Charge Measurements on Individual Ions for Charge Detection Mass Spectrometry. *J. Am. Soc. Mass Spectrom.* 31, 1241–1248. <https://doi.org/10.1021/jasms.0c00081>
- Tresset, G., Decouche, V., Bryche, J.-F., Charpilienne, A., Le Cœur, C., Barbier, C., Squires, G., Zeghal, M., Poncet, D., Bressanelli, S., 2013a. Unusual self-assembly properties of Norovirus Newbury2 virus-like particles. *Arch. Biochem. Biophys.* 537, 144–152. <https://doi.org/10.1016/j.abb.2013.07.003>
- Tresset, G., Le Coeur, C., Bryche, J.-F., Tatou, M., Zeghal, M., Charpilienne, A., Poncet, D., Constantin, D., Bressanelli, S., 2013b. Norovirus Capsid Proteins Self-Assemble through Biphasic Kinetics via Long-Lived Stave-like Intermediates. *J. Am. Chem. Soc.* 135, 15373–15381. <https://doi.org/10.1021/ja403550f>

- Twarock, R., Luque, A., 2019. Structural puzzles in virology solved with an overarching icosahedral design principle. *Nat. Commun.* 10, 4414. <https://doi.org/10.1038/s41467-019-12367-3>
- Utrecht, C., Barbu, I.M., Shoemaker, G.K., van Duijn, E., Heck, A.J.R., 2011. Interrogating viral capsid assembly with ion mobility–mass spectrometry. *Nat. Chem.* 3, 126–132. <https://doi.org/10.1038/nchem.947>
- Utrecht, C., Rose, R.J., van Duijn, E., Lorenzen, K., Heck, A.J.R., 2010. Ion mobility mass spectrometry of proteins and proteinassemblies. *Chem Soc Rev* 39, 1633–1655. <https://doi.org/10.1039/B914002F>
- Van Berkel, G.J., Kertesz, V., 2007. Using the Electrochemistry of the Electrospray Ion Source. *Anal. Chem.* 79, 5510–5520. <https://doi.org/10.1021/ac071944a>
- van de Waterbeemd, M., Fort, K.L., Boll, D., Reinhardt-Szyba, M., Routh, A., Makarov, A., Heck, A.J.R., 2017. High-fidelity mass analysis unveils heterogeneity in intact ribosomal particles. *Nat. Methods* 14, 283–286. <https://doi.org/10.1038/nmeth.4147>
- van de Waterbeemd, M., Snijder, J., Tsvetkova, I.B., Dragnea, B.G., Cornelissen, J.J., Heck, A.J.R., 2016. Examining the Heterogeneous Genome Content of Multipartite Viruses BMV and CCMV by Native Mass Spectrometry. *J. Am. Soc. Mass Spectrom.* 27, 1000–1009. <https://doi.org/10.1007/s13361-016-1348-6>
- van den Heuvel, R.H.H., van Duijn, E., Mazon, H., Synowsky, S.A., Lorenzen, K., Versluis, C., Brouns, S.J.J., Langridge, D., van der Oost, J., Hoyes, J., Heck, A.J.R., 2006. Improving the Performance of a Quadrupole Time-of-Flight Instrument for Macromolecular Mass Spectrometry. *Anal. Chem.* 78, 7473–7483. <https://doi.org/10.1021/ac061039a>
- Van Dycke, J., Cuvry, A., Knickmann, J., Ny, A., Rakers, S., Taube, S., de Witte, P., Neyts, J., Rocha-Pereira, J., 2021. Infection of zebrafish larvae with human norovirus and evaluation of the in vivo efficacy of small-molecule inhibitors. *Nat. Protoc.* 16, 1830–1849. <https://doi.org/10.1038/s41596-021-00499-0>
- Vinje, J., 2015. Advances in Laboratory Methods for Detection and Typing of Norovirus. *J. Clin. Microbiol.* 53, 373–381. <https://doi.org/10.1128/JCM.01535-14>
- Vinje, J., Estes, M.K., Esteves, P., Green, K.Y., Katayama, K., Knowles, N.J., L’Homme, Y., Martella, V., Vennema, H., White, P.A., ICTV Report Consortium, 2019. ICTV Virus Taxonomy Profile: Caliciviridae. *J. Gen. Virol.* 100, 1469–1470. <https://doi.org/10.1099/jgv.0.001332>
- Vongpunsawad, S., Venkataram Prasad, B.V., Estes, M.K., 2013. Norwalk Virus Minor Capsid Protein VP2 Associates within the VP1 Shell Domain. *J. Virol.* 87, 4818–4825. <https://doi.org/10.1128/JVI.03508-12>
- Wang, Z., Chen, Y., Yang, J., Han, Y., Shi, J., Zhan, S., Peng, R., Li, R., Zhang, Runling, Li, J., Zhang, Rui, 2021. External Quality Assessment for Molecular Detection of Severe Acute Respiratory Syndrome Coronavirus 2 (SARS-CoV-2) in Clinical Laboratories. *J. Mol. Diagn.* 23, 19–28. <https://doi.org/10.1016/j.jmoldx.2020.10.008>
- Weinheimer, A.J., 1988. The Charge Induced on a Conducting Cylinder by a Point Charge and Its Application to the Measurement of Charge on Precipitation. *J. Atmospheric Ocean. Technol.* 5, 298–304. [https://doi.org/10.1175/1520-0426\(1988\)005<0298:TCIOAC>2.0.CO;2](https://doi.org/10.1175/1520-0426(1988)005<0298:TCIOAC>2.0.CO;2)

## Bibliography

- Weiss, V.U., Balantic, K., Pittenauer, E., Tripisciano, C., Friedbacher, G., Weber, V., Marchetti-Deschmann, M., Allmaier, G., 2020a. Nano electrospray differential mobility analysis based size-selection of liposomes and very-low density lipoprotein particles for offline hyphenation to MALDI mass spectrometry. *J. Pharm. Biomed. Anal.* 179, 112998. <https://doi.org/10.1016/j.jpba.2019.112998>
- Weiss, V.U., Bereszczak, J.Z., Havlik, M., Kallinger, P., Gösler, I., Kumar, M., Blaas, D., Marchetti-Deschmann, M., Heck, A.J.R., Szymanski, W.W., Allmaier, G., 2015a. Analysis of a Common Cold Virus and Its Subviral Particles by Gas-Phase Electrophoretic Mobility Molecular Analysis and Native Mass Spectrometry. *Anal. Chem.* 87, 8709–8717. <https://doi.org/10.1021/acs.analchem.5b01450>
- Weiss, V.U., Bereszczak, J.Z., Havlik, M., Kallinger, P., Gösler, I., Kumar, M., Blaas, D., Marchetti-Deschmann, M., Heck, A.J.R., Szymanski, W.W., Allmaier, G., 2015b. Analysis of a Common Cold Virus and Its Subviral Particles by Gas-Phase Electrophoretic Mobility Molecular Analysis and Native Mass Spectrometry. *Anal. Chem.* 87, 8709–8717. <https://doi.org/10.1021/acs.analchem.5b01450>
- Weiss, V.U., Denderz, N., Allmaier, G., Marchetti-Deschmann, M., 2021. Online hyphenation of size-exclusion chromatography and gas-phase electrophoresis facilitates the characterization of protein aggregates. *ELECTROPHORESIS* 42, 1202–1208. <https://doi.org/10.1002/elps.202100018>
- Weiss, V.U., Frank, J., Piplits, K., Szymanski, W.W., Allmaier, G., 2020b. Bipolar Corona Discharge-Based Charge Equilibration for Nano Electrospray Gas-Phase Electrophoretic Mobility Molecular Analysis of Bio- and Polymer Nanoparticles. *Anal. Chem.* 92, 8665–8669. <https://doi.org/10.1021/acs.analchem.0c01904>
- Weiss, V.U., Golesne, M., Friedbacher, G., Alban, S., Szymanski, W.W., Marchetti-Deschmann, M., Allmaier, G., 2018. Size and molecular weight determination of polysaccharides by means of nano electrospray gas-phase electrophoretic mobility molecular analysis (nES GEMMA). *ELECTROPHORESIS* 39, 1142–1150. <https://doi.org/10.1002/elps.201700382>
- Wernisch, S., Pennathur, S., 2019. Application of differential mobility-mass spectrometry for untargeted human plasma metabolomic analysis. *Anal. Bioanal. Chem.* 411, 6297–6308. <https://doi.org/10.1007/s00216-019-01719-z>
- Westphall, M.S., Lee, K.W., Salome, A.Z., Lodge, J.M., Grant, T., Coon, J.J., 2022. Three-dimensional structure determination of protein complexes using matrix-landing mass spectrometry. *Nat. Commun.* 13. <https://doi.org/10.1038/s41467-022-29964-4>
- White, L.J., Hardy, M.E., Estes, M.K., 1997. Biochemical characterization of a smaller form of recombinant Norwalk virus capsids assembled in insect cells. *J. Virol.* 71, 8066–8072. <https://doi.org/10.1128/jvi.71.10.8066-8072.1997>
- Wiedensohler, A., Fissan, H.J., 1988. Aerosol charging in high purity gases. *J. Aerosol Sci.* 19, 867–870. [https://doi.org/10.1016/0021-8502\(88\)90054-7](https://doi.org/10.1016/0021-8502(88)90054-7)
- Wilm, M., Mann, M., 1996. Analytical Properties of the Nanoelectrospray Ion Source. *Anal. Chem.* 68, 1–8. <https://doi.org/10.1021/ac9509519>
- Wilm, M.S., Mann, M., 1994. Electrospray and Taylor-Cone theory, Dole's beam of macromolecules at last? *Int. J. Mass Spectrom. Ion Process.* 136, 167–180. [https://doi.org/10.1016/0168-1176\(94\)04024-9](https://doi.org/10.1016/0168-1176(94)04024-9)

- Wobus, C.E., Karst, S.M., Thackray, L.B., Chang, K.-O., Sosnovtsev, S.V., Belliot, G., Krug, A., Mackenzie, J.M., Green, K.Y., Virgin, H.W., 2004. Replication of Norovirus in Cell Culture Reveals a Tropism for Dendritic Cells and Macrophages. *PLoS Biol.* 2, e432. <https://doi.org/10.1371/journal.pbio.0020432>
- Wobus, C.E., Thackray, L.B., Virgin, H.W., 2006. Murine Norovirus: a Model System To Study Norovirus Biology and Pathogenesis. *J. Virol.* 80, 5104–5112. <https://doi.org/10.1128/JVI.02346-05>
- Wörner, T.P., Bennett, A., Habka, S., Snijder, J., Friese, O., Powers, T., Agbandje-McKenna, M., Heck, A.J.R., 2021. Adeno-associated virus capsid assembly is divergent and stochastic. *Nat. Commun.* 12. <https://doi.org/10.1038/s41467-021-21935-5>
- Wörner, T.P., Snijder, J., Bennett, A., Agbandje-McKenna, M., Makarov, A.A., Heck, A.J.R., 2020. Resolving heterogeneous macromolecular assemblies by Orbitrap-based single-particle charge detection mass spectrometry. *Nat. Methods* 17, 395–398. <https://doi.org/10.1038/s41592-020-0770-7>
- Wörner, T.P., Snijder, J., Friese, O., Powers, T., Heck, A.J.R., 2022. Assessment of genome packaging in AAVs using Orbitrap-based charge-detection mass spectrometry. *Mol. Ther. - Methods Clin. Dev.* 24, 40–47. <https://doi.org/10.1016/j.omtm.2021.11.013>
- Wu, W., Zhang, D., Chen, K., Zhou, P., Zhao, M., Qiao, L., Su, B., 2018. Highly Efficient Desalting by Silica Isoporous Membrane-Based Microfluidic Chip for Electrospray Ionization Mass Spectrometry. *Anal. Chem.* 90, 14395–14401. <https://doi.org/10.1021/acs.analchem.8b03934>
- Wu, X., Oleschuk, R.D., Cann, N.M., 2012. Characterization of microstructured fibre emitters: in pursuit of improved nano electrospray ionization performance. *The Analyst* 137, 4150. <https://doi.org/10.1039/c2an35249d>
- Zainazor, C.T., Hidayah, M.S.N., Chai, L.C., Tunung, R., Ghazali, F.M., Son, R., 2010. Retraction: The Scenario of Norovirus Contamination in Food and Food Handlers. *J. Microbiol. Biotechnol.* 20, 229–237. <https://doi.org/10.4014/jmb.0906.06032>
- Zhang, Z., Pulliam, C.J., Flick, T., Cooks, R.G., 2018. Electrophoretic Desalting To Improve Performance in Electrospray Ionization Mass Spectrometry. *Anal. Chem.* 90, 3856–3862. <https://doi.org/10.1021/acs.analchem.7b04529>
- Zhao, Z., Wang, J.C.-Y., Zhang, M., Lyktey, N.A., Jarrold, M.F., Jacobson, S.C., Zlotnick, A., 2021. Asymmetrizing an icosahedral virus capsid by hierarchical assembly of subunits with designed asymmetry. *Nat. Commun.* 12, 589. <https://doi.org/10.1038/s41467-020-20862-1>
- Zheng, D.-P., Ando, T., Fankhauser, R.L., Beard, R.S., Glass, R.I., Monroe, S.S., 2006. Norovirus classification and proposed strain nomenclature. *Virology* 346, 312–323. <https://doi.org/10.1016/j.virol.2005.11.015>
- Zoratto, S., Weiss, V.U., Friedbacher, G., Buengener, C., Pletzenauer, R., Foettinger-Vacha, A., Graninger, M., Allmaier, G., 2021. Adeno-associated Virus Virus-like Particle Characterization via Orthogonal Methods: Nanoelectrospray Differential Mobility Analysis, Asymmetric Flow Field-Flow Fractionation, and Atomic Force Microscopy. *ACS Omega* 6, 16428–16437. <https://doi.org/10.1021/acsomega.1c01443>

## 5. Appendix

### 5.1. Hazardous substances according to the Globally Harmonized System (GHS)

Table 1: Hazard (H) and precautionary statements of hazardous substances used in this work.

SUBSTANCE	PICTOGRAM	HAZARD (H) STATEMENTS	PRECAUTIONARY (P) STATEMENTS
<b>2-MERCAPTOETHANOL</b>	   	H301, H302, H310, H311, H314, H315, H317, H318, H331, H332, H361, H373, H400, H410, H411	P203, P260, P261, P262, P264, P264+P265, P270, P271, P272, P273, P280, P301+P316, P301+P317, P301+P330+P331, P302+P352, P302+P361+P354, P304+P340, P305+P354+P338, P316, P317, P318, P319, P321, P330, P332+P317, P333+P313, P361+P364, P362+P364, P363, P391, P403+P233, P405, P501
<b>ACETIC ACID</b>	 	H226, H314	P210, P233, P240, P241, P242, P243, P260, P264, P280, P301+P330+P331, P302+P361+P354, P303+P361+P353, P304+P340, P305+P354+P338, P316, P321, P363, P370+P378, P403+P235, P405, P501
<b>ACETONE</b>	 	H225, H319, H336	P210, P233, P240, P241, P242, P243, P261, P264+P265, P271, P280, P303+P361+P353, P304+P340, P305+P351+P338, P319, P337+P317, P370+P378, P403+P233, P403+P235, P405, P501

<b>ACETONITRILE</b>	 	H225, H302, H312, H319, H332	P210, P280, P301, P312, P302 + P352, P304 + P340, P305 + P351 + P338
<b>ACRYLAMIDE</b>	 	H301 H312 + H332 H315 H319 H317 H372, H350, H340, H361	P301 + P310, P302 + P352, P304 + P340, P305 + P351 + P338, P333 + P313, P260, P202
<b>AMMONIUM BICARBONATE</b>		H302	P264, P270, P301+P317, P330, P501
<b>AMMONIUM HYDROXIDE</b>	  	H314, H400	P260, P264, P273, P280, P301+P330+P331, P302+P361+P354, P304+P340, P305+P354+P338, P316, P321, P363, P391, P405, P501
<b>AMMONIUM PERSULFATE (APS)</b>	  	H272 H302 - H315 H317 H319 H334 H335	P210 P220, P261, P264 P280 P301 + P312 P302 + P352 P304 + P340 P305 + P351 + P338 P333 + P313 P403 + P233 P501 -
<b>ARGON</b>		H280, H281	P403+P410

Appendix

<p><b>CESIUM CHLORIDE</b></p>	 	<p>H302 (22.38%), H341 (10.49%), H361 (86.71%), H373 (44.06%)</p>	<p>P203, P260, P264, P270, P280, P281, P301+P317, P318, P319, P330, P405, P501</p>
<p><b>CESIUM IODIDE (CSI)</b></p>	 	<p>H302, H315, H317, H319, H335, H361, H400</p>	<p>P203, P261, P264, P264+P265, P270, P271, P272, P273, P280, P301+P317, P302+P352, P304+P340, P305+P351+P338, P318, P319, P321, P330, P332+P317, P333+P313, P337+P317, P362+P364, P391, P403+P233, P405, P501</p>
<p><b>FORMIC ACID</b></p>	  	<p>H226, H290, H302, H314, H331</p>	<p>P210 P280 P303+P361+P353 P304+P340, P305+P351+P338, P310</p>
<p><b>GLUTARALDEHYDE</b></p>	   	<p>H301, H314, H317, H330, H334, H335, H400, H411</p>	<p>P260, P261, P264, P270, P271, P272, P273, P280, P284, P301+P316, P301+P330+P331, P302+P352, P302+P361+P354, P304+P340, P305+P354+P338, P316, P319, P320, P321, P330, P333+P313, P342+P316, P362+P364, P363, P391, P403+P233, P405, and P501</p>

<b>METHANOL</b>	  	H225, H301, H311, H331, H370	P210, P233, P240, P241, P242, P243, P260, P261, P264, P270, P271, P280, P301+P316, P302+P352, P303+P361+P353, P304+P340, P308+P316, P316, P321, P330, P361+P364, P370+P378, P403+P233, P403+P235, P405, P501
<b>NITROGEN</b>		H280, H281	P282, P336+P317, P403, P410+P403
<b>SODIUM DODECYL SULFATE (SDS)</b>	  	H228, H302, H315, H318, H319, H332, H335, H412	P210, P240, P241, P261, P264, P264+P265, P270, P271, P273, P280, P301+P317, P302+P352, P304+P340, P305+P351+P338, P305+P354+P338, P317, P319, P321, P330, P332+P317, P337+P317, P362+P364, P370+P378, P403+P233, P405, P501
<b>SODIUM HYDROXIDE (NAOH)</b>		H314	P260, P264, P280, P301+P330+P331, P302+P361+P354, P304+P340, P305+P354+P338, P316, P321, P363, P405, P501
<b>N,N,N',N'-TETRAMETHYL ETHYLENEDIAMINE (TEMED)</b>	  	H225, H301, H314, H318, H331	P210, P280, P301 + P310, P303 + P361 + P353 P304 + P340, P403 + P235, P501
<b>TRIS HYDROCHLORIDE (TRIS HCL)</b>		H315, H319, H335	P261, P264, P264+P265, P271, P280, P302+P352, P304+P340, P305+P351+P338, P319, P321,

Appendix

			P332+P317, P337+P317, P362+P364, P403+P233, P405, P501
<b>URANYL ACETATE</b>	  	H300+H330, H300, H330, H373, H411	P260, P264, P270, P271, P273, P284, P301+P316, P304+P340, P316, P319, P320, P321, P330, P391, P403+P233, P405, P501
<b>XENON</b>		H280 (73.72%), H281 (26.28%):	P282, P336+P317, P403, P410+P403

## 5.2. Supporting information

### 5.2.1. Virus-like particle size and molecular weight/mass determination applying gas-phase electrophoresis (native nES GEMMA)

Analytical and Bioanalytical Chemistry

Electronic Supplement Material

## **Virus-like particle size and molecular weight/mass determination applying gas-phase electrophoresis (native nES GEMMA)**

Victor U. Weiss<sup>1\*</sup>, Ronja Pogan<sup>2,3\*</sup>, Samuele Zoratto<sup>1</sup>, Kevin Bond<sup>4</sup>, Pascale Boulanger<sup>5</sup>, Martin F. Jarrold<sup>4</sup>, Nicholas Lykтей<sup>4</sup>, Dominik Pahl<sup>6</sup>, Nicole Puffler<sup>1</sup>, Mario Schelhaas<sup>6</sup>, Ekaterina Selivanovitch<sup>4</sup>, Charlotte Uetrecht<sup>2,3</sup>, Günter Allmaier<sup>1</sup>,

<sup>1</sup> *Institute of Chemical Technologies and Analytics, TU Wien, Vienna, Austria*

<sup>2</sup> *Heinrich Pette Institute, Leibniz Institute for Experimental Virology, Hamburg, Germany*

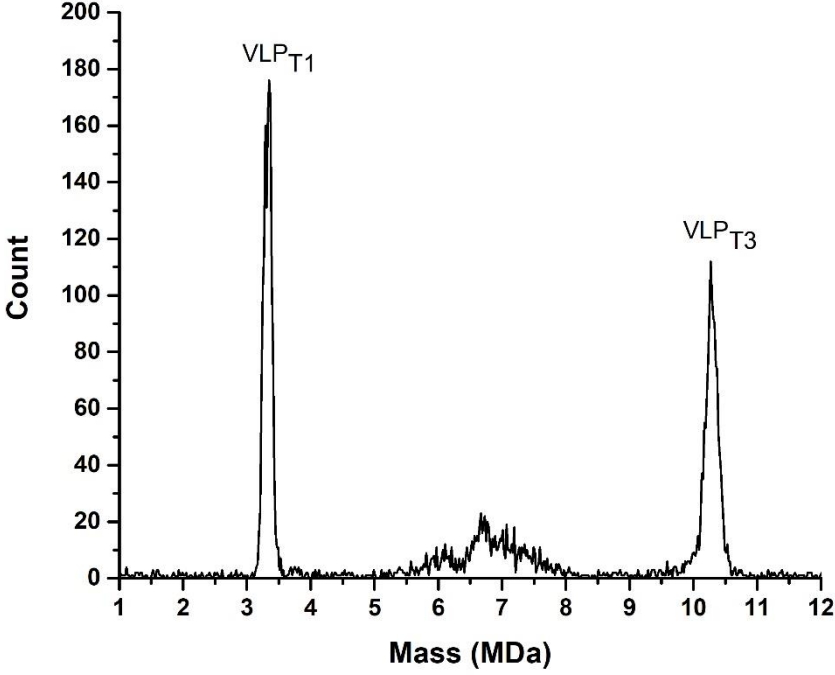
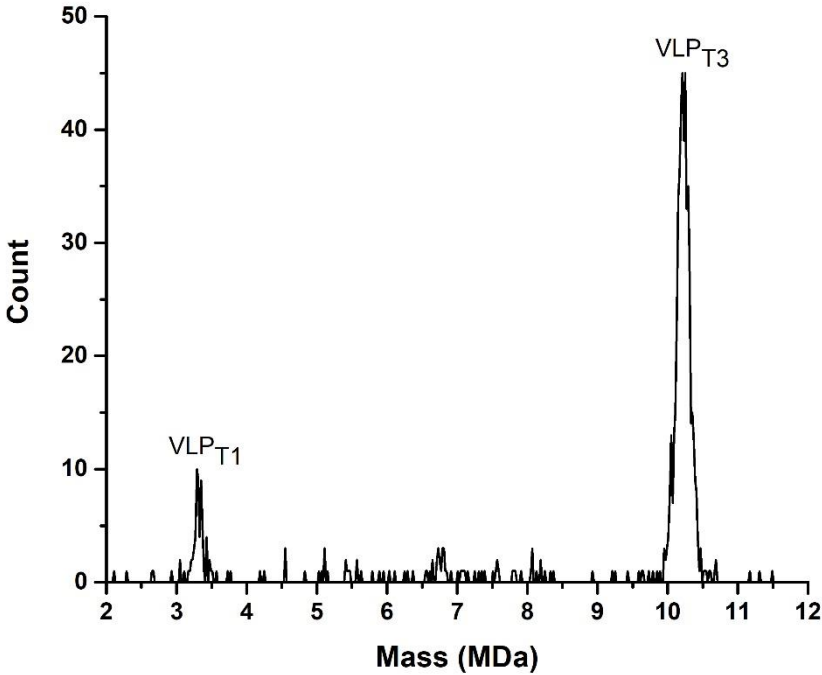
<sup>3</sup> *European XFEL GmbH, Schenefeld, Germany*

<sup>4</sup> *Department of Chemistry, Indiana University, Bloomington, IN, USA*

<sup>5</sup> *Institute for Integrative Biology of the Cell, CEA, CNRS, Université Paris-Sud, Université Paris-Saclay, Gif-sur-Yvette, France*

<sup>6</sup> *Institute of Cellular Virology, WWU Münster, Münster, Germany*

\* Contributed equally



**Electronic supplement material ESM Figure S1:** CDMS spectrum of norovirus West Chester VLPs measured in 50 mM ammonium acetate, pH 6 (top) and 250 mM ammonium acetate, pH 6 (bottom) with peak fitting. 20 kDa bin size were used. Note the overall lower count in the top spectrum indicative of suboptimal spray, which could cause the altered ratios of T1 to T3. Moreover, it is well known that norovirus assembly is sensitive to ionic strength [1, 2].

1. Pogan R, Schneider C, Reimer R, Hansman G, Uetrecht C. Norovirus-like VP1 particles exhibit isolate dependent stability profiles. *J Phys Condens Matter*. 2018;30(6):064006.
2. Shoemaker GK, van Duijn E, Crawford SE, Uetrecht C, Baclayon M, Roos WH, Wuite GJ, Estes MK, Prasad BV, Heck AJ. Norwalk virus assembly and stability monitored by mass spectrometry. *Mol Cell Proteomics*. 2010;9(8):1742-51.

## 5.2.2. Norovirus-like VP1 particles exhibit isolate-dependent stability profiles

### Supplement

## Norovirus-like VP1 particles exhibit isolate-dependent stability profiles

**Ronja Pogan<sup>1</sup>, Carola Schneider<sup>1</sup>, Rudolph Reimer<sup>1</sup>, Grant Hansman<sup>2,3</sup> and Charlotte Uetrecht<sup>1,4</sup>**

<sup>1</sup>Heinrich Pette Institute, Leibniz Institute for Experimental Virology, Hamburg, Germany

<sup>2</sup>Department of Infectious Diseases, Virology, Heidelberg University, Heidelberg, Germany

<sup>3</sup>Schaller Research Group at the University of Heidelberg and the DKFZ, Heidelberg

<sup>4</sup>European XFEL, Schenefeld, Germany

E-mail: [charlotte.uetrecht@xfel.eu](mailto:charlotte.uetrecht@xfel.eu)

Supplementary Figures S1-S6

Supplementary Tables S1-S3

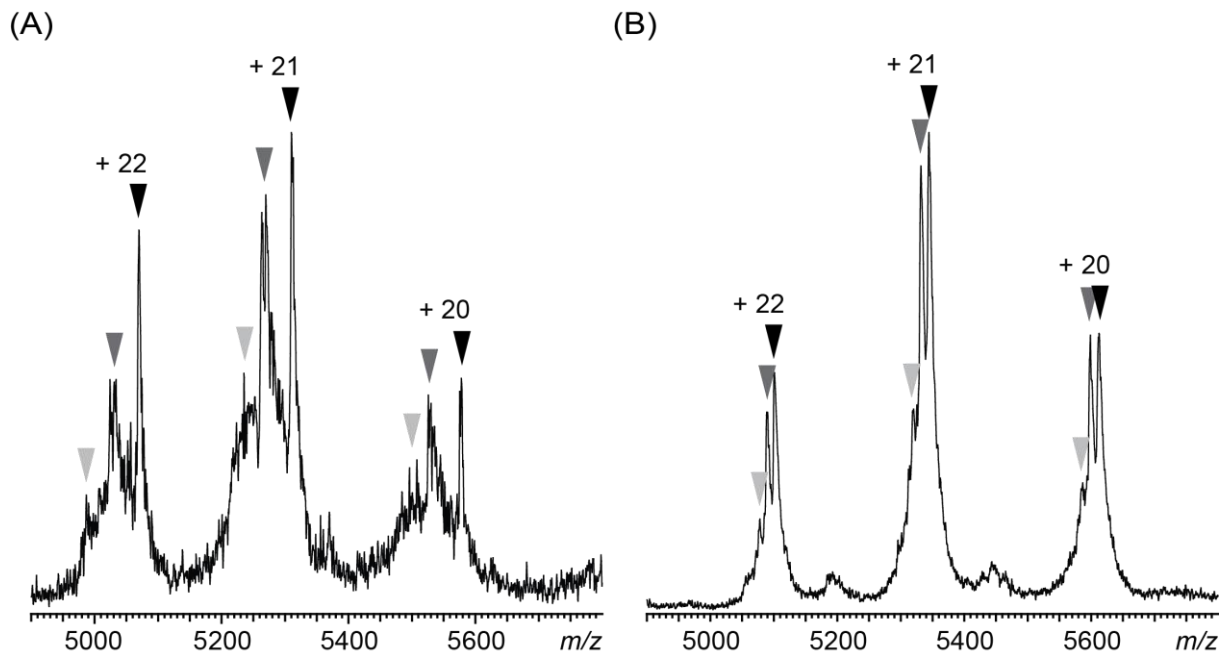


**Figure S1: Zoom-in to VP1 dimer charge state distributions.** Norovirus GII.17 Kawasaki (A) and GI.1 West Chester virus (B) analyzed at 10  $\mu$ M VP1 in 250 mM ammonium acetate, pH 10. Peaks are marked with arrowheads and charge states. (A) Kawasaki virus shows dimer peaks with three species of mass  $109700 \pm 100$  Da (light grey),  $110540 \pm 40$  Da (grey), and  $111530 \pm 20$  Da (black). (B) The West Chester virus shows VP1 dimer peaks with three species of mass  $111717 \pm 10$  (light grey),  $111960 \pm 7$  Da (grey), and  $112257 \pm 3$  Da (black). In Kawasaki free dimer was only observed at pH 10, therefore the observed masses could stem from a truncated subpopulation dissociating earlier. This would be in line with the noisy spectra likely containing more than three species. The West Chester triplet is in line with two distinct versions of the protein differing  $\sim 270$  Da in line with the loss of two N-terminal methionines.

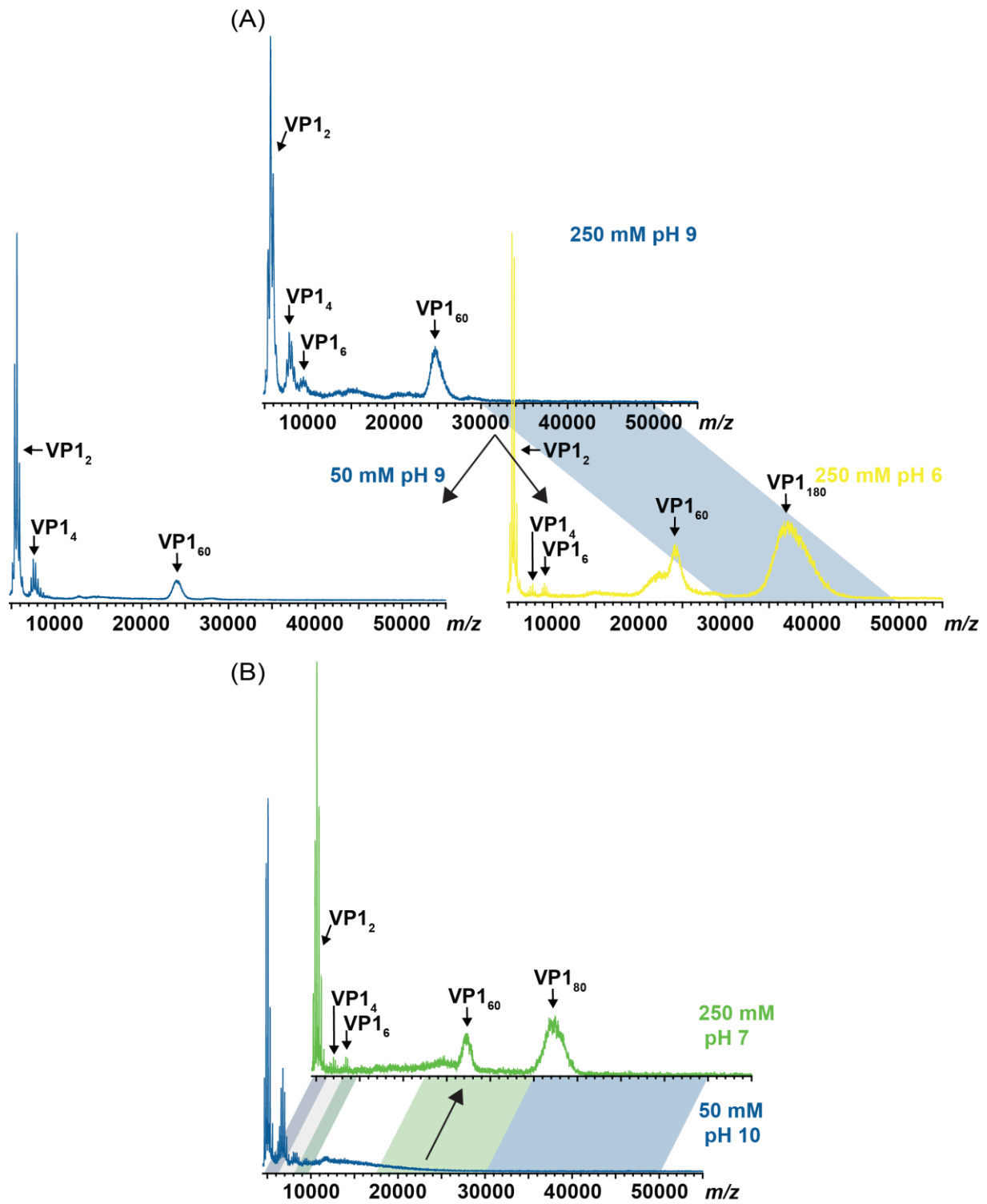


**Figure S2: Reassembly of GI.1 West Chester VLPs.** Representative mass spectra of West Chester VP1 solutions in ammonium acetate. (A) Reassembly of  $T = 3$  particles. A stock solution (120  $\mu$ M VP1) in 250 mM ammonium acetate, pH 9 was diluted 1:10 in 250 mM ammonium acetate, pH 9 (top), 50 mM ammonium acetate, pH 9 (bottom left) and 250 mM ammonium acetate, pH 6 (bottom right). The spectra demonstrate that disassembled  $T = 3$  particles are able to reassemble, indicated by the blue bar. Notably, some VP1 60mers remain upon dilution to lower ionic strength. VP1 60mers were not detected in 50 mM pH 9 after buffer exchange from PBS (Figure 3). However, upon dilution the real ionic strength will be higher (70 mM ammonium acetate), which could stabilize the 60mer. (B) Disassembled capsid

oligomers are able to reassemble also into  $T = 1$  particles. A solution of 10  $\mu\text{M}$  VP1 in 50 mM ammonium acetate pH 10 (bottom) was exchanged to a 250 mM ammonium acetate pH 7 solution, resulting in a final VP1 concentration of 6  $\mu\text{M}$ . Next to VP1 60mers, VP1 80mers were formed at high ionic strength and low pH. At this condition after solution exchange from PBS,  $T = 3$  particles were detected (Figure S3). Note that both the concentration used for solution exchange and for the measurement were lower, indicating that  $T = 3$  assembly is VP1 concentration dependent. This is in line with observations by Shoemaker et al. (2010), who could show that the VP1 concentration is affecting the ratio of VP1 oligomers. Nevertheless, it cannot be excluded that pH 10 introduces structural alterations precluding formation of  $T = 3$ .

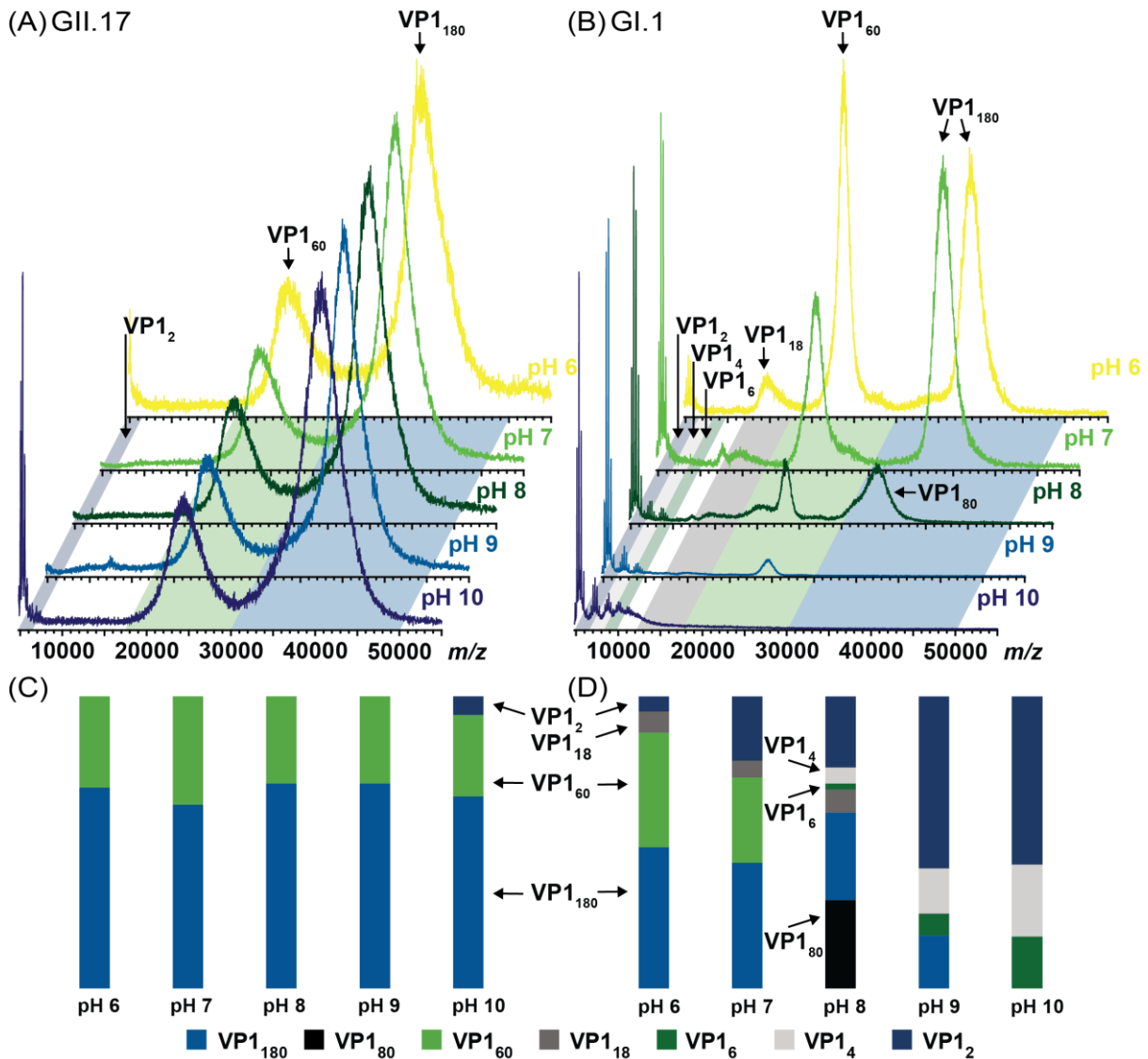


**Figure S3: Comparison of norovirus VLP stability monitored by native MS in 250 mM ammonium acetate solution.** Representative mass spectra of norovirus VLPs (10  $\mu$ M VP1) at pH values indicated (from top to bottom pH 6-10) (A) mass spectra obtained for the GII.17 Kawasaki virus and (B) for the GI.1 West Chester virus. Data are normalized to the highest peak. Colored inlets indicate the respective  $m/z$  range, where intensities were summed for the respective VP1 oligomers. Due to overlapping distributions, the VP1 80mer falls into the same  $m/z$  range as VP1 180mers, the descriptor therefore changes at pH 8 in (D). The intensity fractions of oligomers are shown for GII.17 Kawasaki (C) and for GI.1 West Chester (D) viruses. Note that in panel (B) the same spectrum as in figure 1 is shown.

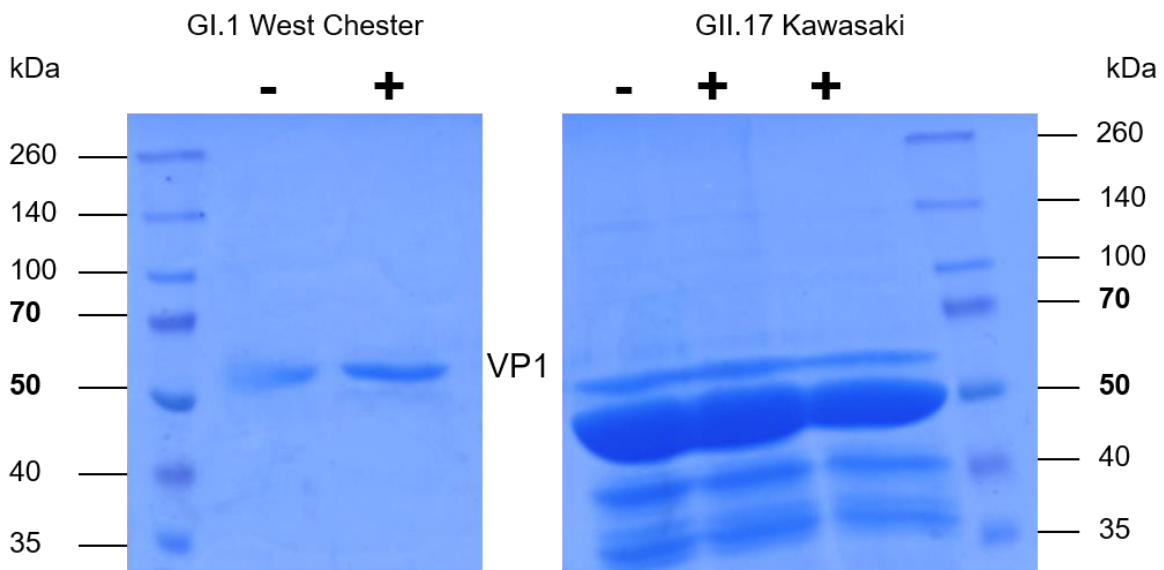


**Figure S4: SDS-PAGE of GI.1 West Chester (30  $\mu$ g) and GII.17 Kawasaki (110  $\mu$ g) preparations.** Protein samples in SDS buffer were subjected to electrophoresis under non-reducing (-) and reducing (+) conditions through a 4-10 % SDS-PAGE gel. The gel was stained with Coomassie blue R250. Molecular mass markers (M) are indicated in kDa.

Sodium dodecyl sulfate polyacrylamide gel electrophoresis (SDS-PAGE) on crude (PBS buffer) VLP solutions were performed following the reported method (Laemmli, 1970). A ten percent polyacrylamide separating gel (25 % acrylamide:bis-acrylamide = 37.5:1, 1% SDS, 0.1% TEMED, 1% APS and 37.5 % Tris-HCl, pH 8.8) and a 4 % stacking gel (15 % acrylamide:bis-acrylamide = 37.5:1, 1% SDS, 0.1% TEMED, 1% APS and 12.5 % Tris-HCl, pH 6.8) were used. Reducing conditions were introduced by adding 2-mercaptoethanol to the loading dye. The gels were stained with a solution containing 0.5% Coomassie brilliant blue R250, 50% ethanol and 7% acetic acid.

Appendix

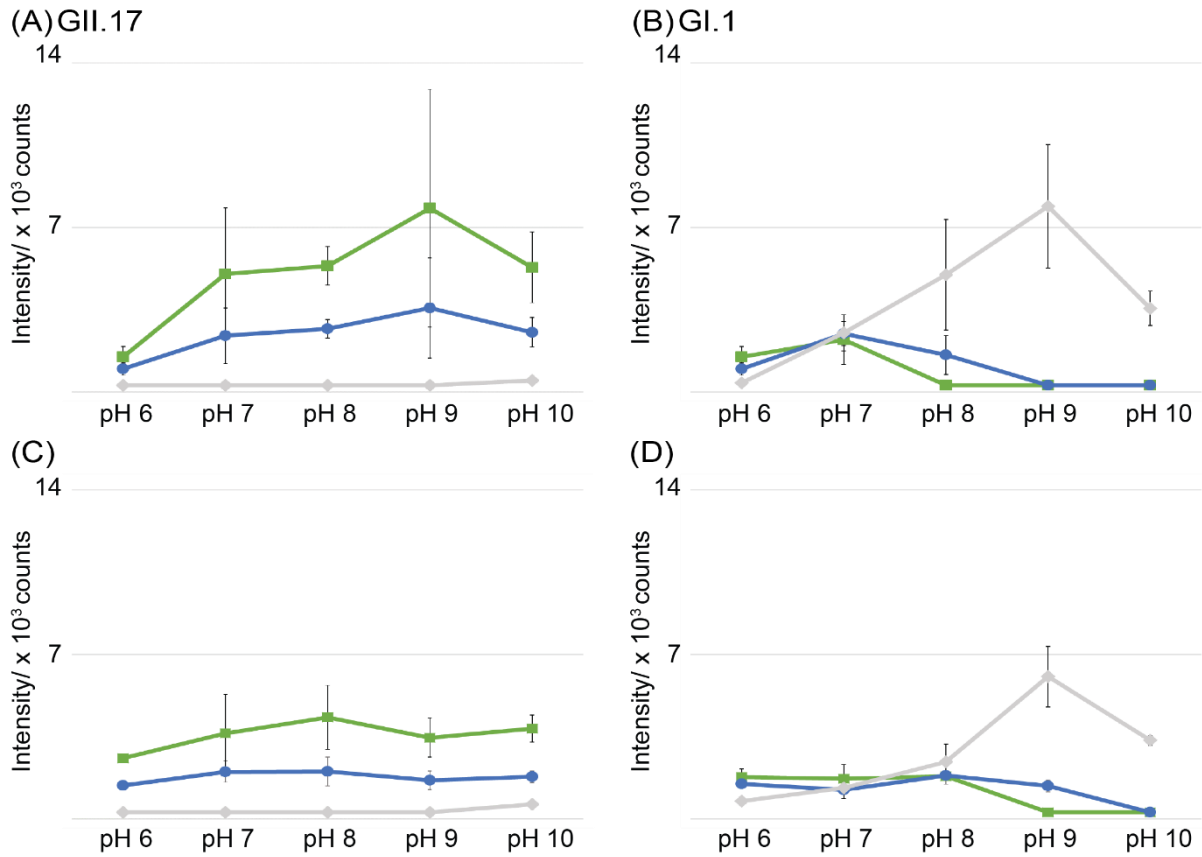


**Figure S5: Comparison of absolute intensities for norovirus GII.17 Kawasaki (A, C) and GI.1 West Chester (B, D) VLPs in 250 mM (A, B) and 50 mM (C, D) ammonium acetate.** Average intensities summed over 100 s at the respective  $m/z$  range are shown in black for  $T = 3$ , in dark grey for  $T = 1$  and light grey for a combined low  $m/z$  region corresponding to smaller oligomers.

Norwalk	1	MMMASKDATSSVDGASGAGQLVPEVNASDPLAMDPVAGSSTAVATAGQVNPIDPWIINNF
West Ch.	1	MMMASKDATSNVDGASGAGQLVPEANTSDPLAMDPVAGSSTAVATAGQVNPIDPWIINNF
Kawasaki	1	MKMASNDAAPSNDAAG---LVPEGNN-ETLPLEPVAGAAIAAPVTGQNNIIDPWIRTNF
Norwalk	61	VQAPQGEFTTISPNNTPGDVLFDSLGLPHLNPFLHLHLSQMYNGWVGNMRVRIMLAGNAFTA
West Ch.	61	VQAPQGEFTTISPNNTPGDVLFDSLGLPHLNPFLHLHLSQMYNGWVGNMRVRIMLAGNAFTA
Kawasaki	57	VQAPNGEFTVSPRNSPGEILLNLELGPDLNPLYLAHLRMYNGYAGGVEVQVLLAGNAFTA
Norwalk	121	GKIIIVSCIPPGFGSHNLTIQAATLFPFHVIADVRTLDPPIEVPLEDVRNVLFHNNDRNQQT
West Ch.	121	GKIIIVSCIPPGFGSHNLTIQAATLFPFHVIADVRTLDPPIEVPLEDVRNVLFHNNDRNQQT
Kawasaki	117	GKILFAAVPPNFPVEFLSPAQITMLPHLIVDVRTLPLEPIMIPLPDVRNTFFHYSNQPNSRM
Norwalk	181	RLVCMLYTPLRTGGGTGDSFVVAGRVMTCPSPDFNFLFLVPPTVEQKTRPFTLPNLPSS
West Ch.	181	RLVCMLYTPLRTGGGTGDSFVVAGRVMTCPSPDFNFLFLVPPTVEQKTRPFTLPNLPSS
Kawasaki	177	RLVAMLYTPLRSNGSGDDVFTVSCRVLTRPTDFEFTYLVPPSVESKTKPFSLPILTLSE
Norwalk	241	LSNSRAPLPISSMGISPDNVQSVQFQNGRCTLGRLVGTTPVSLSHVAKIRGTSNG----
West Ch.	241	LSNSRAPLPISSMGISPDNVQSVQFQNGRCTLGRLVGTTPVSLSQVAKIRGTSNG----
Kawasaki	237	LTNSRFVPIIDSLFTAQNNVLQVQCQNGRCTLGDELQGTQLLPBTGICAFRGRVTAQINQ
Norwalk	297	---TVINLTELDTGTPFFHPFE-GPAPIGFDPDLGGCDWH-----INMTQFGHSSQTQYDVD
West Ch.	297	---TVINLTELDTGTPFFHPFE-GPAPIGFDPDLGGCDWH-----VNMTQFGHSSQTQFDVD
Kawasaki	297	RDRWHMQLQNLNGTTYDPTDDVPAPLGTDFKGVVFGMVSRNVGNDAPGSTRAQQAWVS
Norwalk	347	TPDTEFVPHLGSIQANGIGSGNYVGVLSWISPP---SHPSGSQVDLWKIPNYGSSITEAT
West Ch.	347	TPPETFVPHLGSIQANGVGSNGYIGVLSWISPP---SHPSGSQVDLWKIPNYGSSITEAT
Kawasaki	357	TYSPQFVPKLGSVNLRLISDNDDFQFQPTKFTFVGVNDDDDGHPFRQWELPNYSGELTLNM
Norwalk	404	HLAPSVYPPGFGEVLVFFMFKMPPGAYN---LPCLLPQEYISHLASEQAPTVEAALLH
West Ch.	404	HLAPSVFPPGFGEVLVFFMFKIPGAYN---LPCLLPQEYISHFASEQAPTVEAALLH
Kawasaki	417	NLAPPVAPNFPGEQLLFFRSFVPCSGGYNQGIIDCLIPQEWIQHFYQESAPSQSDVALIR
Norwalk	461	YVDPDTGRNLGEFKAYPDGFLTCTVNGASSGPQQLPINGVFVFSWVSRFYQLKPVGTAS
West Ch.	461	YVDPDTGRNLGEFKAYPDGFLTCTVNGASSGPQQLPINGVFVFSWVSRFYQLKPVGTAS
Kawasaki	477	YVNPDTGRTLFEAKLHRSGYITVAHSG--DYPLVVPANGHFRFDSWVNQFYSLAPMGTGN
Norwalk	521	SARGRLGLRR
West Ch.	521	SARGRLGLRR
Kawasaki	535	GRRAQ----

**identical - similar - different**

**Figure S6: Sequence alignment GI.1 Norwalk, GI.1 West Chester and GII.17 Kawasaki.** S domain covers amino acids 1-225. The alignment was performed using the T-Coffee alignment package (Notredame et al., 2000).

**Table S1: Masses from VP1 oligomers for GI.1 West Chester and GII.17 Kawasaki VLPs** were determined from three MS measurements and listed with standard deviations and the average full width half maximum (FWHM) value. FWHM are given for the whole peak area as the individual species were not fully resolved (see Figure S1). All values in Da.

<b>GI.1 West Chester</b>				
Species	Theor. mass	Exp. mass n = 3	St. dev	Avg. FWHM
VP1 <sub>2</sub>	113218	112257	3	588
VP1 <sub>2</sub> * <sup>1</sup>	112956	111960	7	588
VP1 <sub>2</sub> * <sup>2</sup>	112694	111717	10	588
<b>GI.17 Kawasaki</b>				
	Theor. mass	Exp. mass n = 3	St. dev	Avg. FWHM
VP1 <sub>2</sub>	118768	111530	20	1950
VP1 <sub>2</sub>	118768	110540	40	1950
VP1 <sub>2</sub>	118768	109700	100	1950

\*<sup>1+2</sup>Putative N-terminal processing of two and four methionine residues of one and two monomers, respectively (VP1<sub>2</sub>\*<sup>1</sup> calculated Th. VP1<sub>2</sub> – 2x 131 Da and VP1<sub>2</sub>\*<sup>2</sup> calculated Th. VP1<sub>2</sub> – 4 x 131 Da).

**Table S2: Relative intensities for select  $m/z$  ranges from native MS in 50 mM ammonium acetate in pH 6 – 10 for GI.1 West Chester and GII.17 Kawasaki, corresponding to the intensity plots in figure 4. Signals were summed over 100 s in the respective  $m/z$  range and averaged. Values are given in %.  $N = 3$**

<b>GI.1 West Chester</b>										
	VP1 <sub>180</sub>		VP1 <sub>60</sub>		VP1 <sub>6</sub>		VP1 <sub>4</sub>		VP1 <sub>2</sub>	
	30000 – 50000 $m/z$		17500 - 30000 $m/z$		8200 - 9600 $m/z$		6500 - 8200 $m/z$		4800 - 6500 $m/z$	
pH 6	0.60	± 0.03	0.35	± 0.01					0.05	± 0.01
pH 7	0.28	± 0.13	0.35	± 0.03	0.05	± 0.01	0.09	± 0.02	0.24	± 0.12
pH 8			0.19	± 0.06	0.05	± 0.02	0.15	± 0.06	0.61	± 0.14
pH 9					0.11	± 0.02	0.31	± 0.02	0.58	± 0.04
pH 10					0.19	± 0.04	0.38	± 0.04	0.43	± 0.08
<b>GII.17 Kawasaki308</b>										
	VP1 <sub>180</sub>		VP1 <sub>60</sub>		VP1 <sub>6</sub>		VP1 <sub>4</sub>		VP1 <sub>2</sub>	
	30000 – 50000 $m/z$		17500 - 30000 $m/z$		8200 - 9600 $m/z$		6500 - 8200 $m/z$		4800 - 6500 $m/z$	
pH 6	0.69	± 0.00	0.31	± 0.00						
pH 7	0.69	± 0.01	0.31	± 0.01						
pH 8	0.68	± 0.00	0.32	± 0.00						
pH 9	0.69	± 0.01	0.31	± 0.01						
pH 10	0.67	± 0.01	0.30	± 0.00					0.01	± 0.01

**Table S3: Relative intensities for select  $m/z$  ranges from native MS in 250 mM ammonium acetate in pH 6 – 10 for GI.1 West Chester and GII.17 Kawasaki, corresponding to the intensity plots in figure S3. Signals were summed over 100 s in the respective  $m/z$  range and averaged. Values are given in %.  $N = 3$**

<b>GI.1 West Chester</b>						
	VP1 <sub>180</sub>	VP1 <sub>60</sub>	VP1 <sub>18</sub>	VP1 <sub>6</sub>	VP1 <sub>4</sub>	VP1 <sub>2</sub>
	30000 – 50000 $m/z$	17500 - 30000 $m/z$	12000 - 17500 $m/z$	8200 - 9600 $m/z$	6500 - 8200 $m/z$	4800 - 6500 $m/z$
pH 6	0.48 ± 0.04	0.39 ± 0.04	0.07 ± 0.01			0.05 ± 0.01
pH 7	0.43 ± 0.05	0.29 ± 0.03	0.06 ± 0.00			0.22 ± 0.07
pH 8	0.30 ± 0.03	0.30 ± 0.00	0.08 ± 0.00	0.02 ± 0.00	0.06 ± 0.02	0.24 ± 0.01
pH 9		0.18 ± 0.02		0.08 ± 0.03	0.15 ± 0.05	0.59 ± 0.09
pH 10				0.18 ± 0.01	0.25 ± 0.02	0.58 ± 0.01
<b>GII.17 Kawasaki308</b>						
	VP1 <sub>180</sub>	VP1 <sub>60</sub>	VP1 <sub>18</sub>	VP1 <sub>6</sub>	VP1 <sub>4</sub>	VP1 <sub>2</sub>
	30000 – 50000 $m/z$	17500 - 30000 $m/z$	12000 - 17500 $m/z$	8200_9600 $m/z$	6500_8200 $m/z$	4800_6500 $m/z$
pH 6	0.69 ± 0.00	0.31 ± 0.00				
pH 7	0.63 ± 0.09	0.37 ± 0.09				
pH 8	0.70 ± 0.00	0.30 ± 0.00				
pH 9	0.70 ± 0.01	0.30 ± 0.01				
pH 10	0.66 ± 0.02	0.28 ± 0.01				0.06 ± 0.03

**References**

- LAEMMLI, U. K. 1970. Cleavage of Structural Proteins during the Assembly of the Head of Bacteriophage T4. *Nature*, 227, 680-685.
- NOTREDAME, C., HIGGINS, D. G. & HERINGA, J. 2000. T-Coffee: A novel method for fast and accurate multiple sequence alignment. *J Mol Biol*, 302, 205-17.
- SHOEMAKER, G. K., VAN DUIJN, E., CRAWFORD, S. E., UETRECHT, C., BACLAYON, M., ROOS, W. H., WUIITE, G. J., ESTES, M. K., PRASAD, B. V. & HECK, A. J. 2010. Norwalk virus assembly and stability monitored by mass spectrometry. *Mol Cell Proteomics*, 9, 1742-51.

### 5.2.3. N-terminal VP1 truncations favor $T = 1$ norovirus-like particles

*Supplementary information*

## N-terminal VP1 truncations favor $T = 1$ norovirus-like particles

**Ronja Pogan**<sup>1,2</sup>, **Victor U. Weiss**<sup>3</sup>, **Kevin Bond**<sup>4</sup>, **Jasmin Dülfer**<sup>1</sup>, **Christoph Krisp**<sup>5</sup>, **Nicholas Lykтей**<sup>4</sup>, **Jürgen Müller-Guhl**<sup>1,6</sup>, **Samuele Zoratto**<sup>3</sup>, **Günter Allmaier**<sup>3</sup>, **Martin F. Jarrold**<sup>4</sup>, **Caesar Muñoz-Fontela**<sup>6</sup>, **Hartmut Schlüter**<sup>5</sup>, and **Charlotte Uetrecht**<sup>1,2,\*</sup>

<sup>1</sup> Heinrich Pette Institute, Leibniz Institute for Experimental Virology, Hamburg, Germany

<sup>2</sup> European XFEL GmbH, Schenefeld, Germany

<sup>3</sup> Institute of Chemical Technologies and Analytics, TU Wien, Vienna, Austria

<sup>4</sup> Department of Chemistry, Indiana University, Bloomington, IN, USA

<sup>5</sup> Institute of Clinical Chemistry and Laboratory Medicine, Mass Spectrometric Proteomics Group, University Medical Center Hamburg - Eppendorf, Hamburg, Germany

<sup>6</sup> Bernhard Nocht Institute for Tropical Medicine and German Center for Infection Research (DZIF), Partner site Hamburg-Lübeck-Borstel-Riems, Hamburg, Germany.

\*Correspondence: [charlotte.uetrecht@xfel.eu](mailto:charlotte.uetrecht@xfel.eu)

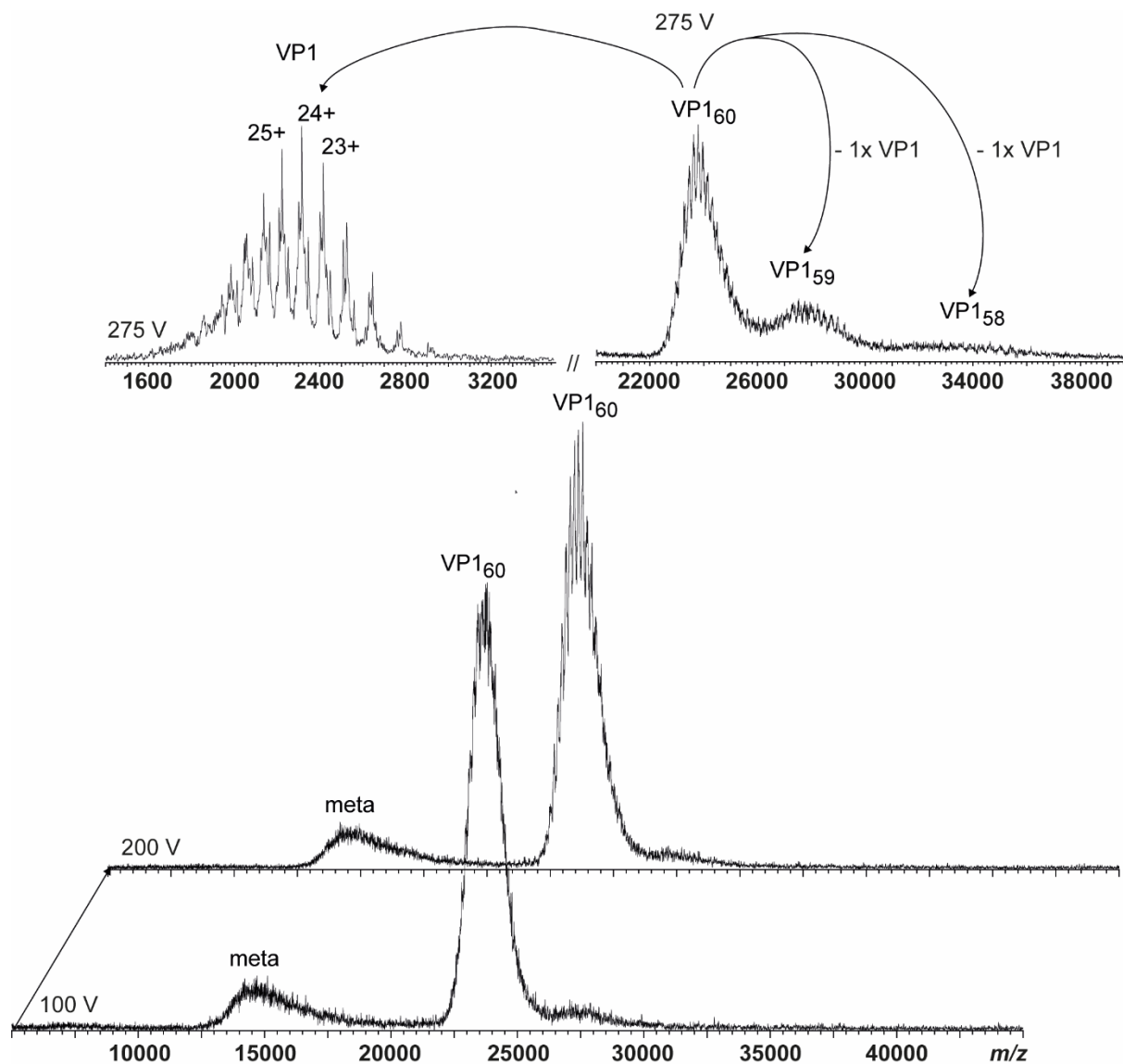
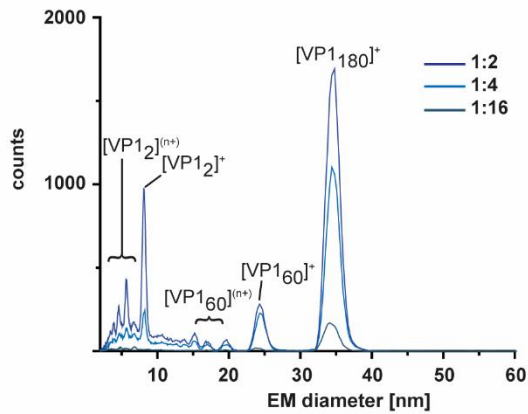


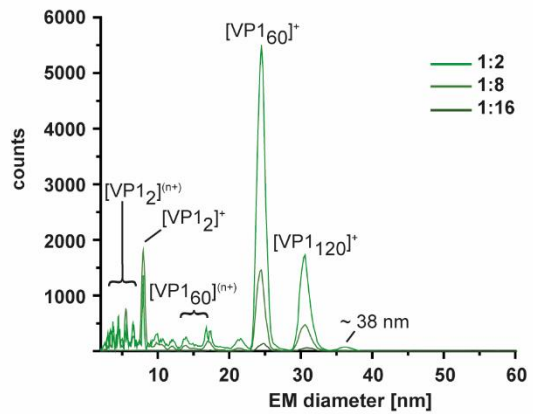
**Figure S1.** Native MS of a GII.10 Vietnam VLPs. Dissociation pathway without selection in the quadrupole shown for GII.10 Vietnam in 250 mM ammonium acetate pH 7 at 10  $\mu$ M VP1. From bottom to top, illustrative mass spectra are shown for 100 V, 200 V, and a zoom in to low  $m/z$  (monomer) and high  $m/z$  (VP1 60-, 59-, 58-mer) at 275 V acceleration into the collision cell. As lower mass ions at approximately 15,000  $m/z$  are annotated as metastable ions (meta), monomer lacking at least 45 aa most likely dissociate from  $T=1$  species.

## Appendix

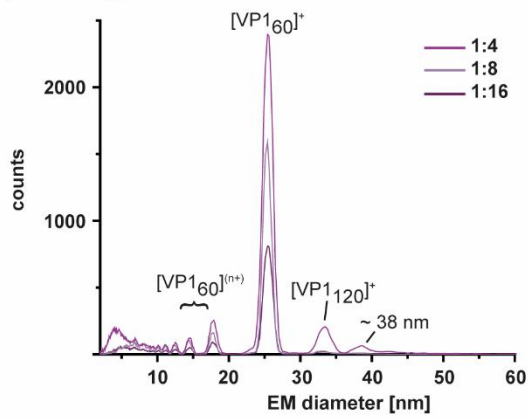
(a) West Chester batch 1



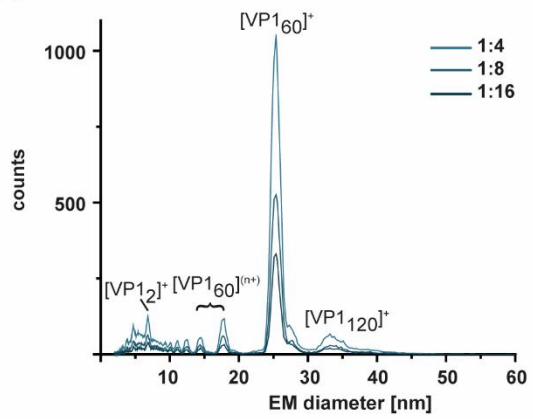
(b) West Chester batch 2



(c) GII.4 Saga



(d) GII.10 Vietnam



(e) GII.17 Saitama

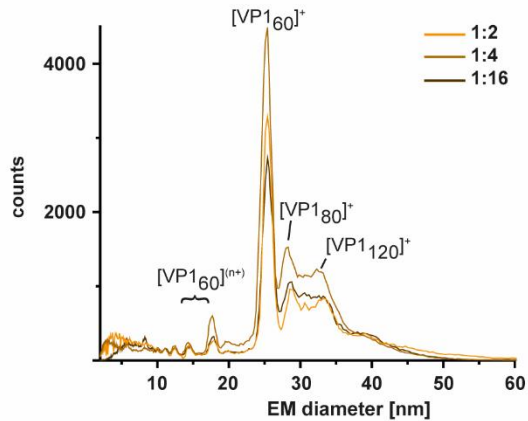


**Figure S2.** GEMMA spectra of different hNoVLPs in 40 mM ammonium acetate at pH 7, 3 different tested dilutions exemplarily shown for (a) West Chester batch 1 (b) West Chester batch 2 (c) GII.4 Saga (d) GII.10 Vietnam and (e) GII.17 Saitama. In GII.1 West Chester batch 2 and GII.4 Saga, additional species at approximately 38 nm were assigned to aggregation due to their appearance only at higher concentrations.

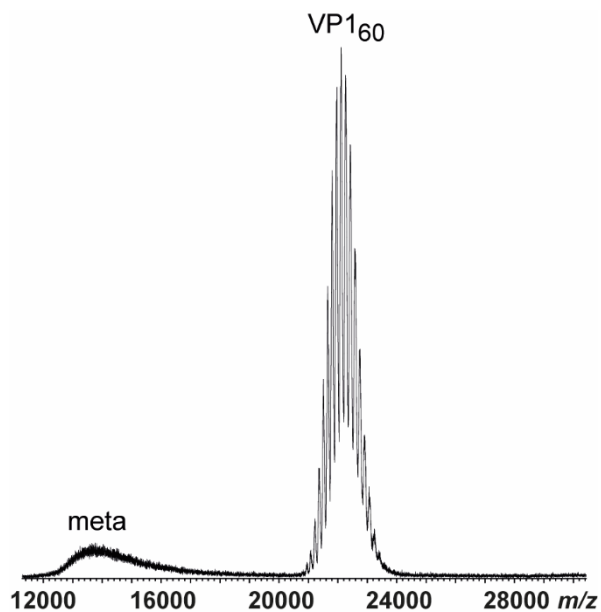
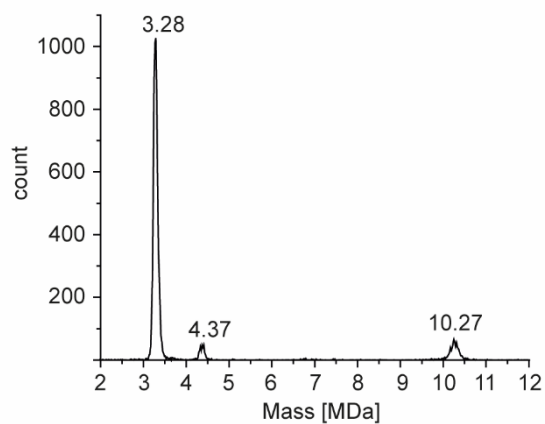


**Figure S3.** Native mass spectrum of GII.4 Saga VLPs at 50 mM ammonium pH 9 at 10  $\mu$ M VP1. In contrast to GEMMA measurements (Figure 5),  $T=1$  particles are detected.

(a) 250 mM AmAc pH 7



(b) 250 mM AmAc pH 8

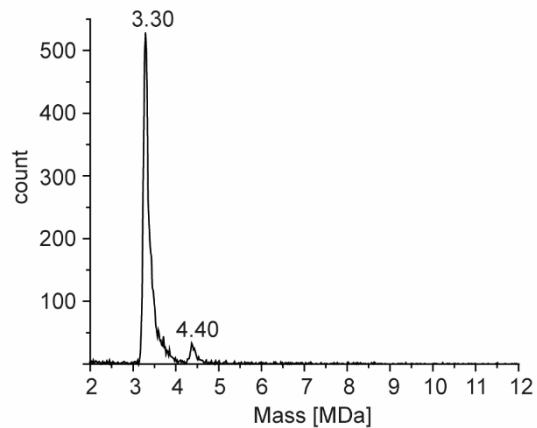
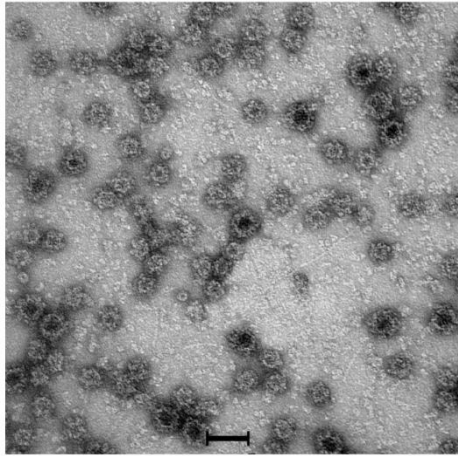


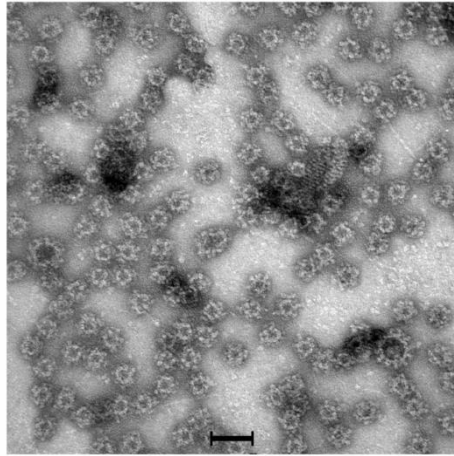
**Figure S4.** Charge detection mass spectra of GI.1 West Chester batch 1 VLPs in 250 mM ammonium acetate at (a) pH 7 and (b) pH 8. Next to  $T=1$  particles, a species at approximately 4.37 MDa at pH 7 and 4.40 MDa at pH 8 is detected. Given the VP1 60-mer mass 4.4 MDa species equal VP1 80-mers. At pH 7, further ions at 10.27 MDa or  $T=3$  particles are observed.

## Appendix

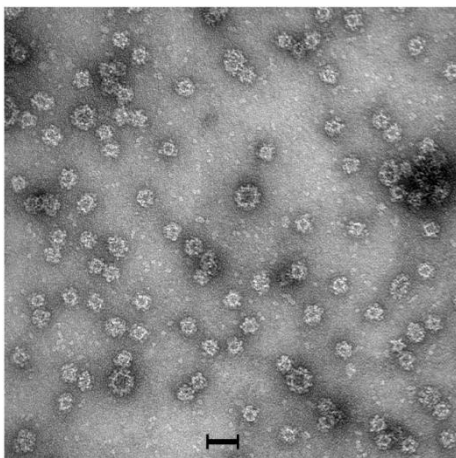
(a) GI.1 West Chester



(b) GII.4 Saga



(c) GII.10 Vietnam



(d) GII.17 Saitama

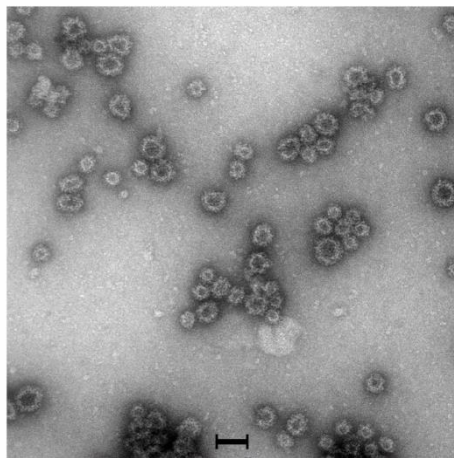


**Figure S5.** Electron micrographs of different hNoVLPs in PBS. (a) GI.1 West Chester (b) GII.4 Saga (c) GII.10 Vietnam and (d) GII.17 Saitama. The bar represents 50 nm. All images are taken at the same magnification. In some cases, particles of similar size to  $T=3$  are observed but the low number precludes detection by other means, moreover our CDMS results suggest that these could also belong to intermediate assemblies in line with the broad GEMMA and native MS distributions.



Pepsin: 524 of 530 - 99%  
 Total: 524 of 530 - 99%

**Figure S6.** VP1 mapping overview of hNoVLP GI.1 West Chester batch 1 after pepsin digestion. In total 524 of 530 aa are covered (coverage 99 %). The first N-terminal residue covered is Ala4, while C-terminally the triplet Leu528-Arg529-Arg530 is missing.

Appendix

M	H	A	S	K	D	A	T	S	N	V	D	G	A	S	G	A	G	O	L	V	P	E	A	N	T	S	D	P	L	A	M	D	P	V	A	G	S	S	T	A	V	A	T	A	G	O	V	N			
1	2	3	4	5	6	7	8	9	10	11	12	13	14	15	16	17	18	19	20	21	22	23	24	25	26	27	28	29	30	31	32	33	34	35	36	37	38	39	40	41	42	43	44	45	46	47	48	49	50		
[Redacted]																																																			
P	I	D	P	H	I	I	N	N	F	V	D	A	P	O	G	E	F	T	I	S	P	N	N	T	P	G	D	V	L	F	D	L	S	L	G	P	H	L	N	P	F	L	L	H	L	S	O	N	Y		
51	52	53	54	55	56	57	58	59	60	61	62	63	64	65	66	67	68	69	70	71	72	73	74	75	76	77	78	79	80	81	82	83	84	85	86	87	88	89	90	91	92	93	94	95	96	97	98	99	100		
[Redacted]																																																			
N	G	V	G	N	M	R	V	R	I	M	L	A	G	N	A	F	T	A	G	K	I	I	V	S	C	I	P	P	G	F	G	S	H	N	L	T	I	A	O	S	T	L	F	P	H	V	I	A			
101	102	103	104	105	106	107	108	109	110	111	112	113	114	115	116	117	118	119	120	121	122	123	124	125	126	127	128	129	130	131	132	133	134	135	136	137	138	139	140	141	142	143	144	145	146	147	148	149	150		
[Redacted]																																																			
D	V	R	T	L	D	P	I	E	V	P	L	E	D	V	R	H	V	L	F	H	N	N	D	R	N	O	Q	T	H	R	L	V	C	M	L	Y	T	P	L	R	T	G	G	G	T	G	D	S	F		
151	152	153	154	155	156	157	158	159	160	161	162	163	164	165	166	167	168	169	170	171	172	173	174	175	176	177	178	179	180	181	182	183	184	185	186	187	188	189	190	191	192	193	194	195	196	197	198	199	200		
[Redacted]																																																			
V	V	A	C	R	V	M	T	C	P	S	P	D	F	N	F	L	F	L	V	P	P	T	V	E	O	K	T	R	P	F	T	L	P	M	L	P	L	S	S	L	S	N	S	R	A	P	L	P	I		
201	202	203	204	205	206	207	208	209	210	211	212	213	214	215	216	217	218	219	220	221	222	223	224	225	226	227	228	229	230	231	232	233	234	235	236	237	238	239	240	241	242	243	244	245	246	247	248	249	250		
[Redacted]																																																			
S	S	M	G	I	S	P	D	N	V	Q	S	V	Q	F	Q	M	G	R	C	T	L	D	T	G	R	L	V	G	T	T	P	V	S	L	S	Q	V	A	K	I	R	G	T	S	N	G	T	V	I	N	
251	252	253	254	255	256	257	258	259	260	261	262	263	264	265	266	267	268	269	270	271	272	273	274	275	276	277	278	279	280	281	282	283	284	285	286	287	288	289	290	291	292	293	294	295	296	297	298	299	300		
[Redacted]																																																			
L	T	E	L	D	G	T	P	F	H	P	F	E	G	P	A	P	I	G	F	P	D	L	G	G	C	D	W	H	V	N	M	T	O	F	G	H	S	S	O	T	O	F	D	V	D	T	T	P	E		
301	302	303	304	305	306	307	308	309	310	311	312	313	314	315	316	317	318	319	320	321	322	323	324	325	326	327	328	329	330	331	332	333	334	335	336	337	338	339	340	341	342	343	344	345	346	347	348	349	350		
[Redacted]																																																			
T	F	V	P	H	L	G	S	I	Q	A	N	G	V	G	S	G	N	Y	I	G	V	L	S	W	I	S	P	P	S	H	P	S	G	S	Q	V	D	L	W	K	I	P	N	Y	G	S	S	I	T		
351	352	353	354	355	356	357	358	359	360	361	362	363	364	365	366	367	368	369	370	371	372	373	374	375	376	377	378	379	380	381	382	383	384	385	386	387	388	389	390	391	392	393	394	395	396	397	398	399	400		
[Redacted]																																																			
E	A	T	H	L	A	P	S	V	F	P	P	G	F	G	E	V	L	V	F	H	S	K	I	P	G	P	G	A	Y	N	L	P	C	L	L	P	O	E	Y	T	S	H	F	A	S	E	O	A			
401	402	403	404	405	406	407	408	409	410	411	412	413	414	415	416	417	418	419	420	421	422	423	424	425	426	427	428	429	430	431	432	433	434	435	436	437	438	439	440	441	442	443	444	445	446	447	448	449	450		
[Redacted]																																																			
P	T	V	G	E	A	A	L	L	H	Y	V	D	P	D	T	G	R	N	L	G	E	F	K	A	Y	P	D	G	F	L	T	C	V	P	N	G	A	S	S	G	P	O	L	P	I	N	G	V			
451	452	453	454	455	456	457	458	459	460	461	462	463	464	465	466	467	468	469	470	471	472	473	474	475	476	477	478	479	480	481	482	483	484	485	486	487	488	489	490	491	492	493	494	495	496	497	498	499	500		
[Redacted]																																																			
F	V	F	V	S	W	V	S	R	F	Y	Q	L	K	P	V	G	T	A	S	S	A	R	G	R	L	G	L	R	R																						
501	502	503	504	505	506	507	508	509	510	511	512	513	514	515	516	517	518	519	520	521	522	523	524	525	526	527	528	529	530																						
[Redacted]																																																			

Peptide: 521 of 530 - 98%  
Total: 521 of 530 - 98%

**Figure S7.** VP1 mapping overview of hNoVLP GI.1 West Chester batch 2 after pepsin digestion. In total 521 of 530 aa are covered (coverage 98 %). The first N-terminal residue covered is Met3 and the C-terminus is covered up to residue Arg523.



Pepsin\_SagaGH: 487 of 540 - 90%  
 Total: 487 of 540 - 90%



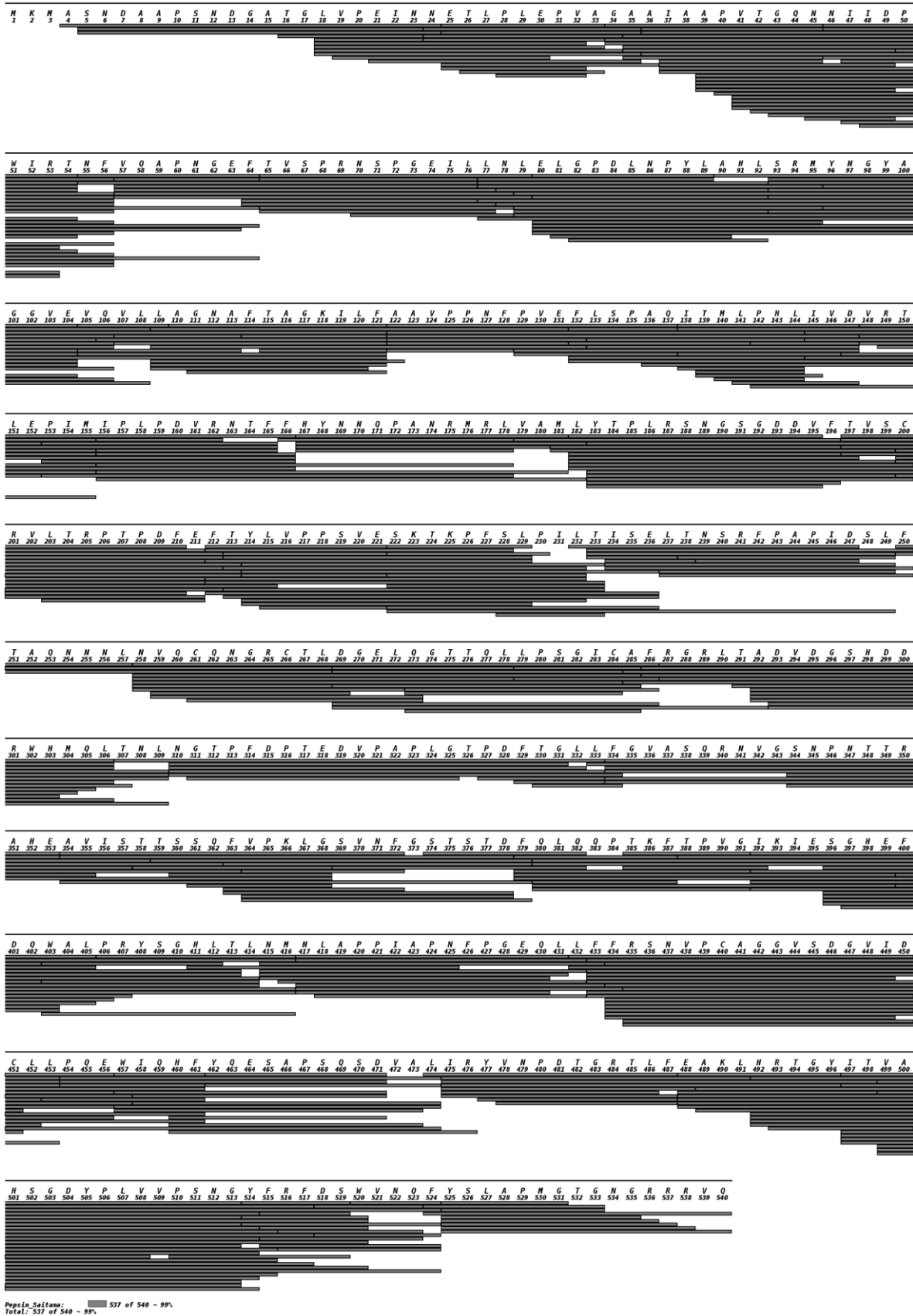
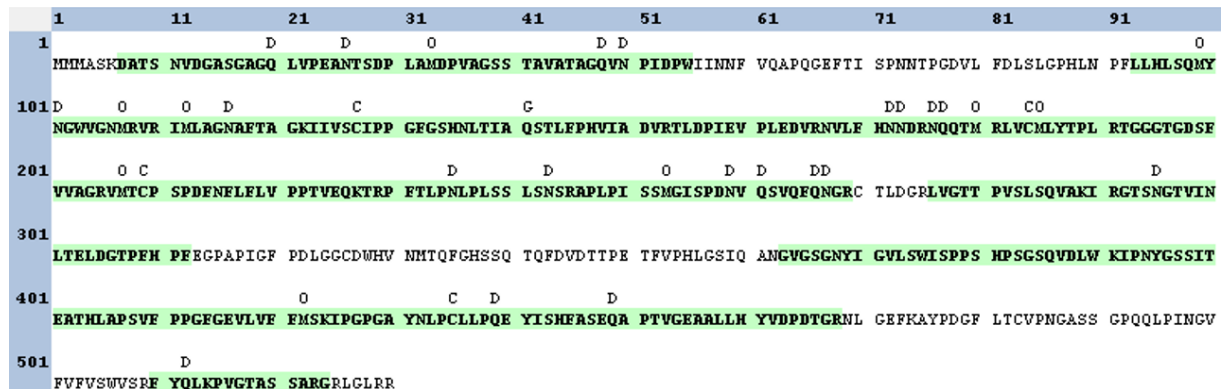


Figure S10. VP1 mapping overview of hNoVLP GII.17 Saitama after pepsin digestion. In total 537 of 540 aa are

## Appendix

covered (coverage 99 %). The first N-terminal residue covered is Ala4, while full-coverage is given for the C-terminus.



**Figure S11.** VP1 mapping overview of hNoVLP GI.1 West Chester batch 1 after trypsin digestion (coverage 72 %). The first N-terminal residue covered is Asp7 and C-terminally six residues are not covered.

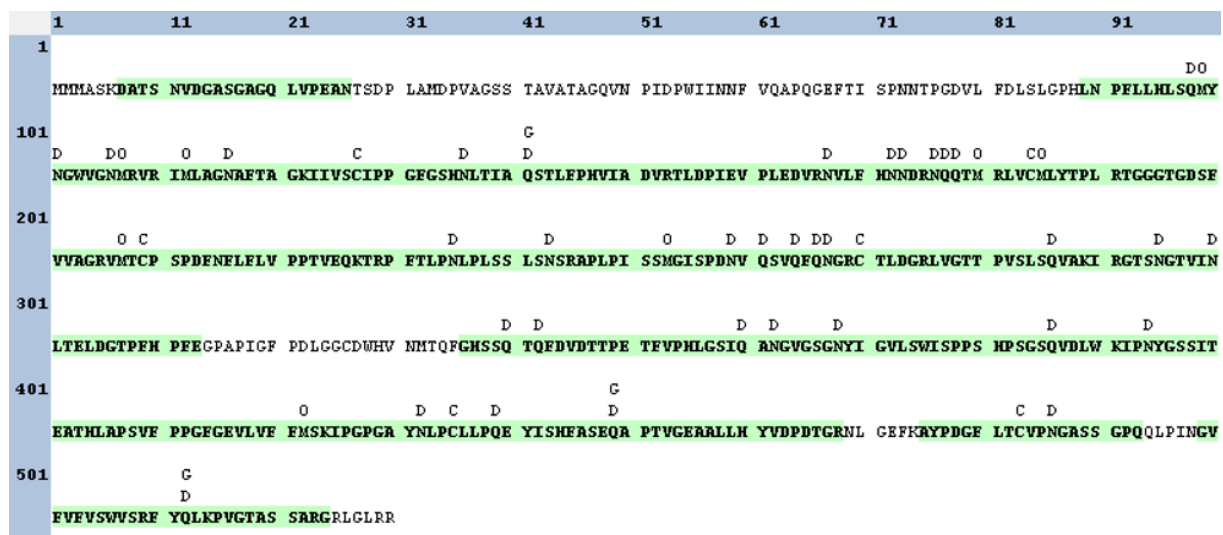


**Figure S12.** VP1 mapping overview of hNoVLP GI.1 West Chester batch 2 after trypsin digestion (coverage 80 %). The first N-terminal residue covered is Asp7 and C-terminally six residues are not covered.

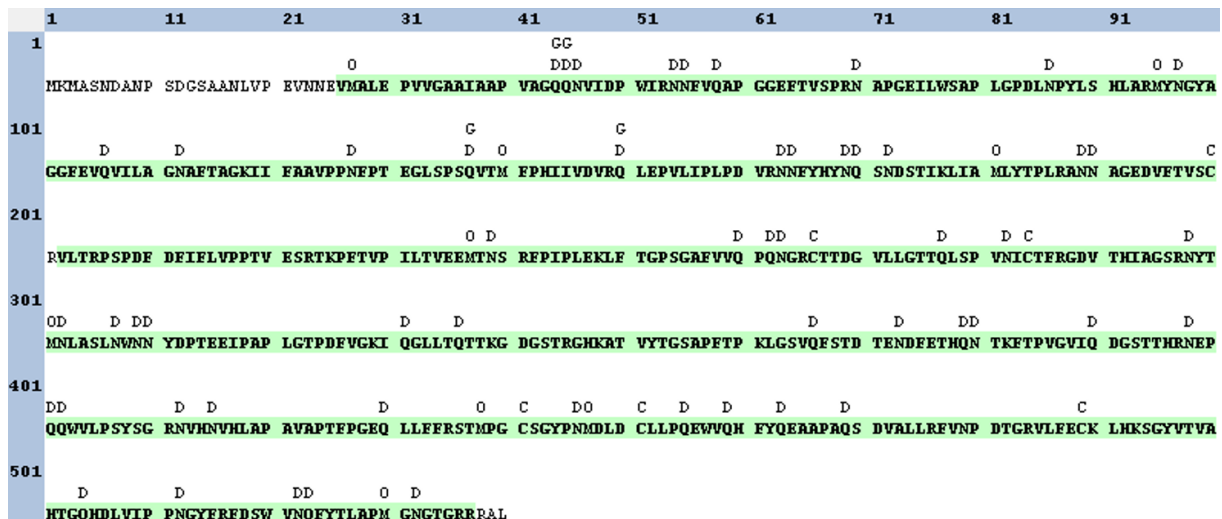


**Figure S13.** VP1 mapping overview of hNoVLP GII.4 Saga after trypsin digestion (coverage 95 %). Semi-tryptic peptide search identifies Val26 as the first N-terminal residue covered, while C-terminally the triplet Arg538-Ala539-Leu540 is not covered.

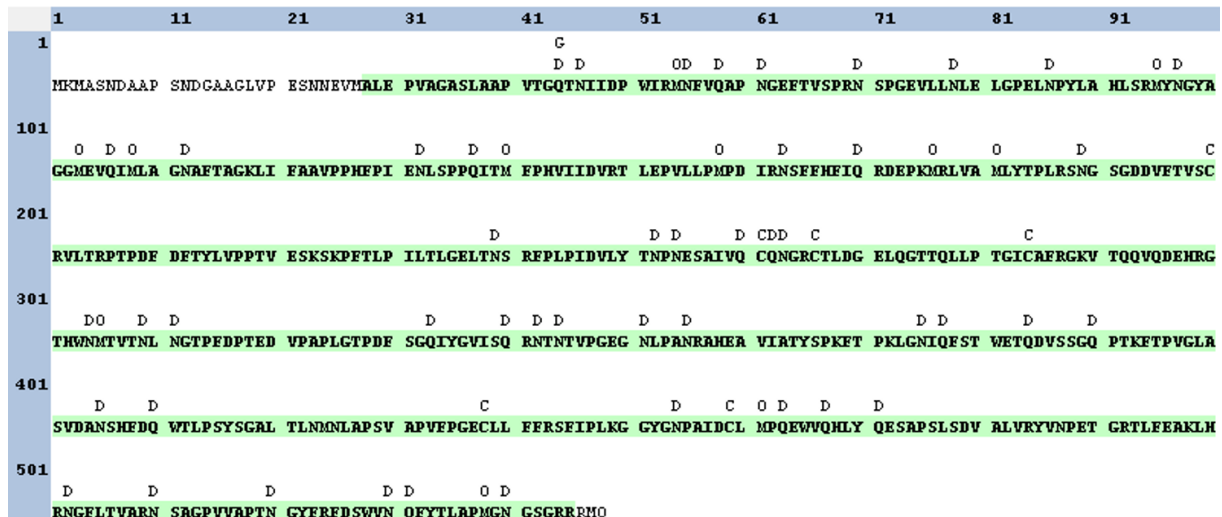


**Figure S14.** VP1 mapping overview of hNoVLP GII.10 Vietnam after trypsin digestion (coverage 95 %). Semi-tryptic peptide search identifies Ala28 as the first N-terminal residue covered, while C-terminally the triplet Arg546-Met547-Gln548 is not covered. Note that the sequence covered starts indeed with a semi-tryptic peptide.

## Appendix

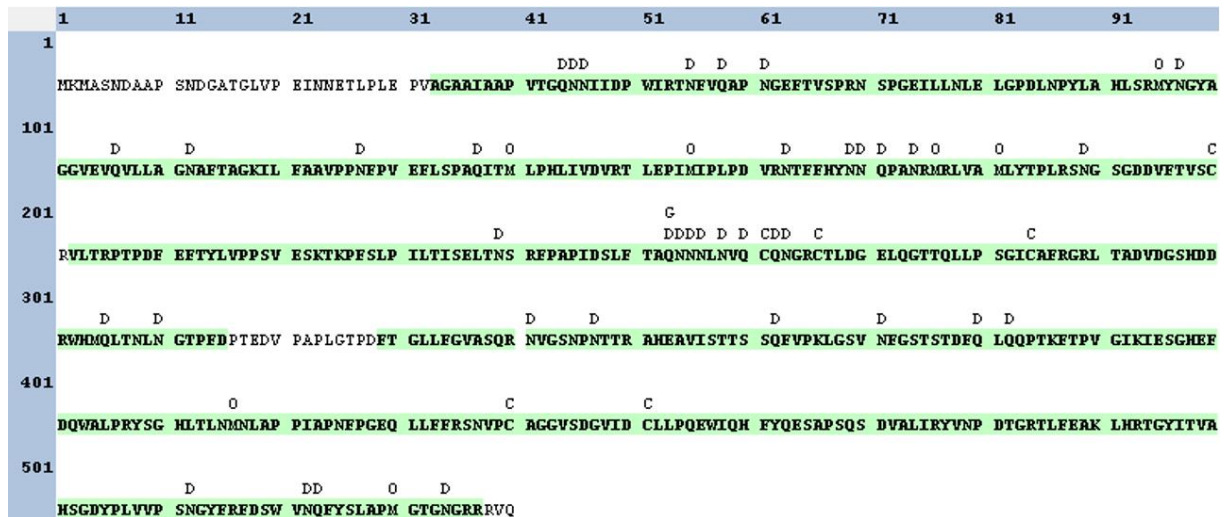


**Figure S15.** VP1 mapping overview of hNoVLP GII.17 Saitama after trypsin digestion (coverage 91 %). Semi-tryptic peptide search identifies Ala33 as the first N-terminal residue covered, while C-terminally the triplet Arg538-Val539-Gln540 is not covered. Note that the sequence covered starts indeed with a semi-tryptic peptide.

Table S1. Data mass table for charge detection mass spectrometry measurements. Abbreviations Th. theoretical, Exp. experimental, Calc. calculated. VP1 Calc. based on VP1 60-mer mass. For VP1 Th. and VP1 Calc. the total aa-amount and aa truncation according to experimental mass are given, respectively. *N* VP1 given for larger assemblies respective to VP1 Calc. \*indicate masses are approximations due to low particle counts.

Variant	VP1 Th.	Complex Exp.	VP1 Calc.	<i>N</i> VP1 Complex
GII.4 Saga	59005 Da 540 aa	3.35 MDa	55800 Da, -31 aa	60
GII.10 Vietnam	59901 Da 548 aa	3.41 MDa ~ 4.5 MDa* ~ 6.9 MDa*	56800 Da, -31 aa	60 79 121
GII.17 Saitama	58957 Da 540 aa	3.44 MDa 4.07 MDa 5.20 MDa 5.72 MDa 6.20 MDa 6.87 MDa	57300 Da, -17 aa	60 71 91 100 108 120

Table S2. Data mass table for conventional QToF measurements. Abbreviations Th. theoretical, Exp. experimental, Calc. calculated. For all tested variants, collision induced dissociation experiments resulted in dissociated VP1 monomer with a main species (VP1 Exp. main) and one or two neighboring species with lower intensity (VP1 Exp. following). VP1 60-mer experimental mass (Complex VP1<sub>60</sub> Exp.) assigned where charge state resolution was obtained and given as approximations for GI.1 West Chester due to low desolvation and associated low charge state resolution. \*approximation.

Variant	VP1 Th.	VP1 Exp. main	VP1 Exp. following	Complex VP1 <sub>60</sub> Exp.
GI.1 West Chester	56609 Da, 530 aa	52760 ± 10 Da, -40 aa	52540 ± 10 Da, -4 aa-	~3.4 MDa*
GII.4 Saga	59005 Da 540 aa	54600 ± 20 Da, -45 aa	54270 ± 20 Da, -48 aa	3.27 ± 0.02 MDa
GII.10 Vietnam	59901 Da 548 aa	55560 ± 10, -45 aa	55220 ± 20, -48 aa 56290 ± 10, -37aa	3.33 ± 0.02 MDa

## Appendix

Table S3 GEMMA Data mass table for gas phase electrophoretic molecular mobility analysis. Abbreviations, Exp. experimental, Calc. calculated. VP1 oligomers given as experimental EMD values and respective molecular weight calculations for low EMD range (<sup>1</sup> Bacher et al 2001) and high EMD range (<sup>2</sup> Weiss et al. 2019) \*approximation due to low particle counts.

Variant	pH	VP1 dimer	VP1 60-mer	VP1 80-mer	VP1 120-mer	VP1 140-mer	VP1 180-mer
		Exp. (nm) Calc. <sup>1</sup> (kDa)	Exp. (nm) Calc. <sup>2</sup> (MDa)				
GI.1 West Chester batch 1	6		24.29 ± 0.09 3.37 ± 0.03				34.54 ± 0.05 8.50 ± 0.03
	7	8.10 ± 0.05 112 ± 2	24.09 ± 0.27 3.30 ± 0.10				34.37 ± 0.13 8.40 ± 0.09
	9	8.03 ± 0.01 109 ± 1					
	6		24.48 ± 0.02 3.44 ± 0.01		30.73 ± 0.05 6.25 ± 0.03		
GI.1 West Chester batch 2	7	8.00 ± 0.07 108 ± 3	24.50 ± 0.12 3.45 ± 0.04		30.71 ± 0.17 6.24 ± 0.09		
	9	7.89 ± 0.01 104 ± 1	24.18 ± 0.06 3.33 ± 0.02				
	5		25.27 ± 0.01 3.74 ± 0.01				
GII.4 Saga	6		25.18 ± 0.01 3.70 ± 0.01				
	7		25.38 ± 0.07 3.8 ± 0.03			33.30 ± 0.08 7.72 ± 0.05	
	8	8.03 ± 0.02 109 ± 1	25.44 ± 0.03 3.80 ± 0.01				
	9	7.88 ± 0.01 104 ± 1					
	5		~ 25*				
GII.10 Vietnam	6		25.11 ± 0.01 3.68 ± 0.02				
	7		25.32 ± 0.02 3.75 ± 0.01			33.41 ± 0.09 7.79 ± 0.06	
	8	7.90 ± 0.02 104 ± 1	25.10 ± 0.02 3.67 ± 0.01			33.31 ± 0.05 7.73 ± 0.03	
	9	7.93 ± 0.02 105 ± 1	25.06 ± 0.02 3.66 ± 0.01				
	5		~ 25*				

	5		25.47 ± 0.09	28.67 ± 0.54	
			3.81 ± 0.04	5.21 ± 0.26	
	6		25.20 ± 0.06		
			3.71 ± 0.03		
GII.17 Saitama	7		25.36 ± 0.06	28.48 ± 0.17	32.62 ± 0.22
			3.77 ± 0.03	5.12 ± 0.08	7.31 ± 0.13
	8	7.99 ± 0.08	25.14 ± 0.05	28.13 ± 0.10	32.33 ± 0.08
		108 ± 3	3.69 ± 0.02	4.96 ± 0.05	7.15 ± 0.05
	9	8.08 ± 0.05	25.22 ± 0.17		
		111 ± 2	3.72 ± 0.07		

<sup>1</sup> Bacher G, Szymanski WW, Kaufman SL, Zollner P, Blaas D, Allmaier G. Charge-reduced nano electrospray ionization combined with differential mobility analysis of peptides, proteins, glycoproteins, noncovalent protein complexes and viruses. *J Mass Spectrom.* 2001;36(9):1038-52.

<sup>2</sup> Weiss VU, Pogan R, Zoratto S, Bond KM, Boulanger P, Jarrold MF, et al. Virus-like particle size and molecular weight/mass determination applying gas-phase electrophoresis (native nES GEMMA). *Anal Bioanal Chem.* 2019;411(23):5951-62

## **6. Declaration on Oath/ Eidesstattliche Versicherung**

---

---

I hereby declare on oath that this doctoral dissertation is written independently and solely by my own based on the original work of my PhD and has not been used other than the acknowledged resources and aids.

Hiermit versichere ich an Eides statt, die vorliegende Dissertation selbst verfasst und keine anderen als die angegebenen Hilfsmittel benutzt zu haben. Die eingereichte schriftliche Fassung entspricht der auf dem elektronischen Speichermedium. Ich versichere, dass diese Dissertation nicht in einem früheren Promotionsverfahren eingereicht wurde.

Datum, Unterschrift